IOWA STATE UNIVERSITY
Digital Repository

Retrospective Theses and Dissertations

Iowa State University Capstones, Theses and Dissertations

1-1-1995

Dynamic behavior of glued laminated timber stringer bridges

Jan Dlabola
Iowa State University

Follow this and additional works at: https://lib.dr.iastate.edu/rtd

Part of the Engineering Commons

Recommended Citation
Dlabola, Jan, "Dynamic behavior of glued laminated timber stringer bridges" (1995). *Retrospective Theses and Dissertations*. 18126.
https://lib.dr.iastate.edu/rtd/18126

This Thesis is brought to you for free and open access by the Iowa State University Capstones, Theses and Dissertations at Iowa State University Digital Repository. It has been accepted for inclusion in Retrospective Theses and Dissertations by an authorized administrator of Iowa State University Digital Repository. For more information, please contact digirep@iastate.edu.

المنارة للاستشارات

www.manaraa.com

Dynamic behavior of glued laminated timber stringer bridges

by

Jan Dlabola

A Thesis Submitted to the

Graduate faculty in Partial Fulfillment of the

Requirements for the Degree of

MASTER OF SCIENCE

Department: Civil and Construction Engineering
Major: Civil Engineering (Structural Engineering)

Signatures have been redacted for privacy

Iowa State University
Ames, Iowa

1995

raa.com

TABLE OF CONTENTS

1. INTRODUCTION 1

1.1 General 1

1.2 Background 2

1.3 Objective of the study 3

1.4 Timber stringer bridge 3

2. ANALYTICAL MODELS 6

2.1 Bridge model 6

2.1.1 General 6

2.1.2 Model 6

2.1.3 Composite action of the cross section 9

2.1.4 Finite element mesh 10

2.2 Vehicle model 11

2.2.1 Vehicle suspensions 11

2.2.1.1 Steel-leaf suspension 11

2.2.1.2 Air suspension 12

2.2.2 Finite element model 13

2.3.2 Model validation 13

2.3.2.1 Modal analysis 13

2.3.2.2 Transient analysis 15

2.3 Vehicle/bridge interaction model 18

raa.com

2.3.1 General 18

2.3.2 Dynamic amplification factor 21

2.3.3 Bridge/vehicle interaction model 23

3. SENSITIVITY STUDY 24

3.1 General 24

3.2 Mode frequency analysis 26

3.3 Transient analysis 33

3.3.1 General 33

3.3.2 Vehicle speed 33

3.3.3 Vehicle initial conditions 40

3.3.4 Analysis in frequency domain 41

3.3.5 Bridge damping 51

3.3.6 Vehicle axle spacing 51

3.3.7 Conclusion 56

4. EXPERIMENTAL INVESTIGATION 57

4.1 General 57

4.1.1 Bridge instrumentation 57

4.1.2 Vehicle instrumentation 60

4.1.3 Test Procedure 64

4.1.4 General format of result discussion 65

4.2 Mud Creek Bridge 66

raa.com

4.2.1 Bridge and vehicle description 66

4.2.2 Discussion of results 72

4.2.2.1 Bridge free vibration response and vehicle vibration..... 72

4.2.2.2 Forced vibration response 72

4.2.2.3 Dynamic amplification 78

4.3 Span 1 of Wittson Bridge 78

4.3.1 Bridge and vehicle description 81

4.3.2 Discussion of results 81

4.3.2.1 Bridge free vibration response and vehicle vibration..... 81

4.3.2.2 Forced vibration response 85

4.3.2.3 Dynamic amplification 91

4.4 Span 3 of Wittson Bridge 94

4.4.1 Bridge and vehicle description 94

4.4.2 Discussion of results 97

4.4.2.1 Bridge free vibration response and vehicle vibration..... 97

4.4.2.2 Forced vibration response 97

4.4.2.3 Dynamic amplification 104

4.5 Chambers Co. Bridge 104

4.5.1 Bridge and vehicle description 104

4.5.2 Discussion of results 109

4.5.2.1 Bridge free vibration response and vehicle vibration..... 109

raa.com

4.5.2.2 Forced vibration response - concentric tests 109

4.5.2.3 Forced vibration response - eccentric tests 113

4.5.2.4 Dynamic amplification 122

4.6 Summary of the experimantal findings 122

4.6.1 Observed bridge behavior 122

4.6.1.1 High speed interval 124

4.6.1.2 Medium speed interval 124

4.6.1.3 Low speed interval 126

4.6.2 Summary of other observations 128

5. SUMMARY AND CONCLUSIONS 131

5.1 Summary 131

5.1.1 Bridge model 131

5.1.2 Vehicle model 132

5.1.3 Sensitivity study 132

5.1.4 Experimental findings 133

5.1.5 Comparison of analytical and experimental results 134

5.2 Conclusions and recommendations 135

REFERENCES 136

ACKNOWLEDGMENTS 139

APPENDIX 1 - RESULTS OF THE ANALYSIS IN FREQUENCY DOMAIN 140

APPENDIX 2 - ADJUSTMENTS FOR DAF CALCULATIONS 153

raa.com

APPENDIX 3 - MODE SHAPES 160

raa.com

LIST OF TABLES

Table 2.1 Finite element assignment to structural components 8

Table 2.2 Vehicle modal shape analysis results 16

Table 3.1 Bridge parameters in sensitivity study 25

Table 3.2 Summary of the modal shape analysis results 31

Table 3.3 Summary of DAF for the sensitivity study 35

Table 4.1 Comparison of computed and experimentally observed modal frequencies for Span 3 of Wittson Bridge 99

Table 4.2 Comparison of computed and experimentally observed modal frequencies for Chambers Co. Bridge 110

Table 4.3 Summary table of observed bridge behavior 125

raa.com

LIST OF FIGURES

Fig. 1.1 Typical glulam beam bridge configuration 4

Fig. 2.1 View of the model 7

Fig. 2.2 Finite element model of the vehicle 14

Fig. 2.3 Modal shapes of the vehicle 17

Fig. 2.4 Vehicle acceleration plot at node 5 19

Fig. 2.5 Frequency content at node 5 19

Fig. 2.6 Vehicle acceleration plot at node 8 20

Fig. 2.7 Frequency content at node 8 20

Fig. 3.1 Full model mode shapes 27

Fig. 3.2 DAF plots for Bridge 1 and Bridge 2 34

Fig. 3.3 Bridge 1 response for 15 mph 36

Fig. 3.4 Bridge 1 response for 25 mph 37

Fig. 3.5 Bridge 1 response for 35 mph 38

Fig. 3.6 Bridge 1 response for 45 mph 39

Fig. 3.7 Monitoring points for the frequency domain analysis 42

Fig. 3.8 Frequency domain analysis - bridge response for smooth vehicle entry and speed 45 mph 44

Fig. 3.9 Bridge 1 response for 45 mph 45

Fig. 3.10 Frequency domain analysis - bridge response for bump vehicle entry and speed 35 mph 47

raa.com

Fig. 3.11 Frequency domain analysis - bridge response for smooth vehicle entry and speed 25 mph 48

Fig. 3.12 Frequency domain analysis - bridge response for bump vehicle entry and speed 25 mph 49

Fig. 3.13 Frequency domain analysis - vehicle response for smooth entry and speed 25 mph 50

Fig. 3.14 Frequency domain analysis - vehicle response for smooth entry and speed 45 mph 52

Fig. 3.15 Frequency domain analysis - vehicle response for bump entry and speed 45 mph 53

Fig. 3.16 Damped and undamped response of the bridge 1 for vehicle speed 25 mph .. 54

Fig. 3.17 DAF variation for different axle spacing of the vehicle 55

Fig. 4.1 Bridge instrumentation 59

Fig. 4.2 Test vehicle..... 61

Fig. 4.3 Vehicle details and accelerometer placement 62

Fig. 4.4 Typical testing vehicle 63

Fig. 4.5 Mud Creek Bridge 67

Fig. 4.6 Mud Creek Bridge - details..... 68

Fig. 4.7 Mud Creek Bridge - layout and instrumentation 70

Fig. 4.8 Mud Creek Bridge - cross section dimensions and transverse position of the vehicle 71

Fig. 4.9 Mud Creek Bridge: accelerometer data and frequency analysis for control run on roadway 73

Fig. 4.10 Dynamic response for Mud Creek Bridge - Stringers G3 (I) and G5 (EI) 74

Fig. 4.11 Frequency content plots for Mud Creek Bridge 76

raa.com

Fig. 4.12 Mud Creek Bridge - DAF plots 79

Fig. 4.13 Wittson Bridge 80

Fig. 4.14 Layout and instrumentation on Span 1 of Wittson Bridge..... 82

Fig. 4.15 Cross section dimensions and transverse position of the vehicle on Span 1 of Wittson Bridge 83

Fig. 4.16 Span 1 of Wittson Bridge - free vibration record and frequency content 84

Fig. 4.17 Wittson Bridge: accelerometer data and frequency analysis for control run on roadway 86

Fig. 4.18 Dynamic response for Span 1 of Wittson Bridge - Stringer G2 87

Fig. 4.19 Frequency content plots for Span 1 of Wittson Bridge..... 89

Fig. 4.20 Frequency content plots for vehicle on Span 1 of Wittson Bridge 92

Fig. 4.21 Span 1 of Wittson Bridge - DAF plots 93

Fig. 4.22 Layout and instrumentation on Span 3 of Wittson Bridge 95

Fig. 4.23 Cross section dimensions and transverse position of the vehicle Span 3 of Wittson Bridge 96

Fig. 4.24 Span 3 of Wittson Bridge - frequency content and acceleration plots of free vibration..... 98

Fig. 4.25 Dynamic response for Span 3 of Wittson Bridge - Stringer G2 100

Fig. 4.26 Frequency content plots for forced vibration of Span 3 of Wittson Bridge 102

Fig. 4.27 Frequency content plots for vehicle on Span 3 of Wittson Bridge 103

Fig. 4.28 Span 3 of Wittson Bridge - DAF plots 105

Fig. 4.29 Chambers Co. Bridge - vehicle on the bridge..... 106

Fig. 4.30 Chambers Co. Bridge - layout and instrumentation 107

raa.com

Fig. 4.31 Chambers Co. Bridge - cross section dimensions and transverse position of the vehicle 108

Fig. 4.32 Wittson Bridge: accelerometer data and frequency analysis for control run on roadway 111

Fig. 4.33 Frequency content plots and acceleration plots for Chambers Co. Bridge..... 112

Fig. 4.34 Dynamic response for concentric tests of Chambers Co. Bridge - Stringer G4 114

Fig. 4.35 Frequency content plots for Chambers Co. Bridge - concentric runs..... 116

Fig. 4.36 Frequency content plots for vehicle on Chambers Co. Bridge 118

Fig. 4.37 Dynamic response for eccentric tests of Chambers Co. Bridge - Stringer G4 119

Fig. 4.38 Frequency content plots for Chambers Co. Bridge - eccentric tests..... 121

Fig. 4.39 Chambers Co. Bridge - DAF plots 123

Fig. 4.40 Acceleration (A2) and frequency content plots for vehicle on Chambers Co. Bridge 127

raa.com

1. INTRODUCTION

1.1 General

Wood has been used as a bridge material in the United States for hundreds of years. Despite the exclusive use of wood bridges during much of the 19th century, the 20th century has brought a significant decline in the percentage of constructed wood bridges compared to bridges made of other materials. Presently, approximately 10% of the bridges listed in the National Bridge Inventory are made of wood. There has recently been a renewed interest in wood as a bridge material and in promoting the use of timber for bridge construction.

The United States government passed the Timber Bridge Initiative in 1988. This program, headed by the United States Department of Agriculture Forest Service, helps local governments construct timber bridges. The Forest Products Laboratory evaluates and monitors these bridges through a series of periodic tests. Information from these tests provide insight into changes that can be made to improve performance, design and cost effectiveness.

raa.com

1.2 Background

To account for the dynamic loads imposed by passing vehicles, Standard Specifications for Highway Bridges created by the American Association of State Highway and Transportation Officials (AASHTO) [1] prescribes that dynamic allowance be applied. AASHTO has not required the application of the impact factor for wood because of its ability to absorb shock and carry larger loads for a short duration. Recently, the exclusion of wood bridges from dynamic loading requirements has been questioned. Studies have shown that the dynamic impact can account for a significant portion of the total response and thus should be considered.

The dynamic behavior of steel and concrete bridges has been studied analytically and experimentally by many researchers. The dynamic behavior is affected by many characteristics and is relatively difficult to quantify when using only a few parameters. Material properties, vehicle characteristics, path and velocity of the vehicle, riding surface quality and initial conditions combine to affect the dynamic response of the bridge.

Solutions to the problem of bridge vibration produced by moving vehicles have been obtained by various researchers by using bridge and vehicle models of various sophistication. Models of vehicles have included moving constant forces, rolling masses, a single sprung mass, and sprung mass systems with multi degrees of freedom. A review of analytical and experimental findings by Paultre et. al. [2] suggests that vehicle spring models can be used with reasonable accuracy to represent vehicle behavior. Although 2D models are most frequently used, Wang et. al. [3] introduced a 3D 12 degree of freedom model.

raa.com

When modeling a structure's dynamic behavior, more advanced models will not generally produce more accurate results. Results have shown that a model improved by adding springs and dampers is harder to validate due to uncertainty associated with values of mechanical constants. These typically vary over a considerable range; therefore, many authors (Bakht and Pinjarkar [4]) suggest that analytical investigation must always be compared to a full scale experiment.

1.3 Objective of the study

Since 1993, this program of timber bridge investigation has been ongoing at Iowa State University. The initial phases of the study concentrated on stress-laminated and longitudinal glulam deck bridges. The objective of this study is to develop a model capable of simulating dynamic behavior and to study this behavior. In the next step to perform a test of several field bridges and to study their behavior.

1.4 Timber stringer bridge

Typical timber stringer bridge cross and longitudinal sections are shown in Fig. 1.1. Ritter [5] describes general design and construction parameters. A timber stringer bridge superstructure consists of a series of longitudinal timber beams and a transverse deck. Historically, this arrangement has been the most common and economical type of timber bridge. For the past 20 years, these bridges have been almost exclusively constructed from glued-laminated (glulam) timber because of their performance superiority and availability in

raa.com

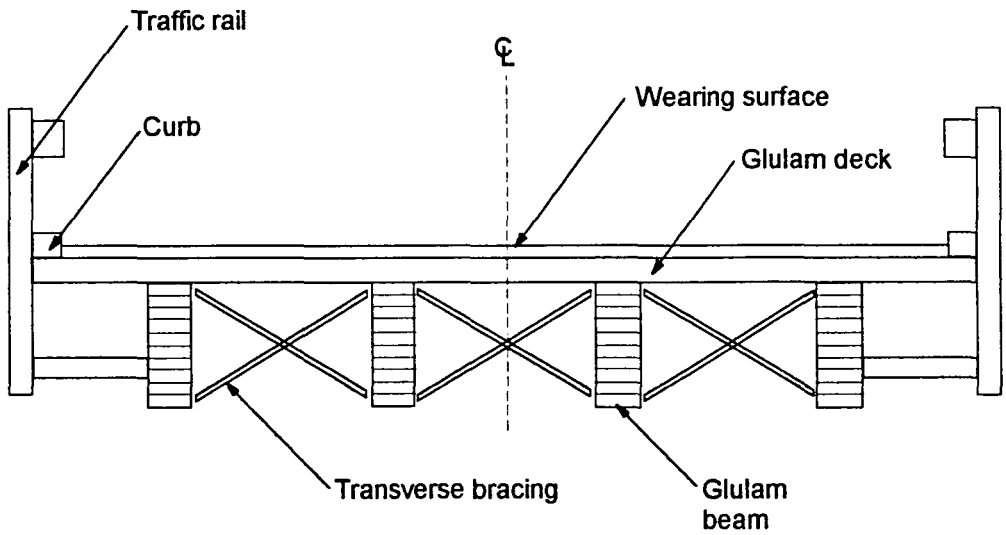

a) Cross section

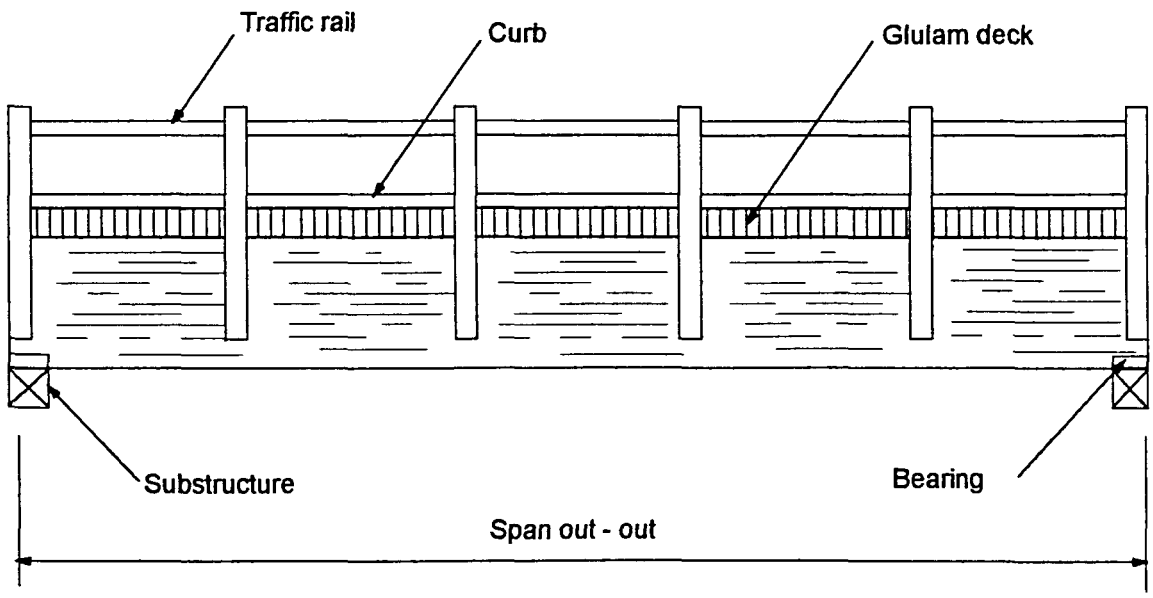

b) Side elevation

Fig. 1.1 Typical glulam beam bridge configuration

raa.com

larger sections. To enhance their performance further, different species of timber are used within one beam so that laminae with a higher modulus of elasticity can be used for outer fibers of beam sections.

Timber stringer bridges are the most practical for clear spans between 20 to 100 ft. The most economical and practical beam spacing for transverse glulam decks supporting highway loads is between 4.5 to 6.5 ft, depending on performance of the deck. The beams and deck are connected with various types of connectors, the most typical being aluminum brackets and through bolts. The deck panels may or may not be interconnected with steel dowels. Depending on the volume of traffic on the bridge, the deck is laid over with an asphalt wearing surface.

raa.com

2. ANALYTICAL MODELS

2.1 Bridge model

2.1.1 General

Although beam - deck bridges are a very common type of structure, related literature is lacking in published material pertinent to the topic of timber stringer bridges. To describe the bridge behavior, analysis of a three dimensional finite element (full) model utilizing the ANSYS software package [6] was used. The main objective of this step was to develop a model to correspond with typical field bridge. This chapter describes the composition of the model.

2.1.2 Model

The model was assembled using stringers, deck panels, stringer-deck connectors, transverse bracing, and supports, and appears in Fig. 2.1. Stringers exposed to in-plane loads only were modeled using quadrilateral shell (SHELL 63) elements. This element has six degrees of freedom for each node (three rotations and three translations). Material properties of the element are determined by a set of four independent engineering constants, E_x, E_y, G_{xy} and ν_{xy}. Deck panels were modeled using the same element as the stringers.

raa.com

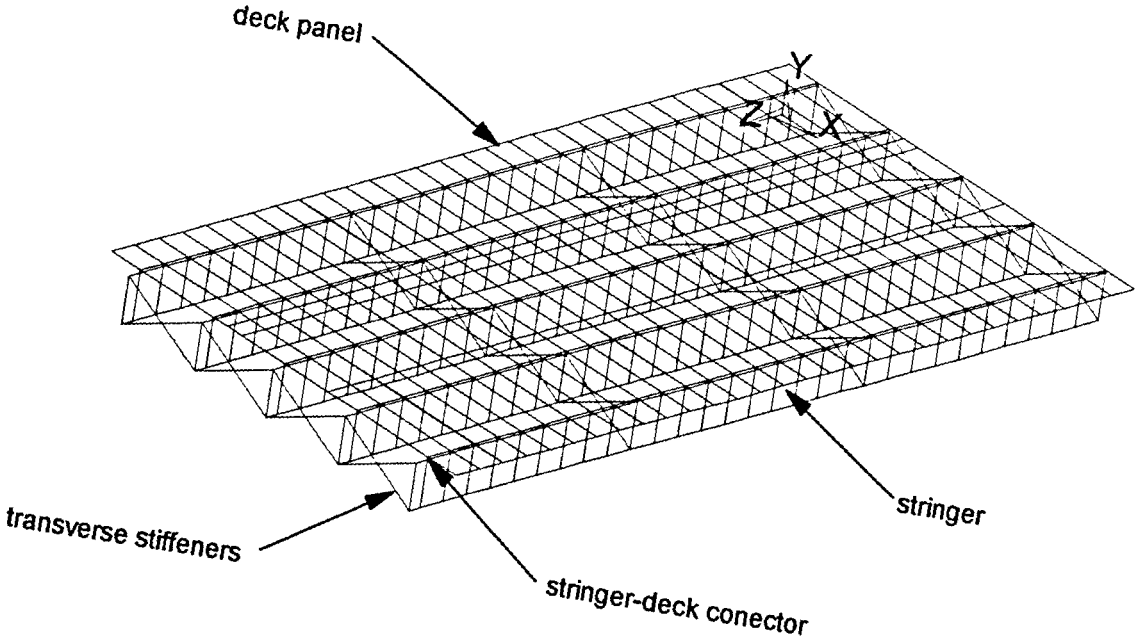

Fig. 2.1 View of the model

raa.com

Because the panel's deflections are mainly influenced by bending, the membrane stiffness of the element was neglected. Stringer-deck connectors were modeled by flexible 3D links (BEAM 4). When the bending stiffness of the connections is known from experimental measurement, its flexural properties (product EI) are typically calculated as follows:

$$k=12\frac{EI}{L^3}$$

where k is the experimentally determined stiffness of the connector and L is its length in the model. Transverse bracing (X-bracing) was modeled by tension-only spars (LINK 8). Supports were modeled by pin constraints in all x, y and z directions, with longitudinal release at one end. The structural elements and the finite elements used to model them are summarized in Table 2.1.

Table 2.1 Finite element assignment to structural components

STRUCTURAL ELEMENT	FINITE ELEMENT [6]
stringer	quadrilateral shell (SHELL 63)
deck	quadrilateral shell (SHELL 63)
stringer-deck connector	flexible link (BEAM 4)
transverse bracing	tension-only spar (LINK 8)
supports	pin constraints

raa.com

2.1.3 Composite action of the cross section

Glulam decks are constructed of panels manufactured of vertically laminated lumber. The panels are placed transverse to supporting beams, and loads act parallel to the wide face of the laminations. The two basic types of glulam decks are non-interconnected decks and doweled decks. Non-interconnected decks have no mechanical connectors between adjacent panels. Doweled decks are interconnected with steel dowels to distribute loads between the panels. In this study only the case of deck without dowels was considered.

In the case of non-interconnected deck, the transfer of longitudinal force through the composite deck, which determines the degree to which the sections behave as a composite, depends on the following factors:

- Condition of the surfaces facing the gap.

  The deck is on the compression side of the composite section. Under gravity loads, negative strains may close the gaps and some portion of the compression force can be generated through bearing between the panels.

- Geometrical position of the panel

  Placement of the stringers assumes high stiffness (E_L) in the longitudinal direction of the bridge. The same direction for the panel, however, is associated with the transverse modulus of elasticity E_T, which is about 1/8 -1/10 of the E_L value.

- Flexural stiffness of the fasteners

raa.com

The amount of composite action exhibited by the glulam stringer - deck section was experimentally studied by Gutkowski et. al. [7] as a function of all the three factors identified above. Ritter [5] suggests there are various types of deck attachments to glulam beams, the most common being aluminum brackets and lag screws. Gutkowski experimentally measured the stiffness of lag screw connections. Depending upon the timber grade, the average stiffness values were 47 kips/in. and 46 kips/in. for southern pine and Douglas fir, respectively. Considering only the case of interest (non-interconnected deck) we can conclude that for the practical stiffness values of the connectors shown above, the amount of composite action is between 0 and 1% depending on the grade of the used timber. The difference between deflection of a specimen with no composite action (the stringers carry all the load) and the deflection of a specimen where the composite contribution of the deck is allowed, was within 1%. Considering that conclusion, it was decided to neglect the composite action entirely and proceed with the model that would allow for no composite action at all.

2.1.4 Finite Element Mesh

For this model, the mesh size was established by considering the following factors:

- Longitudinal dimension of the mesh must be able to accommodate the changing position of a vehicle for dynamic analysis.
- The layout of the mesh of the stringers must enable attachment of the deck.

raa.com

- The non-restrained dimensions of the mesh will be kept to maintain small aspect ratio, yet a reasonable number of elements in terms of computation time will be used. The size of elements in a longitudinal direction of the bridge was then established at 17 in. to match a step of the vehicle.

2.2 Vehicle model

The first chapter briefly discussed the approach to modeling a vehicle for dynamic analysis. This study continues as an ongoing project, and the concept of the model developed and validated by Wijesooriya [8] was adopted for this analysis. Nevertheless, since the research suggests that the vehicle model and parameters have a prominent effect on the response of the bridge, more attention was paid to the vehicle model than in the previous study. The research [2] has shown that the following vehicle parameters are important to the bridge response:

- axle spacing
- suspension parameters
- initial conditions

2.2.1 Vehicle suspensions

2.2.1.1 Steel leaf suspension

It was found that the force-deflection behavior of mechanical steel leaf suspensions that are commonly fitted in commercial vehicles is generally non-linear [9]. The test results

raa.com

indicate that truck leaf springs may exhibit varying levels of effective spring rate in addition to damping, coulomb friction or hysteresis depending upon the loading of the spring and amplitude of the oscillation. The load test and behavior of this type of suspension is thoroughly described in references [9], [10] and [11]. In order to model this behavior, researchers used two approaches to the model. First is a linear spring-damper combined with a coulomb friction element model used by Drosner [12] and Wang [3]. Second is the analytical description developed by Francher [11], and used by Nowak [13] and Green et. al. [14]. The model accounts for nonlinearity of the spring rate, which is typically exhibited by multi-leaf rear springs.

2.2.1.2 Air suspensions

The air suspensions, sometimes also referred to as "road friendly" suspensions, were developed in attempt to reduce damage afforded to infrastructure and cargo. These suspensions display linear behavior with a natural frequency of about 2 Hz, and damping greater than 20%. Hardy and Cebon [15] modeled this type of suspension with a linear spring/viscous damper model.

It has been recognized that air sprung vehicles usually apply smaller dynamic loads to the bridge, and produce smaller dynamic amplification compared to the steel suspensions. The bridge response is less dependent upon speed [14], [16]. The frequencies of the body bounce modes of vibration in vehicles fitted with air suspensions are also lower than the frequencies of steel suspension fitted vehicles. It is the opinion of the author that the higher (axle related) frequencies are the same regardless of the vehicle suspension.

raa.com

2.2.2 Finite element model

In the model shown in Fig. 2.2a, the largest portion of the vehicle mass is attributed to the rigid chassis, and is represented by mass M1 (MASS 21). Masses M2, M3, and M4 are associated with the axles. Suspension of the front axle and the common suspension of the rear tandem and tires are modeled by linear spring-damper elements (COMBIN 14). These elements are connected with rigid links (BEAM 4). With regard to the previous discussion it is apparent that the vehicle is representative of one fitted with the air suspension.

Based on the previous research [13], [14] and [15], the values of stiffnesses associated with the suspensions and tires were assumed to be 7 and 14 kips/in./axle for the front and rear suspensions, and 20 kips/in./axle for tires. To validate the model and justify these values, two sensitivity studies were considered:

- mode shape analysis of the vehicle to determine its mode frequencies
- transient analysis of the vehicle subjected to an impact load

The criteria used to validate the model were frequencies exhibited by the vehicle.

2.3.2 Model validation

2.3.2.1 Modal analysis

It was found that heavy commercial vehicles exhibit two vibration modes: body bounce vibration at frequencies ranging from 2 - 5 Hz, and wheel hop vibration at

raa.com

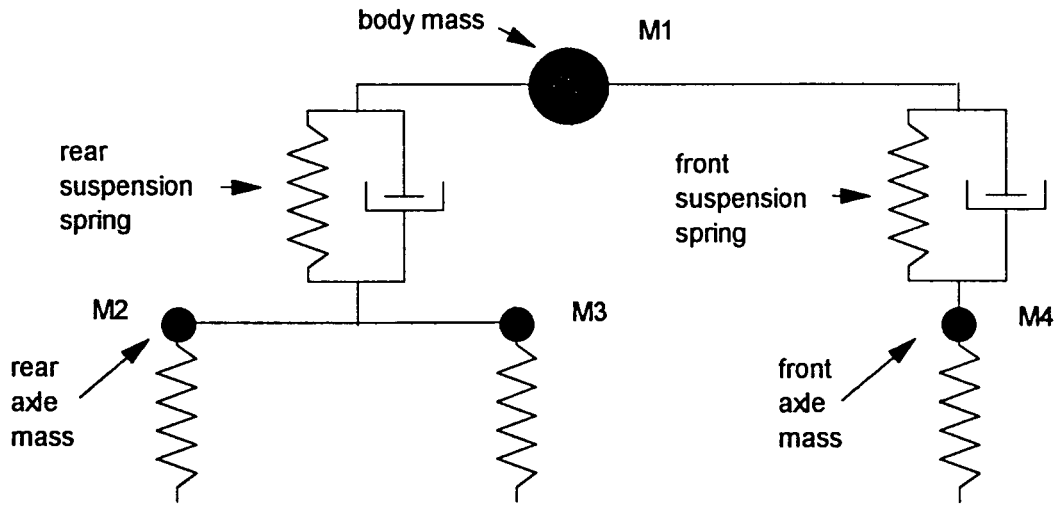

a) Model of the vehicle

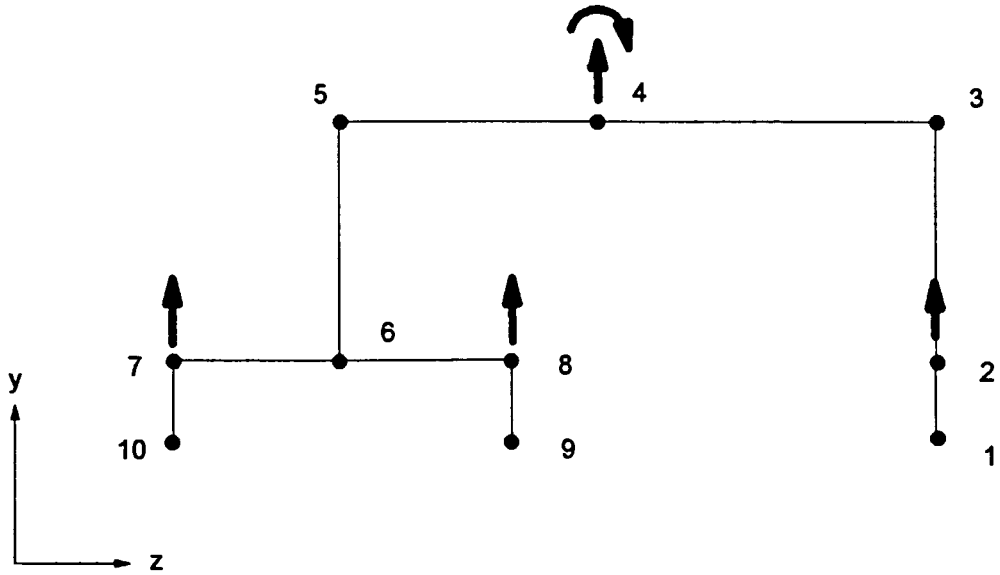

b) node numbering and master degrees of freedom

Fig. 2.2 Finite element model of the vehicle

nanaraa.co

frequencies greater than 7 Hz and typically around 15 Hz [14], [16]. For case of the air suspension, the vibration mode associated with the body is typically lower than 2 Hz.

Two sets of values for suspension and tire stiffness were considered for the purpose of the analysis; they appear in Table 2.2. The vehicle was assumed to have five degrees of freedom, as shown in Fig. 2.2b. The summary of mode frequencies appears in Table 2.2 and the respective mode shapes appear in Figs. 2.3. The first two modes are associated with the vehicle's body (body bounce and body pitch) and the other three modes describe action of the wheels (pitch and bounce). The literature often refers to the axle bounce modes as "axle hop". It can be concluded that, for the set of values selected for the analysis (set 1), both of the frequencies associated with the body and with the axles satisfy the assumptions for an air suspended vehicle. The frequencies determined for the other set, especially those associated with the wheels, are rather high.

2.3.2.2 Transient analysis

According to Green [14], an air sprung vehicle riding on rigid pavement imposes wheel forces with a frequency of less than 2 Hz. The transient analysis was conducted to validate this feature of the model. In lieu of analysis of the vehicle riding on a rough surface an impact of the magnitude of one-half of the weight of the truck was suddenly applied to the center of gravity of the vehicle for the time of 1 sec. and was then suddenly removed. Free vibration of one of the rear axles and of a point directly above the suspension were monitored for another two seconds (see nodes 8 and 5, respectively, in Fig. 2.2a).

ıanaraa.co

Table 2.2 Vehicle modal shape analysis results

Vehicle parameters	Units	Set 1	Set 2
Front suspension stiffness	K/in./axle	7	10
Rear suspension stiffness	K/in./axle	14	20
Coefficient of suspension damping	K-sec/in.	0.05	0.05
Tire stiffness	K/in./axle	20	30
Mass of the chassis	K-sec^2/in.	0.115	0.115
Axle mass	K-sec^2/in.	0.002	0.002
Modal shape frequencies			
1st mode shape - body bounce	Hz	1.7	2.0
2nd mode shape - body pitch	Hz	3.1	3.7
3rd mode shape - axle pitch	Hz	15.9	19.5
4th mode shape - axle hop	Hz	18.5	22.5
5th mode shape - axle hop	Hz	18.6	22.6

ıanaraa.cc

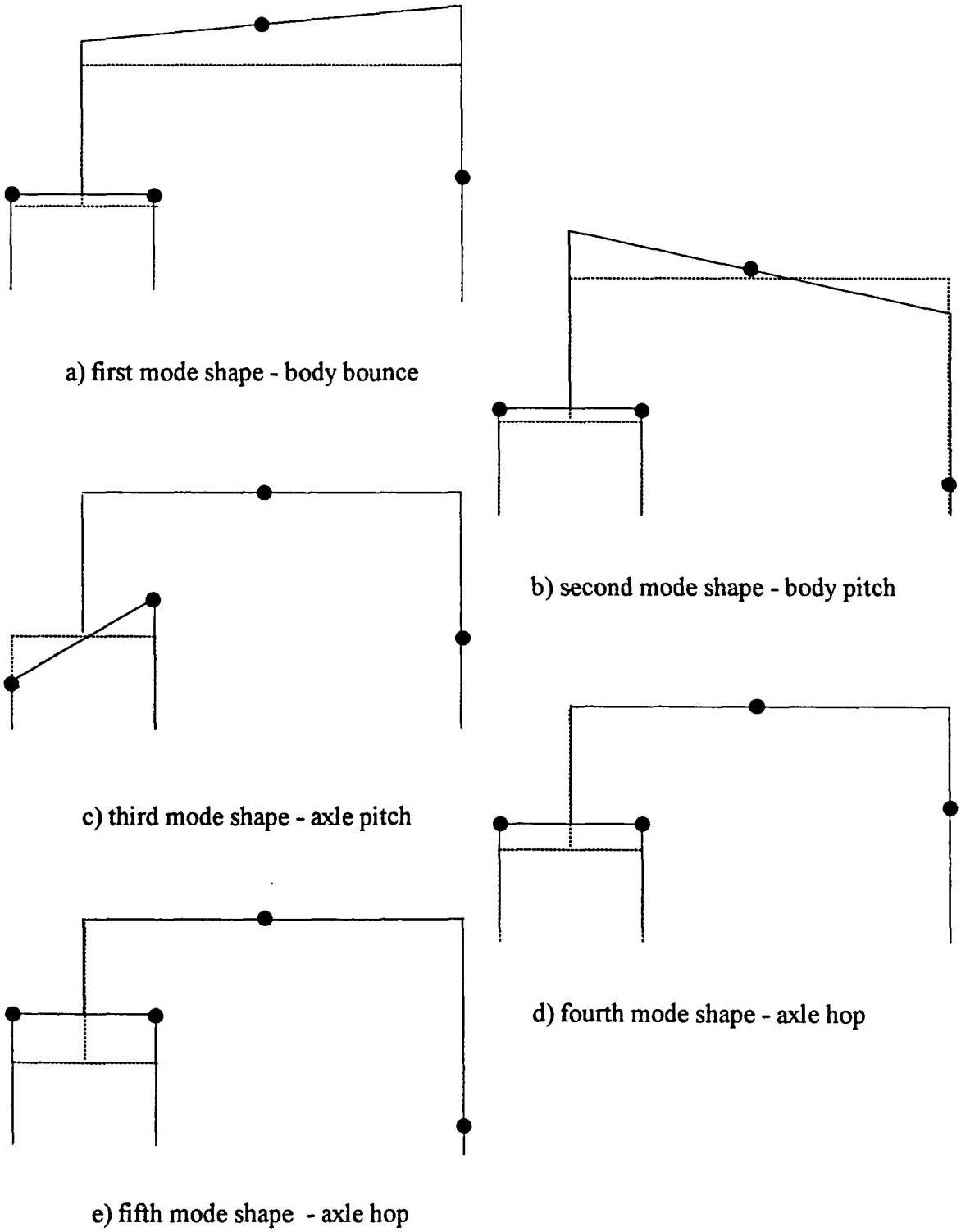

Fig. 2.3 Modal shapes of the vehicle

ıanaraa.co

The time history plots of accelerations and frequency content plots are presented in Figs. 2.4 through and 2.7. The time history plots show only the free vibration parts of the response. The results correspond to observations from field tests made by Green [14] and Heywood [16], and provide evidence that frequency of the dynamic loads exerted by the wheels occur in the frequency of about 1.6 Hz and 3.1 Hz (Fig. 2.5 and 2.7), which corresponds to the first (body bounce) and second (body pitch) modes of the vehicle. The frequency of the axle hop was observed to be 18 Hz (Fig. 2.7). These frequencies also well correspond to the results of the mode analysis presented in Table 2.2 Hence both of the studies confirm the validity of the vehicle model.

2.3 Vehicle/bridge interaction model

2.3.1 General

In the past, researchers have been trying to determine the most important factors that influence the dynamic response of a bridge subjected to moving vehicular forces and have concluded that the most important ones are:

- Bridge natural frequency.
- Speed of the vehicle.
- Roadway roughness.
- Approach to the bridge (bump).

ıanaraa.co

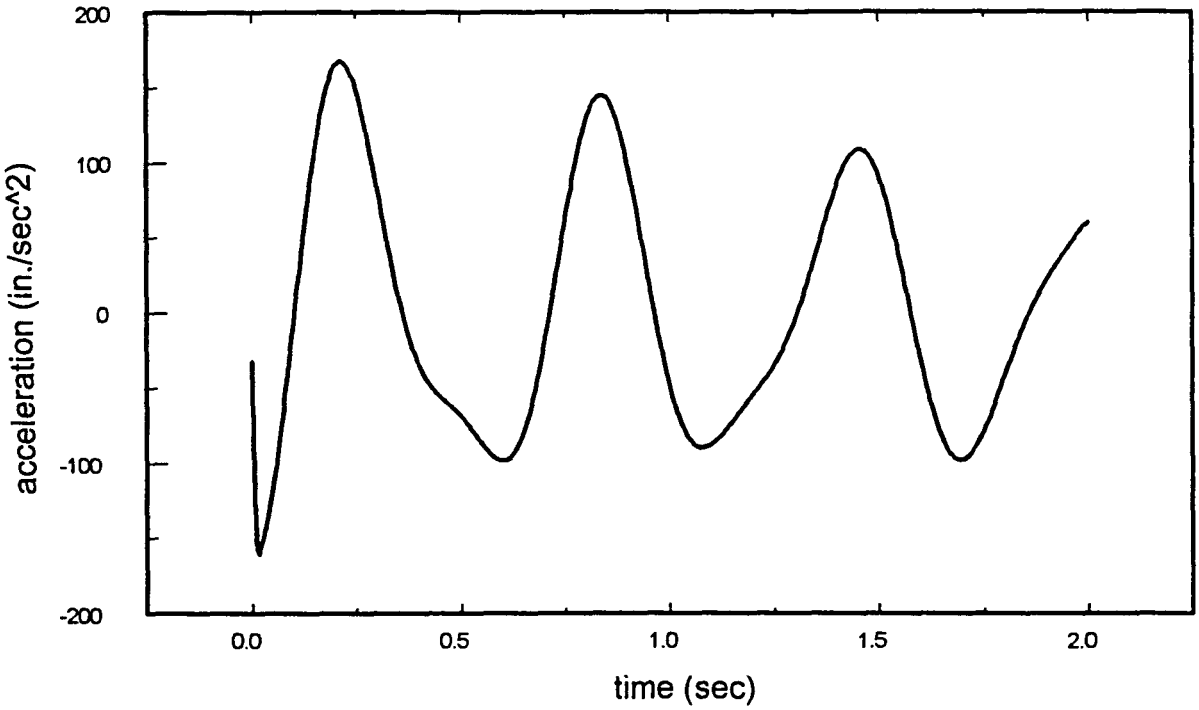

Fig. 2.4 Vehicle acceleration at node 5

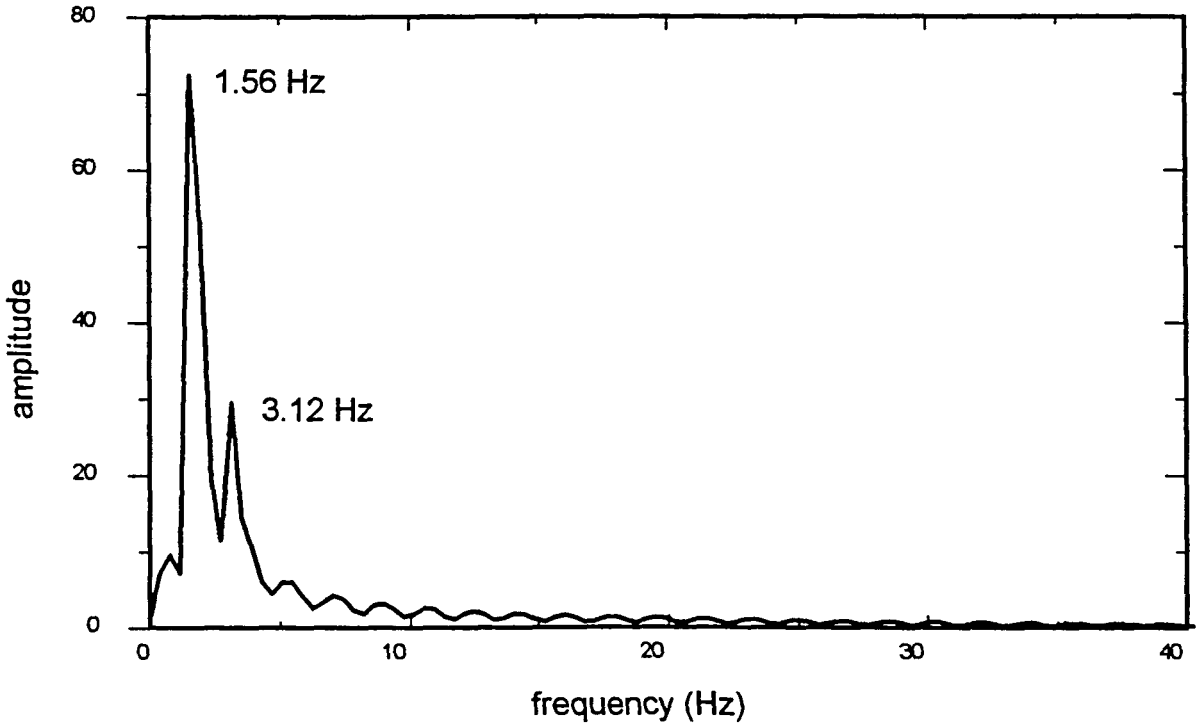

Fig. 2.5 Vehicle frequency content at node 5

hanaraa.co

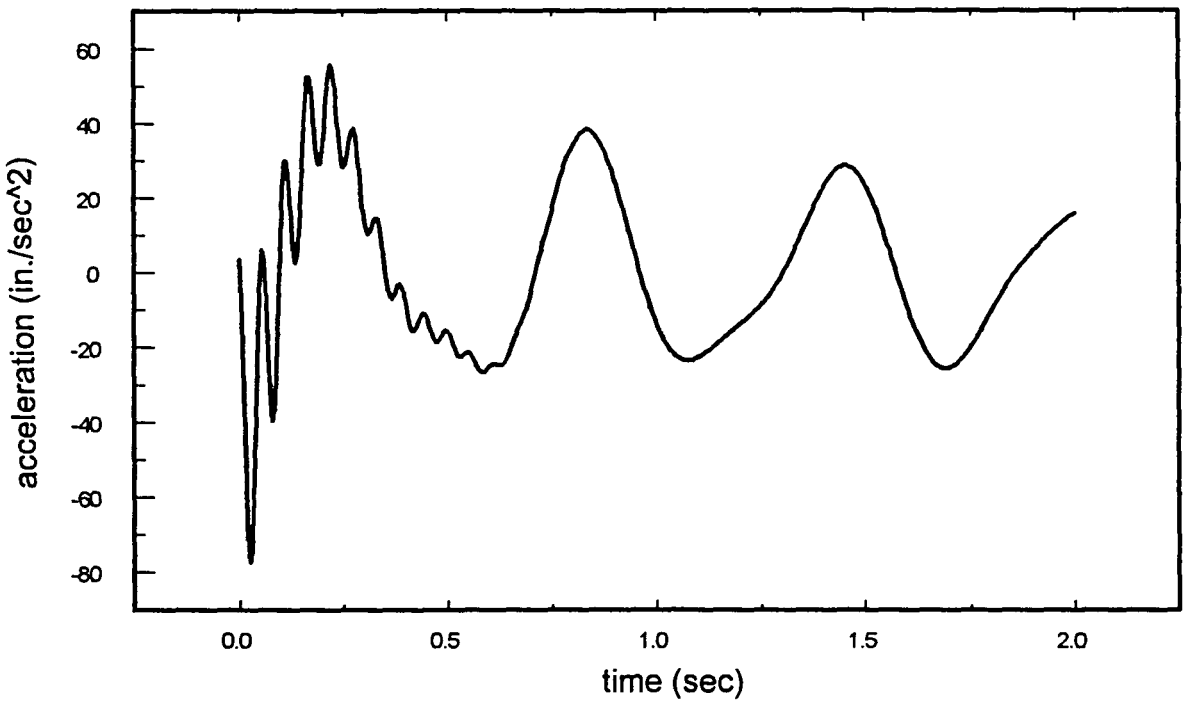

Fig. 2.6 Vehicle acceleration at node 8

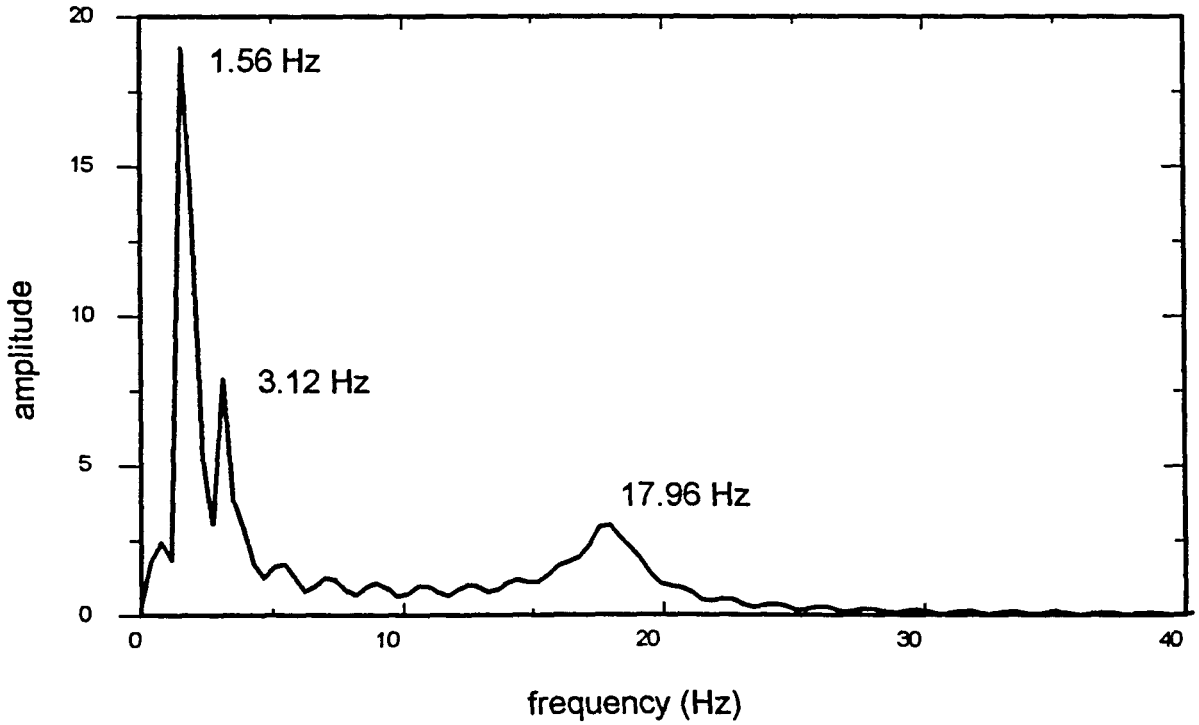

Fig. 2.7 Vehicle frequency content at node 8

hanaraa.co

2.3.2 Dynamic Amplification Factor

The dynamic character of the response of bridges to traffic is presently well established. A moving vehicle on a bridge generates deflections and stresses that are generally greater than those caused when the same vehicle loads are applied statically. The dynamic amplification (DA) resulting from the passage of vehicle on a specific bridge is defined as:

$$DA = \frac{\delta_{dyn} + \delta_{stat}}{\delta_{dyn}} \qquad \frac{\delta_{dyn} - \delta_{stat}}{\delta_{stat}}$$

The dynamic amplification factor (DAF) used herein to quantify comparison between different bridges is defined as:

$$DAF = 1 + DA$$

where:

δ_{dyn} = Maximum deflection under the vehicle traveling at normal speed

δ_{stat} = Maximum deflection under the vehicle traveling at crawling speed

DAF = Dynamic amplification factor

This definition is consistent with most recently published work [2], [14], [16], etc., and allows for direct comparison of results and findings. The maximum deflection under a vehicle traveling at crawling speed is usually very close to the static value. The published

hanaraa.co

research [2], [13], [14], [15], [16], [17] also agrees on some factors that influence the DAF, which can be summarized as follows:

- The maximum dynamic amplification occurs when the dynamic component of a load varies at the bridge's first natural frequency. Therefore some national codes (Canada, Switzerland) increase the dynamic allowance for bridges with natural frequencies between 2 - 5 Hz. Heywood [16] points out that similar dynamic coupling with the wheel frequencies may occur for bridges with high natural frequencies.
- Large amplification occurs when the maximum response due to succeeding axles coincide.
- The maximum response (DAF, max) is not affected by damping.
- The dynamic factor is smaller for two vehicles than for one.
- The heavier the weight carried by a vehicle, the lower the impact factors are

Some of these findings will be addressed in the sensitivity study presented in the subsequent chapter.

ıanaraa.co

2.3.3 Bridge/vehicle interaction model

The differential equation of motion defining the bridge/vehicle interaction is:

$$[M]\{\ddot{x}\} + [C]\{\dot{x}\} + [K]\{x\} = \{F\},$$

where [M],[C] and [K] are the known mass, damping and stiffness matrices of the bridge, respectively. {F} is the vector of dynamic excitation and {x} is the vector of the sought nodal displacements. The solution is obtained under the following assumptions:

- The vehicle travels at a constant speed.
- All the components move with the same velocity in a longitudinal direction.
- Each tire contacts the roadway at a single point.
- Force inputs are limited to the vertical direction.
- The structural damping of the bridge is assumed 5% of critical.

The solution for the displacement {x} was also developed and validated by Wijesooriya [8], and will not be discussed here.

ıanaraa.co

3. SENSITIVITY STUDY

3.1 General

The main objective of this chapter is to investigate the behavior of the model and its sensitivity to parameters as identified in Chapter 2. Models of two bridges were selected to carry out this investigation. These bridges were carefully chosen to be representative of bridges with different structural characteristics. The first bridge is a 40 ft. long, two lane, five stringer bridge. The other is a 30 ft., one lane, four stringer bridge. For the purpose of the following discussion, they will be referred to as Bridge 1 and Bridge 2, respectively.

With regard to transverse stiffness, Bridge 1 is rather flexible compared to Bridge 2. Although both bridges have a deck of the same depth (5 in.), the stringers of Bridge 1 are farther apart (60 in. compared to 51 in. for Bridge 2); thus, Bridge 1 is more flexible. Also, the transverse stiffeners of Bridge 1 are twice as rigid as those of Bridge 2. A summary of the relevant structural bridge parameters appears in Table 3.1. The vehicle parameters conform to Set 1 in Table 2.2.

ıanaraa.co

Table 3.1 Bridge parameters in sensitivity study

Bridge parameters	Units	Bridge 1	Bridge 2
Length	in.	501	366
Width	in.	288	190
Number of stringers	-	5	4
Stringer spacing	in.	60	51
Stringer dimensions (depth, width)	in., in.	41 1/4 x 6 5/8	31 5/8 x 5
Deck thickness	in.	5	5
Longitudinal Modulus E_L	Ksi	1830	1830
Transverse Modulus E_T	Ksi	180	180
Shear Modulus G_{LT}	Ksi	100	100
Density	pcf	50	50
Structural damping	% crit.	5	5

ıanaraa.cc

3.2 Mode frequency analysis

Mode frequencies are elementary dynamic characteristics of a bridge. In the second chapter it was mentioned that when the first mode frequency matches the vehicle body bounce or axle hop frequencies, large dynamic amplifications may occur. The first mode shape of Bridge 2 is longitudinal because of its transverse rigidity. In transversely flexible Bridge 1 the first mode shape is transverse and non-symmetrical. The first eight mode shapes of Bridge 1 appear in Fig. 3.1 and are summarized in Table 3.2.

The first mode shape (Fig. 3.1a) is transverse, where the stringers have deflected in a half-sine wave shape. The deflection is maximum for the outside stringers (positive for one and negative for the other) and zero for the middle one at any section. The second shape (Fig. 3.1b) is the first longitudinal one, where all the stringers underwent the same deflection in a transverse direction. The third shape (Fig. 3.1c) is a transverse shape similar to the first one, except both the outside stringers underwent downward deflection and the middle stringers underwent upward deflection. The transverse deflection of the section is no longer linear. In the fourth shape (Fig. 3.1d), the outside stringers already exhibit full sine-wave deflection and the transverse deflection of the section is linear. The fifth shape (Fig. 3.1e) is the second longitudinal one and all the stringers underwent the same full sine-wave deflection. In the sixth shape (Fig. 3.1f), the stringers have deflected in a half sine wave shape, and the section has transversely deflected in full sine wave. The seventh (Fig 3.1g) shape is similar to the fourth one, except the outside stringers underwent the same

ıanaraa.cc

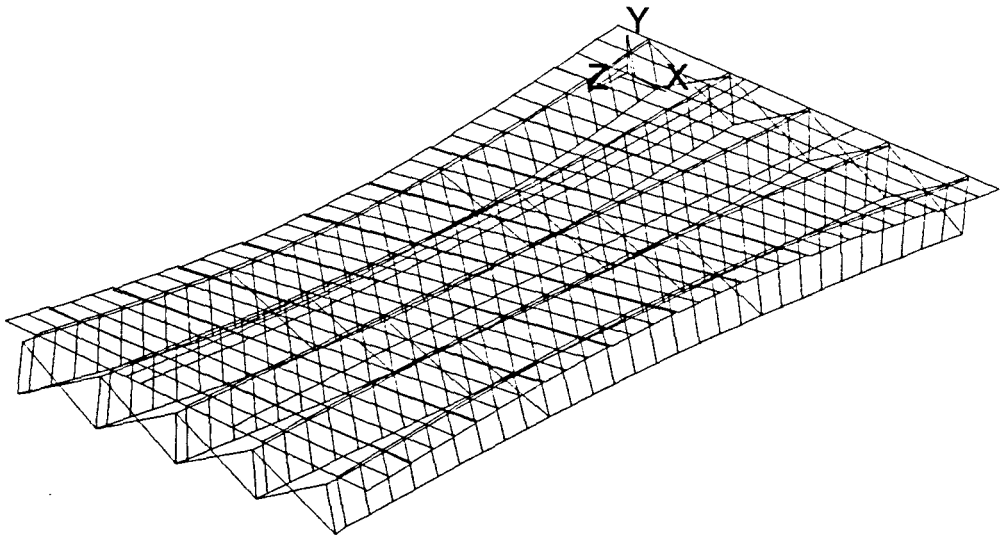

a) First mode shape, f = 7.4 Hz

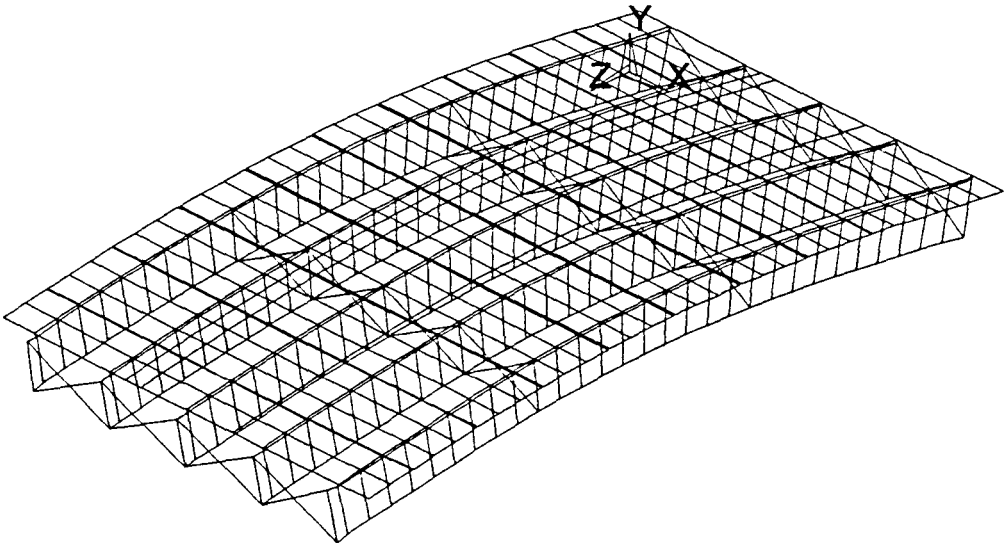

b) Second mode shape, f = 7.5 Hz

Fig. 3.1 Full model mode shapes

hanaraa.co

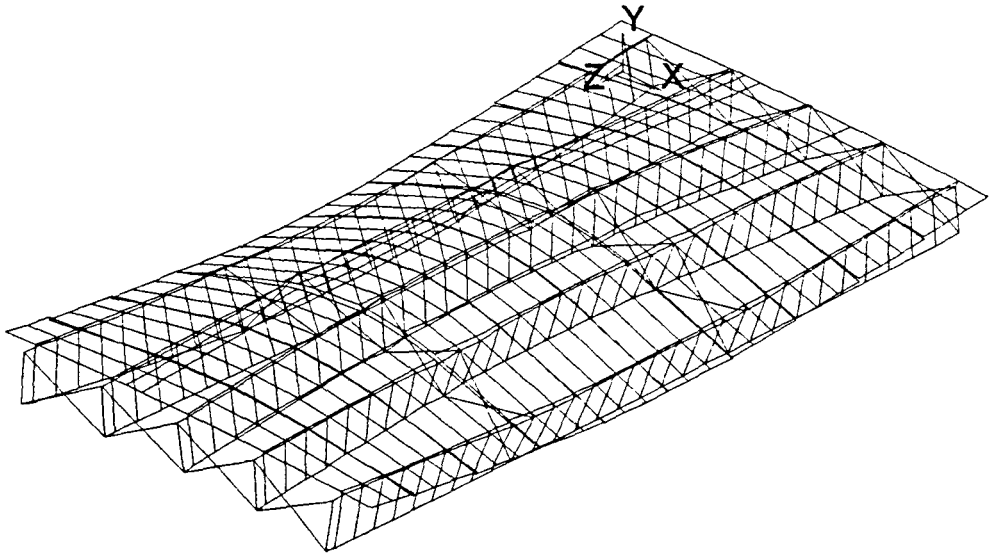

c) Third mode shape, f = 13.9 Hz

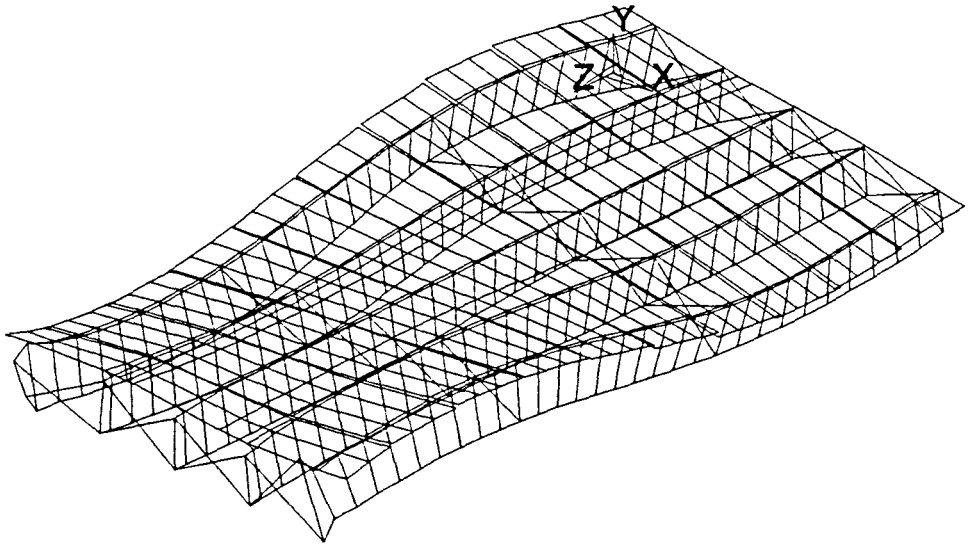

d) Fourth mode shape, f = 24.7 Hz

Fig. 3.1 (continued)

ıanaraa.co

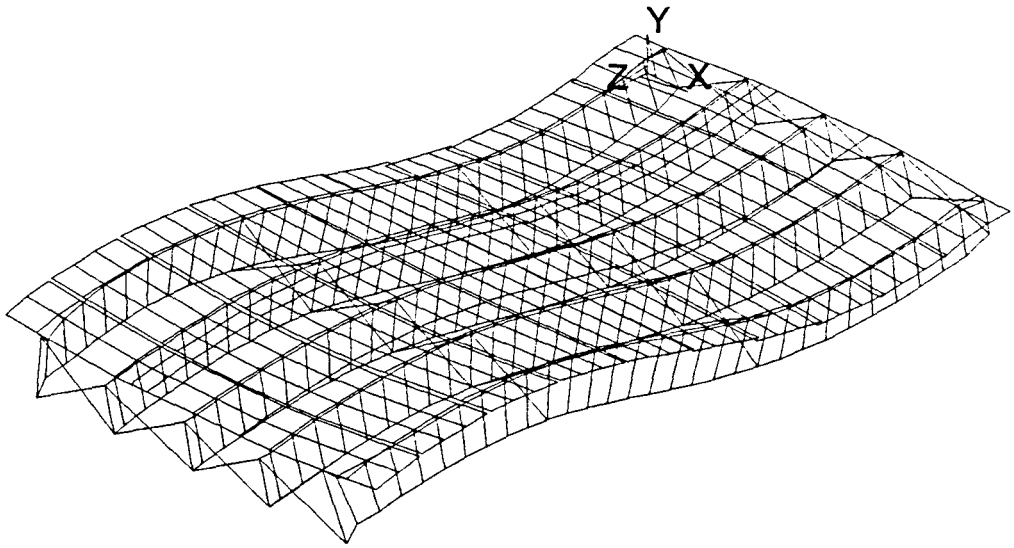

e) Fifth mode shape, f = 25.6 Hz

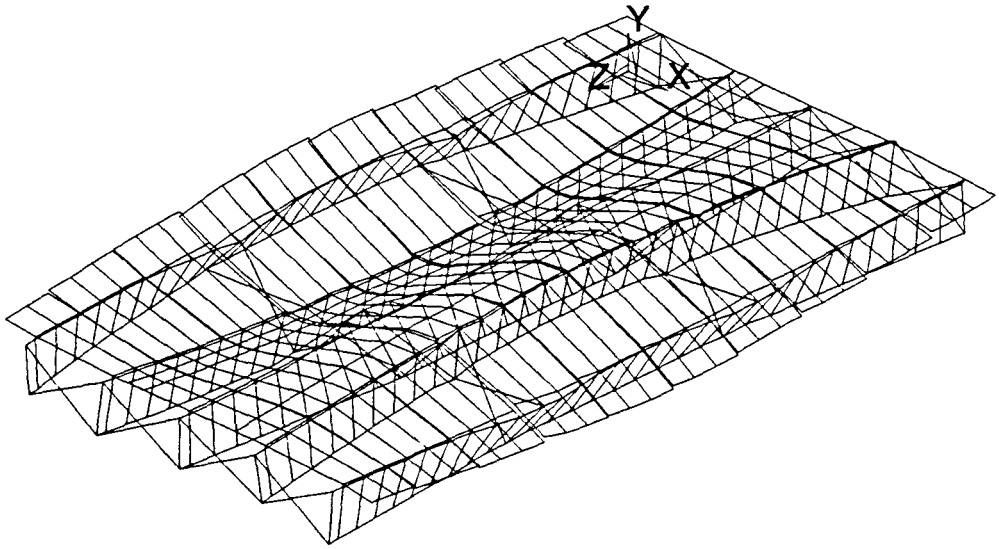

f) Sixth mode shape, f = 27.6 Hz

Fig. 3.1 (continued)

nanaraa.co

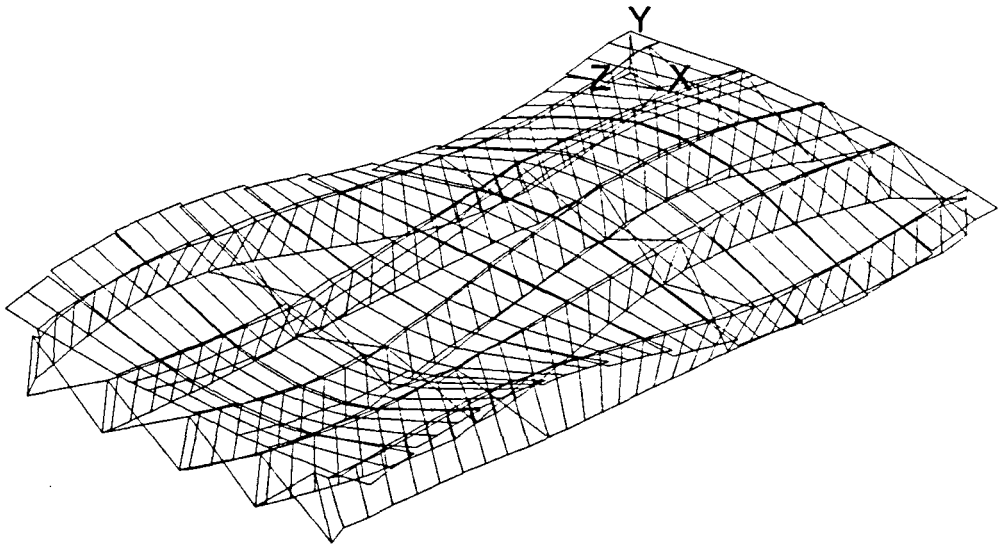

g) Seventh mode shape, f = 28.5 Hz

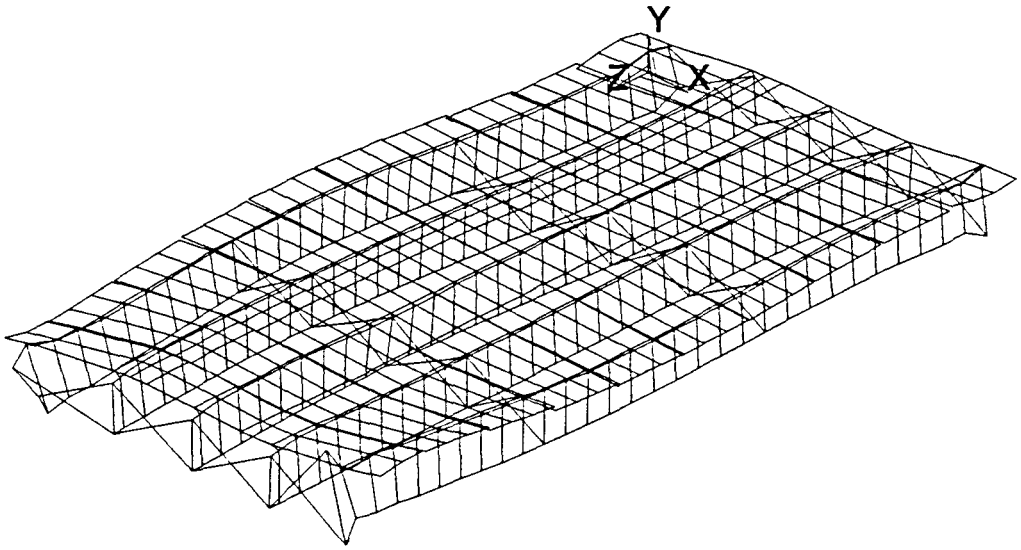

h) Eighth mode shape, f = 32.7 Hz

Fig. 3.1 (continued)

ıanaraa.co

Table 3.2 Summary of the modal shape analysis results

	Bridge 1		Bridge 2	
Mode	Frequency [Hz]	Shape	Frequency [Hz]	Shape
1	7.4	transverse	9.8	longitudinal
2	7.5	longitudinal	10.1	transverse
3	13.9	transverse	30.9	transverse
4	24.7	transverse	33.1	transverse
5	25.6	longitudinal	33.3	longitudinal
6	27.3	transverse	41.4	transverse
7	28.5	transverse	46.1	transverse
8	32.7	transverse	64.3	longitudinal

The vehicle mode frequencies appear in Table 2.2.

ıanaraa.co

(downward) deflection, opposite to the middle one. The eight shape is again a transverse one, where the stringers exhibit one and a half sine wave deflection.

The frequencies of the first longitudinal modes from the computer analysis were also compared to a hand calculation utilizing a formula for a simply supported beam with distributed properties:

$$f=\frac{\pi}{2l^2}\sqrt{\frac{EI}{m}}$$

The results produced by the formula agreed with the ANSYS computation results within a 10% degree. When compared with Paultre [2], there is an agreement. For the hand calculation, the stiffness of the stringers was assumed to contribute toward the longitudinal stiffness of the bridge. Any effect of the deck was ignored.

The effect of the finite element mesh coarseness on the mode frequency response was also investigated. The standard model of Bridge 1 was compared to a model with a finer mesh of the stringers (every finite element of the standard mesh was further horizontally divided into three elements). The differences were smaller than 2% and provided evidence that a finer mesh would not significantly improve the model. The values are also included in Table 3.2.

ıanaraa.co

3.3 Transient analysis

3.3.1 General

The objective of the time history analysis was to investigate how the following parameters influence the model's dynamic response:

- Vehicle speed
- Initial conditions of the vehicle
- Structural damping of the bridge
- Axle spacing of the vehicle

In order to simplify the comparison, the parameters of interest were varied. The response was compared to the standard conditions of the model. The summary of these standard conditions was already presented in Table 3.1.

3.3.2 Vehicle speed

Because timber stringer bridges are commonly found on county roads and lower grade highways, a spectrum of speeds between 15 and 45 mph was considered. The results for both bridges in terms of DAF are shown in Fig. 3.2 and Table 3.3. For Bridge 1, four time - deflection plots of static and dynamic displacements for speeds of 15, 25, 35, and 45 mph, respectively, are presented in Figs 3.3a, 3.4a, 3.5a and 3.6a. It is apparent that the response changes with velocity. A large amplitude of vibration can be noted for the speed

hanaraa.co

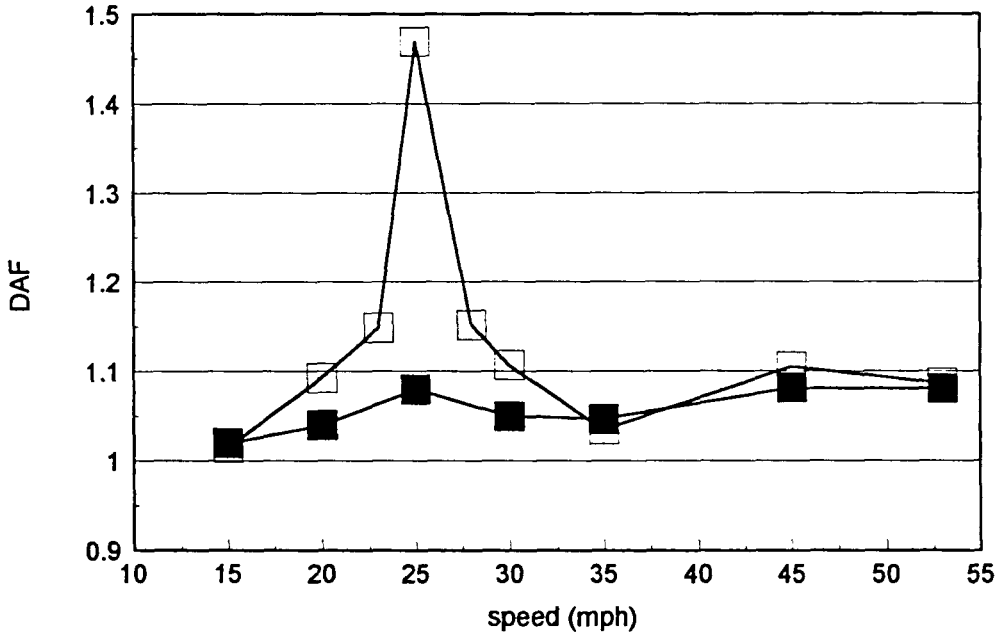

a) Bridge 1

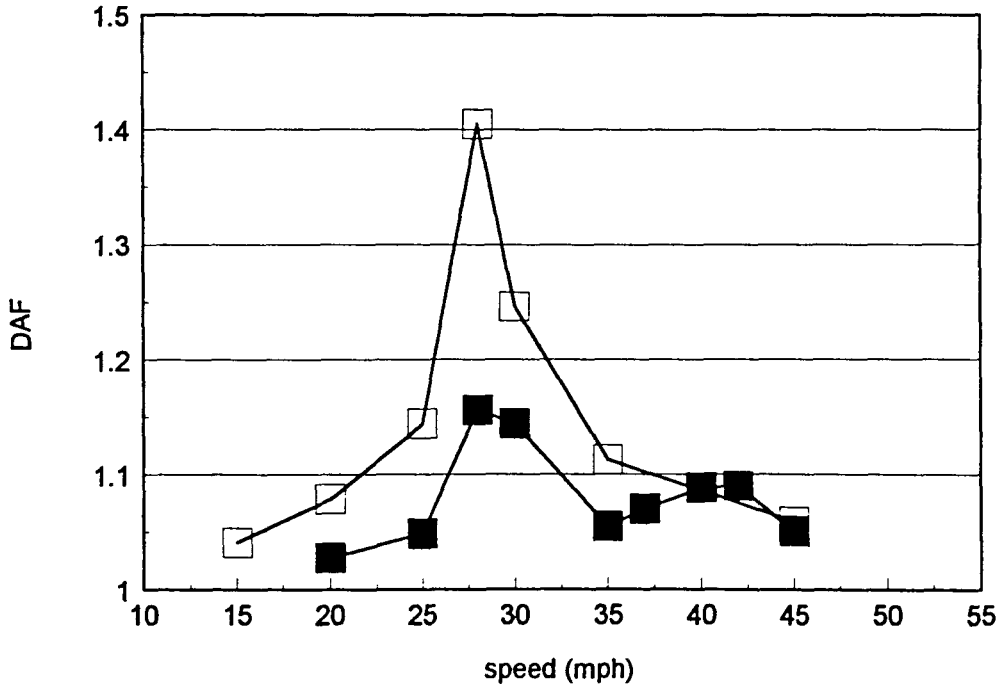

b) Bridge 2

Fig. 3.2 DAF plots for Bridge 1 and Bridge 2

nanaraa.co

Table 3.3 Summary of DAF for the sensitivity study

	BRIDGE 1		BRIDGE 2		
SPEED	SMOOTH	BUMP	SMOOTH	BUMP	AXLE (*)
15	1. 02	1.02	N/A	1.04	N/A
20	1.04	1.09	1.03	1.08	N/A
23	N/A	1.15	N/A	N/A	N/A
25	1.08	1.47	1.05	1.14	1.05
28	N/A	1.15	1.16	1.41	1.10
30	1.05	1.11	1.14	1.25	1.09
35	1.05	1.04	1.06	1.11	1.07
37	N/A	N/A	1.07	N/A	1.09
40	N/A	N/A	1.09	N/A	1.10
42	N/A	N/A	1.09	N/A	1.09
45	1.08	1.11	1.05	1.06	1.07
53	1.08	1.09	N/A	N/A	N/A

* = Vehicle with longer axle spacing

nanaraa.co

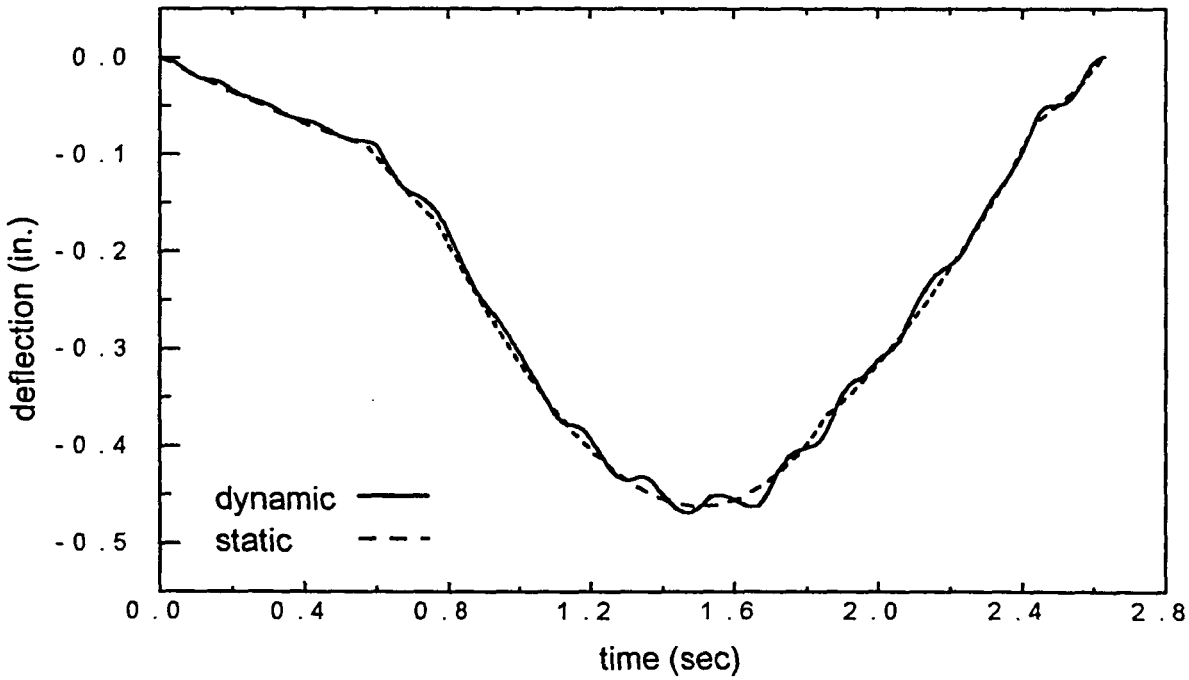

a) response for smooth entry

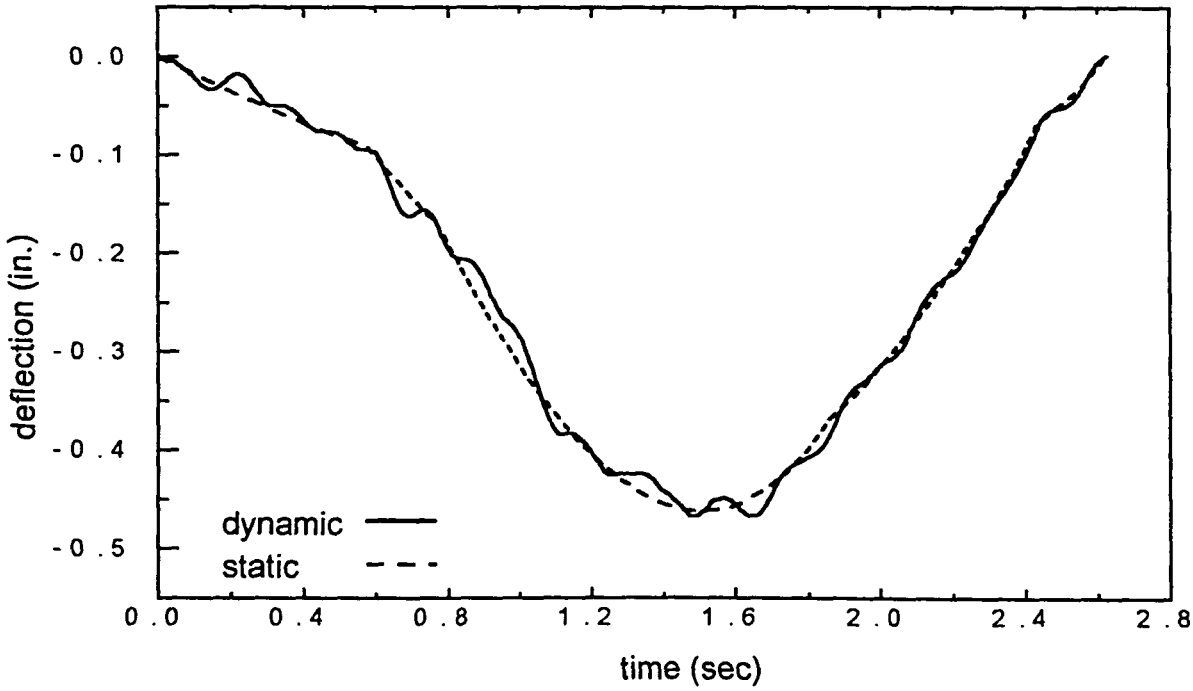

b) response for bump entry

Fig. 3.3 Bridge 1 response for 15 mph

nanaraa.co

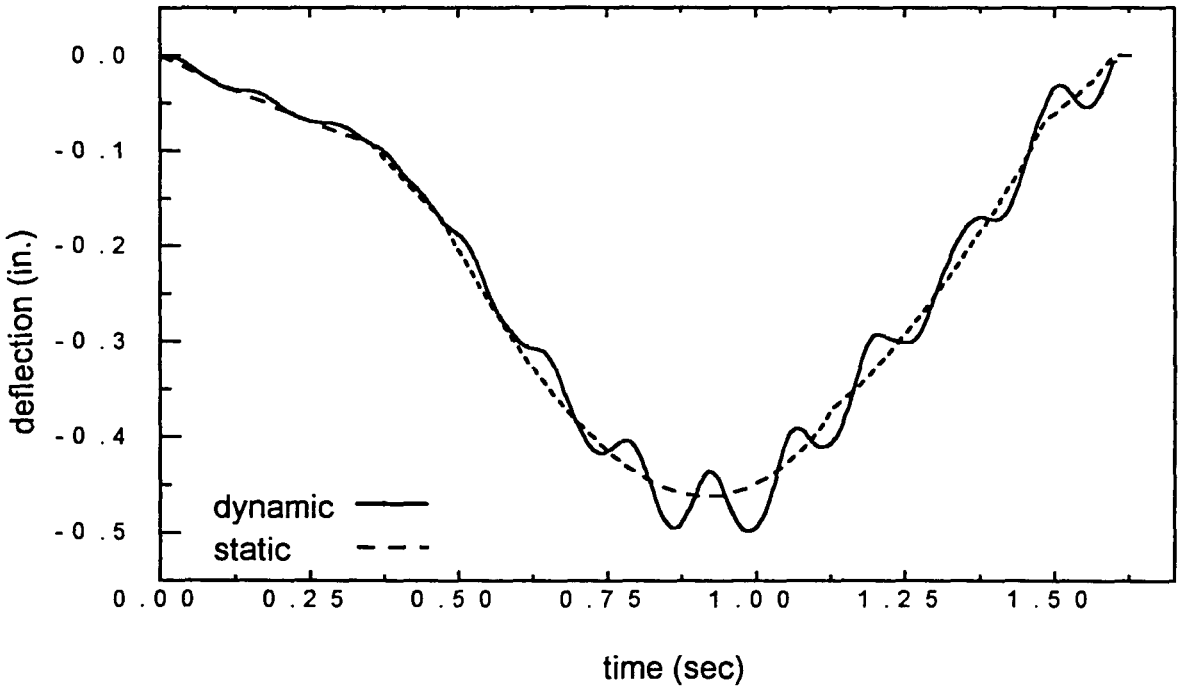

a) response for smooth entry

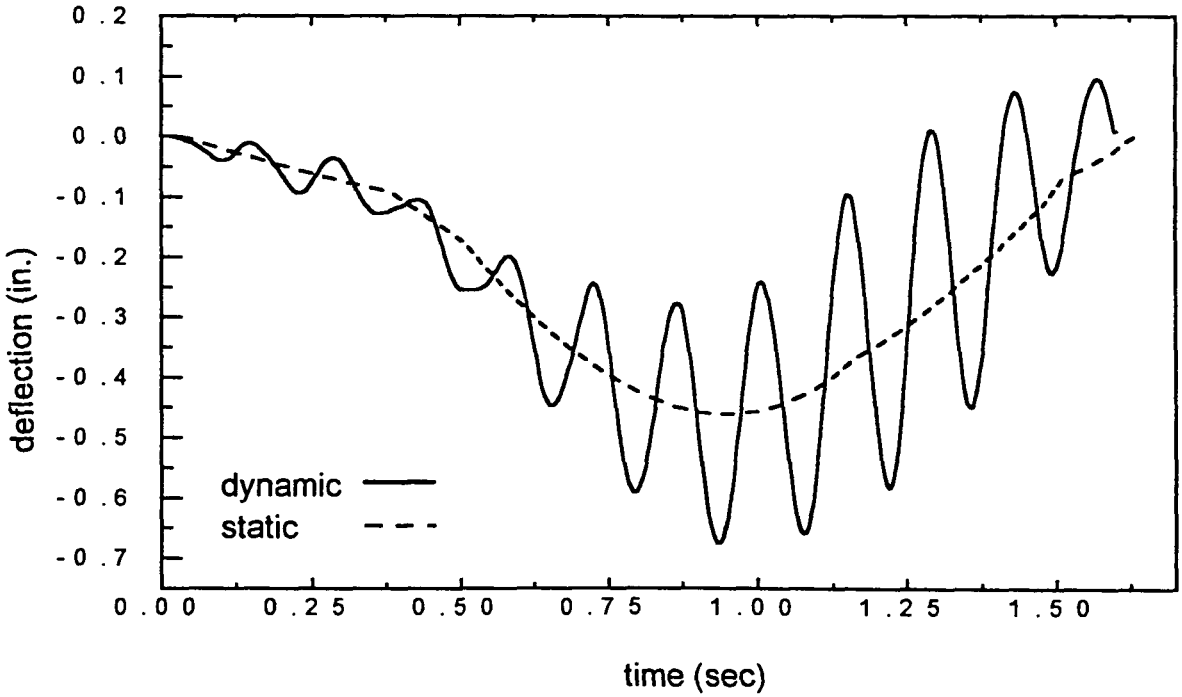

b) response for bump entry

Fig. 3.4 Bridge 1 response for 25 mph

nanaraa.co

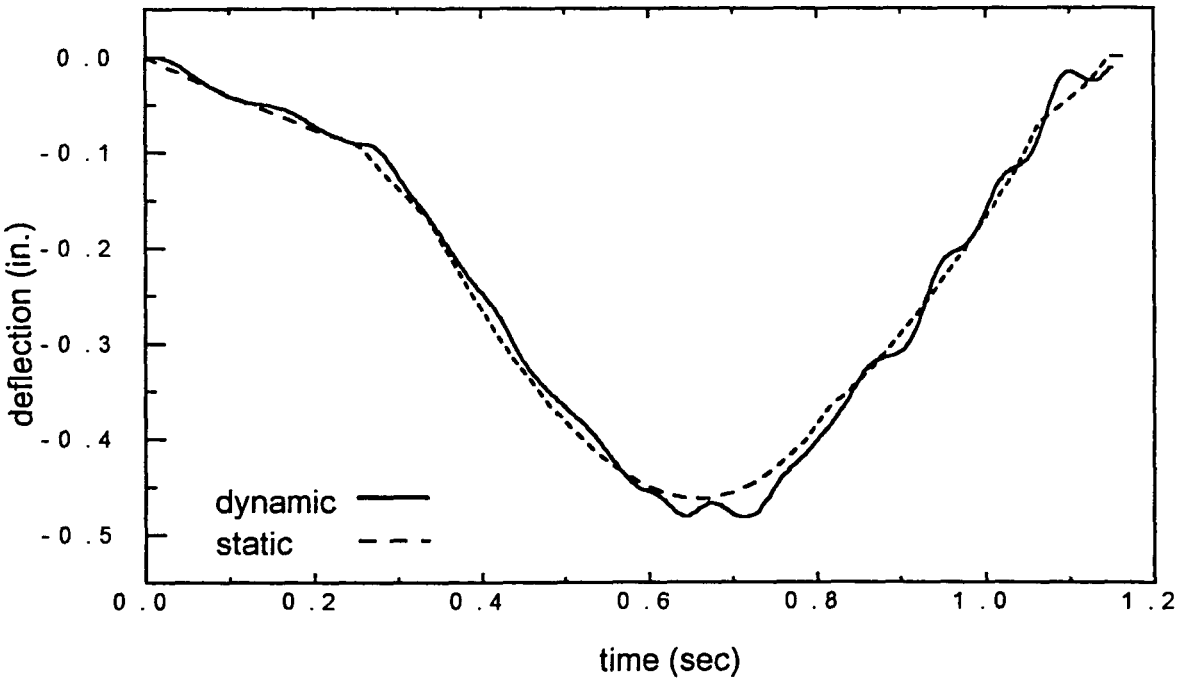

a) response for smooth entry

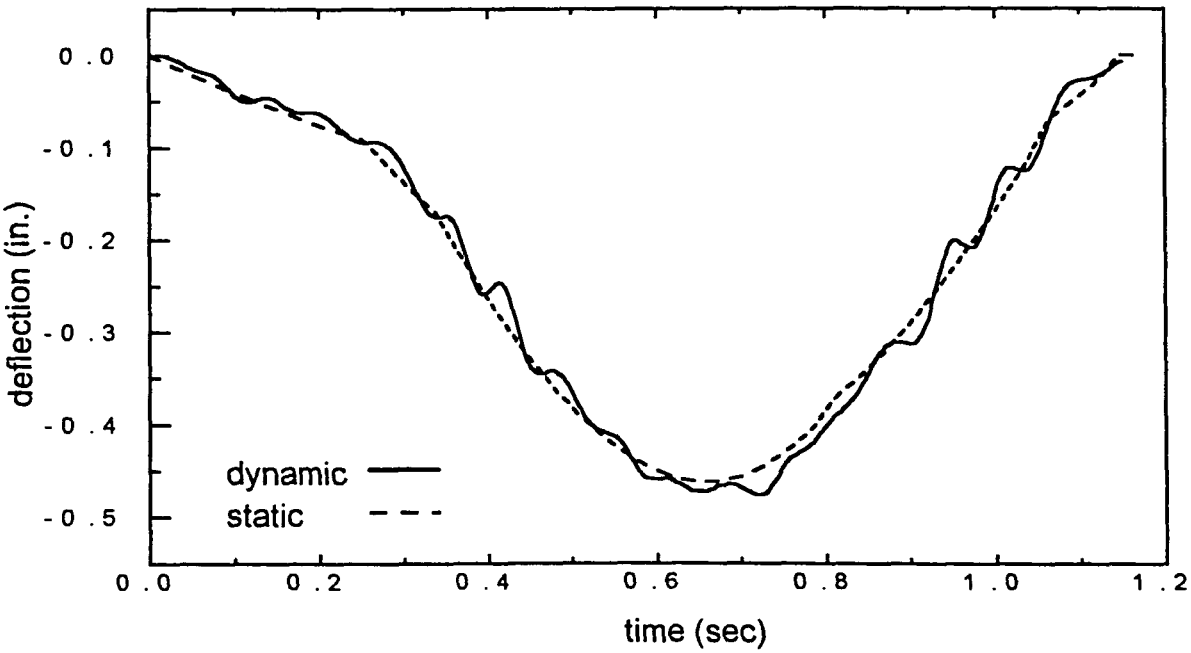

b) response for bump entry

Fig. 3.5 Bridge 1 response for 35 mph

nanaraa.co

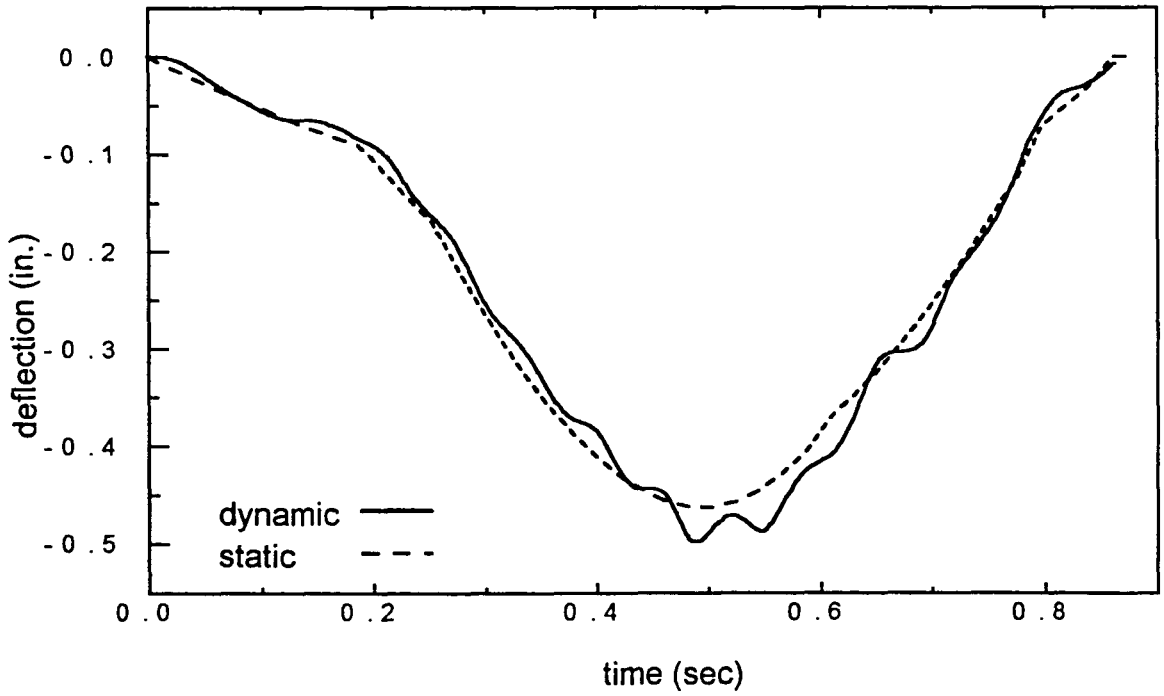

a) response for smooth entry

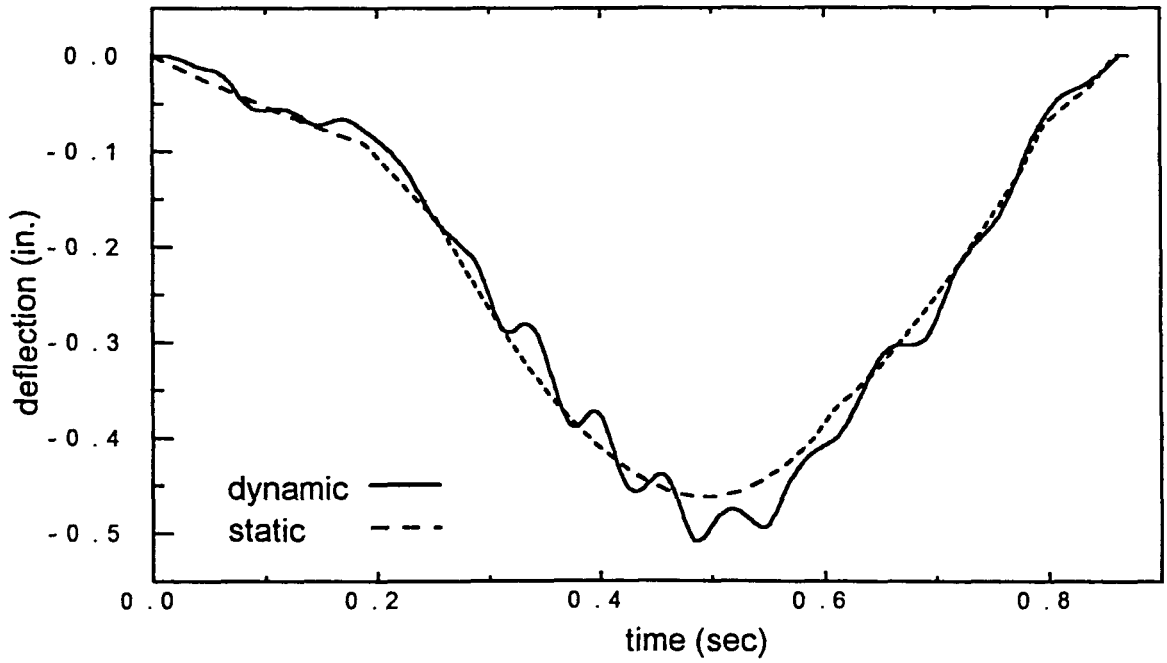

b) response for bump entry

Fig. 3.6 Bridge 1 response for 45 mph

nanaraa.co

of 25 mph. The dynamic amplification is high (1.47) at this speed and decreases afterwards. The dynamic amplification increases again for speeds greater than 35 mph.

3.3.3 Vehicle initial conditions

A 4 in. long and 1.5 in. high artificial bump placed at the entrance to the bridge was included in the model to excite vehicle vibration before it enters the bridge. The path of the tire riding over the bump was modeled as follows. The tire climbs on and off the bump gradually and follows a straight line path. The horizontal length of the ascending part of the tire path is 1.5 in. The next 1 in. the tire follows a horizontal straight line path on the top of the bump and then descents for another 1.5 in. The use of the bump to account for pavement irregularities is common in both analytical and experimental studies. Bakht and Pinjarkar [4] note, however, that this case may produce overestimated results if the bridge and approach pavement are well maintained. The results for both bridges in terms of DAF are shown in Fig. 3.2 and Table 3.3 and time deflection plots for Bridge 1 are shown in Figs. 3.3b, 3.4b, 3.5b and 3.6b. It is shown, that for a given bridge/vehicle system, there exists a critical speed at which the response is amplified for a bump condition. Although the amplification for this speed is very high (DAF = 1.47 for Bridge 1), the speed range for the high amplification is very narrow (the DAF drops to 1.18 at speeds which are higher or lower by as little as 3 mph). The response of the bridge for speeds other than the critical ones does not seem to be influenced by the bump to a significant degree for the same

nanaraa.co

bridge. For Bridge 2 (see Fig. 3.2b), however, the difference is apparent for a wider range of speeds.

3.3.4 Analysis in frequency domain

To obtain a more in-depth understanding of the behavior at the critical speed, a detailed analysis in time and frequency domain was carried out for both bridges. Since the produced results were similar, only the case of Bridge 1 will be discussed. Three points on the bridge and three points on the vehicle were monitored (Fig. 3.7). Those for the bridge are:

point 1 - midspan, at the bottom of the middle stringer

point 2 - midspan, at the bottom of the most external stringer

point 3 - quarterspan, at the bottom of the middle stringer

Those for the vehicle are (Fig 3.7):

point 1 - the center of the body mass

point 2 - directly above the rear suspension

point 3 - first axle of the rear tandem

Barton et. al. [18] notes that most of the mode shapes can be identified with this layout of accelerometers. For each of the speeds, there are two cases (smooth and bump vehicle entry). For each of the two cases, there are three time-deflection plots for the bridge points, six time acceleration plots for the bridge and vehicle points and six frequency content plots

nanaraa.co

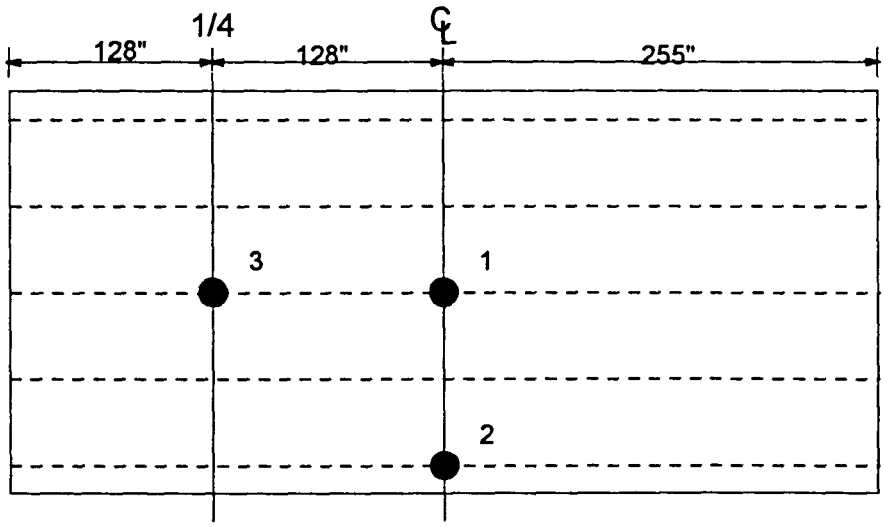

a) bridge 1

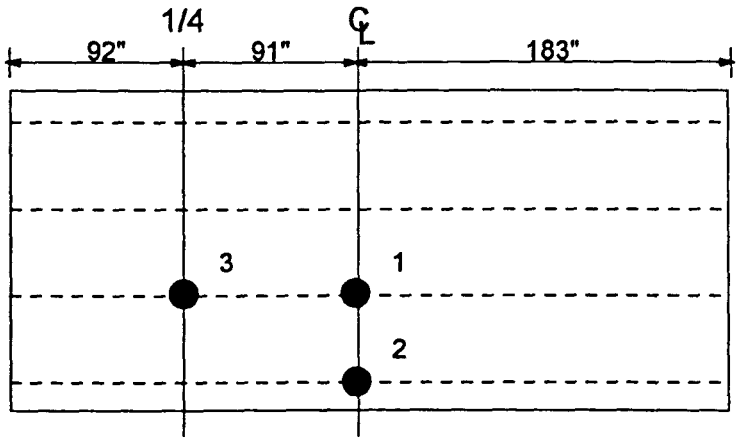

b) bridge 2

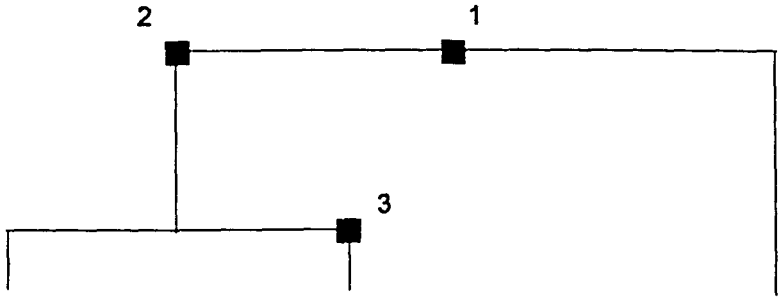

c) vehicle

Fig. 3.7 Monitoring points for the frequency domain analysis

nanaraa.co

for the bridge and vehicle points. A Fast Fourier Transform (FFT) was utilized to obtain the frequency content plots.

In Fig. 3.8 (smooth entry of the vehicle traveling at the speed of 45 mph) it is apparent that two frequencies dominate the response. Since the frequency of 15.2 Hz is apparent at all three bridge monitoring points, it is implied that the bridge vibrates in the third mode shape (mode frequency 13.9 Hz, Fig. 3.1c). Further proof can be observed through the time-deflection plots in Fig. 3.9. In Fig. 3.1c, the dynamic deflection should be maximum for the outside and minimum for the middle stringers at a given instant (and vice versa after a time equal to one-half of the natural period of the mode). This is consistent with the time deflection record, and is particularly noticeable in Fig. 3.9 at time t=0.45 sec, where the dynamic component of the deflection for points 1 and 3 (middle stringer) is exactly 180 degrees out of phase from point 2 (outside stringer). The other dominant frequency is 30.3 Hz, which is prominent only at point 3. The point is at the quarterspan of the middle stringer. This frequency is very close to the frequency of the seventh mode shape (28.5 Hz). In Fig.3.1g the points where the bridge vibration record is available, the seventh mode should contribute only at point 3 (points 1 and 2 are located at midspan which is a point of contraflexure for this shape and thus does not contribute to the response).

nanaraa.co

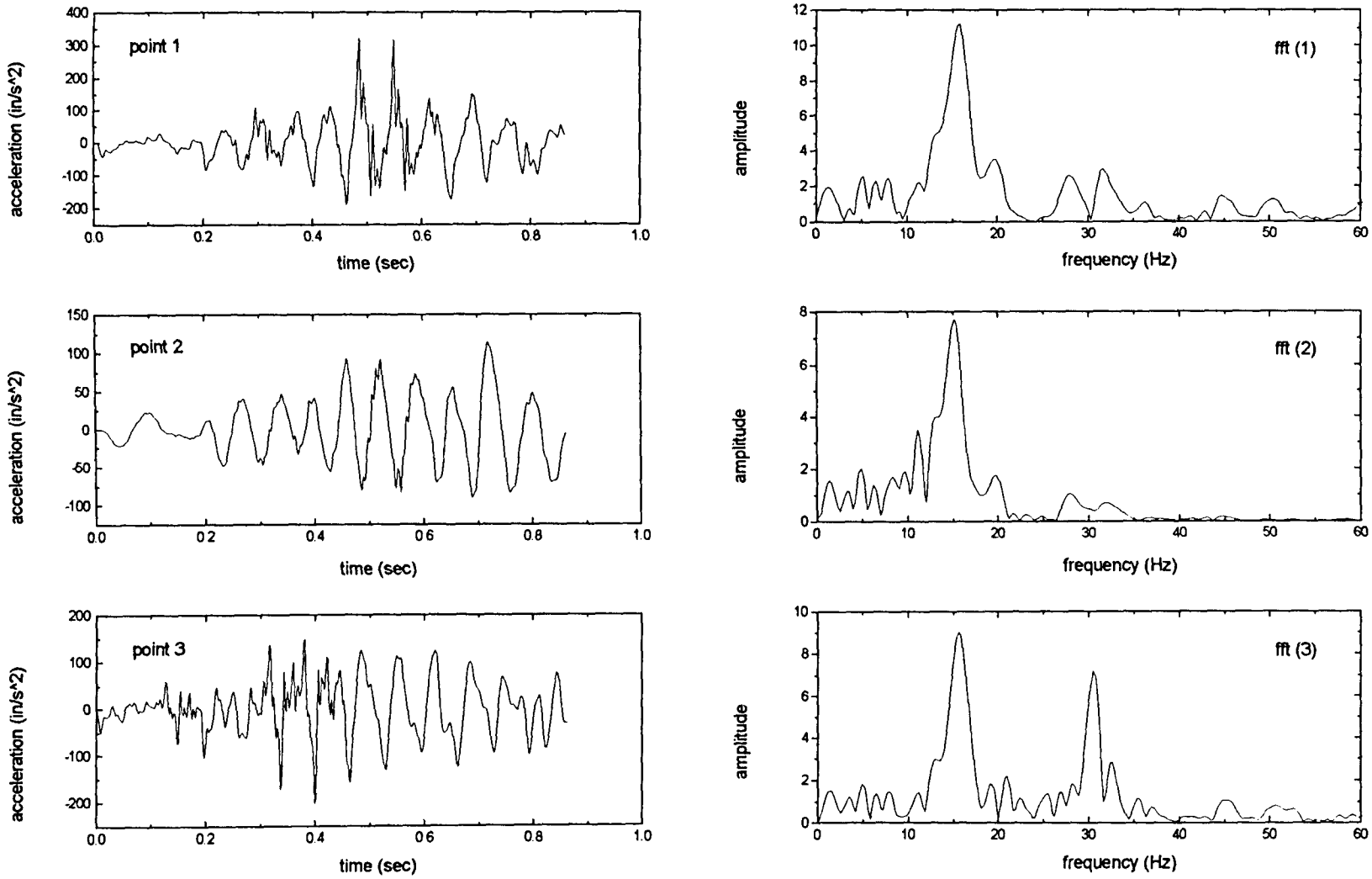

Fig. 3.8 Frequency domain analysis - bridge response for smooth vehicle entry and speed 45 mph

nanaraa.co

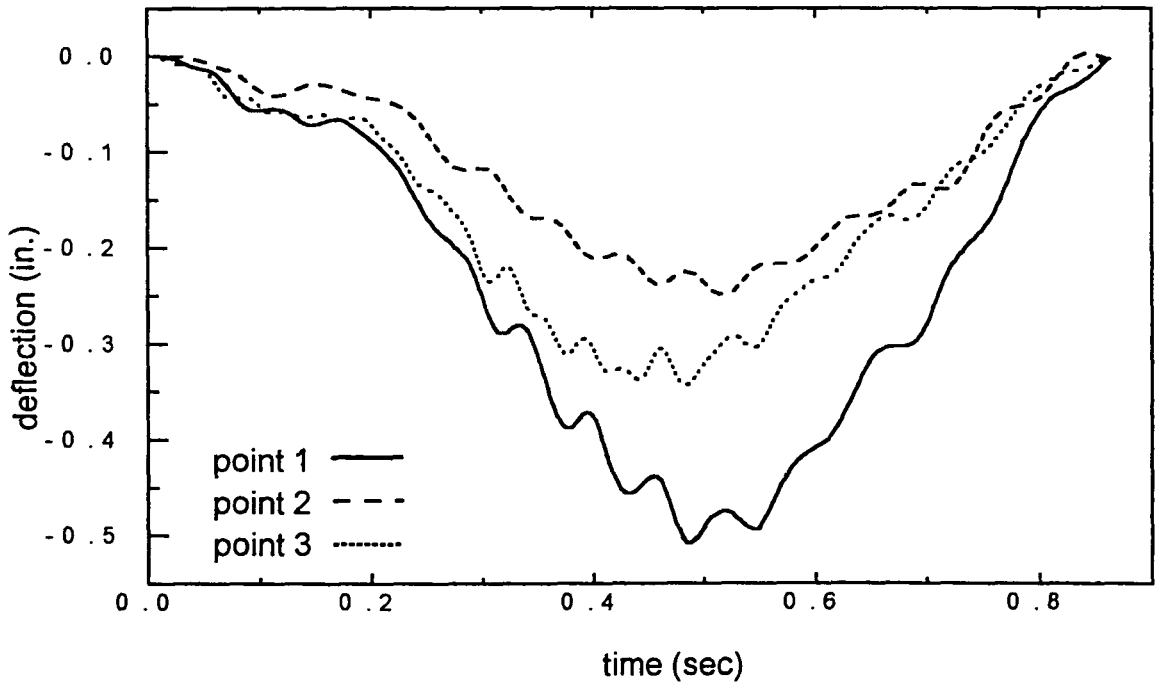

a) response for smooth entry

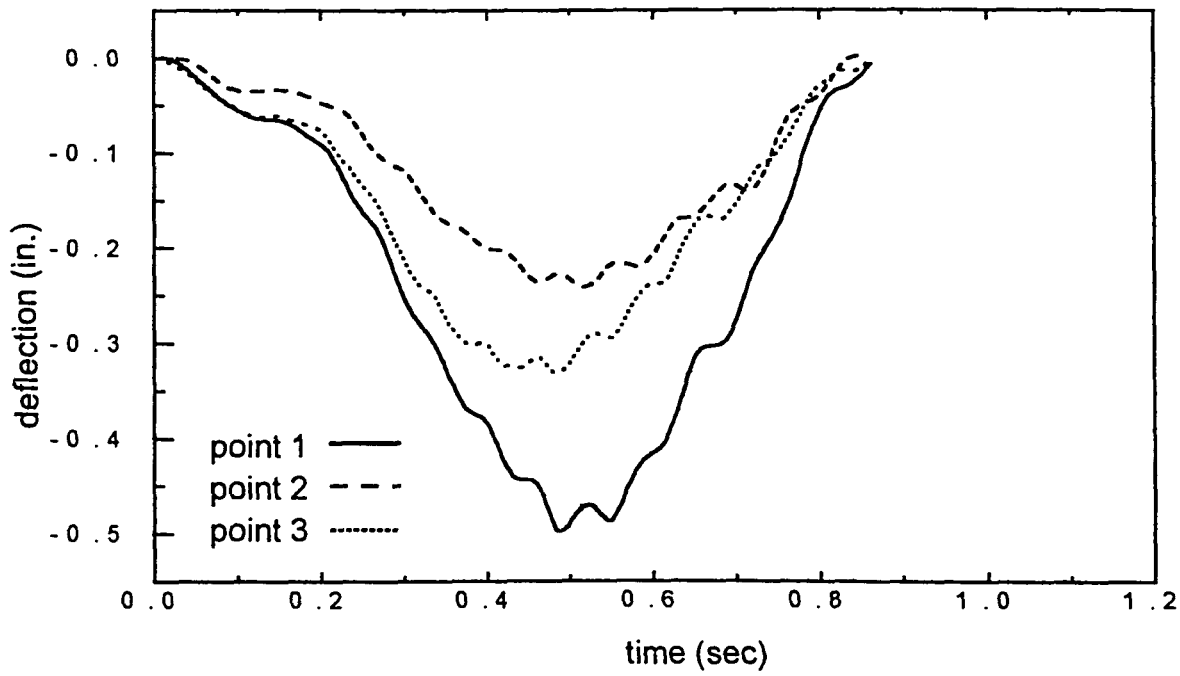

b) response for bump entry

Fig. 3.9 Bridge 1 deflections for 45 mph

nanaraa.co

Based on the results of the analysis the following conclusions about the bridge behavior can be made:

- Since the vehicle was in a concentric transverse position on the bridge, only the transversely symmetric modes of the bridge vibration were excited.
- The participation of the modes differs with speed.
- For smooth entry of the vehicle, the second mode (first longitudinal) dominated the response.
- The bump case excites higher modes of vibration and the second (first longitudinal) mode is not always the dominant one. The third mode is dominant at 35 and 45 mph (Figs. 3.10 and 3.8). The fifth (second longitudinal) mode is excited at 20 mph (plots not included). The seventh mode is excited at 45 mph (Fig. 3.8).
- When examining higher speeds (35 and 45 mph) for the bump condition, the higher modes tend to dominate the bridge response.
- For the critical speed (25 mph), the second (first longitudinal) mode dominates the smooth entry condition (Fig. 3.11), and is the only participating mode for the bump case (Fig. 3.12).

The following conclusions about the vehicle behavior can be made:

- The level of accelerations measured on the axle (point 3) was always higher by an order of magnitude for the bump case.
- Both the vehicle's body and axle related modes were excited. (Fig. 3.13)

nanaraa.co

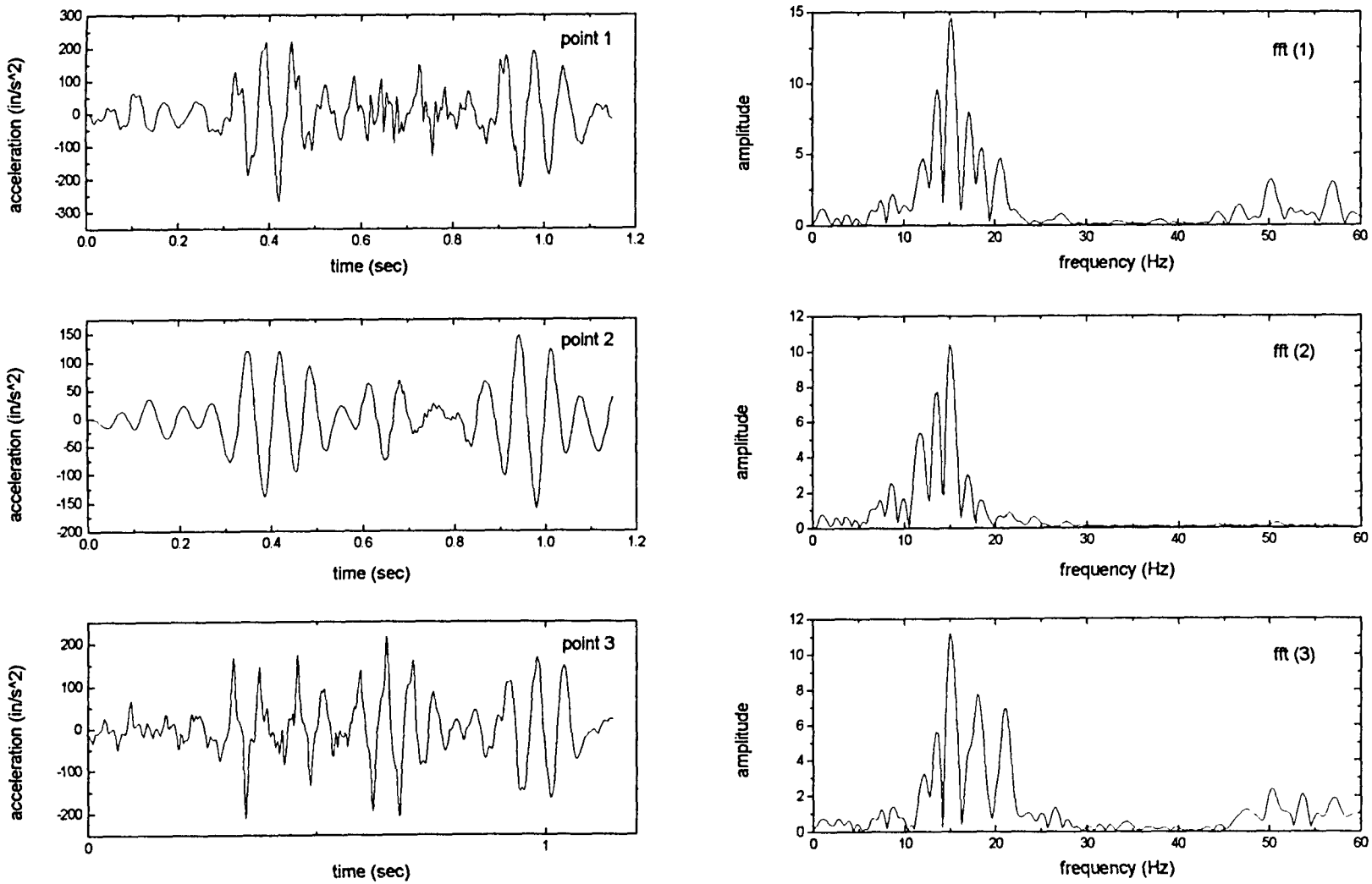

Fig. 3.10 Frequency domain analysis - bridge response for bump vehicle entry and speed 35 mph

nanaraa.co

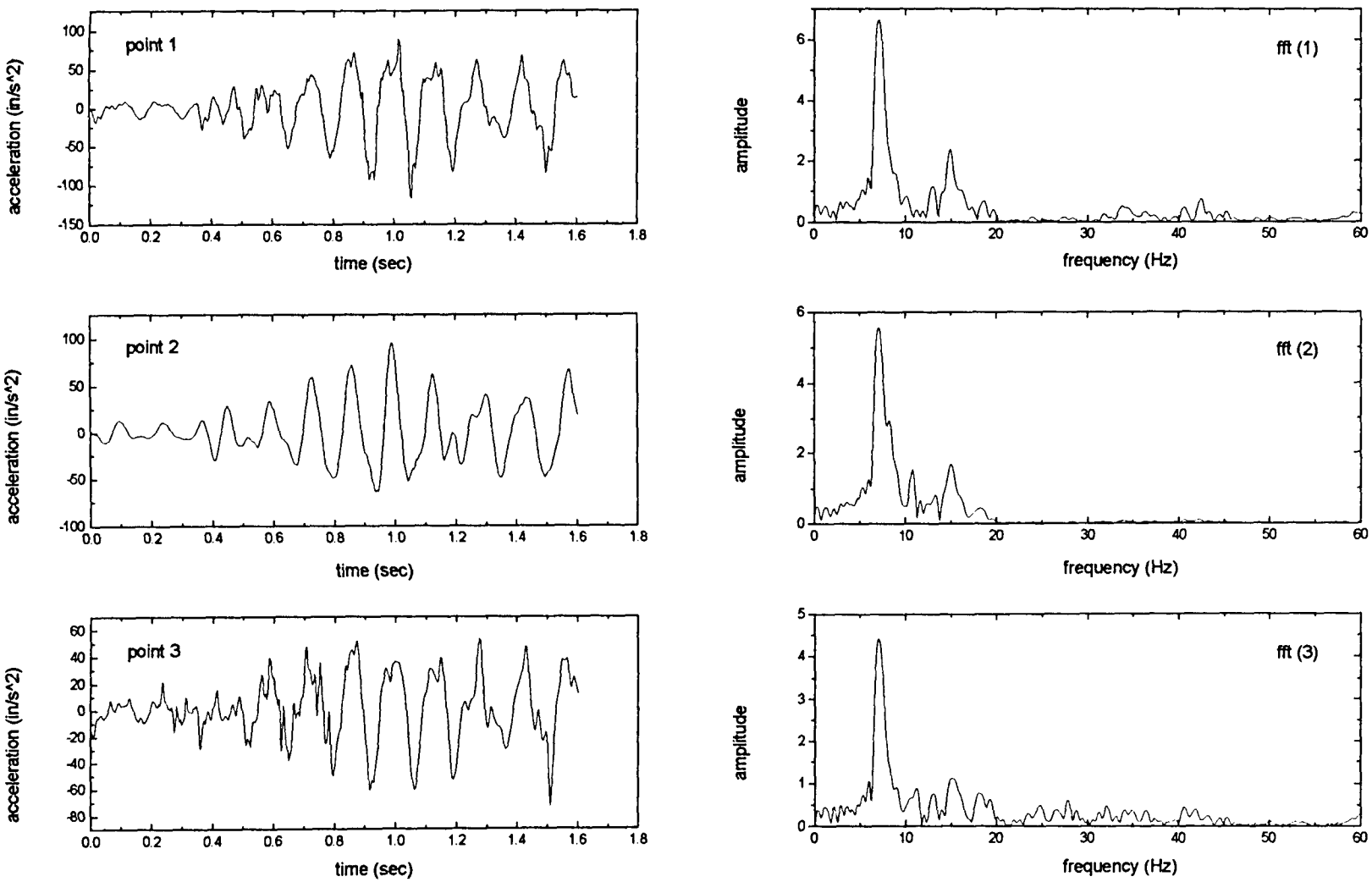

Fig. 3.11 Frequency domain analysis - bridge response for smooth vehicle entry and speed 25 mph

nanaraa.co

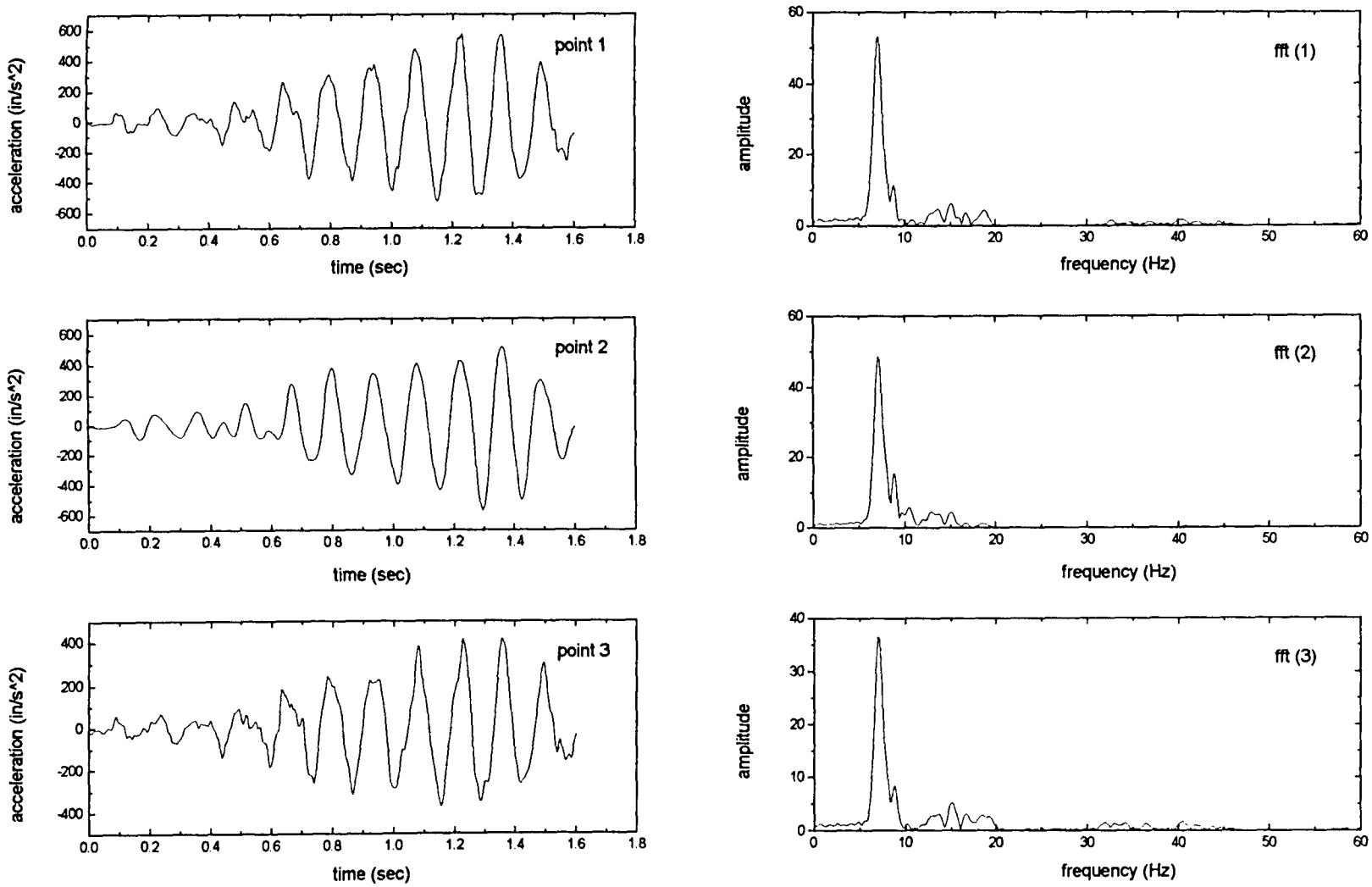

Fig. 3.12 Frequency domain analysis - bridge response for bump vehicle entry and speed 25 mph

nanaraa.co

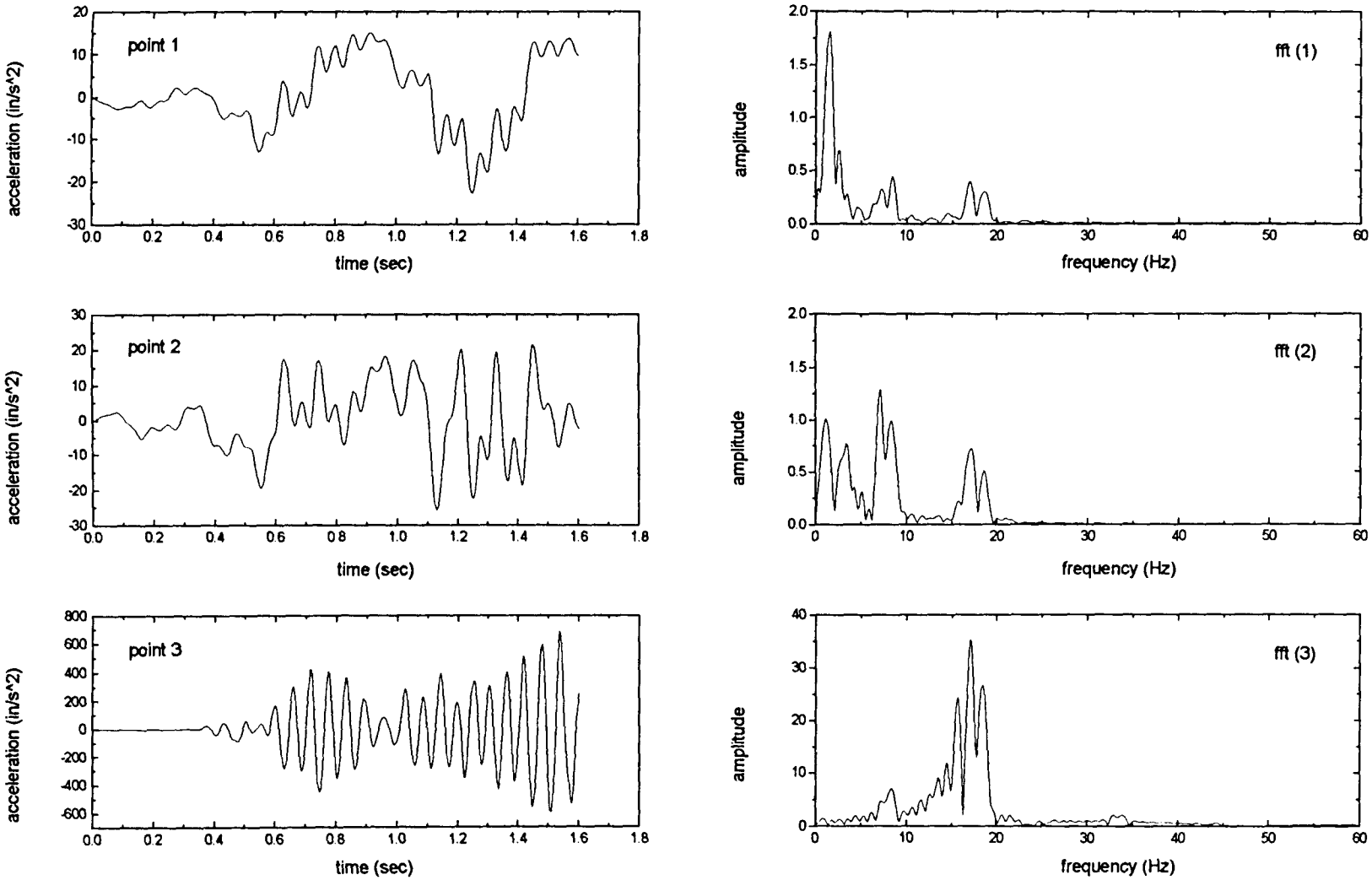

Fig. 3.13 Frequency domain analysis - vehicle response for smooth entry and speed 25 mph

nanaraa.co

- Within the axle related frequencies, both axle hop (Fig. 3.14) and axle pitch (Fig. 3.15) modes were excited.
- The high axle frequencies are dominant at the center of the body mass for the critical speed of the vehicle (Fig. 3.13)

The plots of the analysis results not discussed in the text appear in Appendix 1.

3.3.5 Bridge damping

The undamped response of Bridge 1 was considered for smooth entry of the vehicle at the critical speed of 25 mph. Time-deflection plots of the damped response (5% critical) and undamped response appear in Fig. 3.16. The undamped response produced higher maximum amplification and amplitudes of the bridge vibration. The observed DAFs were 1.083 for the damped and 1.149 for the undamped responses.

3.3.6 Vehicle axle spacing

A case of longer distance between the rear tandem axles was considered. The standard 51 in. longer, 68 in. spacing was considered. The vehicle traveled over Bridge 2 in speeds ranging from 20 to 45 mph. The results in terms of DAF appear in Fig. 3.17. Compared to the response under the standard vehicle, the DAF is lower for the standard vehicle critical speed and higher for the speeds around 40 mph. The observation supports of the hypothesis that the DAF for a bridge is maximized when the loads due to succeeding axles coincide. Considering the natural frequency of the bridge (f = 9.764 Hz), the speed

nanaraa.co

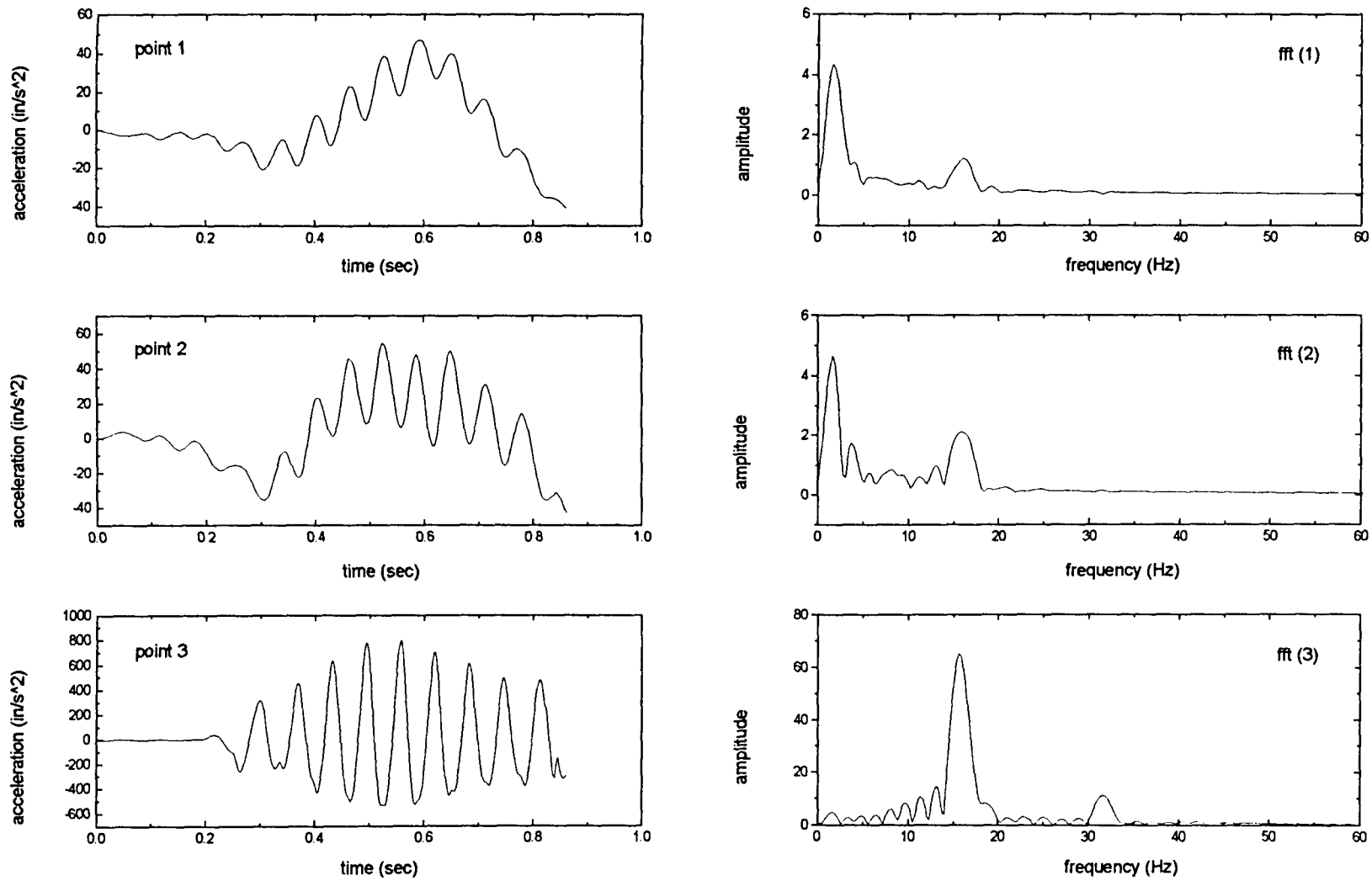

Fig. 3.14 Frequency domain analysis - vehicle response for smooth entry and speed 45 mph

nanaraa.co

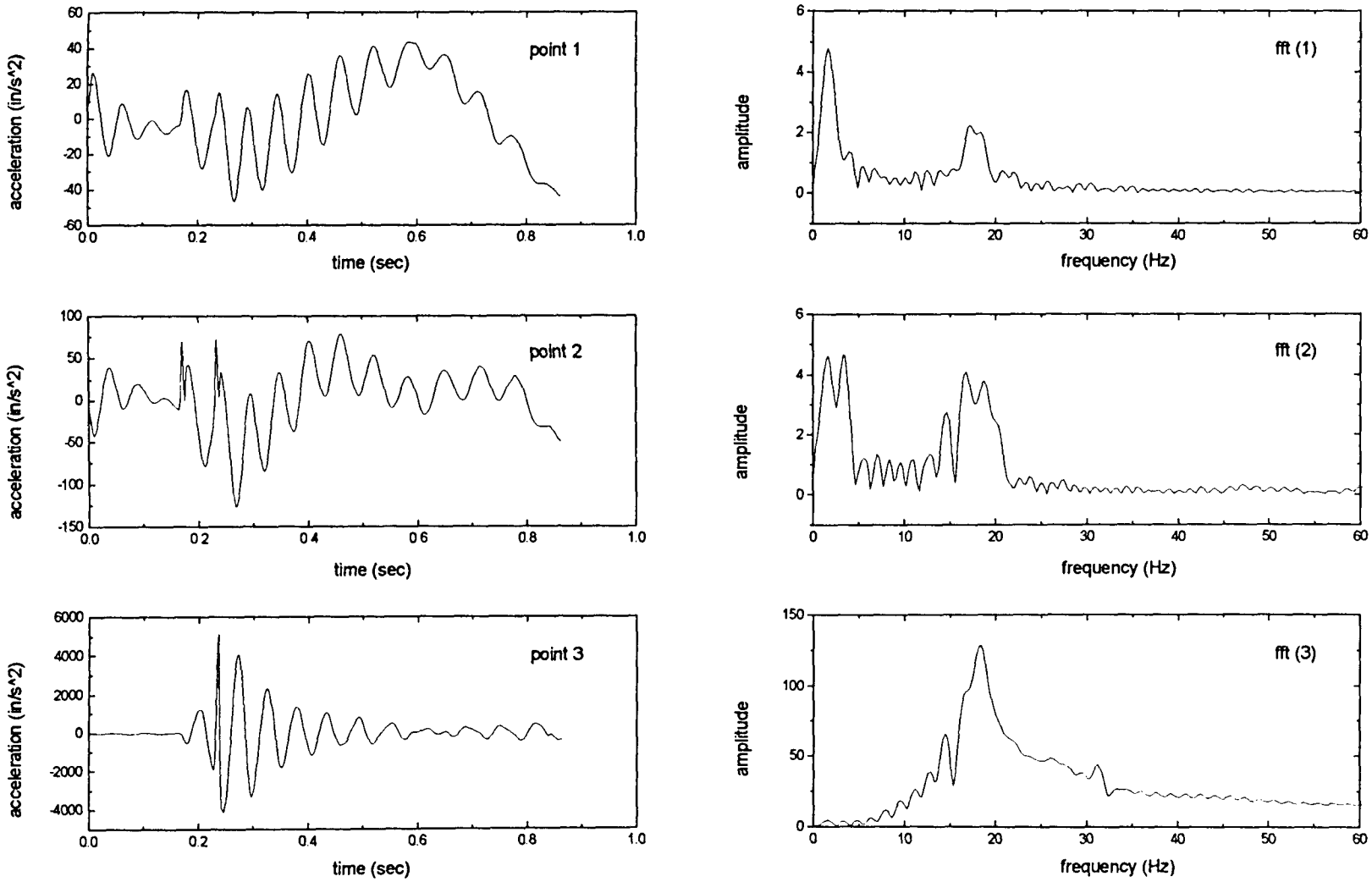

Fig. 3.15 Frequency domain analysis - vehicle response for bump entry and speed 45 mph

nanaraa.co

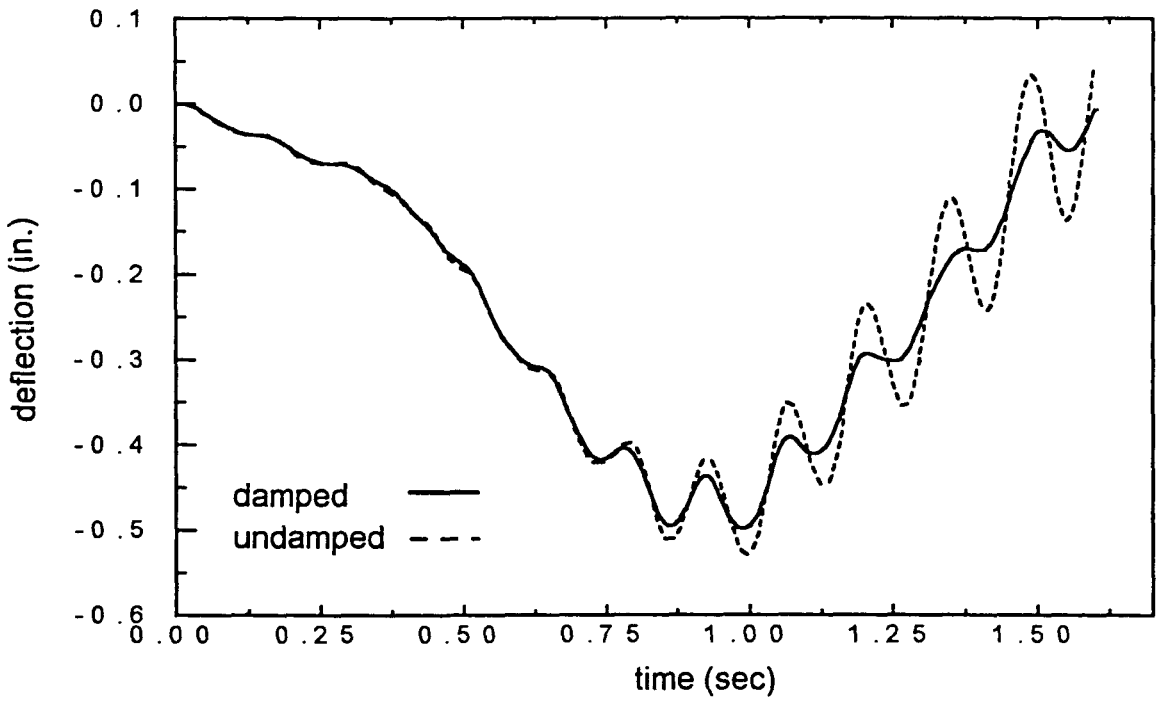

Fig. 3.16 Damped and undamped response of the bridge 1 for vehicle speed 25 mph

nanaraa.co

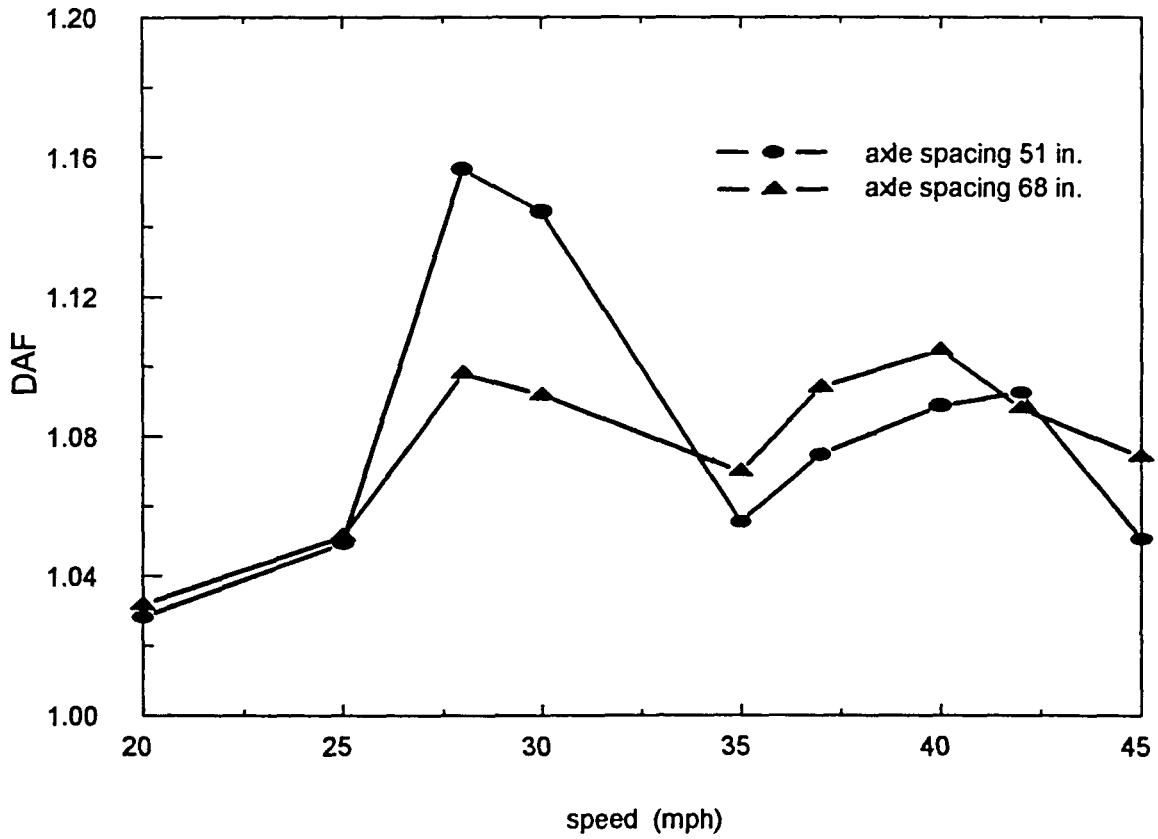

Fig. 3.17 DAF variation for different axle spacing of the vehicle

nanaraa.co

for the rear tandem axles to pass the same point is 28 and 38 mph for the standard and modified vehicle, respectively. The higher amplification for the standard vehicle may be explained by the fact that it occurs for a lower speed, and thus, more oscillations can occur with the vehicle on the bridge.

3.3.7 Conclusion

Based upon the presented sensitivity study, the following conclusions can be made:

- For both smooth and bump entry cases, a critical speed can be found for the particular vehicle/bridge system, for which the dynamic amplification is the highest.
- The highest amplification (DAF) occurs for the speed, where time for the rear axles to pass the same point coincides with the natural period of the bridge. Also, for the critical speed the bridge appears to respond in the first longitudinal mode shape.
- The bump placed at the entrance of the bridge amplifies the maximum dynamic deflection, possibly multiple times.
- Higher modes participate or even dominate in the bridge response, particularly for higher speeds.
- The undamped response seems to produce a higher DAF.
- Different axle spacing of the vehicle changes the variation of DAF with speed.

nanaraa.co

4. EXPERIMENTAL INVESTIGATION

4.1 General

The objectives of the experimental investigation were to determine the dynamic characteristics and performance of several field bridges and to acquire data to validate the analytical models discussed in Chapters 2 and 3. The bridges selected for the tests were the Mud Creek Bridge, Wittson Bridge and Chambers Co. Bridge, each located in the state of Alabama. The first two bridges consisted of four simple spans, and the last one was a single span bridge. Mud Creek and Chambers Co. Bridge each have two traffic lanes, while Wittson Bridge has one. The instrumentation for the bridges and the testing procedures were generally the same for all of the bridges and will be discussed prior to the results for each bridge. A concluding summary of the results for all the bridges is presented at the end of this chapter.

4.1.1 Bridge instrumentation

The tests were designed according to Ritter et. al. [19] and Barton et. al. [18] to acquire data to determine the bridge's natural frequencies, dynamic amplification and structural damping. General layout and schematic of the bridge instrumentation appear in

nanaraa.co

Fig. 4.1. The dynamic response of the bridge was recorded during the passage of the testing vehicle traveling at a constant velocity and for several more seconds after the vehicle left the bridge to acquire both forced and free vibration data. Deflections were measured at midspan of each of the stringers, and at quarterspan of the middle stringer (or the one closest to the middle in the case of even number of stringers) using a Celesco string-type direct current potentiometer. A frame consisting of surveying tripods supporting a 2- by 12-in. board was used to support the displacement transducers. Data was collected using a Hewlett-Packard 3852 data acquisition/control system (DAS) equipped with two HP 44711, 24 channel FET multiplexers and HP 44702, 14 bit high speed voltmeter. The DAS was controlled and the data was processed and stored in a portable 486DX-33 PC running IBASIC for windows. The entire system was triggered when the vehicle crossed the tape switch at the bridge entrance. Another tapeswitch was installed at the end of the bridge to determine the actual velocity of the test truck. The system was powered by a portable generator.

Three accelerometers [Seismic Accelerometer, Model 393C by PCB Piezotronics] were mounted on the bridge. Two of them were placed at midspan on two stringers (middle and exterior one) and one at quarterspan of the middle stringer (Fig. 4.1). This layout corresponds to the one used for the analytical study.

nanaraa.co

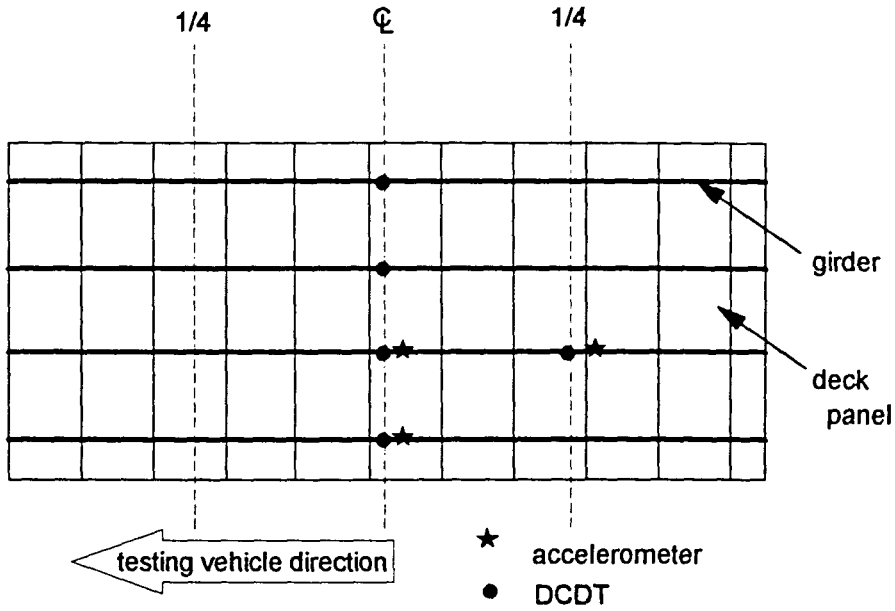

a) schematic of instrumentation layout

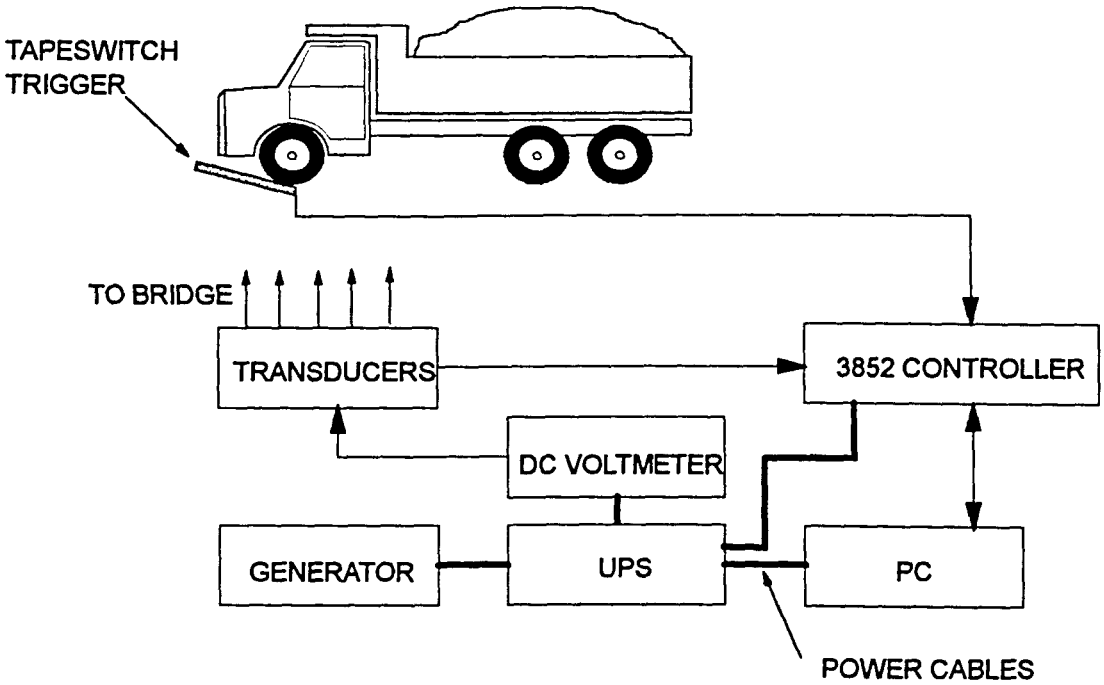

b) schematic of instrumentation arrangement

Fig. 4.1 Bridge instrumentation

nanaraa.co

4.1.2 Vehicle instrumentation

The vehicles used in this testing were three axle dump trucks with multi-leaf steel springs. The front axle had two tires and the rear axles had four tires each. The test vehicles were instrumented with two accelerometers to acquire a record of the vehicle vibration before it entered the bridge and while on the bridge. These accelerometers were mounted on the vehicle frame directly above the suspension (A2) and on the rear axle (A1) to determine frequency of the vehicle body and axle vibration. A schematic of the test vehicle and the vehicle instrumentation are shown in Fig. 4.2. A schematic of the vehicle suspension and placement of the accelerometers appear in Fig. 4.3. A photo of a typical test vehicle appears in Fig. 4.4.

The vehicle acceleration data was collected simultaneously with the bridge displacement and acceleration data. The setup consisted of a Gould digital oscilloscope (DSO) and two PCB accelerometers. The accelerometers were high sensitivity integrated circuit piezoelectric with a quartz tri-shear design. The accelerometers were wired into conditioner modules and from there into the DSO. The DSO was connected to a laptop computer via IEEE-488 interface. Transition software from Gould controlled the DSO so that it waited for a trigger to collect the signals from both channels. Data was then transferred to the laptop and the DSO was reset for the next trigger. Power to the laptop and oscilloscope was provided by either batteries or the electrical system of the vehicle through the fuse box or cigarette lighter. Digital filtering of the acquired data was done during the reduction as needed.

nanaraa.co

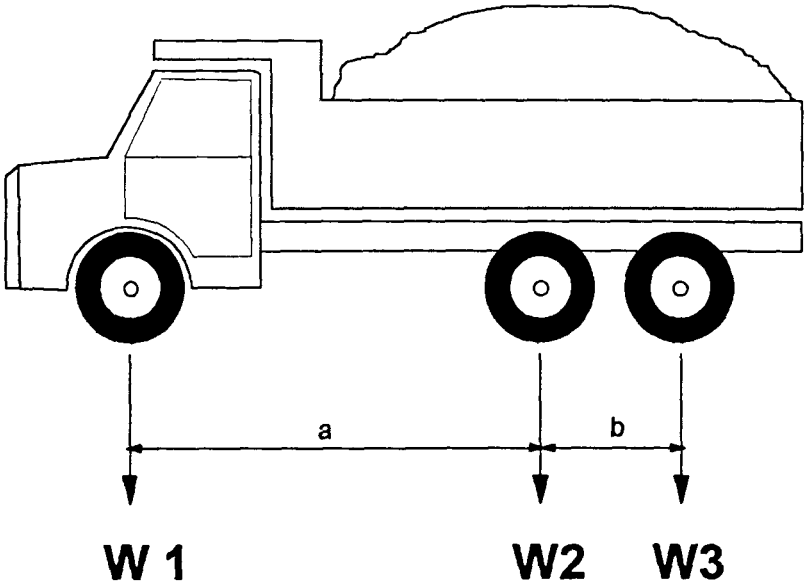

a) vehicle schematic

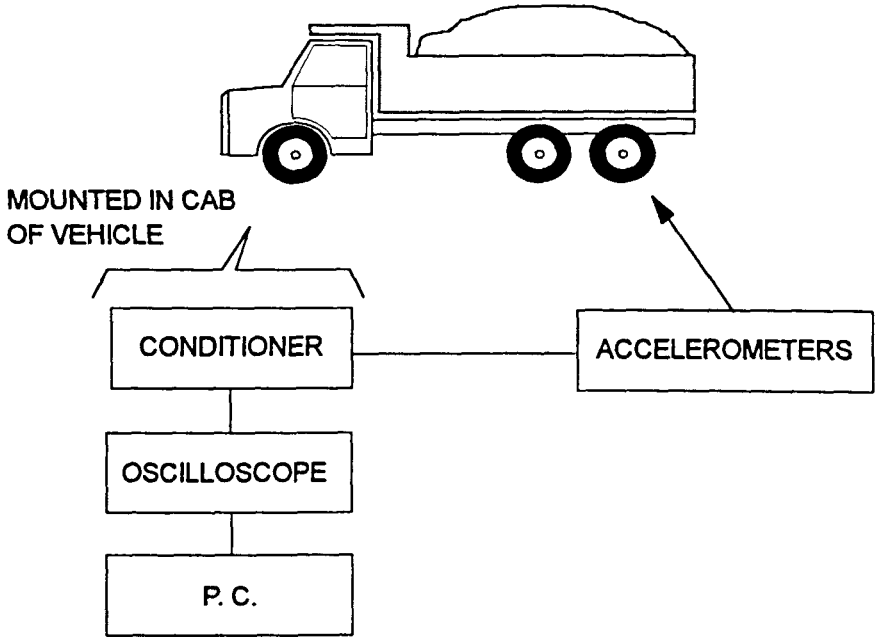

b) vehicle instrumentation arrangement

Fig. 4.2 Test vehicle

nanaraa.co

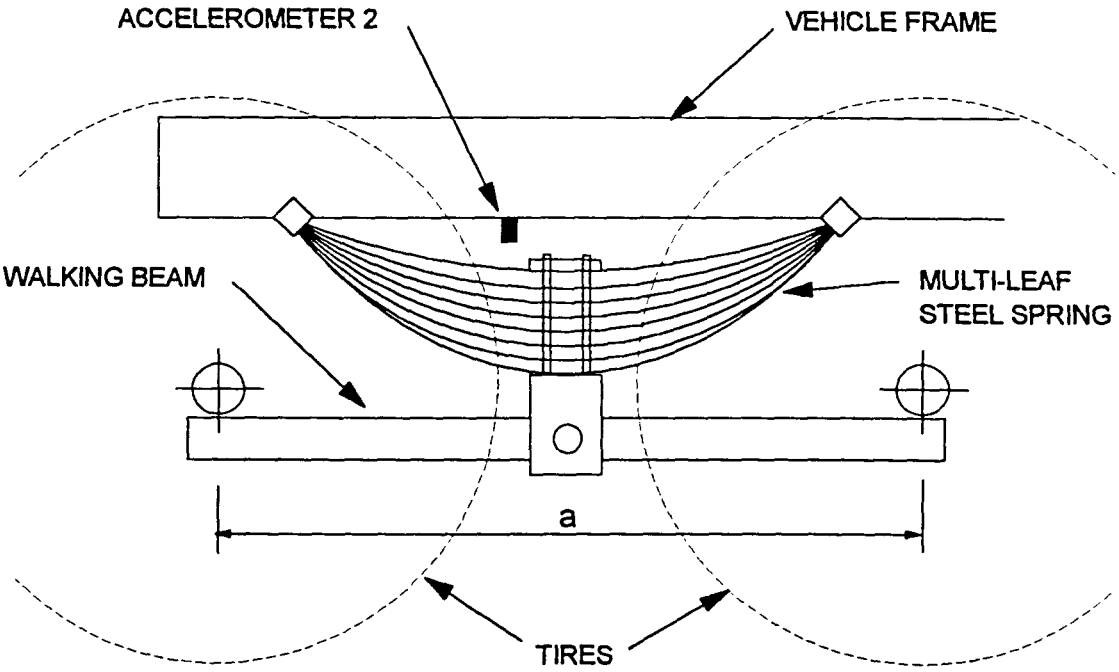

a) schematic of the suspension

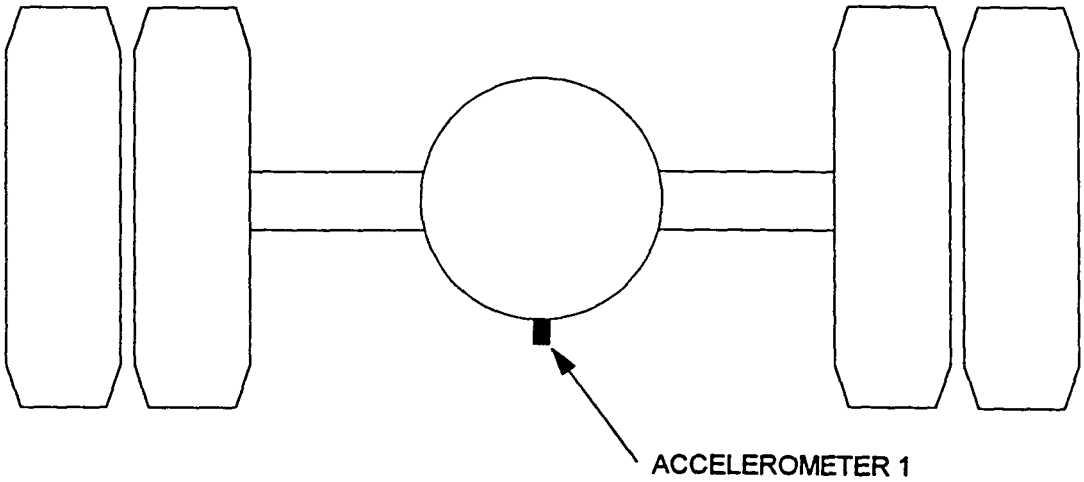

b) view of a rear-most axle

Fig. 4.3 Vehicle details and accelerometer placement

nanaraa.co

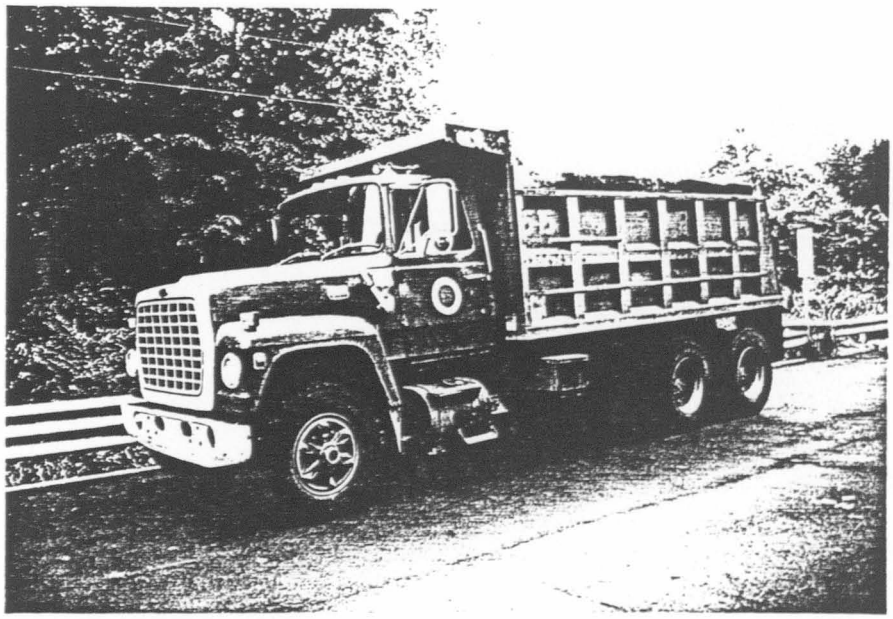

Fig. 4.4 Typical testing vehicle

araa.com

A tapeswitch that was mounted to the front bumper of the vehicle was used to trigger the DSO. A 2- by 4-in. board was attached parallel to the bumper to extend the tapeswitch approximately 2 ft to the side of the truck to hit a vertical rod placed on the roadway to trigger the DSO. The rod was positioned so that the DSO was triggered 20 ft before the front axle of the vehicle entered the bridge.

4.1.3 Test procedure

The dynamic behavior of the bridge was evaluated for several vehicle velocities, generally between 10 and 40 mph with 5 mph increments. Two approach conditions were considered: in situ approach conditions and an artificial rough approach, which was simulated by a 2- by 4-in. board placed at the entrance of the bridge. For the two lane bridges two transverse positions of the vehicle were also considered: Concentric, with the axle of the truck centered on the bridge and eccentric, with the left wheel line right of the centerline.

String lines were used to provide a guide for the driver to follow. Visual records were obtained on each test indicating the vehicle deviation from the string line position. The magnitude of the response was influenced by the differences in transverse position of the vehicle on the bridge for each test (tracking). Therefore, the maximum deflections were adjusted for calculation of the dynamic amplification. These adjustments are explained in detail in the appendix.

nanaraa.co

A crawl test was performed for each loading position to obtain a basis for a dynamic amplification evaluation. The crawl time-deflection plot was fitted with a smooth curve which was used for the actual amplification evaluation. The crawling speed of the truck was approximately 2 mph. The velocity of the truck was determined by the tapeswitches installed at the entrance and end of the bridge or bride span. Visual observation was made at each test site to assess the surface roughness of the approach road and the bridge wearing surface. The surface roughness was classified according to a scale presented by Dodds [20].

4.1.4 General format of results discussion

The respective bridges will be discussed in the following format:

Bridge and vehicle description

Bridge dimensions, detailed layout of instrumentation, roadway roughness conditions and data pertaining to the vehicle will be discussed.

Bridge free vibration response and vehicle vibration

Observed natural frequencies and calculated damping from the free vibration record of the bridge and record of vehicle vibration on pavement will be discussed.

Forced vibration response

Forced vibration response will be discussed based on analysis in time and frequency domain.

nanaraa.co

Dynamic amplification

The bridge response will be discussed in terms of dynamic amplification factors calculated according to Chapter 2.3.2

The following notation will be used in the discussion of results:

I = in situ approach conditions and concentric vehicle test

EI = eccentric vehicle test and in situ approach conditions

B = artificial bump approach conditions and concentric test of the vehicle

EB = eccentric vehicle test and artificial bump approach conditions

L = vehicle test with a decreased tire pressure to simulate a low tire stiffness

8.7EB = vehicle test at speed specified in mph, approach conditions and vehicle position

A1 = accelerometer placed at the rear-most axle of the vehicle (Fig. 4.3b)

A2 = accelerometer placed at the frame of the vehicle (Fig. 4.3a)

4.2 Mud Creek Bridge

4.2.1 Bridge and vehicle description

Mud Creek Bridge is a two lane bridge consisting of four simple spans. A photo of the bridge appears in Fig. 4.5. The stringers of adjacent spans are placed end to end with no visible gaps between them. Also, deck panels overlap at the ends of stringers on adjacent spans (Fig. 4.6a). The 41.75 ft long south end span was selected for the test. The

nanaraa.co

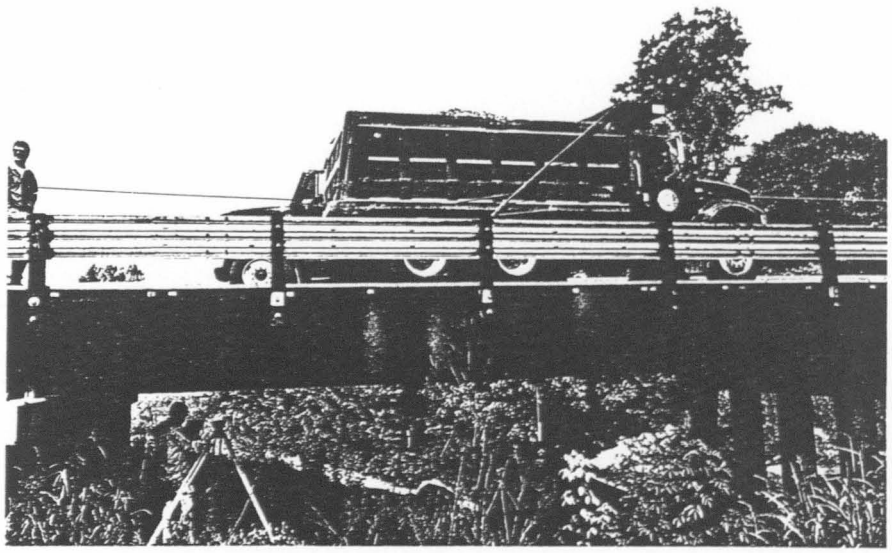

a) vehicle on the bridge

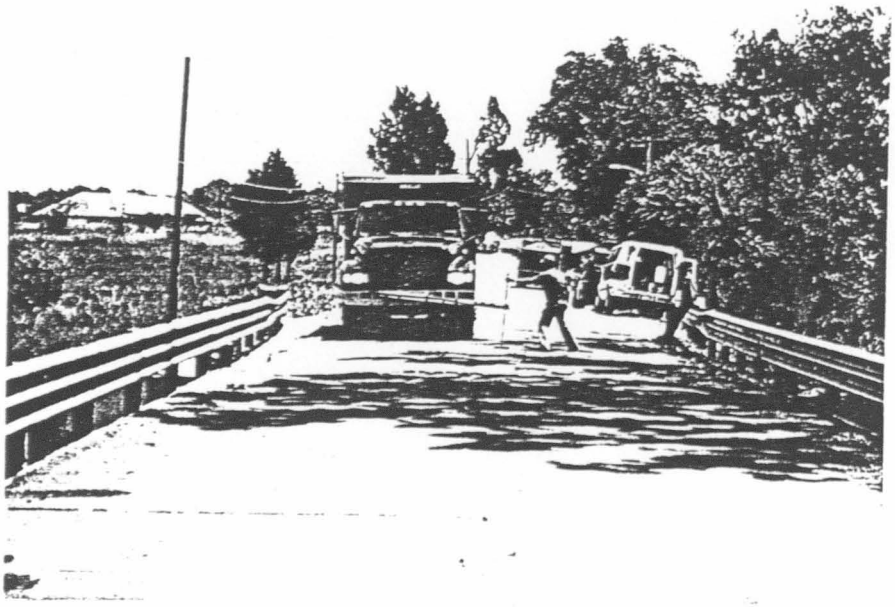

b) vehicle entering the bridge for an eccentric run

Fig. 4.5 Mud Creek Bridge

ınaraa.cor

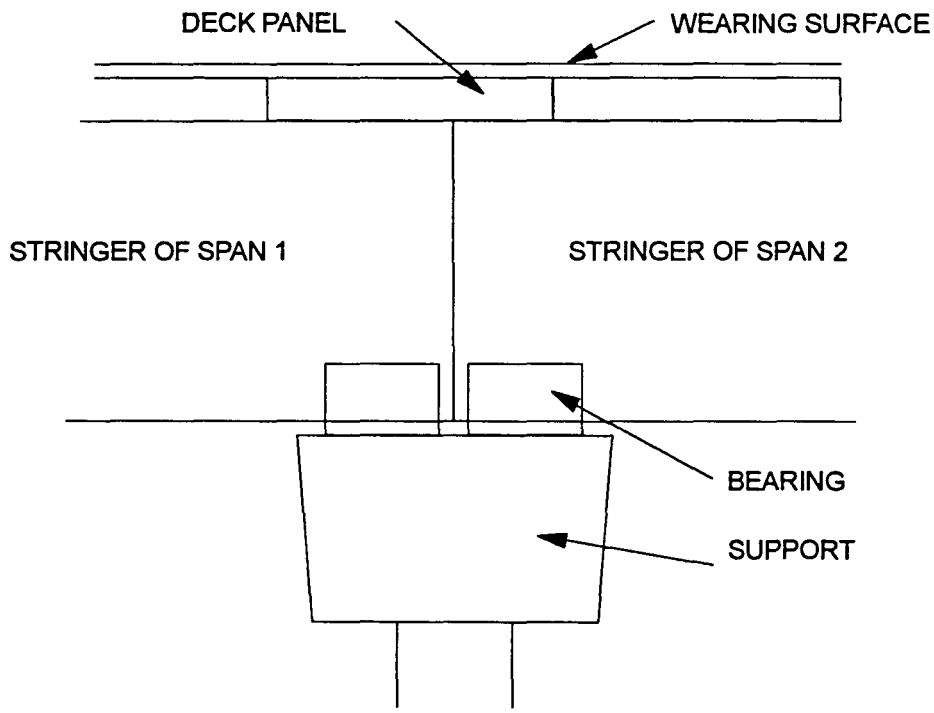

a) detail at internal support

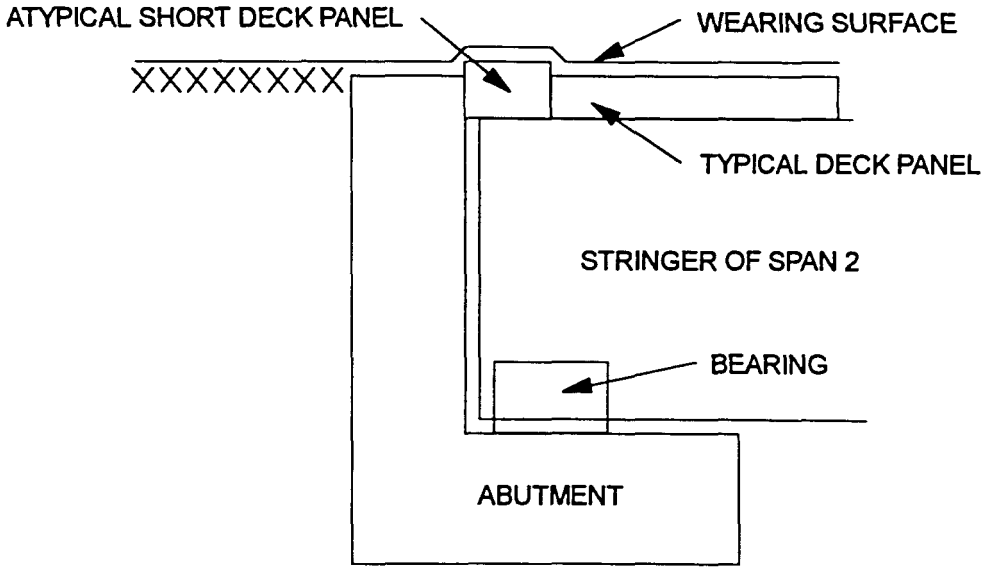

b) detail at external support

Fig. 4.6 Mud Creek Bridge - details

nanaraa.co

22.5 ft long, 51 in. wide and 5 in. deep deck panels are supported by five stringers at 60 in. on centers; A cross section of each is 43 in. deep and 6.75 in. wide. The stringers are made of Southern Yellow Pine (E_L = 1,920 to 2,160 ksi). Steel guardrail on timber posts are is installed on both sides of the bridge. The layout of the bridge and the instrumentation appear in Fig. 4.7. The cross section is shown in Fig. 4.8.

Travelling from the south, the approach road to the bridge is in a downward grade that levels at 150 ft before the bridge. An upward grade of 0.4% is constant along the bridge. According to a visual observation, the approach road surface roughness conditions could be characterized as good. The bridge pavement surface roughness could be characterized as very good. The first deck panel of the bridge was only 5 in. wide and elevated by approximately 0.75 in. above the riding surface in the panel's immediate vicinity. This created a natural bump (Fig. 4.6b).

The test truck was a three axle dump truck with 145 in. between the steering axle and the first rear tandem axle (dimension 'a' in Fig. 4.1) and 53 in. between the rear tandem axles (dimension 'b' in Fig. 4.1). The axle loads W1, W2 and W3 were 11 kips, 25.2 kips and 25.2 kips, respectively; total truck weight thus was 61.4 kips. Accelerometer data was taken while the truck was driven on the approach road to determine the frequencies inherent to the truck.

nanaraa.co

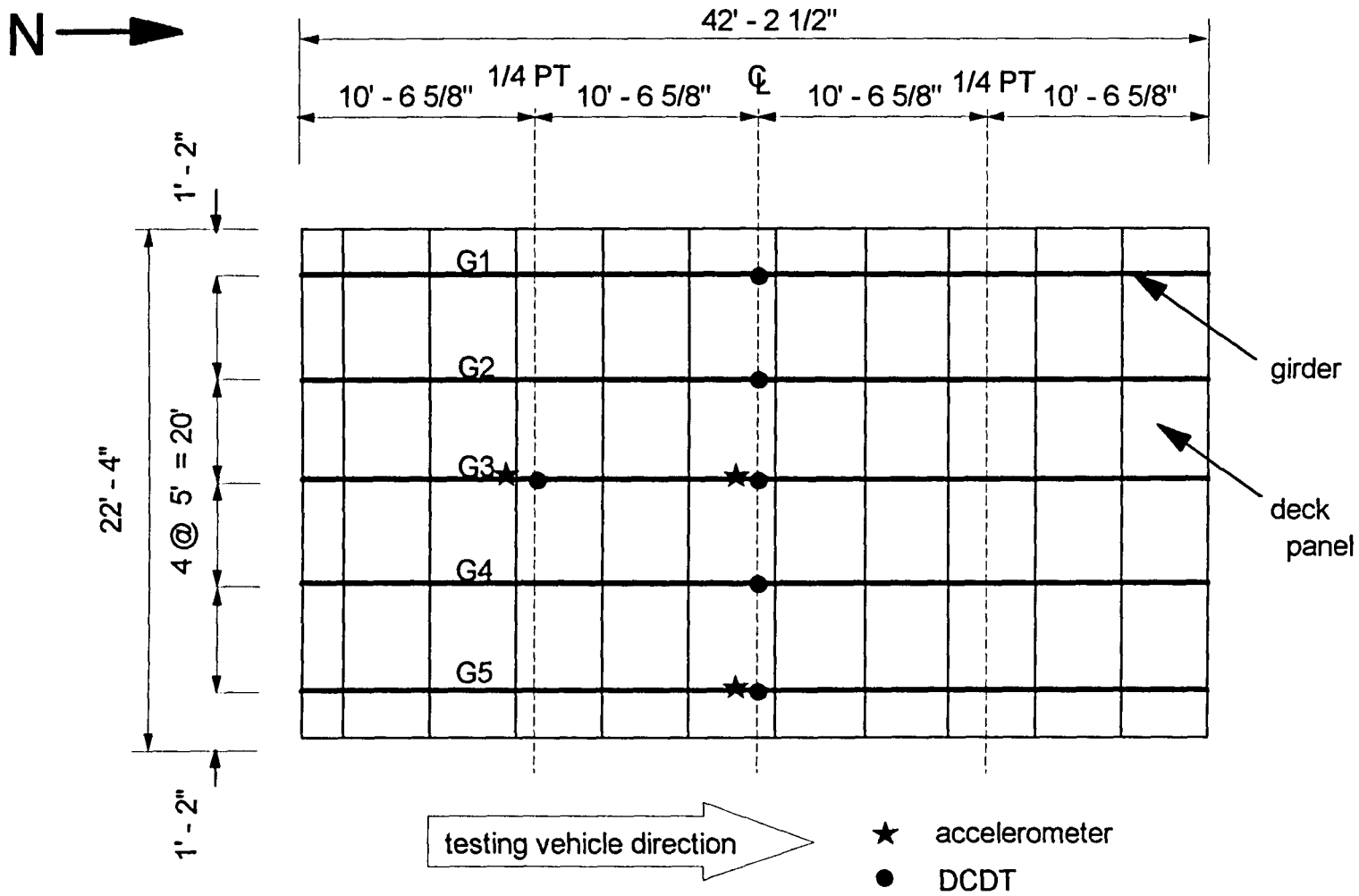

Fig. 4.7 Mud Creek Bridge - layout and instrumentation

nanaraa.co

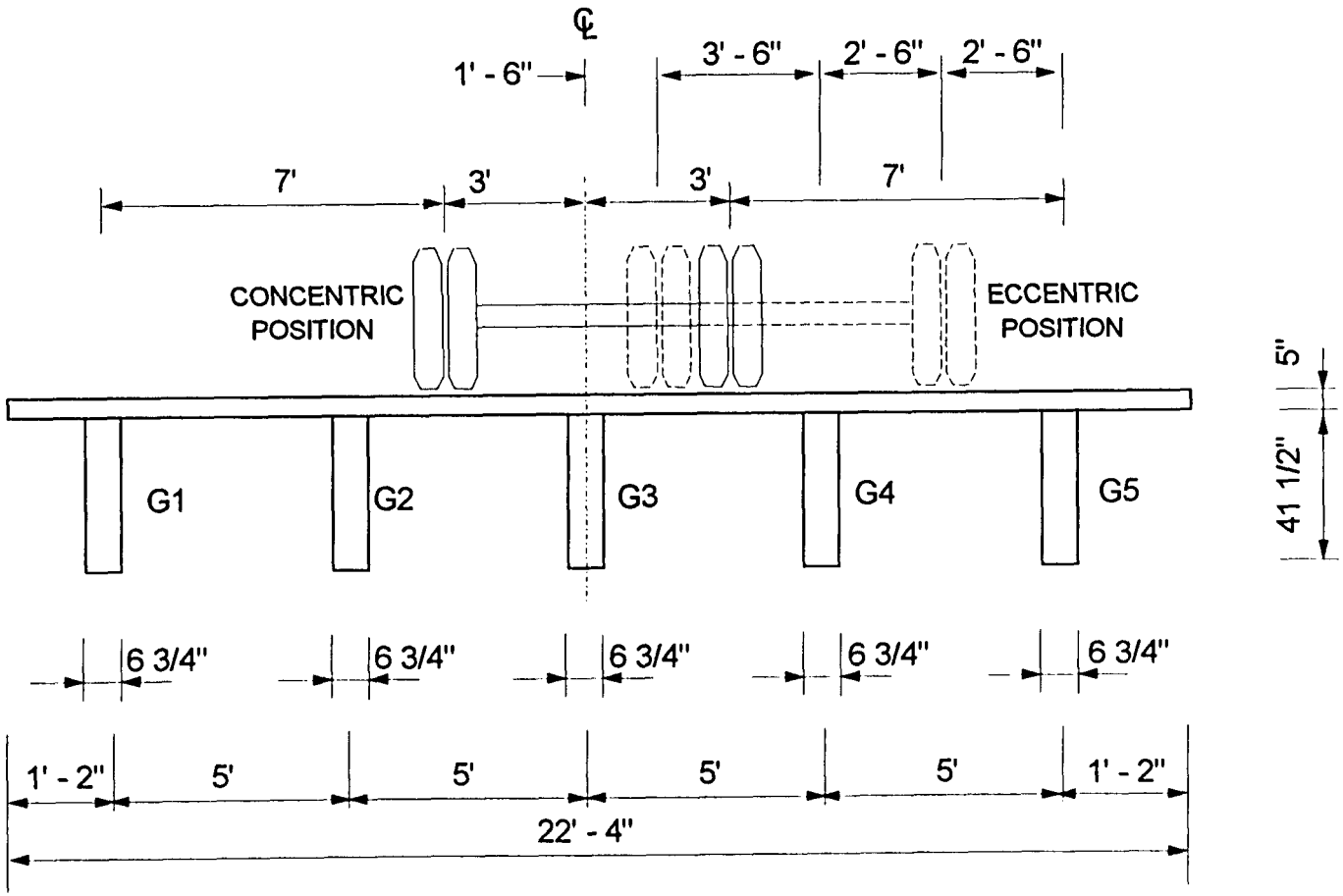

Fig. 4.8 Mud Creek Bridge - cross section dimensions and transverse positions of the vehicle

nanaraa.co

4.2.2 Discussion of the results

4.2.2.1 Bridge free vibration response and vehicle vibration

Because of the deck panel placement at the stringer joint of adjacent spans, a certain degree of continuity was exhibited by the bridge. The accelerometer record of the free vibration was disturbed by the presence of the vehicle on subsequent spans of the bridge; therefore it was difficult to determine structural damping. The fundamental frequency of the bridge was determined to be 8.9 Hz. The frequency of the vehicle body bounce was found to be 2.5 Hz. The frequency of the vehicle axle hop was 10.2 Hz (Fig. 4.9).

4.2.2.2 Forced vibration response

Due to the rough in situ approach to the bridge, only in situ tests were performed (i.e. no artificial bump was used). The vehicle transverse positions for both of the tests are shown in Fig. 4.8. The plots of bridge deflection and vehicle position along the bridge are shown in Fig. 4.10. The deflections of the middle stringer G3 and the exterior stringer G5 are shown in the figures for the concentric and eccentric tests respectively. Observation of this data show three different patterns of bridge behavior. These patterns can be observed for both concentric and eccentric tests at these speed intervals: low (up to 10 mph), medium (11 to 24 mph) and high (over 25 mph). three speed intervals will be discussed in following paragraphs.

The response of the vehicle in the low speed interval is dominated by a low frequency of 2.6 Hz (Fig. 4.11a). The frequency of the bridge vibration at speeds at 7.5I, 10.4I and 10.4E (2.54 Hz, Fig. 4.11b) is very close to the body bounce frequency of the

nanaraa.co

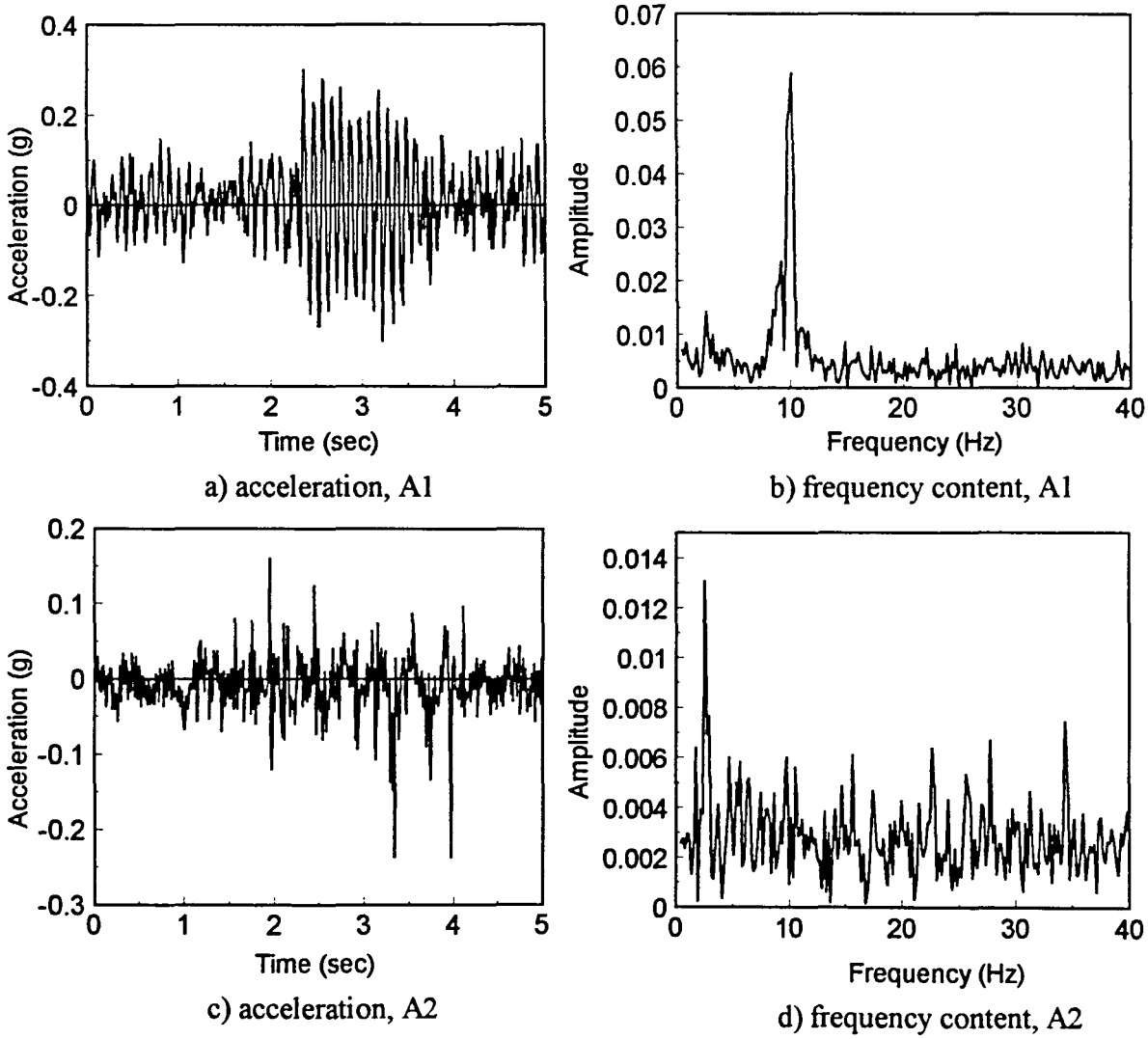

Fig. 4.9 Mud Creek Bridge - accelerometer data and frequency analysis for control run on roadway

nanaraa.co

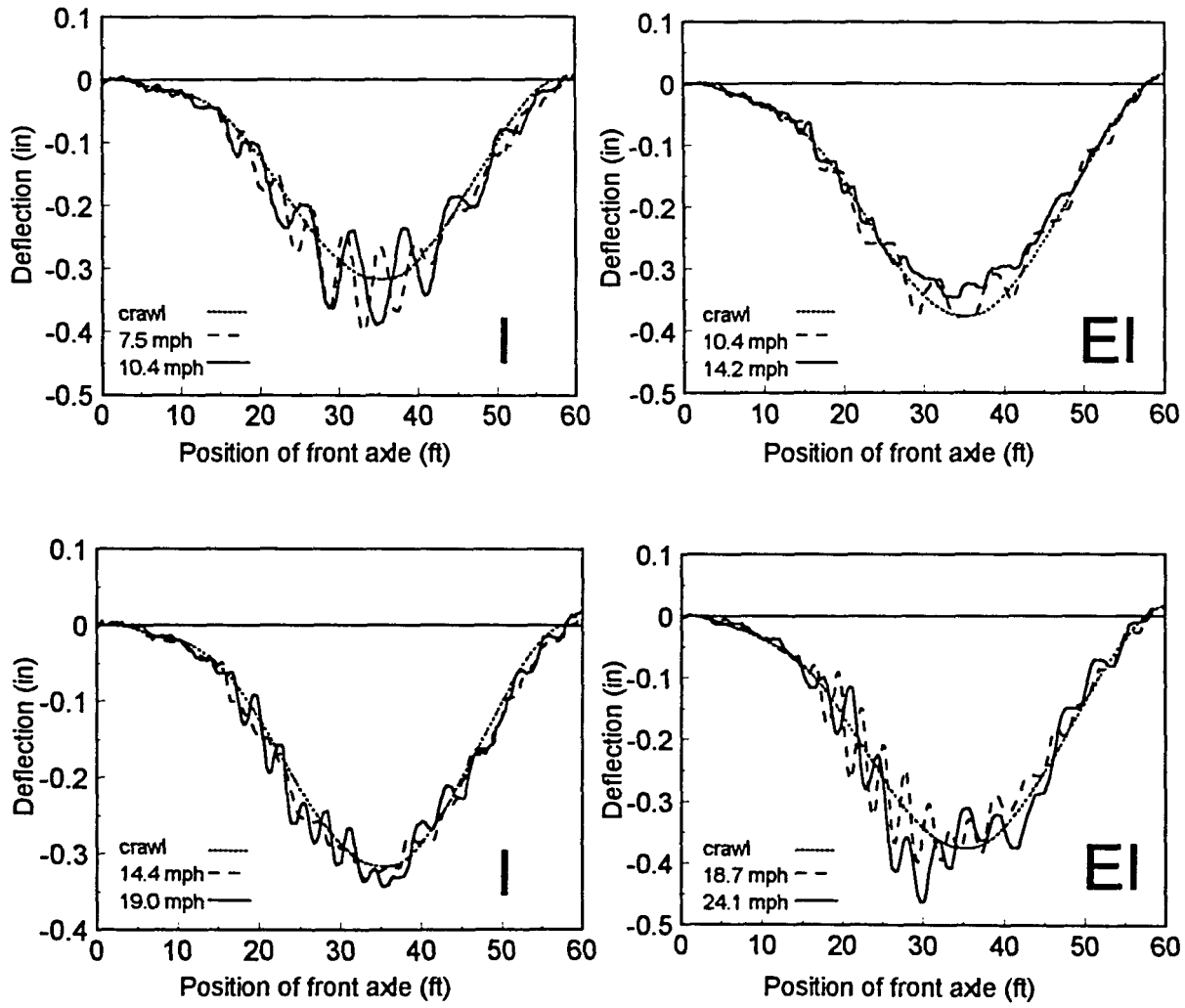

Fig. 4.10 Dynamic response for Mud Creek Bridge - Stringers G3 (I) and G5 (EI)

nanaraa.co

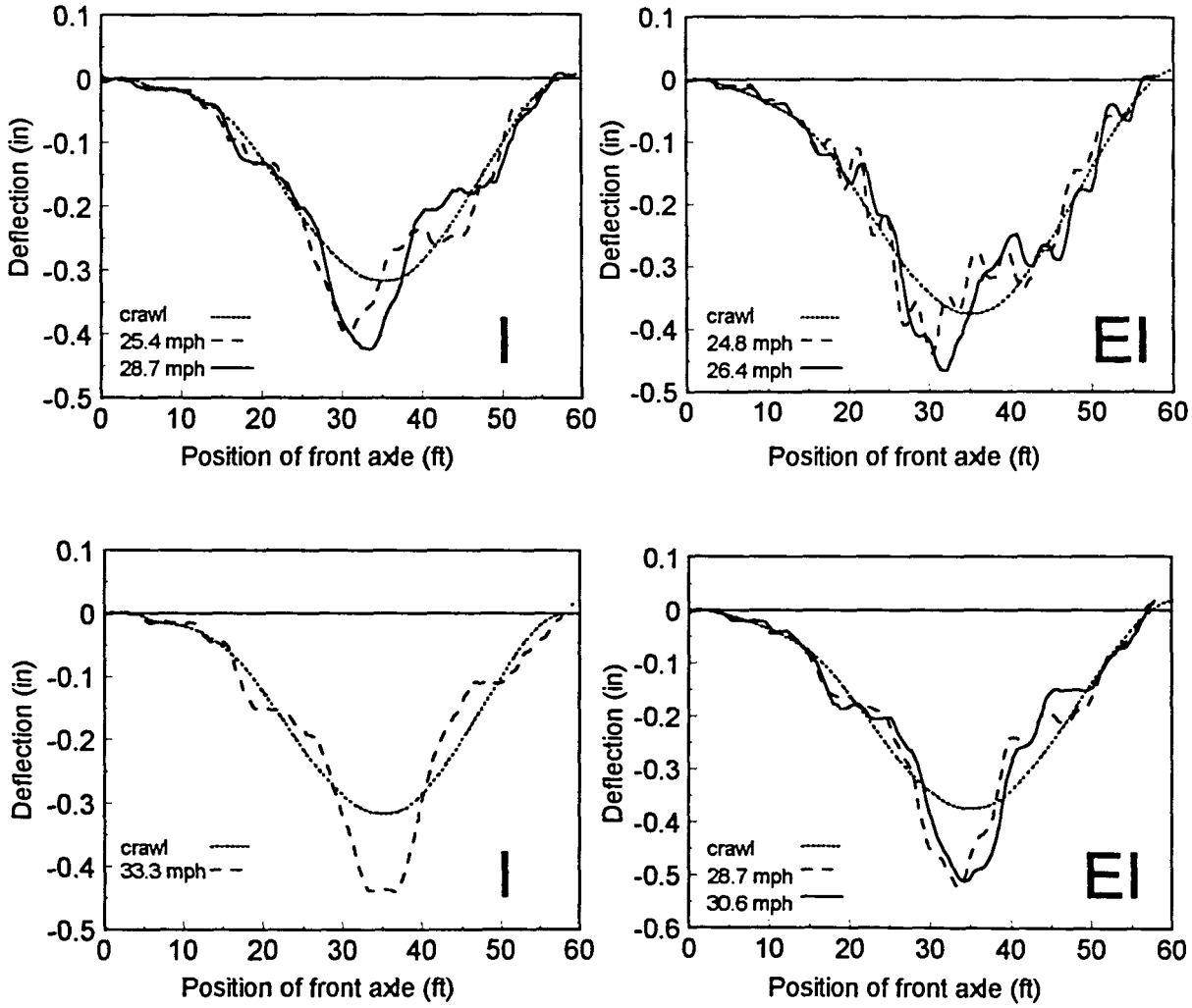

Fig. 4.10 (continued)

nanaraa.co

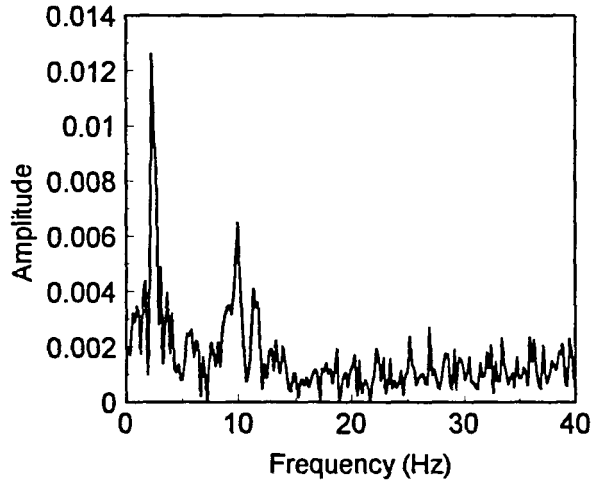

a) vehicle, A1, 7.5I mph

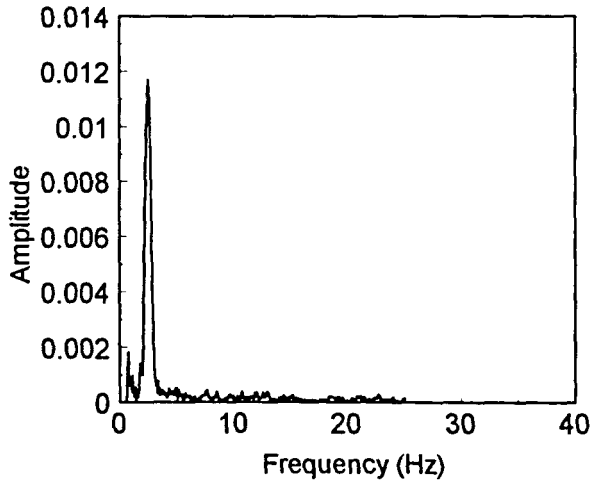

b) bridge, 7.5I mph

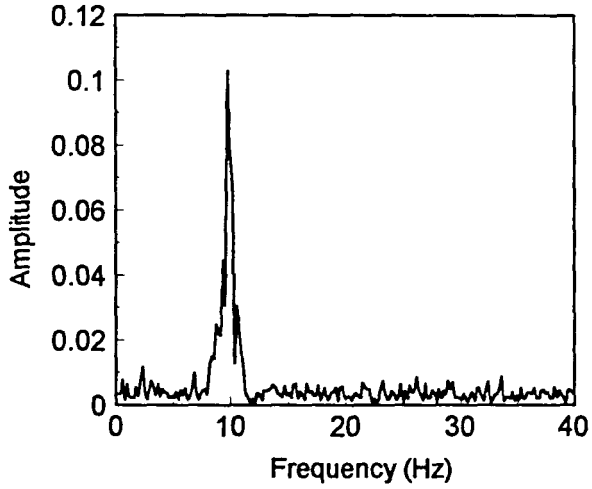

c) vehicle, A1, 19.0I mph

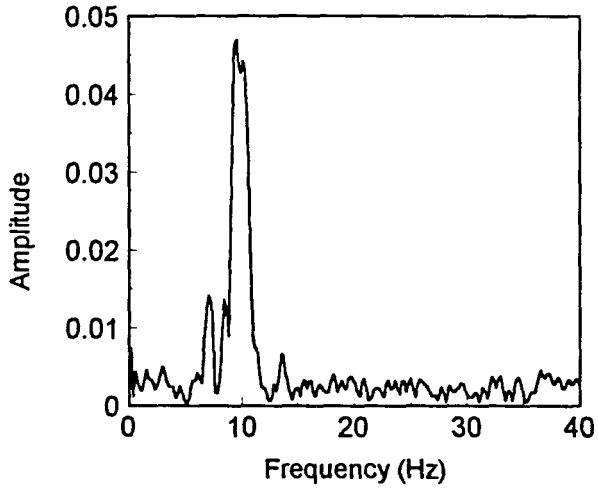

d) bridge, 19.0I mph

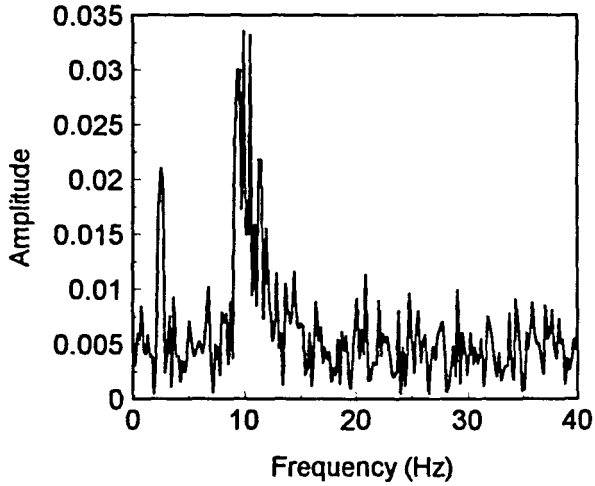

e) vehicle, A1, 26.4E mph

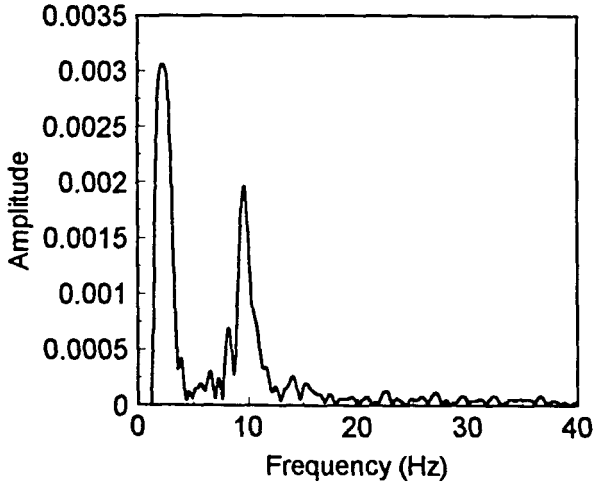

f) bridge, 26.4E mph

Fig. 4.11 Frequency contents plots for Mud Creek Bridge

nanaraa.co

vehicle for that test. In this case, the vehicle is the source of the forcing function for the bridge response.

At the speed of 14 mph, the bridge begins to respond in the frequency of 10 Hz, which is close to the frequency of the first longitudinal mode of the bridge (8.9 Hz). The vehicle response is dominated by the axle hop frequency (10.4 Hz, Fig. 4.11c). The frequencies of the bridge and vehicle response are very similar and for some tests they are identical. The bridge behaves similarly for the speeds up to 20 mph for both concentric and eccentric tests. A typical bridge response at this speed interval is shown in Fig. 4.11d. It should be noted that for speeds up to 20 mph, the bridge always exhibits a regular pattern of vibration regardless of the frequency of the vibration. This observation is true for both concentric and eccentric positions of the vehicle (Fig. 4.10).

A change in the pattern of bridge vibration can be noticed for vehicle velocities above 24 mph in the bridge response. The response is dominated by a low frequency of 2.3 Hz, which is again close to the body bounce frequency of the vehicle. A higher frequency of 10 Hz can be observed superimposed on the low frequency (see deflection plots in Fig. 4.10 and a frequency content plot in Fig. 4.11f). The contribution of the forced response due to the body bounce mode of the vehicle is significantly higher than the contribution of the bridge's natural frequency. This behavior can be observed at all high speeds (above 24 mph) for both concentric and eccentric tests. The body bounce frequency becomes prominent again in the vehicle vibration (compare Fig. 4.11e to Fig. 4.11c).

nanaraa.co

4.2.2.3 Dynamic amplification

The plot of dynamic amplification of the bridge response (DAF) and vehicle speed are shown in Fig. 4.12. When observing the DAF for the concentric tests, it was noted that the amplification was high for low speed ranges (i.e. when the bridge vibration was dominated by the low frequencies). The largest amplification of 1.38 was observed for the speed of 33.3 mph. The amplification is low, when the bridge's first longitudinal frequency dominates the response at speeds of 14.4 and 19 mph. The same conclusions holds true for the eccentric tests. The largest amplification for the eccentric test (1.33) was observed at the speed of 30.6 mph.

4.3 Span 1 of Wittson Bridge

Wittson Bridge is a single lane bridge consisting of four simple spans; 51.3 ft Span 1, 51.3 ft Span 2, 102 ft Span 3, and 35 ft Span 4. A photo of the bridge appears in Fig. 4.13. Although the ends of the stringers of adjacent spans were separated by a 1.5 to 3 in. gap, the deck panels overlapped from one span to another, creating possible rotational continuity. The stringers is made of Southern Yellow Pine (E_L = 2,020 to 2,090 ksi). Steel guardrail on timber posts are installed on both sides of the bridge. The first and the third span were tested and will be called Span 1 and Span 3, respectively, and discussed separately.

nanaraa.co

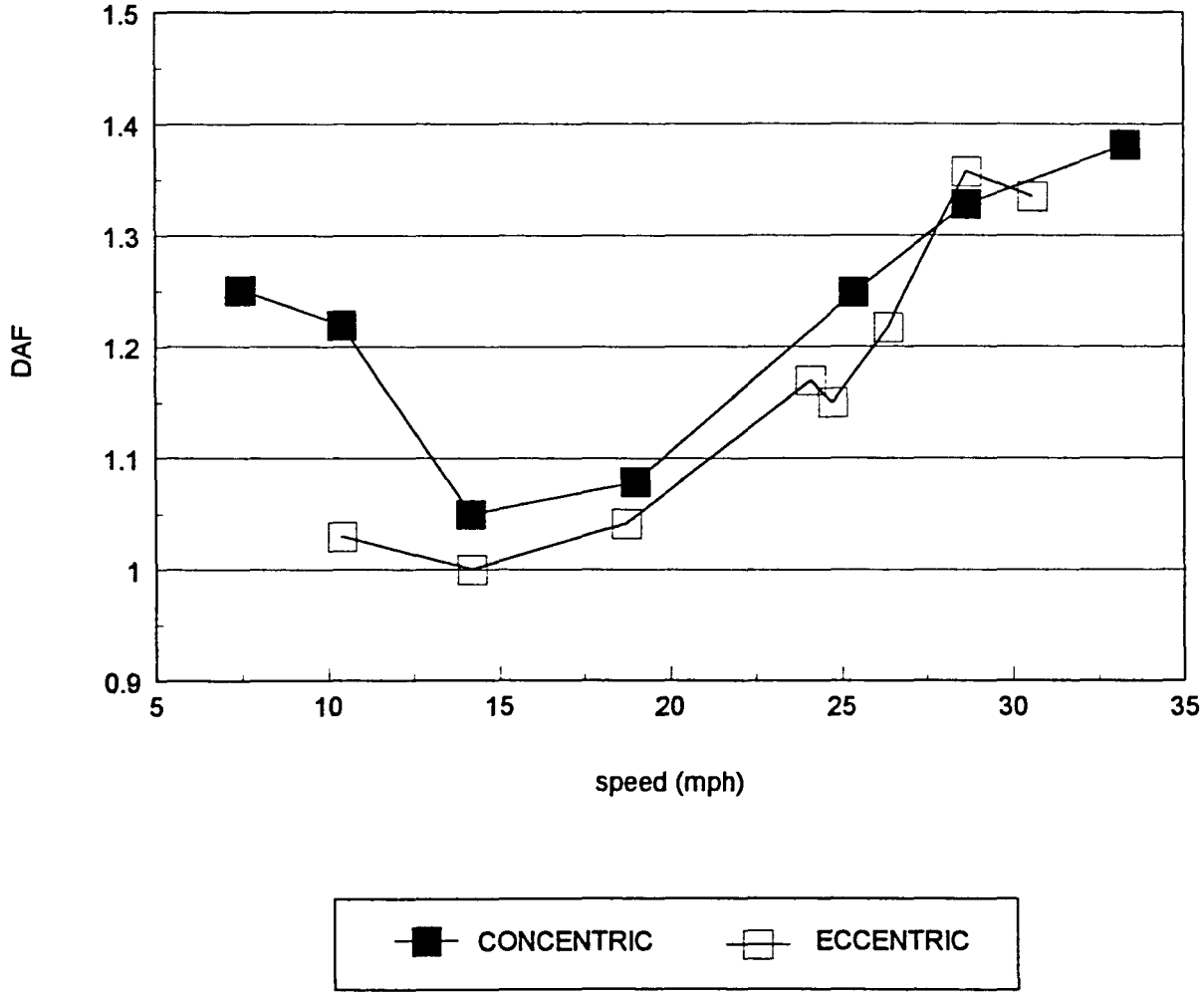

Fig. 4.12 Mud Creek Bridge - DAF plots

nanaraa.co

a) overall view of Wittson Bridge

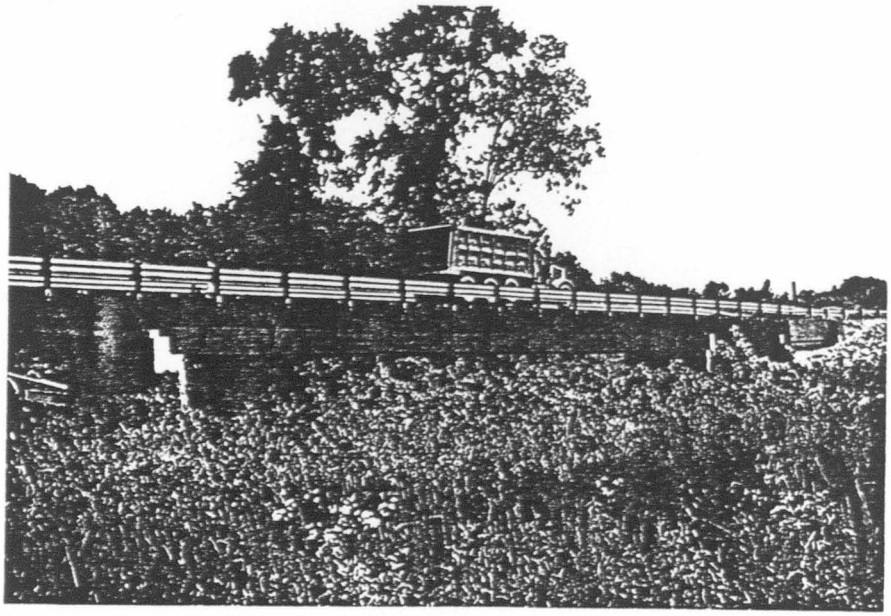

b) vehicle on Span 3

Fig. 1.13 Wittson Bridge

ınaraa.cor

4.3.1 Bridge and vehicle description

A downward grade of 1.6% from North to South is constant along the bridge. The roadway approach to the bridge and the bridge surface are paved. The surface conditions of the approach road could be characterized as very good. The approach beyond 600 ft on the northern side of the bridge is a gravel road.

The layout of the bridge and instrumentation used appear in Fig. 4.14. The cross section is shown in Fig. 4.15. The deck panels are 25 ft long, 48 in. wide and 5 in. deep. The deck is supported by four stringers at 51 in. on centers. The cross section of each is 43 in. deep and 6.75 in. wide.

The test truck was a three axle dump truck with 194 in. between the steering axle and the first rear tandem axle (dimension 'a' in Fig. 4.2) and 53 in. between the rear tandem axles (dimension 'b' in Fig. 4.2). The axle loads W1, W2 and W3 were 18.68 kips, 19.27 kips and 19.27 kips, respectively; total truck weight thus was 57.22 kips.

4.3.2 Discussion of the results

4.3.2.1 Bridge free vibration response and vehicle vibration

Due to a certain degree of rotational continuity exhibited by the bridge, the free vibration record was disturbed by the presence of the vehicle on the subsequent spans and it was possible to determine only the fundamental frequency of the bridge. The plot of the accelerometer record and the frequency content are shown in Fig. 4.16 with a fundamental frequency of 5.9 Hz. The structural damping was evaluated from the plot in Fig. 4.16a

nanaraa.co

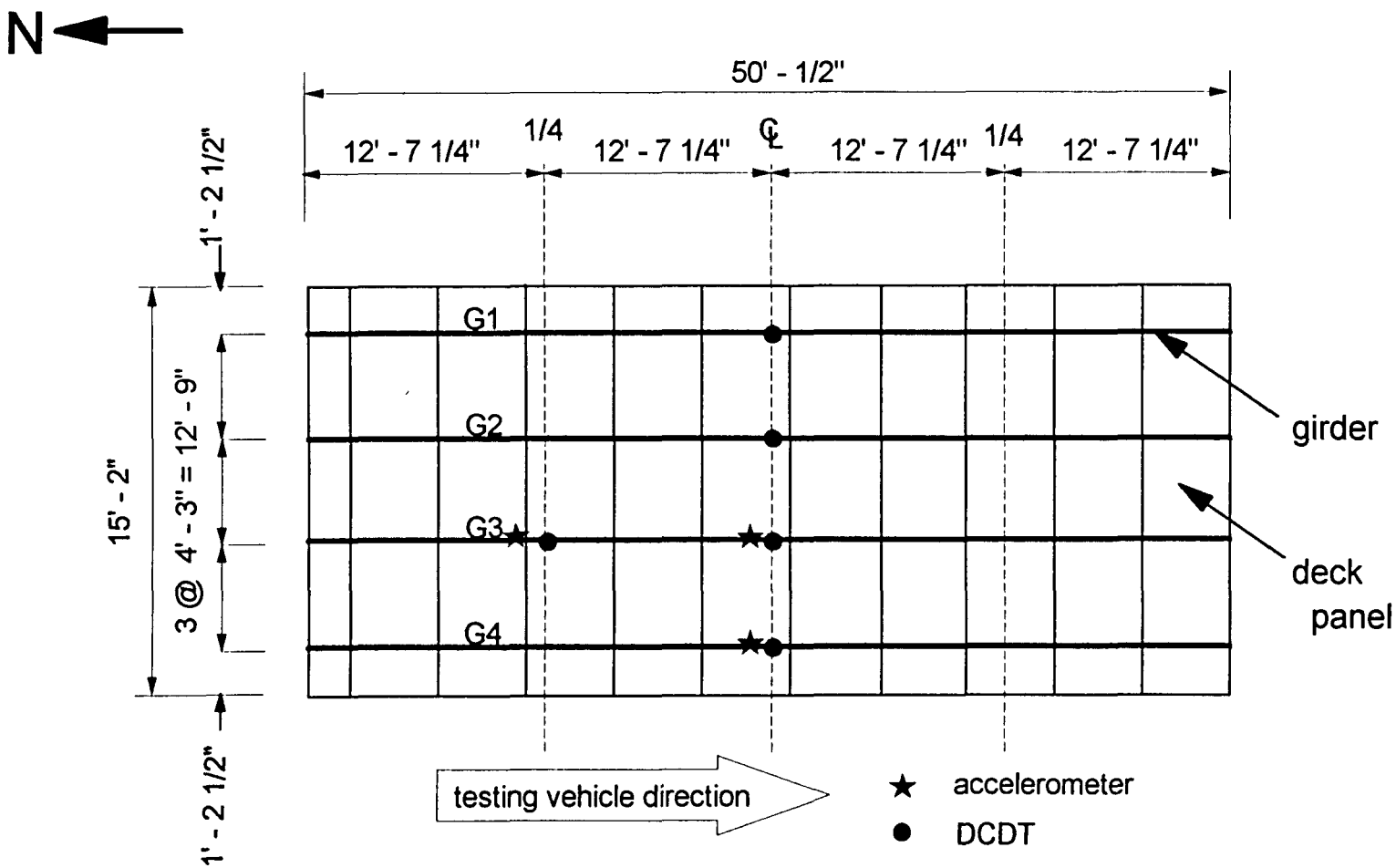

Fig. 4.14 Layout and instrumentation on Span 1 of Wittson Bridge

nanaraa.co

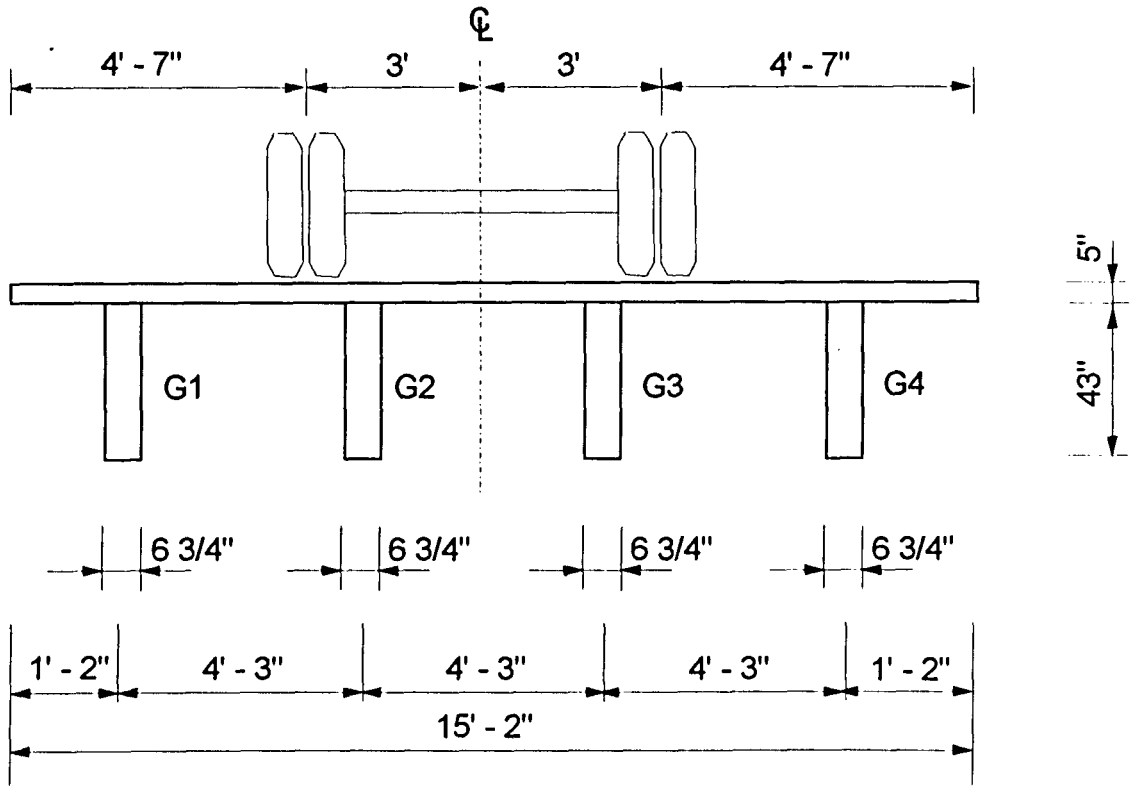

Fig. 4.15 Cross section dimensions and transverse position of the vehicle on Span 1 of Wittson Bridge

nanaraa.co

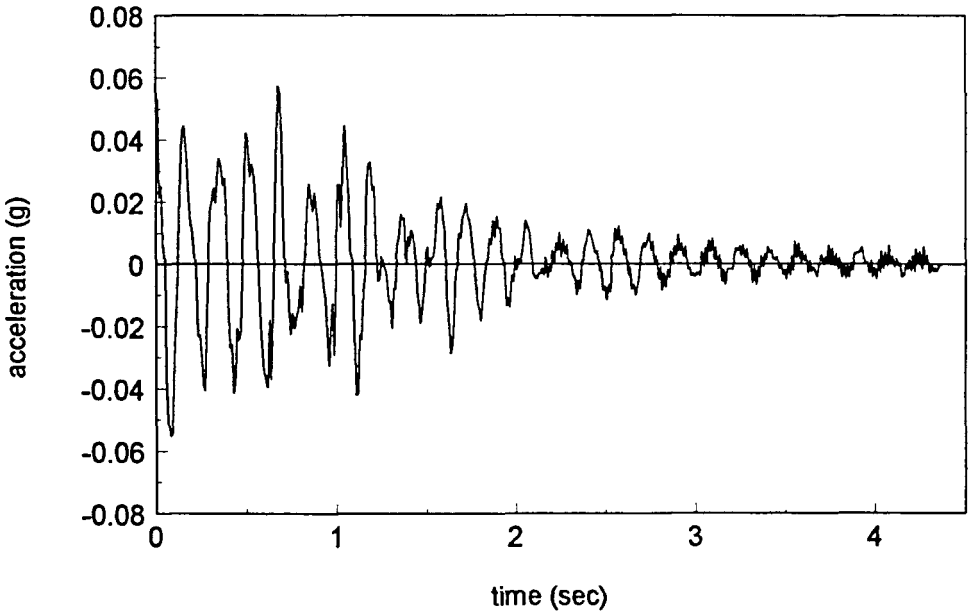

a) free vibration record

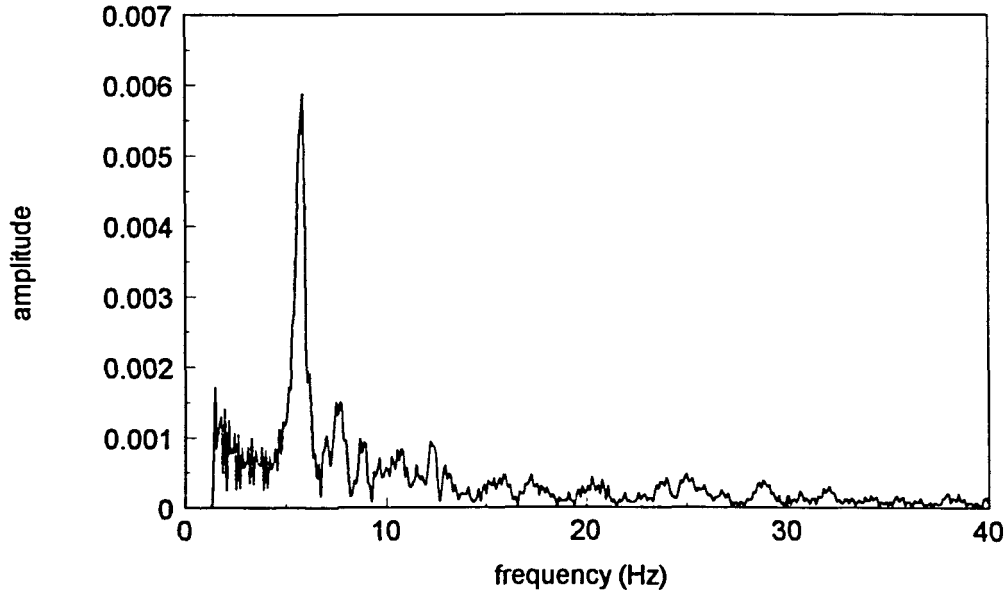

b) frequency content

Fig. 4.16 Span 1 of Wittson Bridge - free vibration record and frequency content

nanaraa.co

using the logarithmic decrement method. The calculated structural damping was found to be 4.3% of critical.

Frequencies inherent to the vehicle were determined while the truck was driven on the approach roadway. Plots of acceleration and frequency content for accelerometers A1 and A2 appear in Fig. 4.17. The frequency of the body bounce was found to be 3.1 Hz and the frequency of axle hop was found to be 10.7 Hz.

4.3.2.2 Forced vibration response

Concentric tests with in situ and bump approaches were performed. The transverse position of the vehicle is shown in Fig. 4.15. Plots of the bridge deflection against the vehicle position along the bridge for the stringer with the largest observed deflections (G2) are shown in Fig. 4.18. Two different patterns of the bridge vibration can be observed at these speed intervals: low (up to 27 mph) and high (over 30 mph) speed.

The bridge response being dominated by one mode is a common observation during all tests in the low speed interval. A regular pattern of vibration can be observed at the low speeds. The frequency of the forced response is 5.3 Hz at the speed at 15I mph (Fig. 4.19a), which is close to the bridge fundamental frequency of 5.6 Hz. The frequency of the response increases as the speed of the vehicle increases. The frequency of the bridge response is 7.0 Hz at the speed of 19.5I mph (Fig. 4.19c) and 8.2 Hz at the speed of 26.3I mph (Fig. 4.19e). The same observations can be made for the bump approach conditions. The frequency of the bridge response is 5.7 Hz at the speed of 16.2B mph (Fig. 4.19b), and 7.2 Hz at the speed of 20.9B mph (Fig. 4.19d).

nanaraa.co

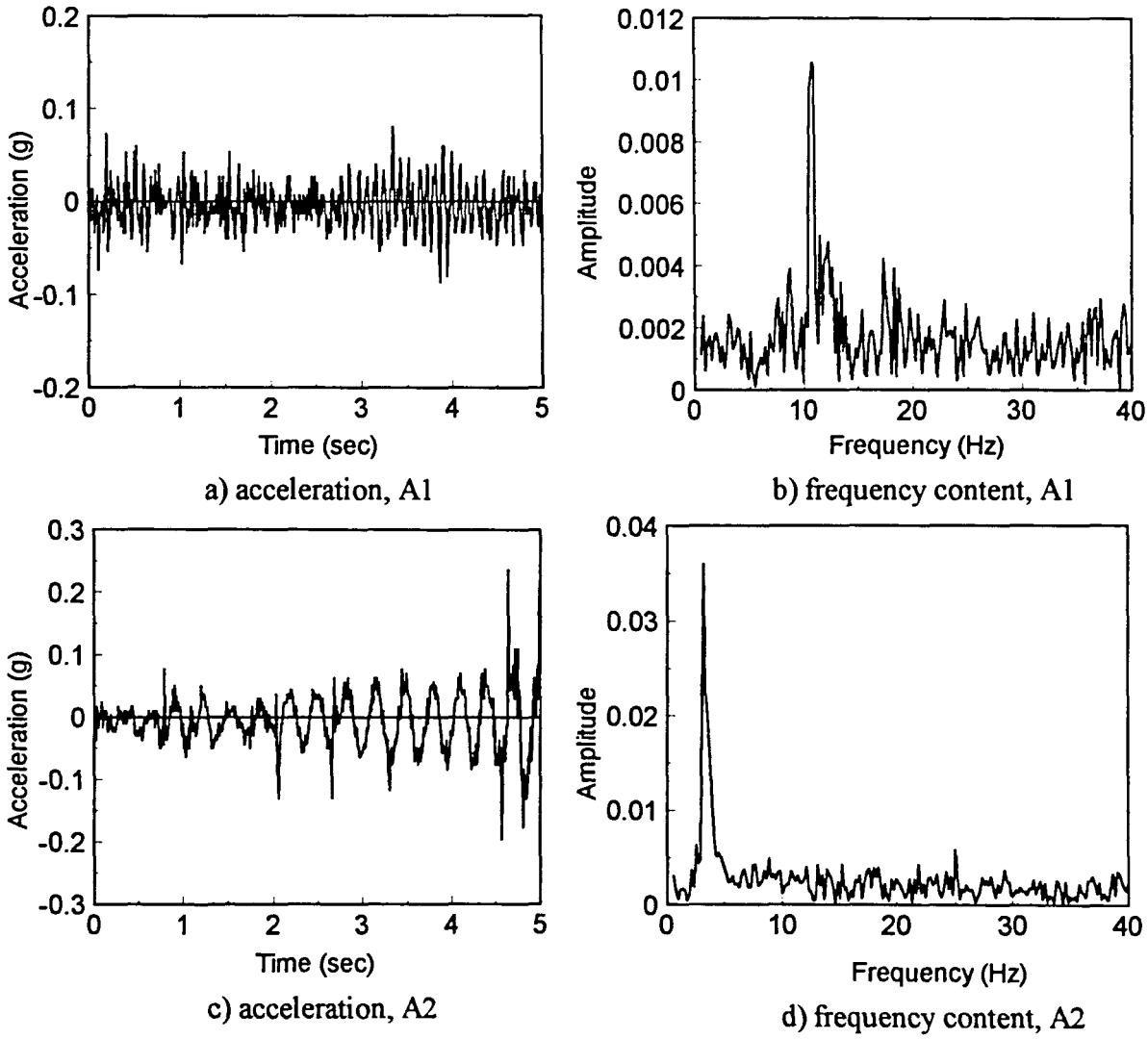

Fig. 4.17 Wittson Bridge - accelerometer data and frequency analysis for control run on roadway

nanaraa.co

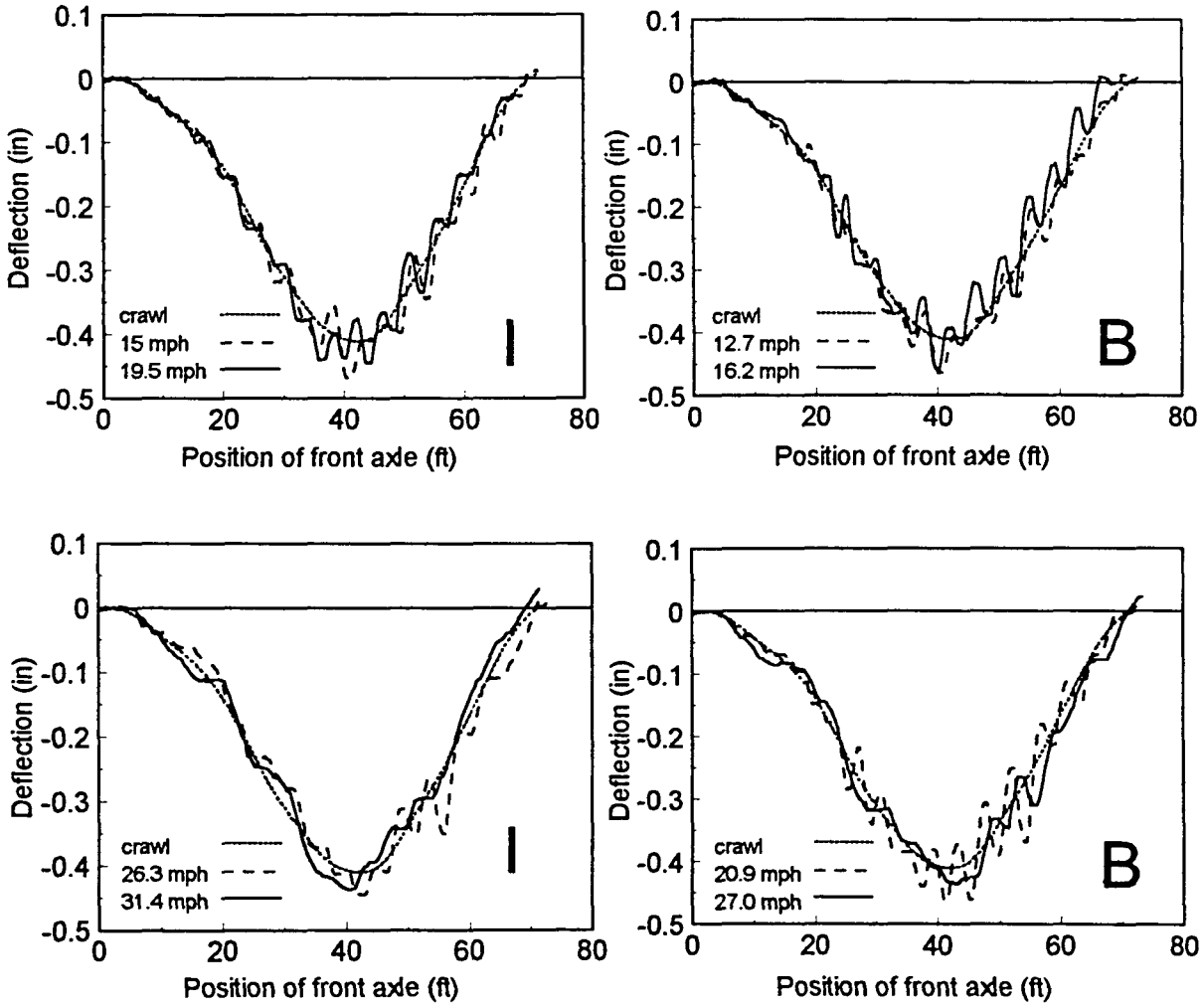

Fig. 4.18 Dynamic response for Span 1 of Wittson Bridge - Stringer G2

nanaraa.co

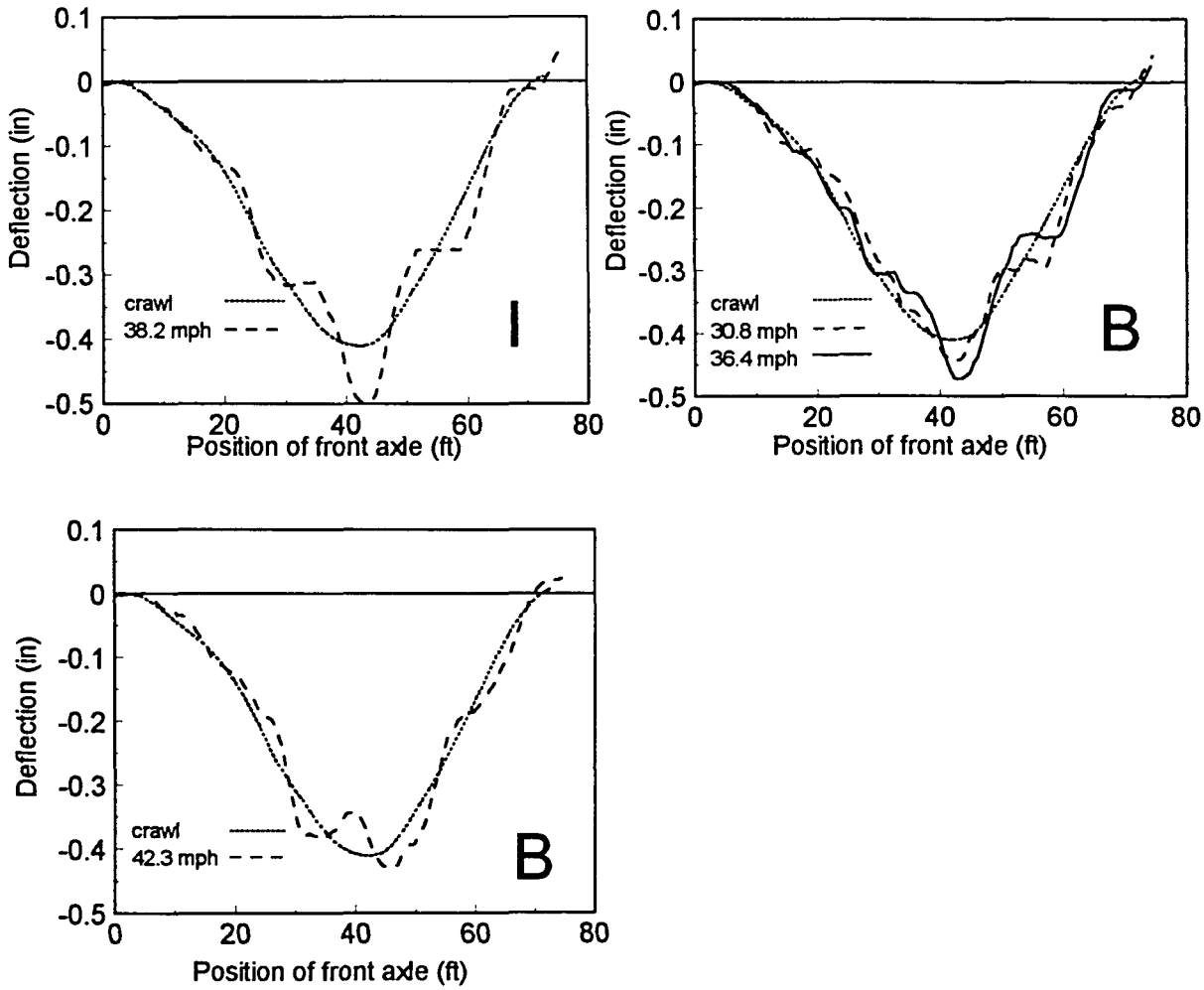

Fig. 4.18 (continued)

nanaraa.co

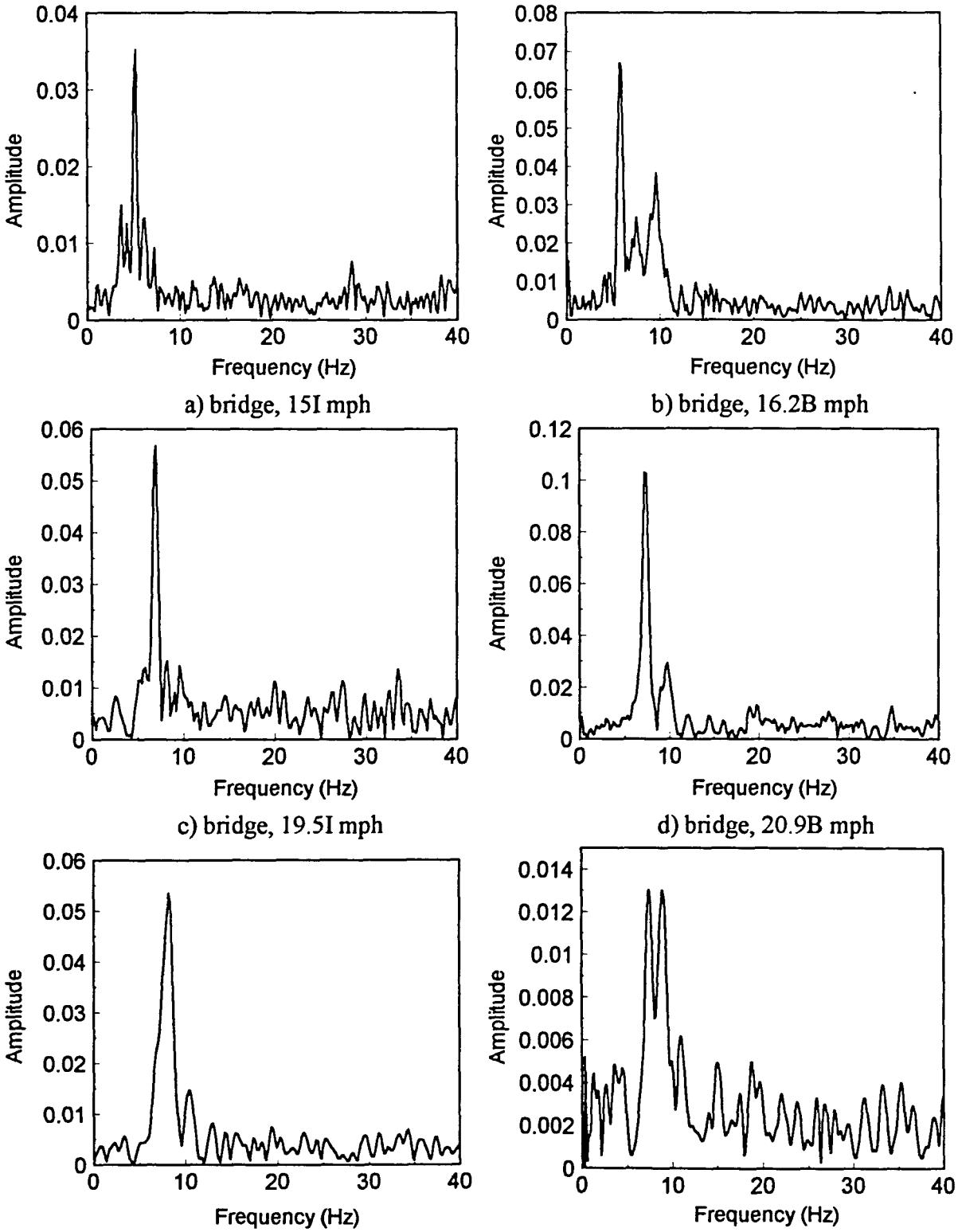

a) bridge, 15I mph

b) bridge, 16.2B mph

c) bridge, 19.5I mph

d) bridge, 20.9B mph

e) bridge, 26.3I mph

f) bridge, 27.0B mph

Fig. 4.19 Frequency contents plots for Span 1 of Wittson Bridge

nanaraa.co

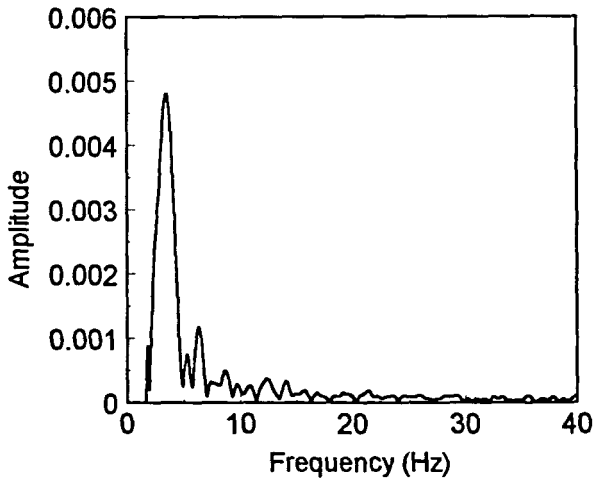

g) bridge, 38.2I mph

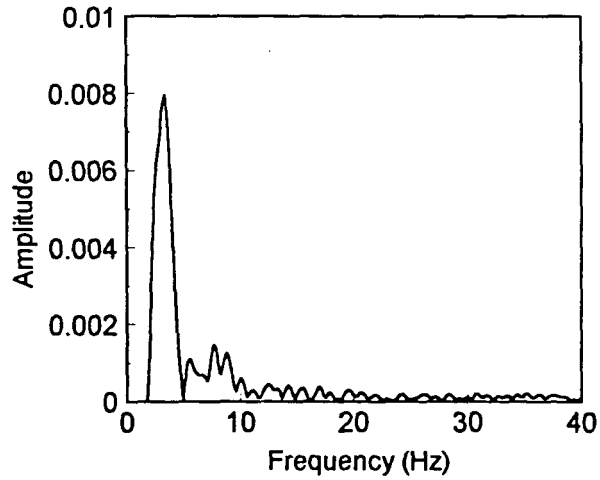

h) bridge, 36.4B mph

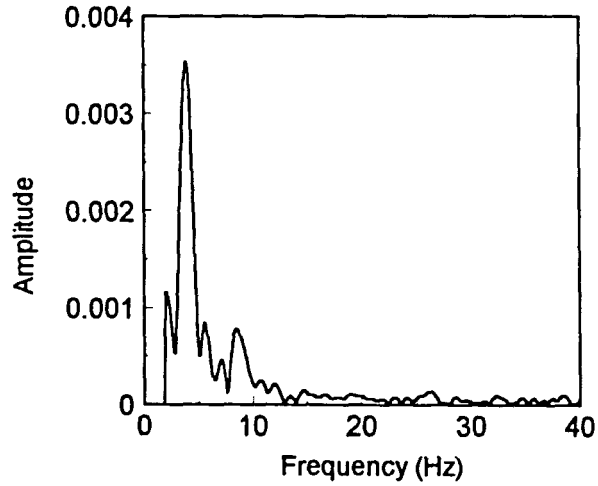

i) bridge, 42.3B mph

Fig. 4.19 (continued)

nanaraa.co

Note that the frequency of the response is close at comparable speeds regardless of the approach conditions of the bridge (5.3 Hz at 15I mph and 5.7 at 16.2B mph; 7.0 Hz at 19.5I and 7.2 Hz at 20.9B mph). A frequency of 10 Hz appears in plots 4.19b and 4.19d. This frequency is not contained in the response for in situ approach conditions; it comes from the axle hop vibration mode of the vehicle, which was excited by the bump.

A change in the pattern of bridge vibration occurs as the vehicle speed increases above 30 mph. The response is dominated by a low frequency (Fig. 4.19g-i), which is close to the body bounce frequency of the vehicle, and again increases with speed. The frequency is 3.3 Hz at the speed of 36.5B mph, 3.5 Hz at the speed of 38.2I mph, and 3.9 at the speed of 42.3B mph. This observation is true for in situ and bump approach conditions.

Analysis of the vehicle behavior appears in Fig. 4.20a-f. An observation common to all the plots is that the vehicle exhibits vibration in the axle hop mode (f = 10 Hz). This behavior remains unchanged regardless of vehicle speed, with the exception of the speed of 15I mph. where the body bounce frequency can be observed.

4.3.2.3 Dynamic amplification

The plot of the DAF for the middle stringer (G3 versus speed) is shown in Fig. 4.21. For the lower speeds, the amplification is higher for the bump condition. In the analytical study presented in Chapter 3, the observation was made that the amplification is high when the time for the two rear axles to pass a common point is equivalent to the natural period of the bridge (pseudo-resonance). Based on the natural frequency of the bridge (5.6 Hz), the natural period is 0.176 sec. If the rear axle spacing is 53 in., the speed required for the rear

nanaraa.co

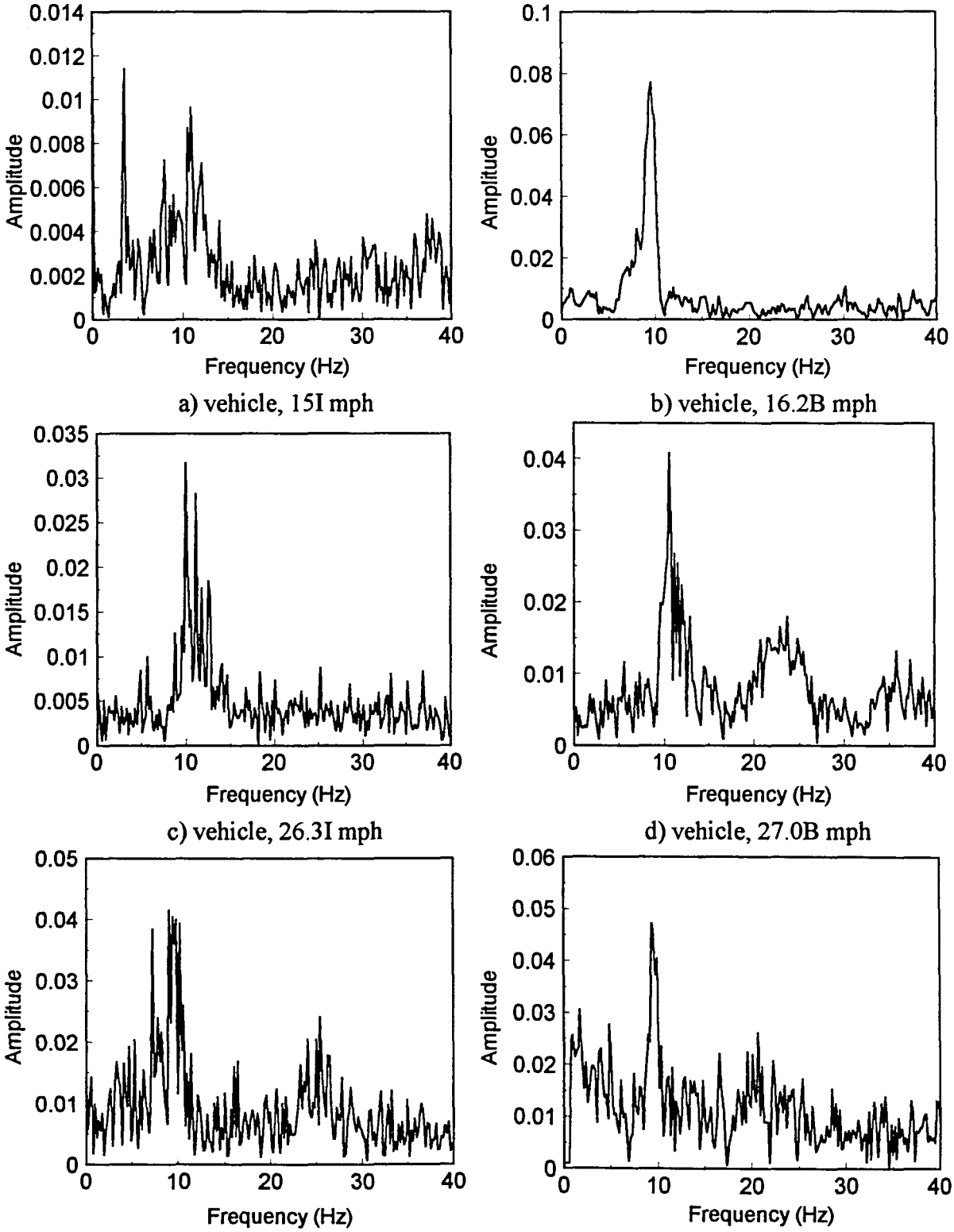

a) vehicle, 15I mph

b) vehicle, 16.2B mph

c) vehicle, 26.3I mph

d) vehicle, 27.0B mph

e) vehicle, 38.2I mph

f) vehicle, 36.4B mph

Fig. 4.20 Frequency contents plots for vehicle on Span 1 of Wittson Bridge

nanaraa.co

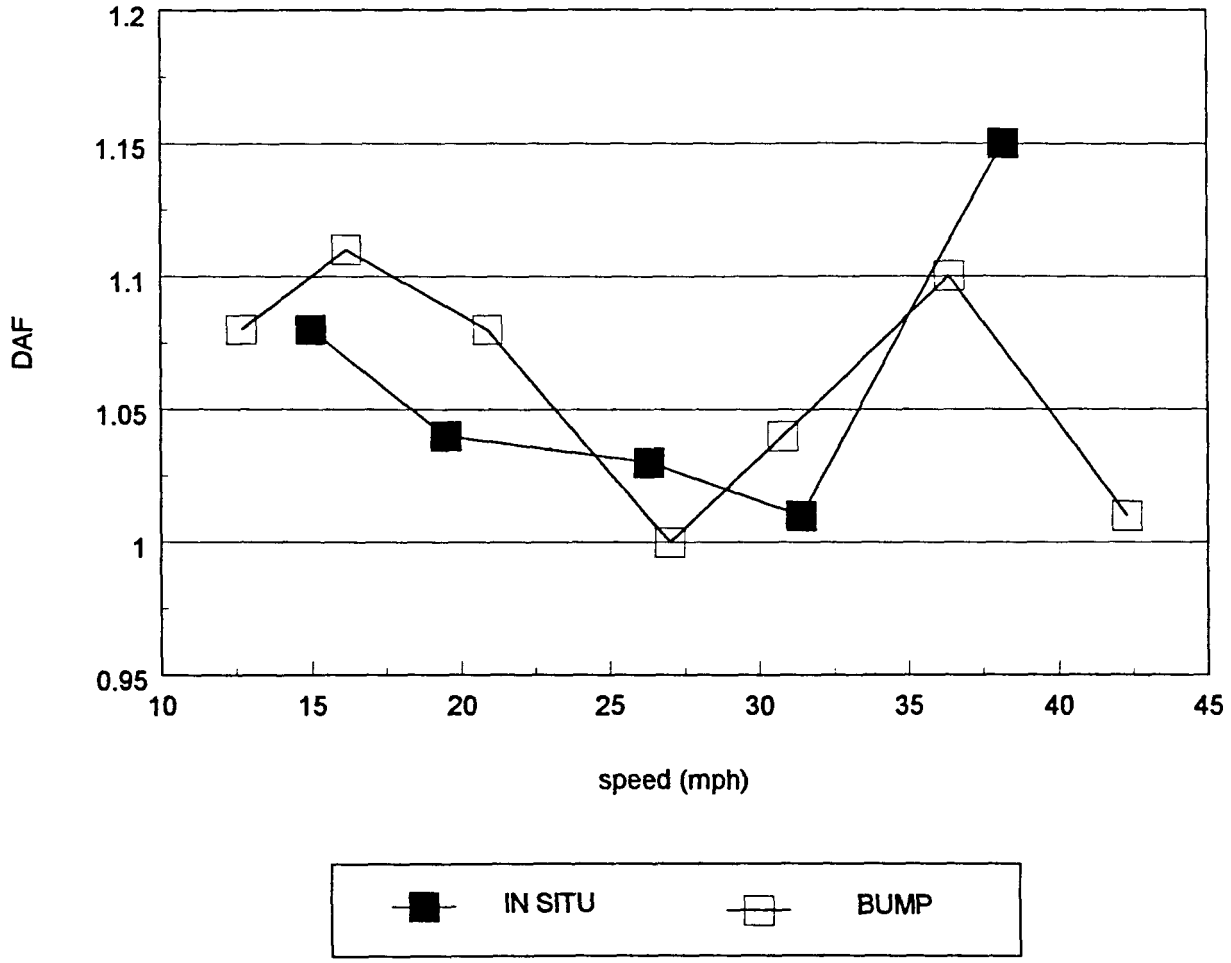

Fig. 4.21 Span 1 of Wittson Bridge - DAF plots

nanaraa.co

axles to satisfy this condition is 16.9 mph. According to the DAF plot, it is apparent that the amplification is high at this speed for the bump condition. This is logical, since the presence of the bump made the loading effect of the axles more prominent.

The bridge amplification increases after the bridge begins to exhibit vibration in low frequencies close to the vehicle body bounce (from about 25 mph). At the speed of 42.3B mph, however, the amplification is low. In the author's opinion, this fact can be inferred by observing the deflection plots in Fig. 4.18. At the speed of 36.4B and 38.2I the downward vehicle oscillation occurs at the same moment the vehicle is in the position to cause maximum static (crawl) deflection; therefore, the maximum dynamic deflection is large. At the speed of 42.3B, the vehicle oscillation goes upward for the same position of the truck. Thus, the maximum dynamic deflection is small.

4.4 Span 3 of Wittson Bridge

4.4.1 Bridge and vehicle description

The layout of the bridge and instrumentation used appear in Fig. 4.22 and the cross section is shown in Fig. 4.23. The stringers is made of Southern Yellow Pine (E_L = 1,690 to 1,930 ksi). The deck panels are 25 ft long, 48 in. wide, and 5 in. deep. The deck is supported by four stringers at 51 in. on center. The cross section of each stringer is 43 in. deep and 6.75 in. wide. Other details pertaining to the bridge and vehicle are equal to those of Span 1 of Wittson Bridge.

nanaraa.co

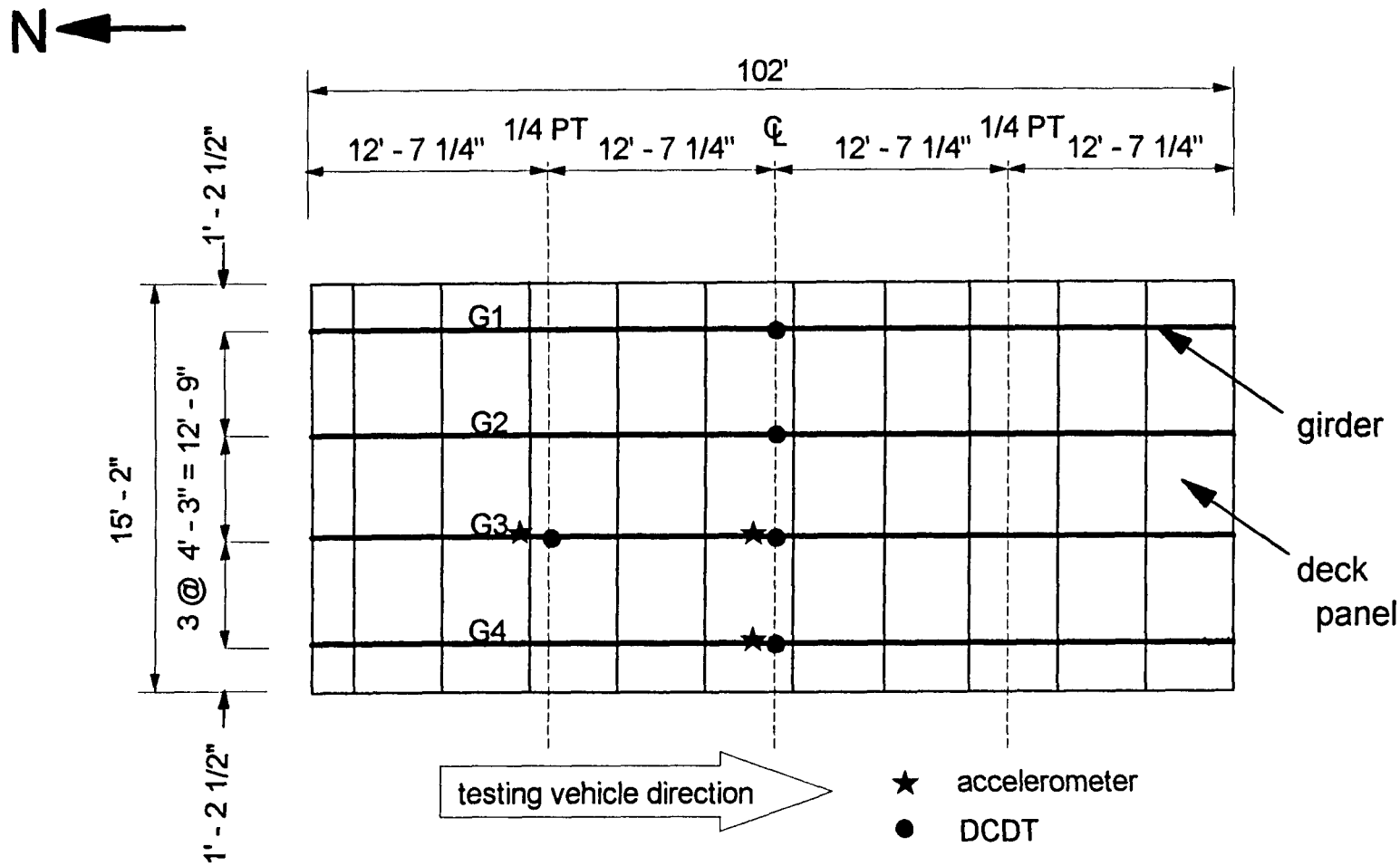

Fig. 4.22 Layout and instrumentation on Span 3 of Wittson Bridge

nanaraa.co

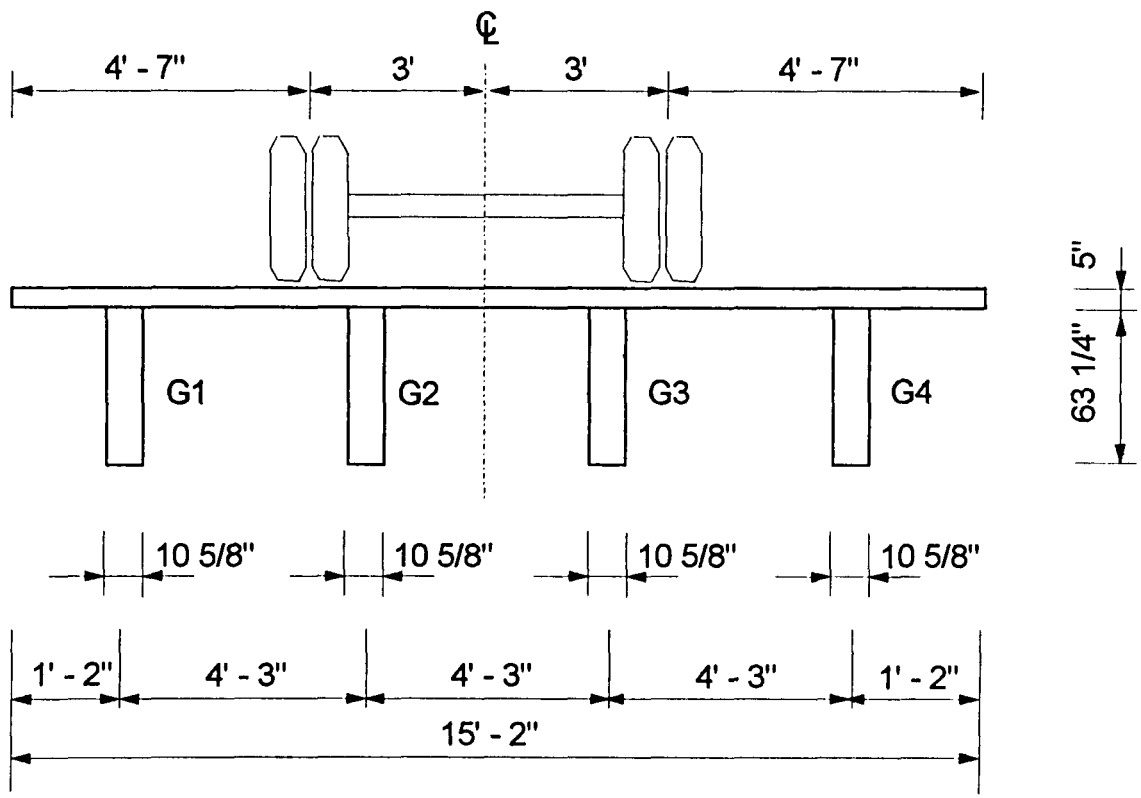

Fig. 4.23 Cross section dimensions and transverse position of the vehicle on Span 3 of Wittson Bridge

nanaraa.co

4.4.2 Discussion of the results

4.4.2.1 Bridge free vibration response and vehicle vibration

Three normal mode frequencies were determined from the free vibration record. Figure 4.24a,c and d shows frequencies of 2.8 Hz, 8.8 Hz, and 10.6 Hz, respectively. A computer model of the bridge was created to identify mode shapes of the observed frequencies (see Appendix 3). Table 4.1 presents a comparison of results of the computer analysis and field observation. Structural damping was evaluated using free vibration records as shown in Figs. 4.24b and d. The calculated structural damping was found to be 3.2% of critical.

4.4.2.2 Forced vibration response

Concentric tests with in situ and bump approaches were performed. The plots of the bridge deflection versus the vehicle position along the bridge for the stringer with the largest observed deflections (G2) are shown in Fig. 4.25. Selected typical frequency content plots of the bridge forced vibration response are shown in Fig. 4.26. The bridge response is dominated by one mode at the speed of 8.9I mph (Fig. 4.26a). The second longitudinal mode appears at the speed of 24.6I mph (Fig. 4.26c). The second longitudinal mode is excited at the speeds of 9.7B mph and 15.6B mph. Only lower speeds have dominant frequencies of vibration. At the high speeds no particular frequency dominates the response. The vehicle response is dominated by the body bounce frequency at the lowest speed (8.9I and 9.7B) and at speeds between 25 and 30 mph (Fig. 4.27). At other speeds (10 to 25 mph) the response is dominated by the axle hop.

nanaraa.co

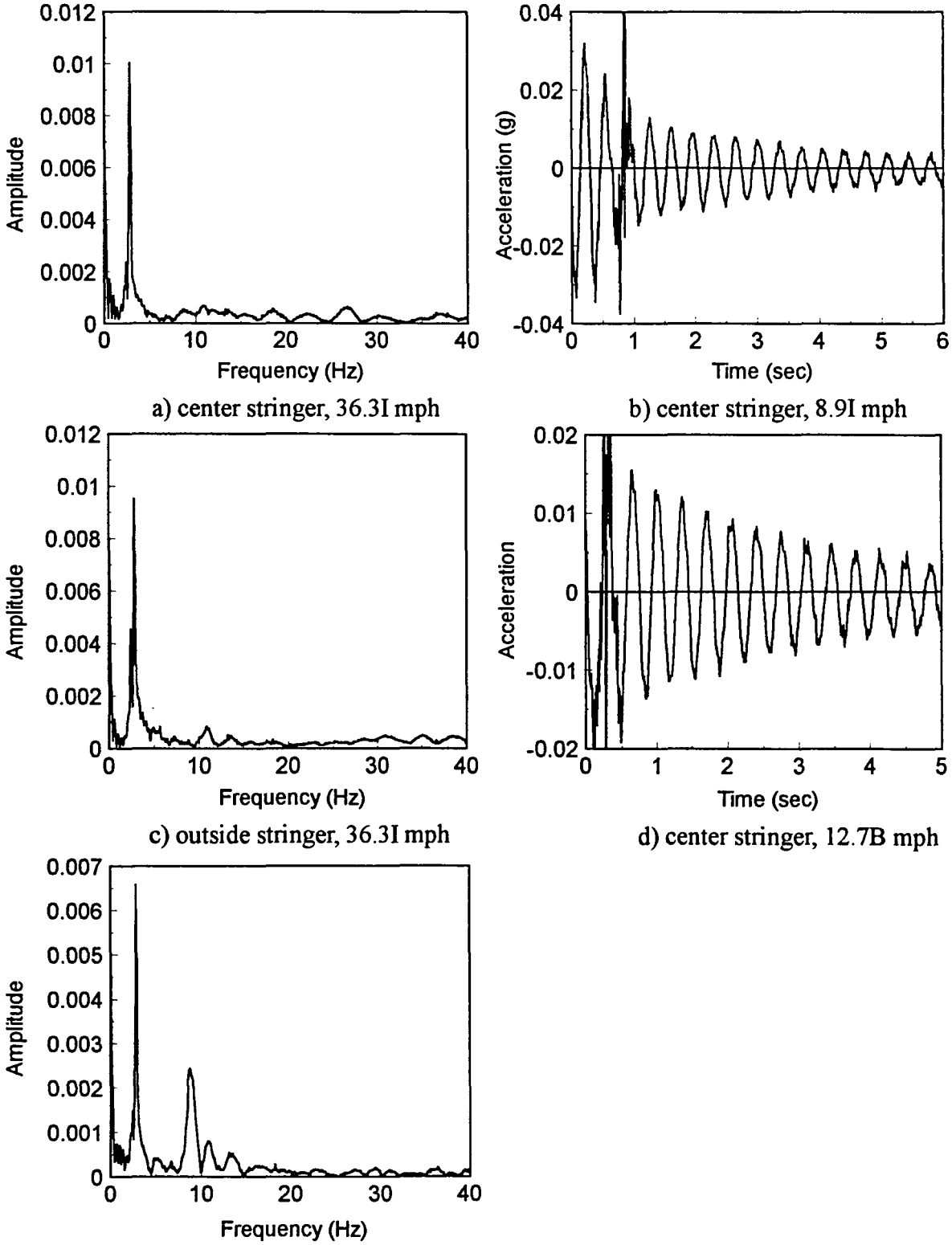

a) center stringer, 36.3I mph

b) center stringer, 8.9I mph

c) outside stringer, 36.3I mph

d) center stringer, 12.7B mph

e) quarter span, 36.3I mph

Fig. 4.24 Span 3 of Wittson Bridge -frequency content and acceleration plots of free vibration

nanaraa.co

Table 4.1 Comparison of computed and experimentally observed modal frequencies for Wittson Bridge - Span 3

COMPUTER RESULT [Hz]	FIELD OBSERVATION [Hz]	DESCRIPTION	SHAPE
2.5	N/A	asymmetric transverse	Fig. A3.1a
2.7	2.8	first longitudinal	Fig. A3.1b
9.4	N/A	asymmetric transverse	Fig. A3.1c
9.5	8.8	second longitudinal	Fig. A3.1d
11.7	11.7	symmetric transverse	Fig. A3.1e

nanaraa.co

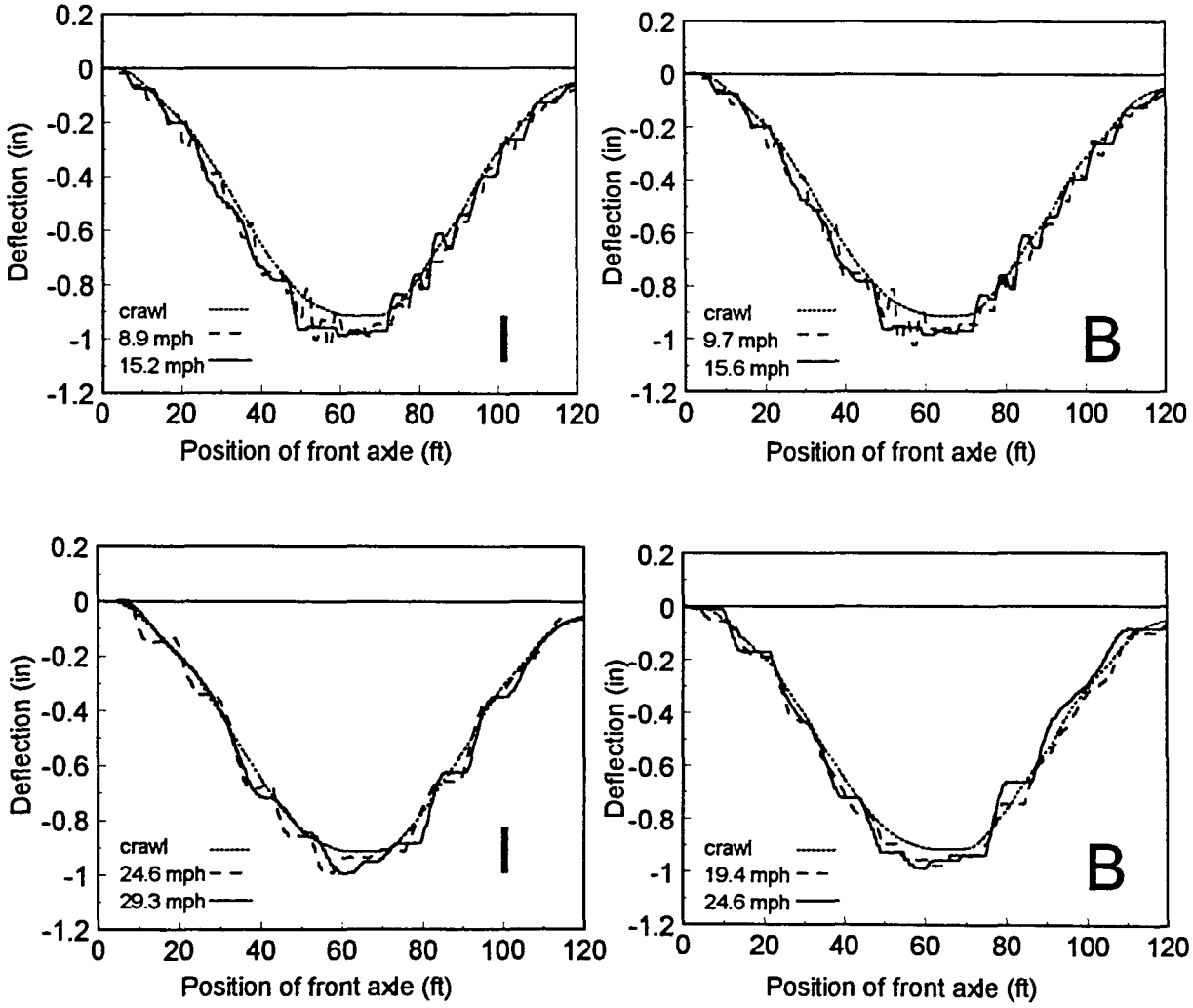

Fig. 4.25 Dynamic response for Span 3 of Wittson Bridge - Stringer G2

nanaraa.co

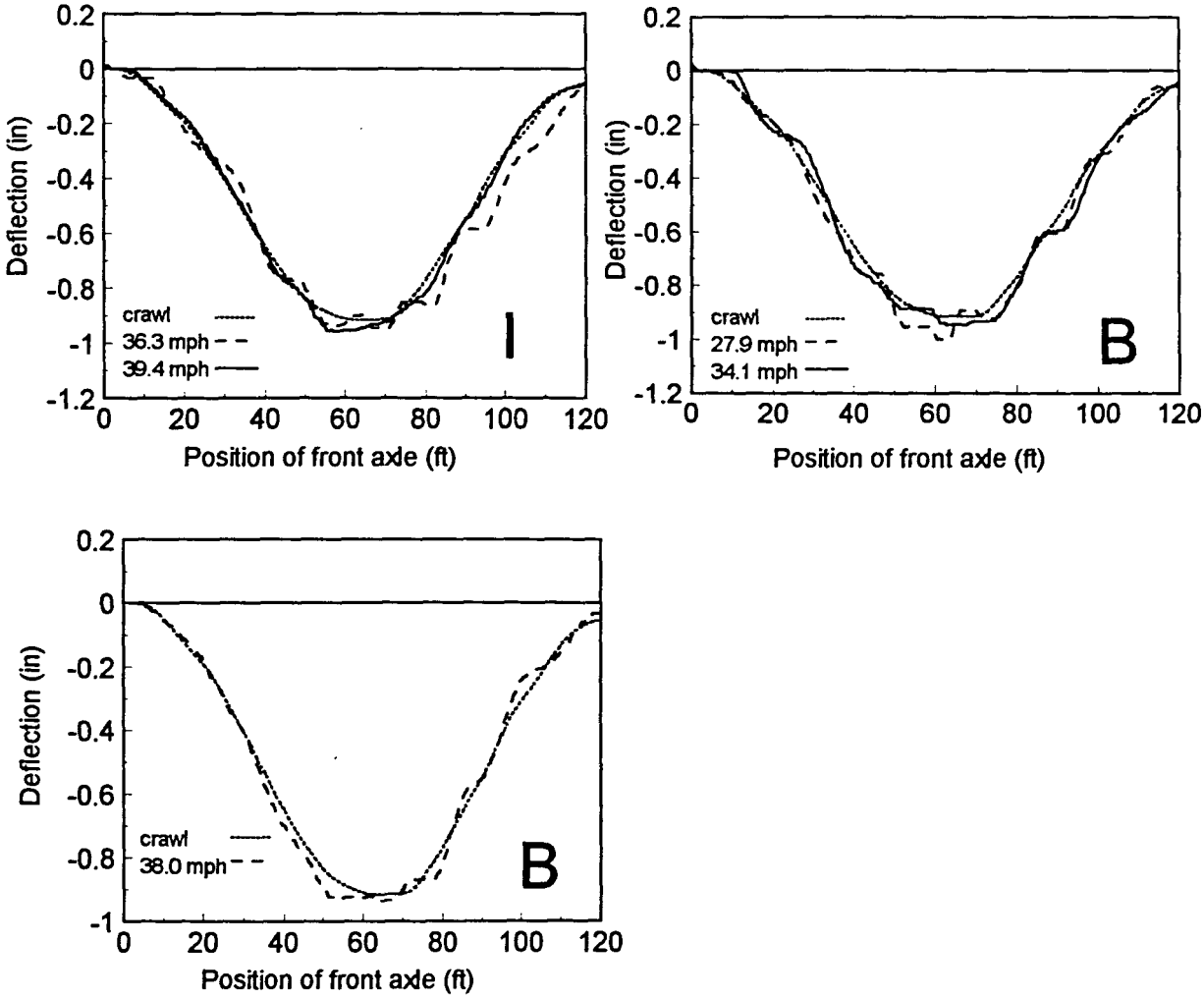

Fig. 4.25 (continued)

nanaraa.co

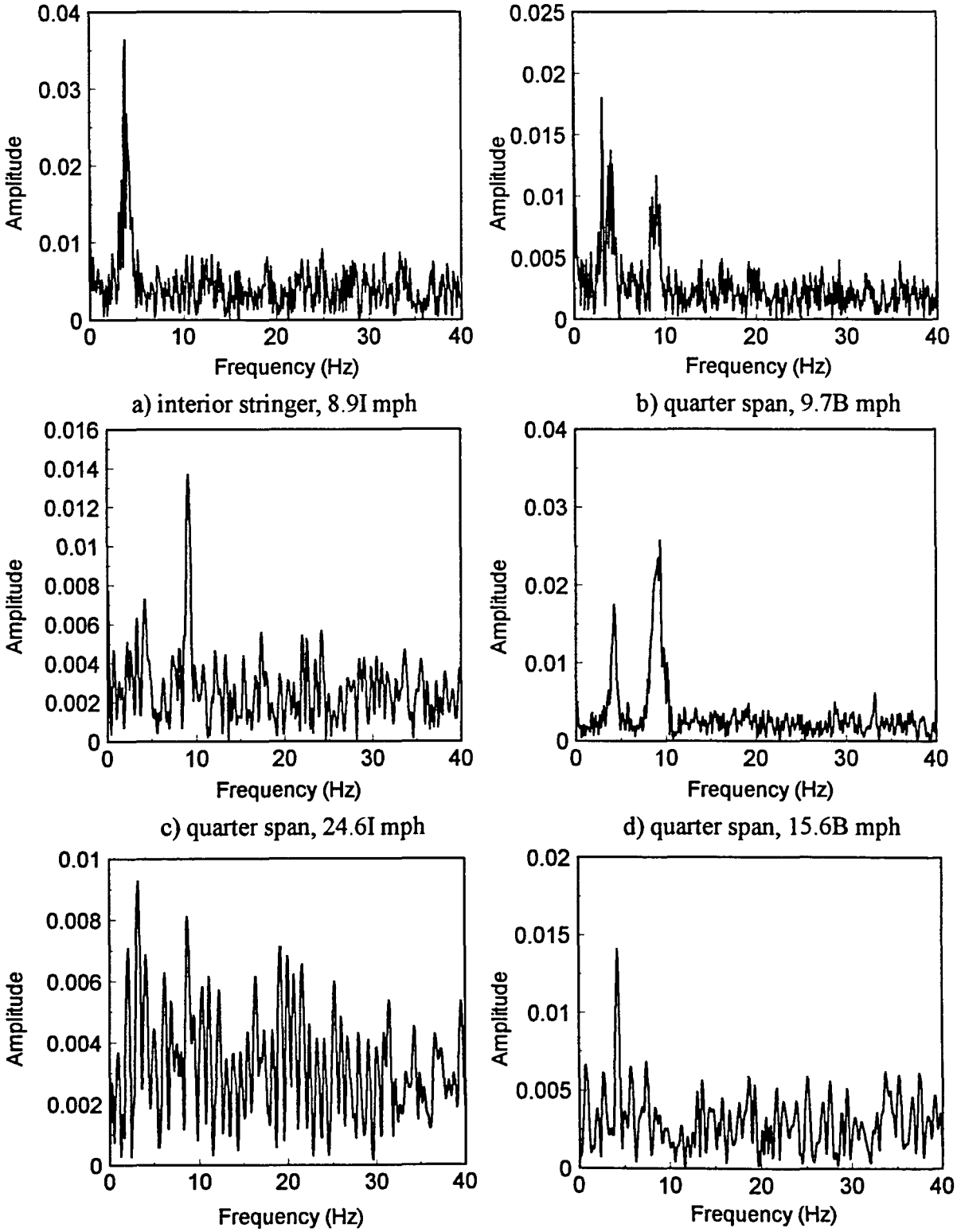

a) interior stringer, 8.9I mph

b) quarter span, 9.7B mph

c) quarter span, 24.6I mph

d) quarter span, 15.6B mph

e) interior stringer, 29.3I mph

f) interior stringer, 27.9B mph

Fig. 4.26 Frequency content plots for forced vibration of Span 3 of Wittson Bridge

nanaraa.co

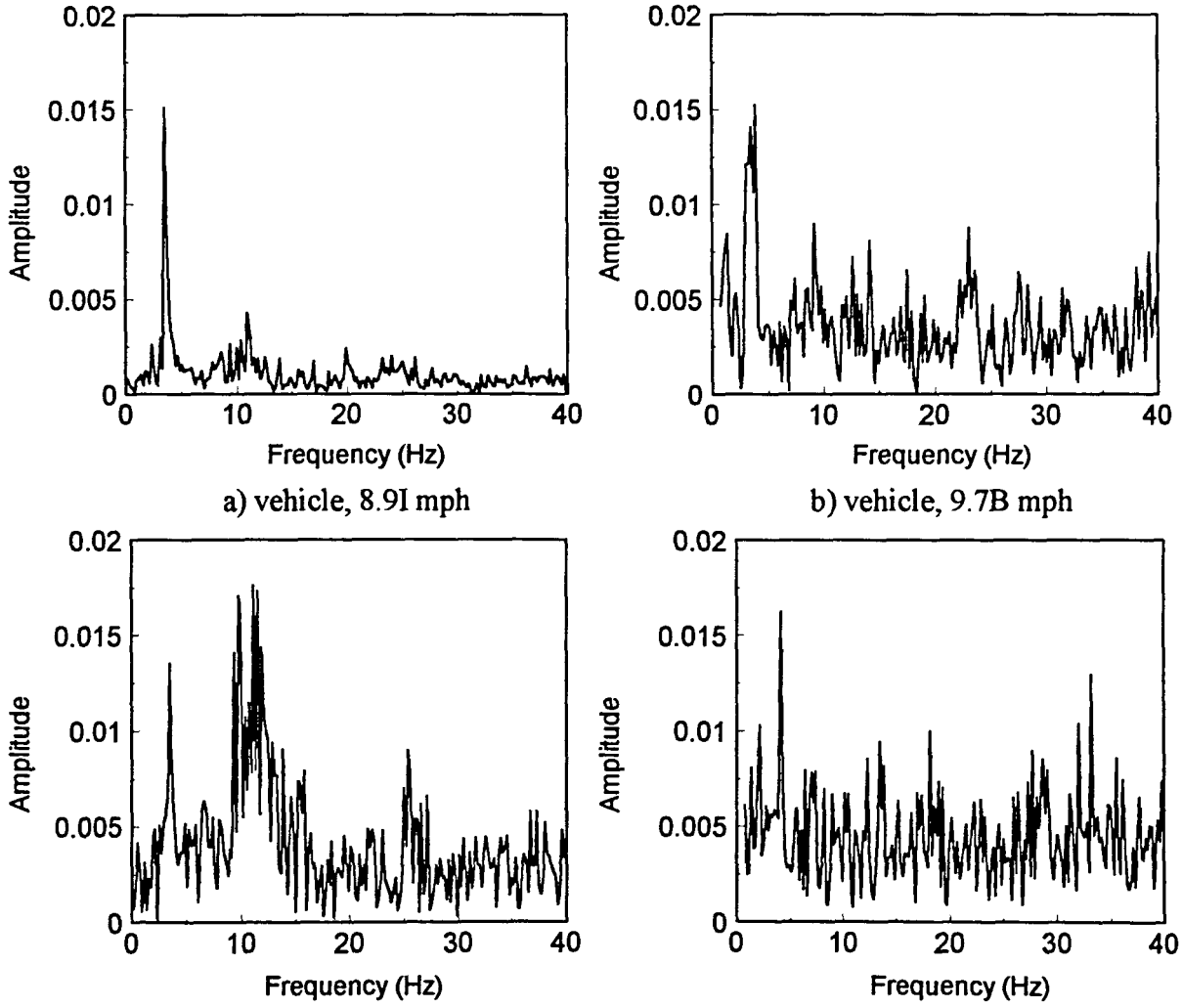

a) vehicle, 8.9I mph

b) vehicle, 9.7B mph

c) vehicle, 24.6I mph

d) vehicle, 27.9B mph

Fig. 4.27 Frequency content plots of vehicle on Span 3 ofWittson Bridge

nanaraa.co

4.4.2.3 Dynamic amplification

The plot of dynamic amplification against speed appears in Fig. 4.28. The highest amplification occurs at the lower speeds of 8.9I mph and 9.7B mph. Based on the natural period of the first mode of vibration (0.357 sec), the speed of 9 mph satisfies the condition for the pseudo-resonance with passage of the rear tandem axles. In the author's oppinion the pseudo-resonance is the reason for the high DAF. The amplification also increases at speeds around 25 to 30 mph. The body bounce dominates the response of the vehicle at these speeds.

4.5 Chambers Co. Bridge

4.5.1 Bridge and vehicle description

Chambers Co. Bridge is a 53.1 ft long single span two lane bridge. A photo of the bridge appears in Fig. 4.29. The 29 ft long, 48 in. wide and 5 in. deep deck panels are supported by six stringers at 60 in. on center. A cross section of each was 53 1/2 in. deep and 8 5/8 in. wide. The stringers are made of Southern Yellow Pine (E_L = 1,850 to 1,930 ksi). Steel guardrail on timber posts are installed on both sides of the bridge. The bridge and instrumentation layout appear in Fig. 4.30. The cross section of the bridge is shown in Fig. 4.31.

Travelling from the South, the approach roadway to the bridge has a downward grade that levels 350 ft before the bridge. According to the visual observation, the approach road surface roughness conditions could be characterized as good (asphalt

nanaraa.co

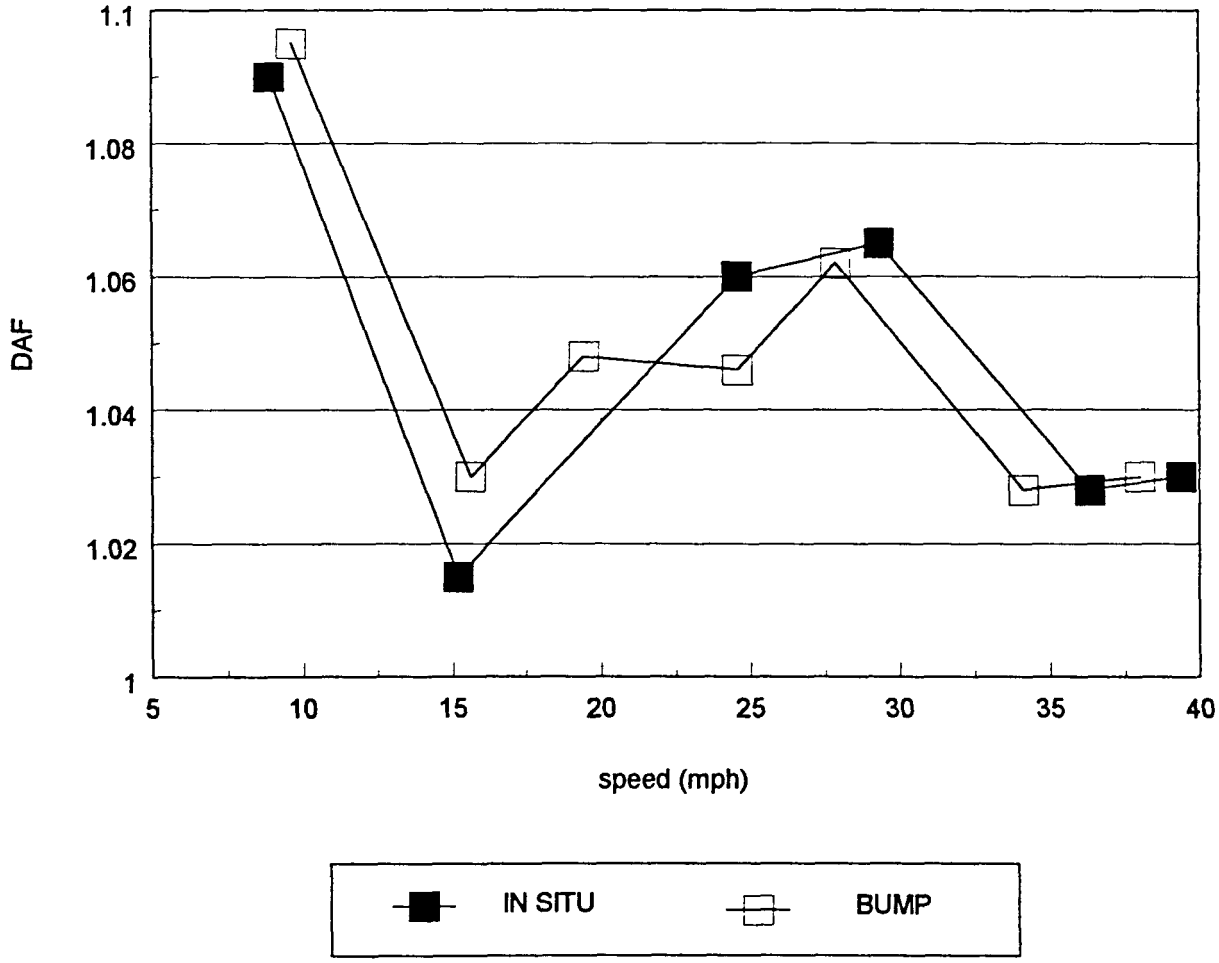

Fig. 4.28 Span 3 of Wittson Bridge - DAF plots

nanaraa.co

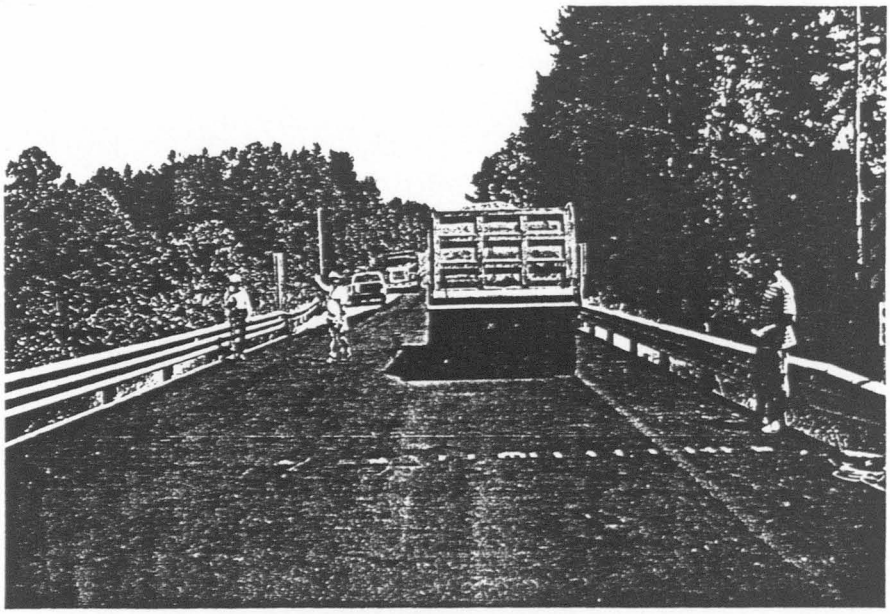

Fig. 4.29 Chambers Co. Bridge - vehicle on the bridge during crawl rest

.naraa.cor

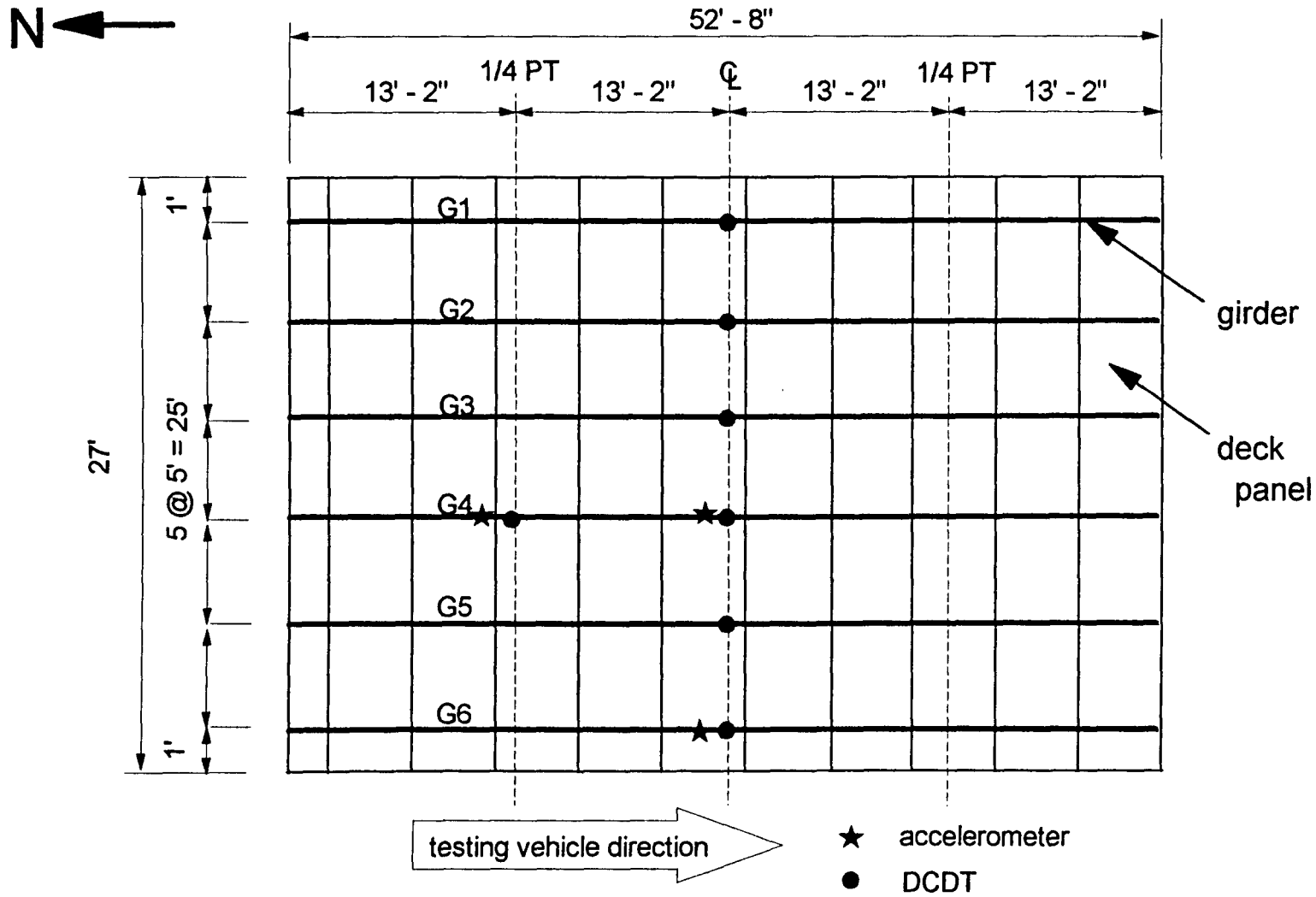

Fig. 4.30 Chambers Co. Bridge : layout and instrumentation

nanaraa.co

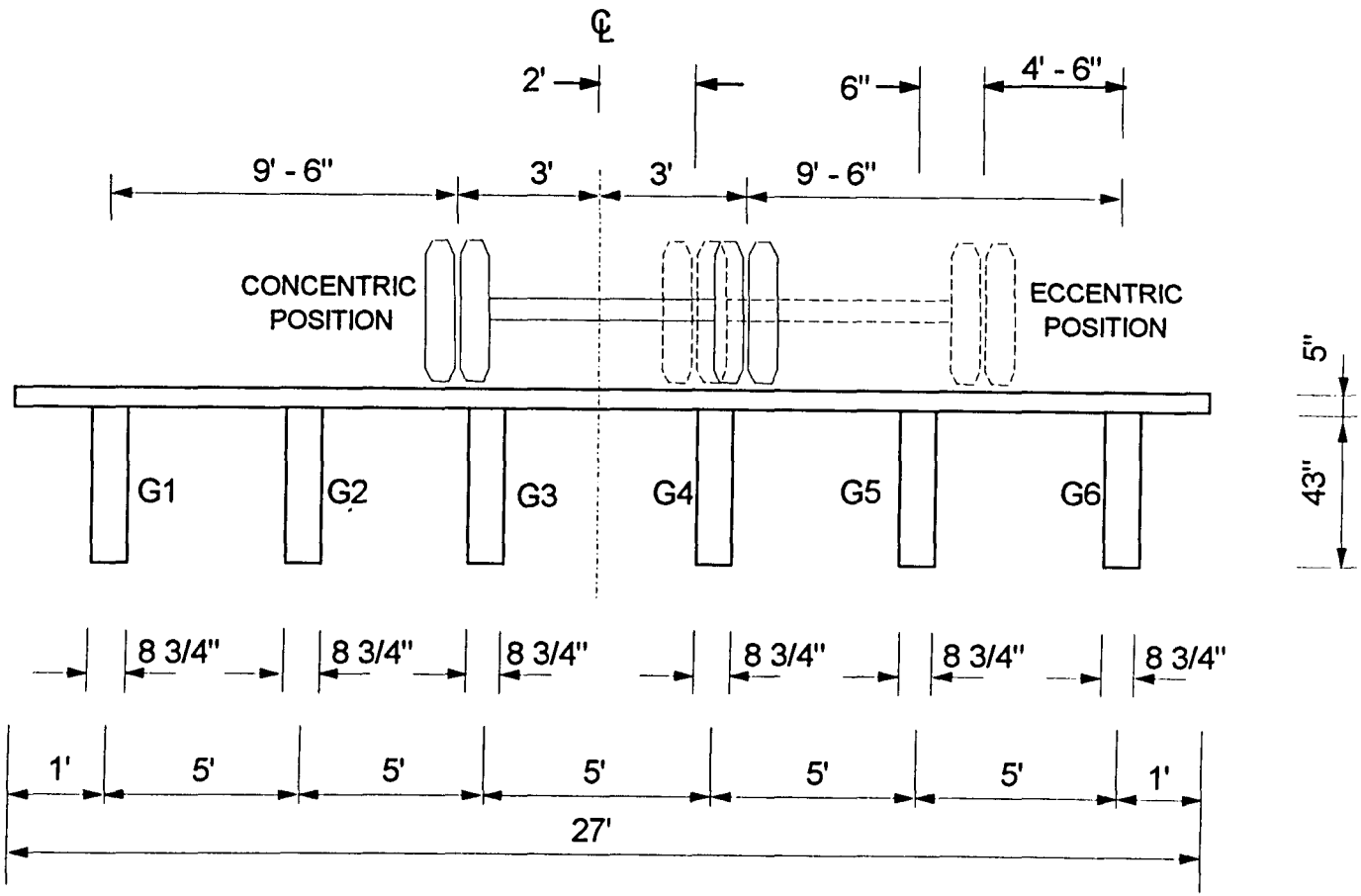

Fig. 4.31 Chambers Co. Bridge - cross section dimensions and transverse positions of the vehicle

nanaraa.co

pavement). The bridge pavement surface roughness could be characterized as very good. During the testing a depression about 1 in. deep developed in the middle of the immediate approach to the bridge.

The test truck was a three axle dump truck with 179 in. between the steering axle and first rear tandem axle (dimension 'a' in Fig. 4.2) and 53 in. between the rear tandem axles (dimension 'b' in Fig. 4.2). The axle loads W1, W2, and W3 were 14.3 kips, 24.8 kips, and 24.8 kips, respectively; total truck weight thus was 62.9 kips.

4.5.2 Discussion of the results

4.5.2.1 Bridge free vibration response and vehicle vibration

Four normal mode frequencies were determined from the free vibration record. Figure 4.33b, c show frequencies of 6.4 Hz, 11.0 Hz, 17.5 Hz and 21.7 Hz. A computer model of the bridge was created to identify mode shapes of these observed frequencies (see Appendix 3). Table 4.2 presents a comparison of results of the computer analysis and field observations. Structural damping was evaluated from the free vibration record in Fig. 4.33a and the calculated damping was found to be 5.8% of critical. Frequencies inherent to the vehicle were determined and the frequency of the vehicle body bounce was found to be 2.7 Hz. The frequency of the vehicle axle hop was found to be 10.2 Hz (Fig. 4.32).

4.5.2.2 Forced vibration response - concentric tests

Three types of concentric vehicle tests were performed; in situ and bump approaches and a test with an adjusted tire pressure to simulate a vehicle with a lower

nanaraa.co

Table 4.2 Comparison of computed and experimentally observed modal frequencies for Chambers Co. Bridge

COMPUTER RESULT [Hz]	FIELD OBSERVATION [Hz]	DESCRIPTION	SHAPE
6.6	6.44	first longitudinal	Fig. A3.2a
6.9	N/A	asymmetric transverse	Fig. A3.2b
10.7	11.0	symmetric transverse	Fig. A3.2c
20.8	17.1	asymmetric transverse	Fig. A3.2d
22.3	21.7	second longitudinal	Fig. A3.2e

nanaraa.co

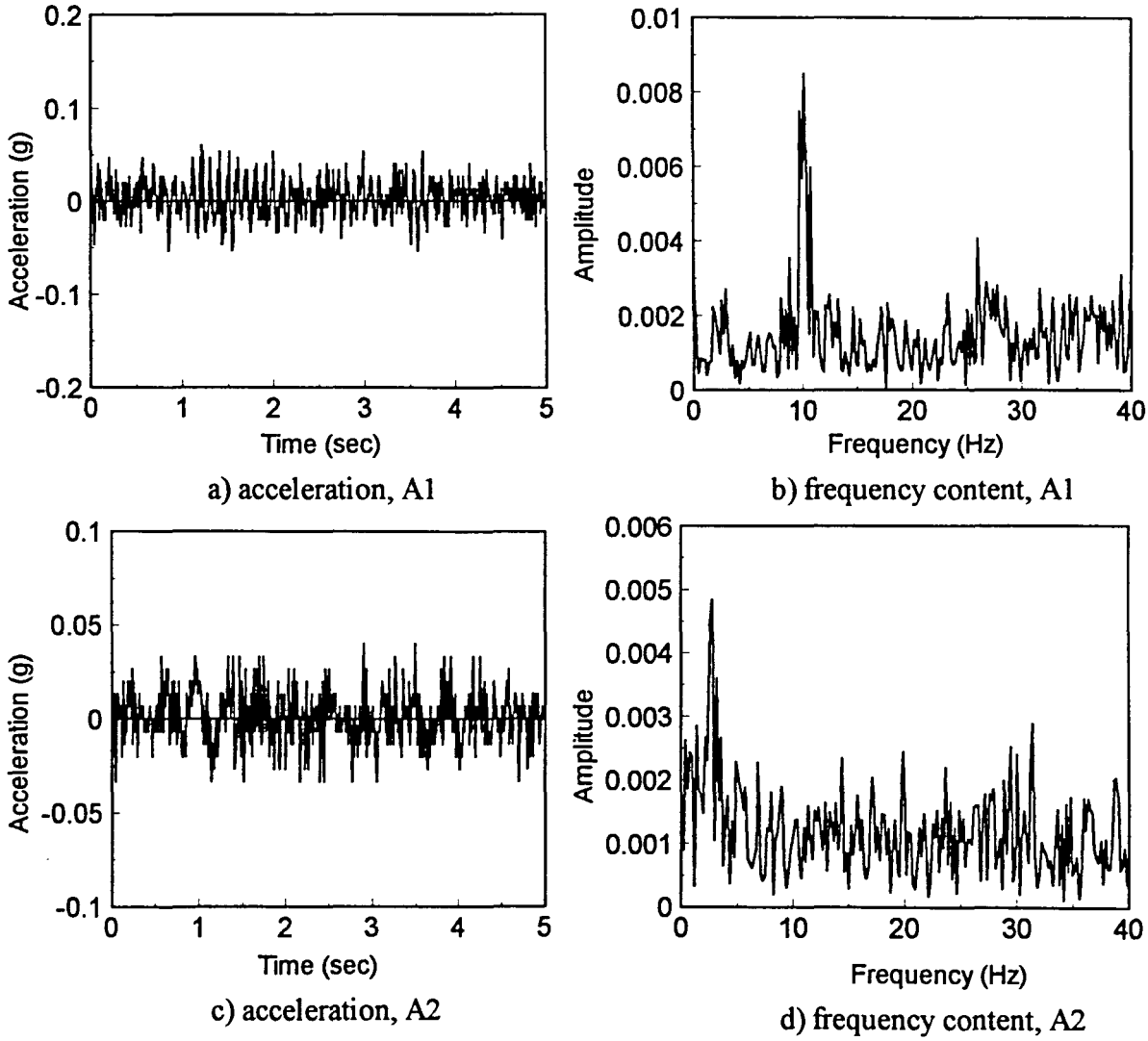

Fig. 4.32 Chambers Co. Bridge - accelerometer data and frequency analysis for control run on roadway

nanaraa.co

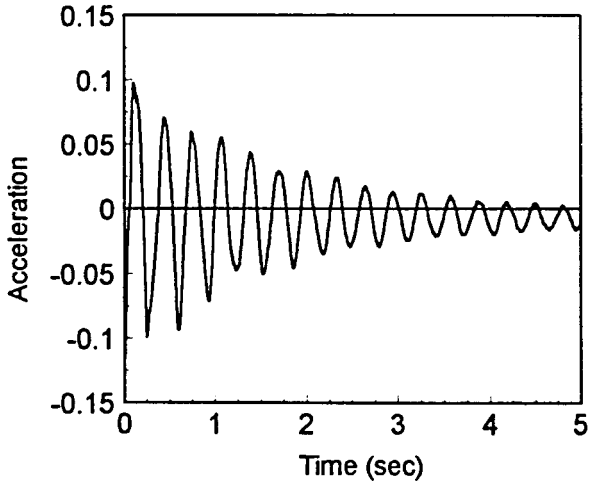

a) free vibration record of interior stringer, 23.0I mph

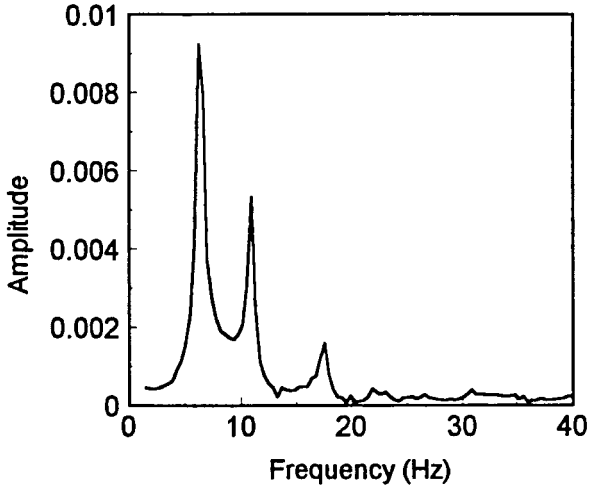

b) interior stringer, 22.0EI mph

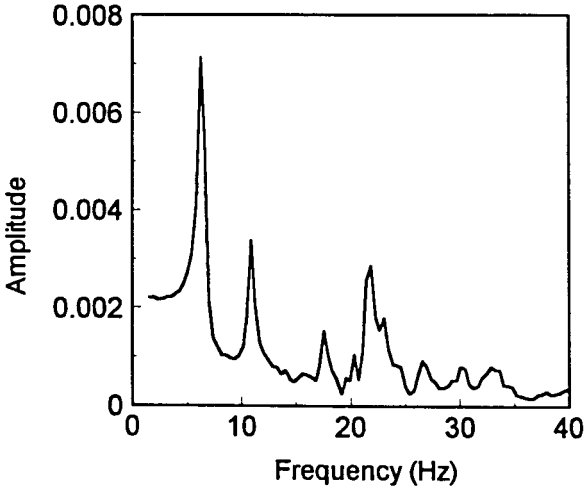

c) quarter span, 33.0I mph

Fig. 4.33 Frequency content plots and acceleration plot for Chambers Co. Bridge

nanaraa.co

vehicle tire stiffness. For this test, the pressure in the vehicle tires was decreased by 20%, from 115 psi to 90 psi. The deflections of the middle stringer G4 versus position of the vehicle along the bridge are shown in Fig. 4.34. Typical frequency content plots of the bridge response are shown in Fig. 4.35. Typical frequency content plots of the vehicle response are shown in Fig. 4.36. Three speed intervals with different bridge behavior were identified: low (up to 10 mph), medium (10 mph to 25 mph), and high (over 25 mph). A similar observation was made at Mud Creek Bridge. Generally, the bridge behavior was the same for all the three types of tests in each interval.

At the low speed interval, the bridge vibrates at the frequency of 2.7 Hz (Figs. 4.35 a,b,g). The vehicle response is dominated by the low frequency of 2.6 Hz (Fig. 4.36b). At medium speed interval, the bridge responds in frequencies of 6.9 Hz and 10.6 Hz (Fig. 4.35 c,d,h). These frequencies are close to the observed bridge mode frequencies of 6.4 Hz and 11.0 Hz. The transverse mode (f = 11.0 Hz) dominated the response for the bump tests. Also, the bridge oscillates regularly about the crawl curve. At high speeds, the pattern of vibration is different. The frequency of 2.6 Hz appears in the response along with the normal mode frequencies of 6.4 and 11.0 Hz (Fig. 4.35 e,f,i). The low frequency of 2.6 Hz is also present in the vehicle response (Fig. 4.36d).

4.5.2.3 Forced vibration response - eccentric tests

The deflections of the stringer with the largest observed deflection (G4) versus position of the vehicle along the bridge are shown in Fig. 4.37. Typical frequency content plots of the bridge response are shown in Fig. 4.38. The frequency domain analysis results

nanaraa.co

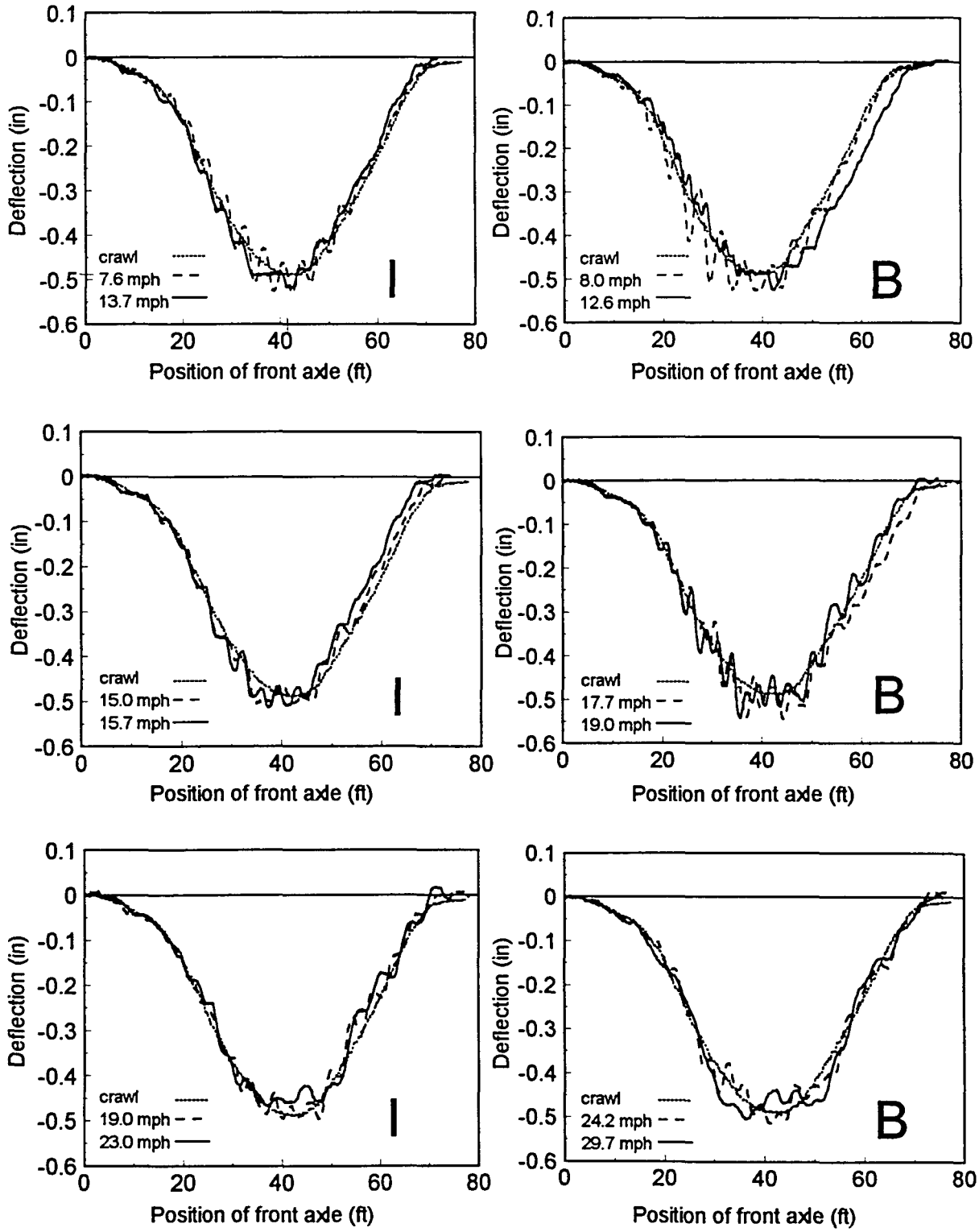

Fig. 4.34 Dynamic response for concentric tests of Chambers Co. Bridge - Stringer G4

nanaraa.co

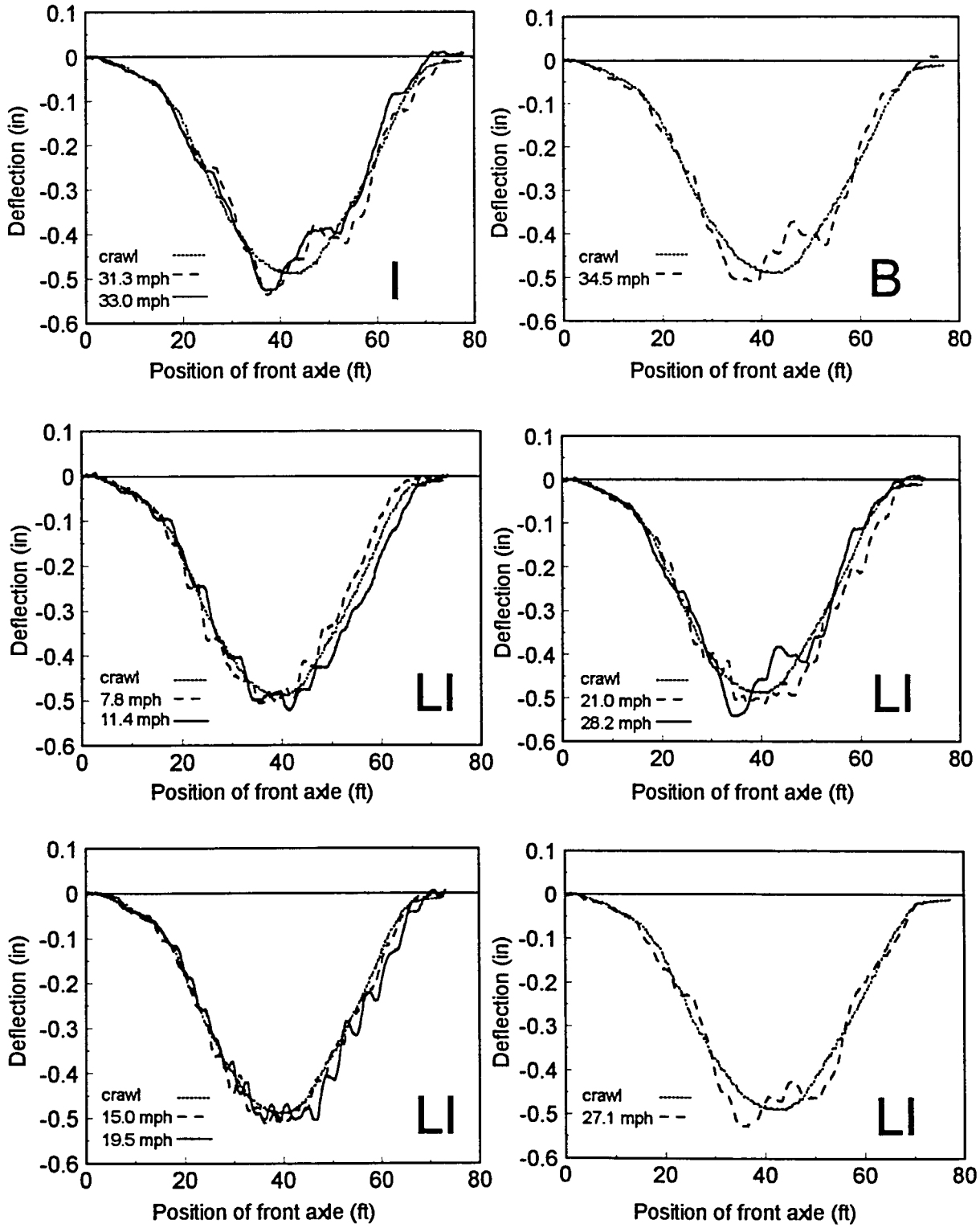

Fig. 4.34 (continued)

nanaraa.co

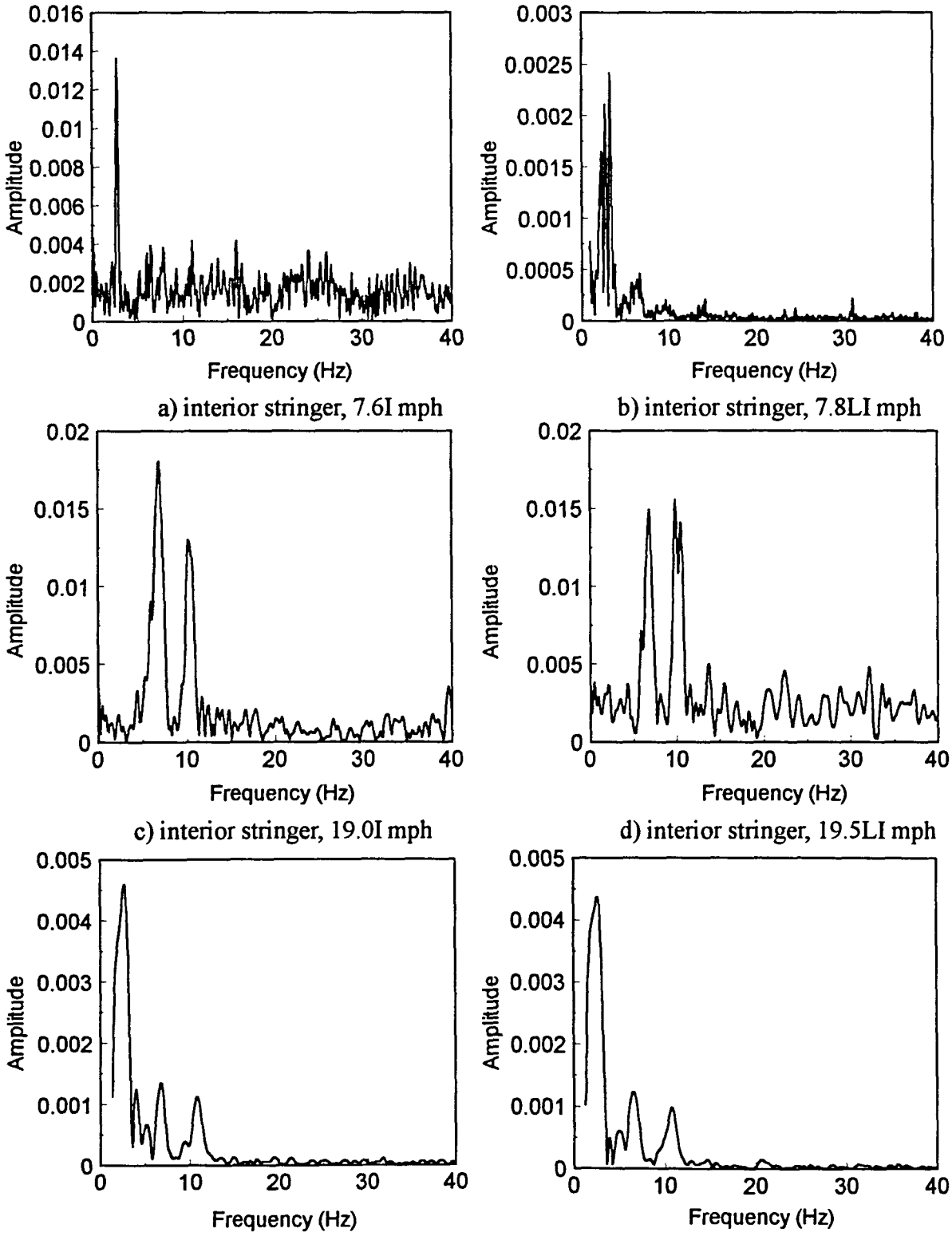

a) interior stringer, 7.6I mph

b) interior stringer, 7.8LI mph

c) interior stringer, 19.0I mph

d) interior stringer, 19.5LI mph

e) interior stringer, 31.3I mph

f) interior stringer, 28.2LI mph

Fig. 4.35 Frequency content plots for Chambers Co. Bridge - concentric runs

nanaraa.co

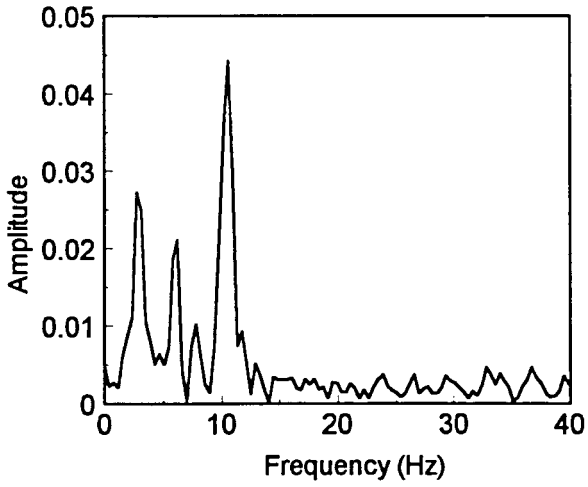

g) interior stringer, 8.0B mph

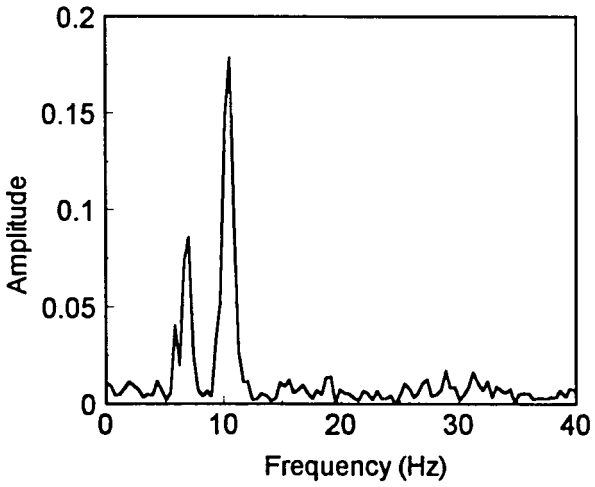

h) interior stringer, 19.0B mph

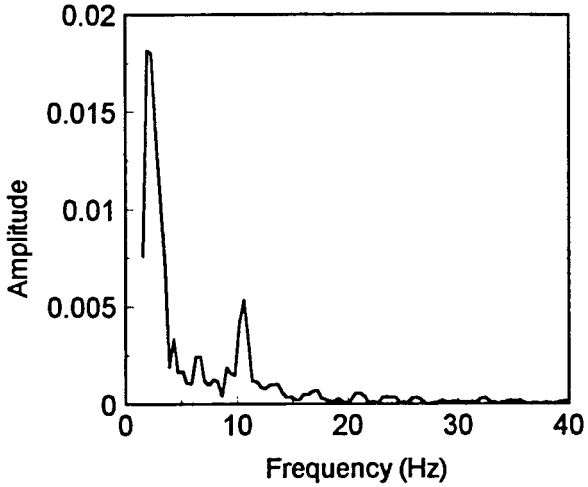

i) interior stringer, 34.5B mph

Fig. 4.35 (continued)

nanaraa.co

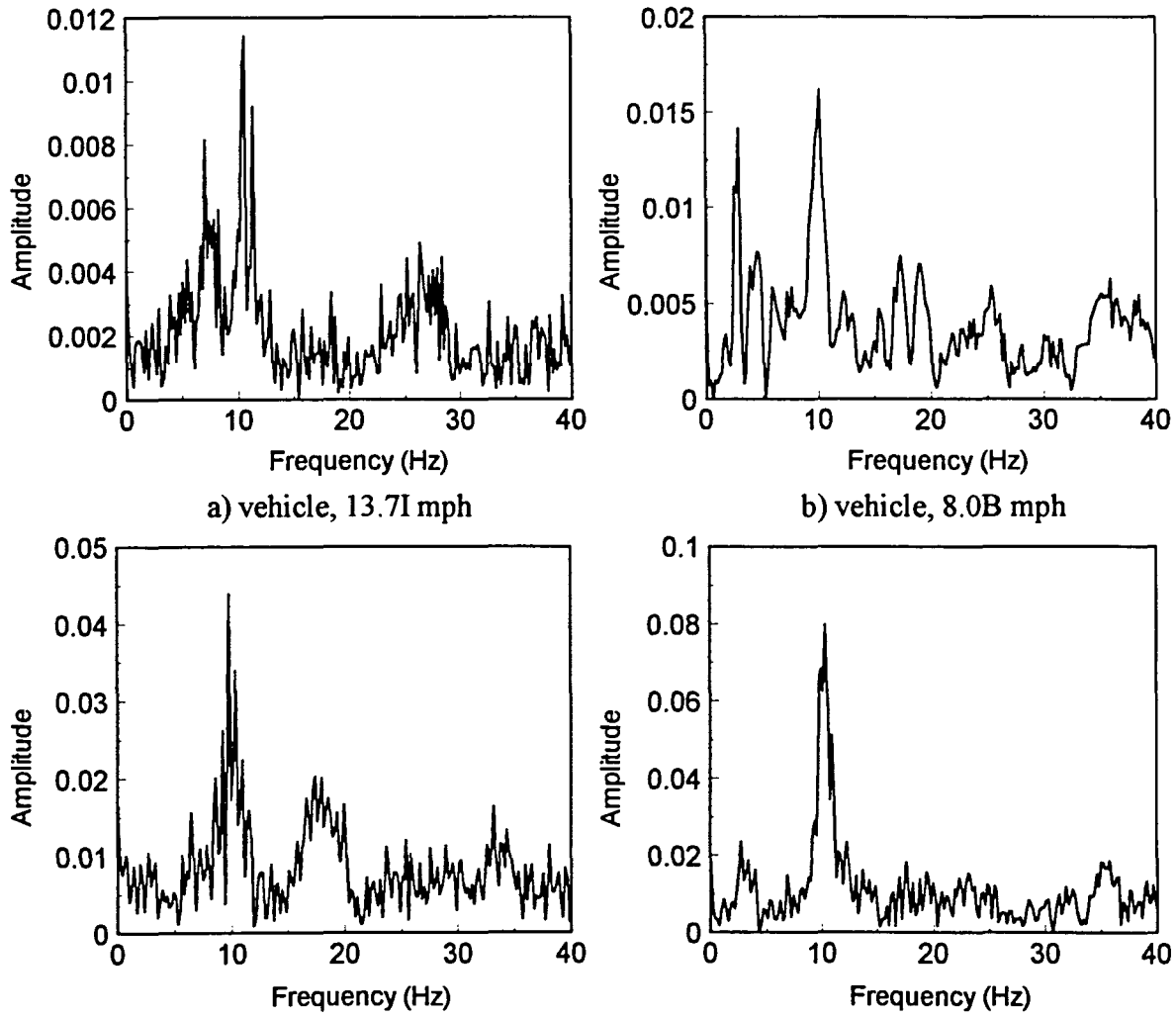

a) vehicle, 13.7I mph

b) vehicle, 8.0B mph

c) vehicle, 23.0I mph

d) vehicle, 24.2B mph

Fig. 4.36 Frequency content plots for vehicle on Chambers Co. Bridge

nanaraa.co

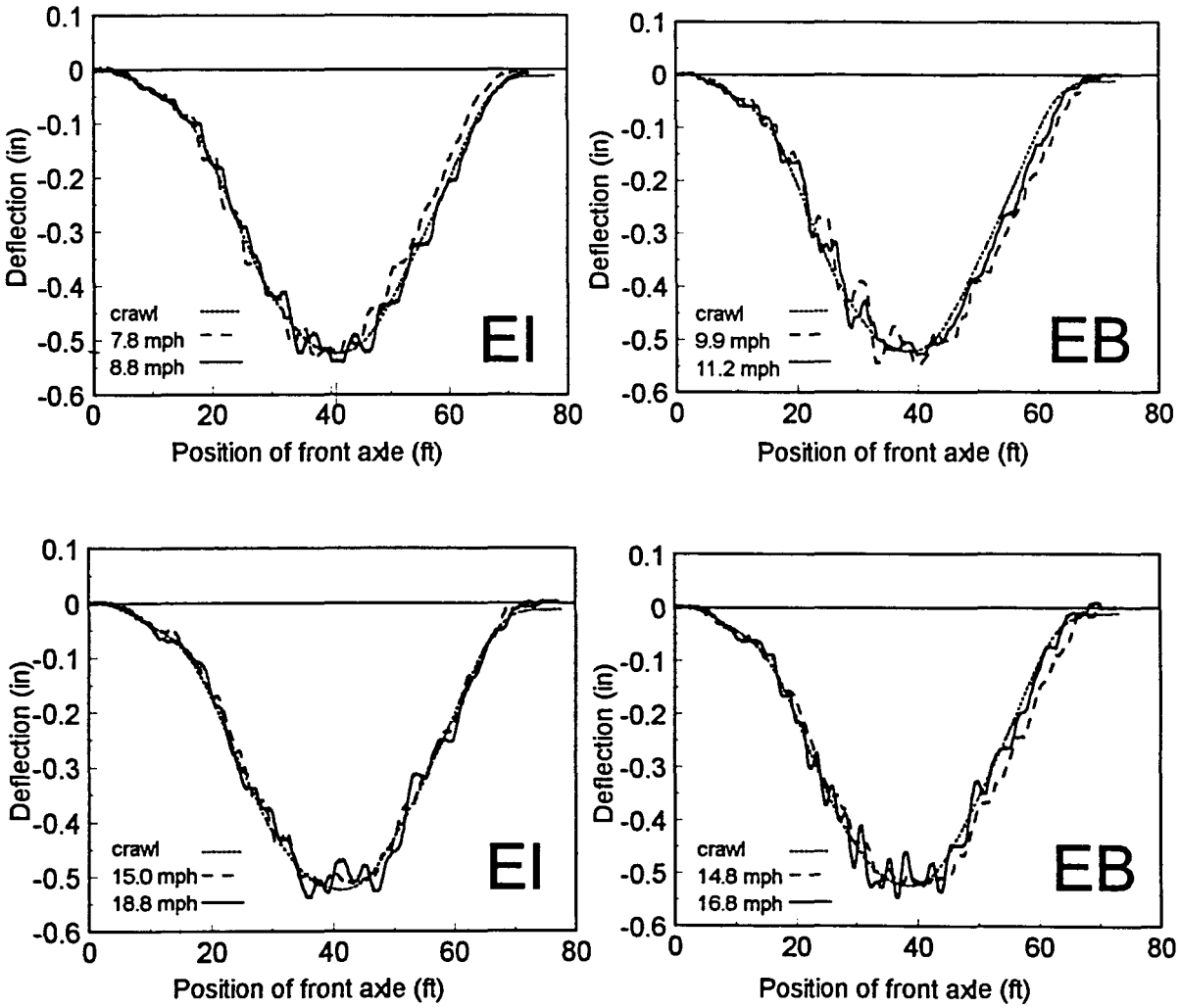

Fig. 4.37 Dynamic response for eccentric test of Chambers Co. Bridge - Stringer G4

nanaraa.co

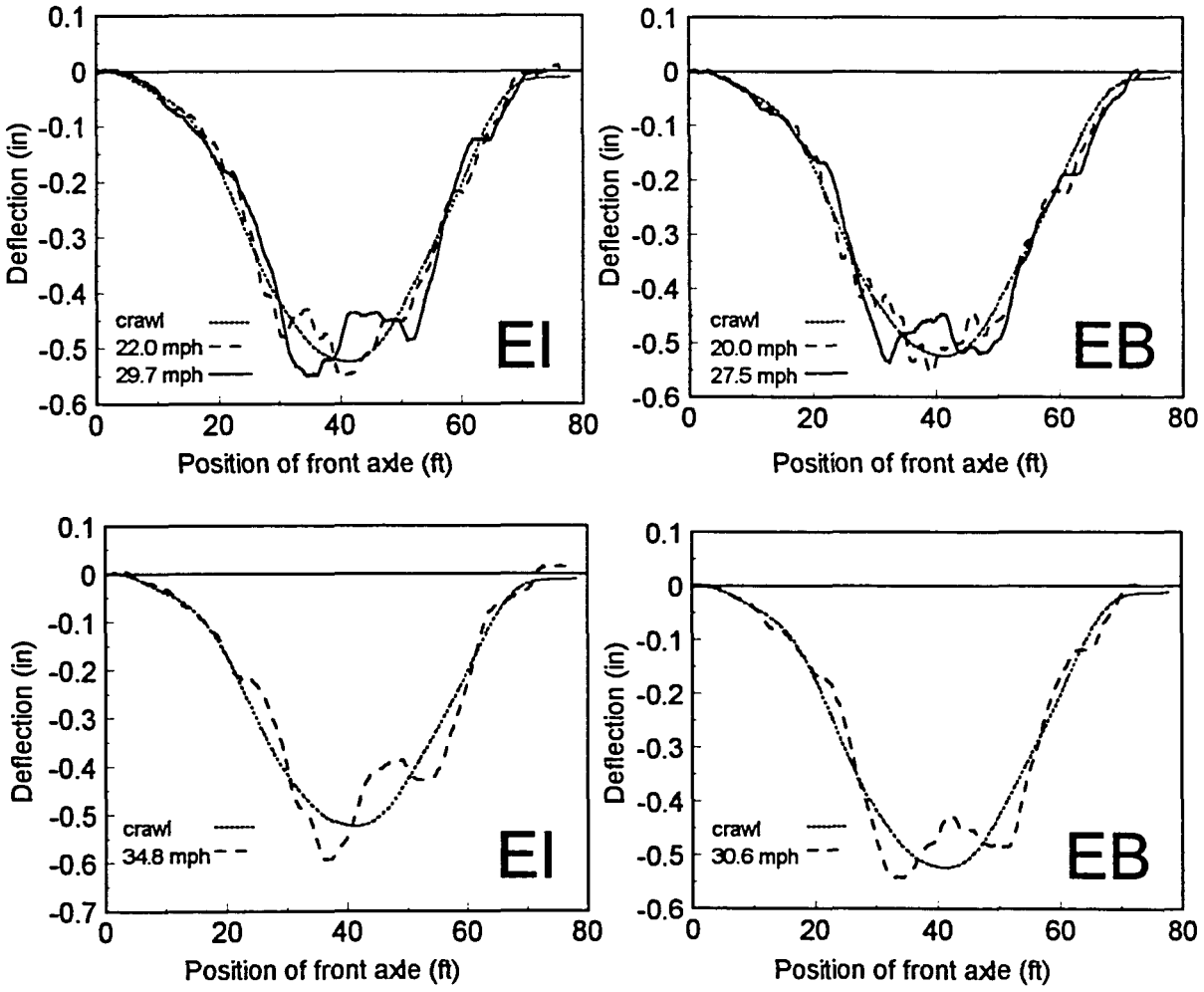

Fig. 4.37 (continued)

nanaraa.co

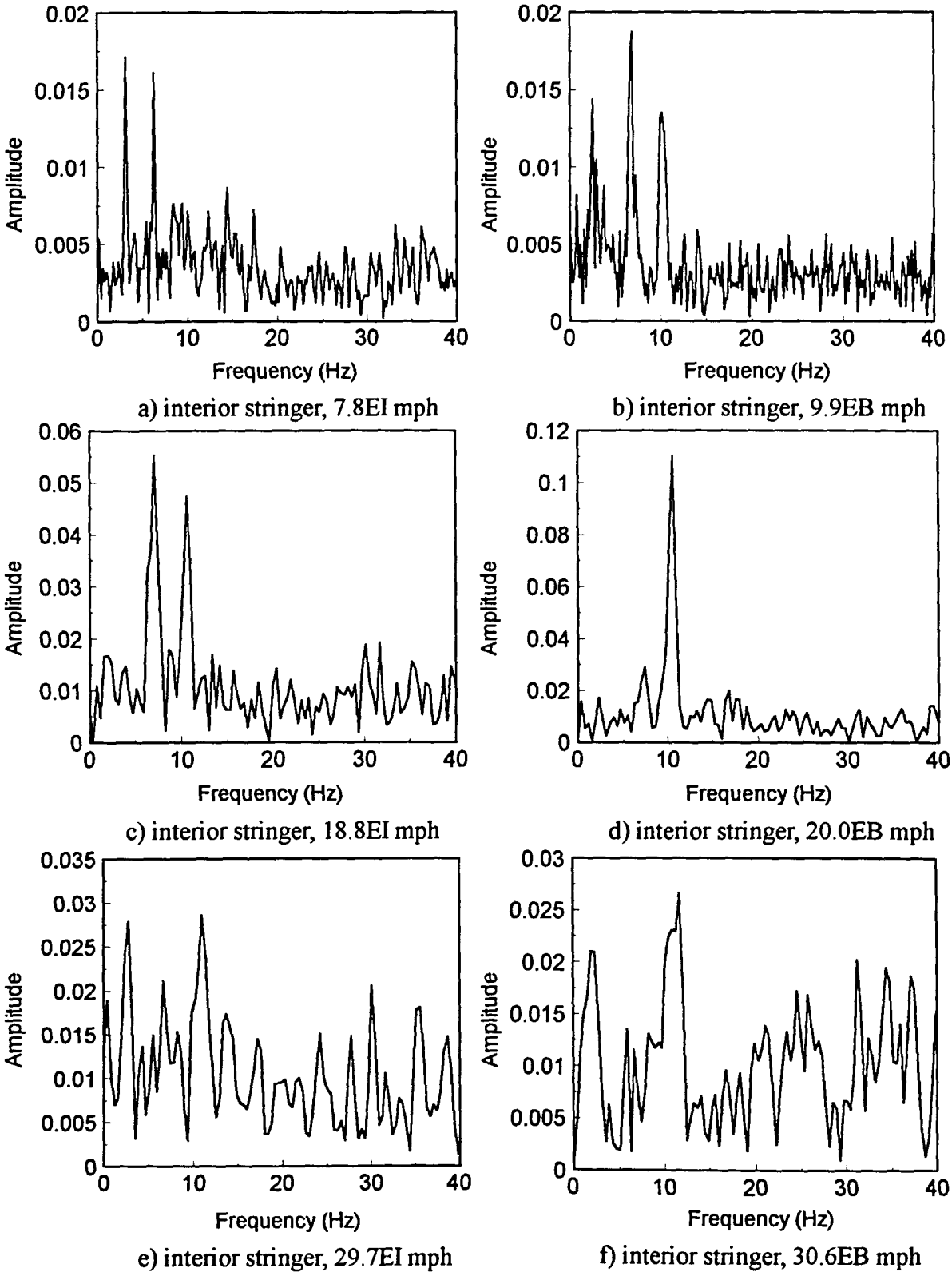

Fig. 4.38 Frequency content plots for Chambers Co. Bridge - eccentric tests

nanaraa.co

of the eccentric tests is similar to the concentric tests. Bridge response at the low speed interval is shown in Fig. 4.38a,b, at the medium speed interval in Fig. 4.38c,d, and at the high speed interval in Fig. 4.38e,f. The bump tests excited the transverse normal mode of vibration (f = 11.0 Hz) rather than the longitudinal one (f = 6.4 Hz).

4.5.2.4 Dynamic amplification

The plots of dynamic amplification appear in Fig. 4.39. Based on the natural period of the bridge of 0.155 sec, the speed to satisfy the condition of the pseudo-resonance with passage of the rear tandem axles is 19.4 mph. At this speed, the amplification is high for the bump approach for both concentric and eccentric tests. The amplification increases as the speed of the vehicle increases over 25 mph. The low amplification at the speed of 29.5B mph occurs due to the upward amplitude of the truck vibration while the truck passes the midspan of the bridge. There is a 4% difference in the amplification at speeds of 7.5I mph and 7.5L mph. This difference may be due to the effect of the lower tire pressure during the test at 7.5L. For the speeds above 10 mph the bridge response for the vehicle with low tire pressure is very similar to the response for vehicle with the regular tire pressure (Fig. 4.39a).

4.6 Summary of the experimental findings

4.6.1 Observed bridge behavior.

One aspect of the bridge behavior was found to be common for Mud Creek Bridge, Span 1 of Wittson Bridge and Chambers Co. Bridge. Three distinct and different patterns

nanaraa.co

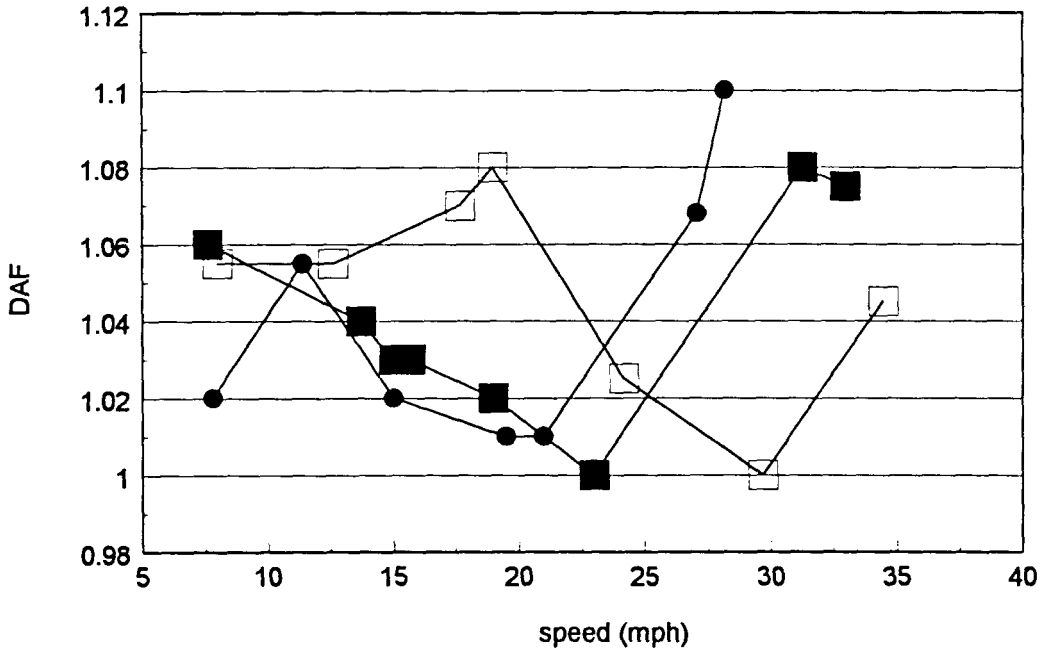

a) concentric runs

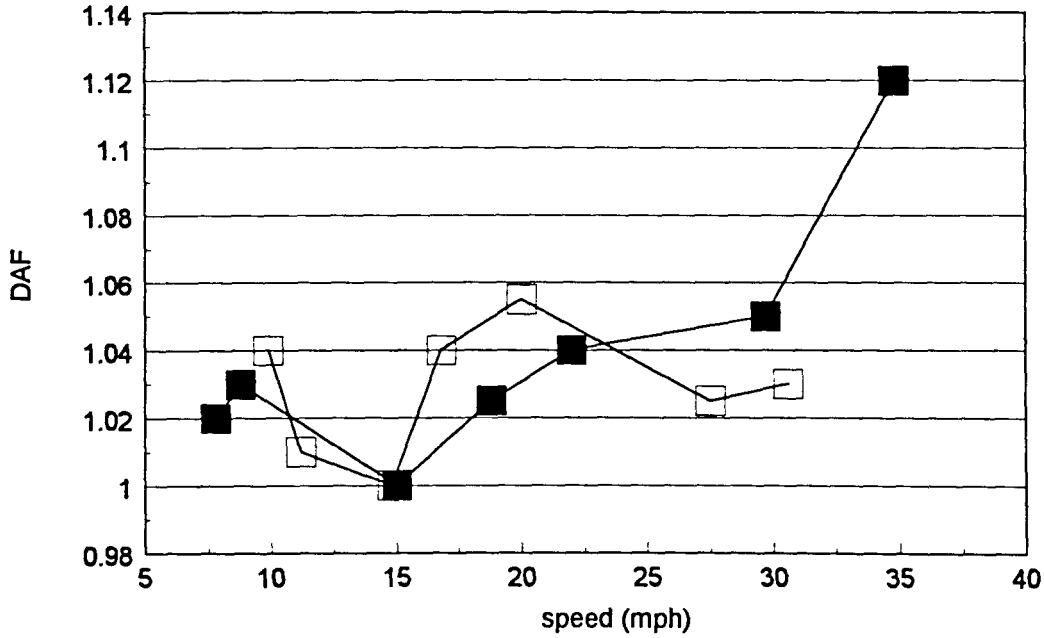

b) eccentric runs

Fig. 4.39 Chambers Co. Bridge - DAF plots

nanaraa.co

of vibration were observed at low, medium and high vehicle speeds. This behavior is summarized in Table 4.3, and discussed below. These patterns were consistently observed, regardless of the approach condition or transverse position of the vehicle and were not clearly observed for Span 3 of Wittson Bridge because the bridge natural frequency was close to the body bounce frequency of the vehicle.

4.6.1.1 High speed interval

The high speed interval includes speeds higher than 25 mph. At this interval each bridge vibrated at low frequencies between 2.5 and 3.5 Hz, which was the same as the frequency of response found in the low speed interval. Both body bounce and axle hop frequencies were usually present in the vehicle response. The dynamic amplification was usually relatively high in this speed interval. However, it was also observed that the amplification could have been low due to longitudinal position of the vehicle on the bridge at certain speeds.

A possible explanation for the body bounce frequency of the vehicle dominating the response at high speeds is that the excitation of the truck vibration (i.e. initial conditions) is high due to the high speed. The higher vibration causes a higher variation in the vehicle forces. The high forces cause a forced response of the bridge, with a frequency equal or close to the vehicle body bounce frequency.

4.6.1.2 Medium speed interval

The medium speed interval includes velocities between 10 mph and 25 mph. Within this speed interval, the frequency of the bridge vibration tends to be similar to one or more

nanaraa.co

Table 4.3 Summary table of observed bridge behavior

SPEED RANGE	OBSERVED BEHAVIOR
low (up to 10 mph)	*low frequency vibration* frequency of the vibration between 2.5 Hz and 3.5 Hz
medium (10 mph to 25 mph)	*high frequency vibration* frequency of vibration close to bridge normal mode frequency
high (over 25 mph)	*low frequency vibration* frequency of the vibration between 2.5 Hz and 3.5 Hz

nanaraa.co

of the lower natural frequencies (longitudinal or transverse) of the bridge. The vehicle response was dominated by the axle hop frequency. It is possible that the effect of the body bounce of the vehicle was not as significant as in the case of high speeds because of the lower amplitude of the vehicle excitation (i.e. initial conditions) at medium speeds.

4.6.1.3 Low speed interval

The low speed interval includes speeds up to 10 mph. At this interval, the bridge was vibrating at a low frequency between 2.5 and 3.5 Hz. The bridge exhibited regular oscillation about the crawl curve. The body bounce frequency dominated the behavior of the vehicle. A typical plot of this behavior can be found in Fig. 4.37 (speeds 7.6I mph and 8.0B mph).

A possible explanation of the body bounce frequency dominating the response in the case of the low speeds is due to pseudo resonance. Although the amplitude of the vehicle excitation and vibration is lower than in case of medium speeds, the effect of this excitation is higher. The vibrating truck hit the bridge with its maximum force several times with a period very close to the time taken by the axles to pass a common point. This explanation is supported by observing bridge deflection curves (e.g. Fig. 4.10, speeds 7.5I mph and 10.4I mph). The amplitude of the bridge vibration about the crawl curve increases as the vehicle approaches midspan.

A frequency analysis was performed to determine whether the low frequency was present in the truck vibration before it entered the bridge. Figure 4.40a shows a plot of acceleration (A2) versus time for a test of 8.7B mph on Chambers Co. Bridge. The low

nanaraa.co

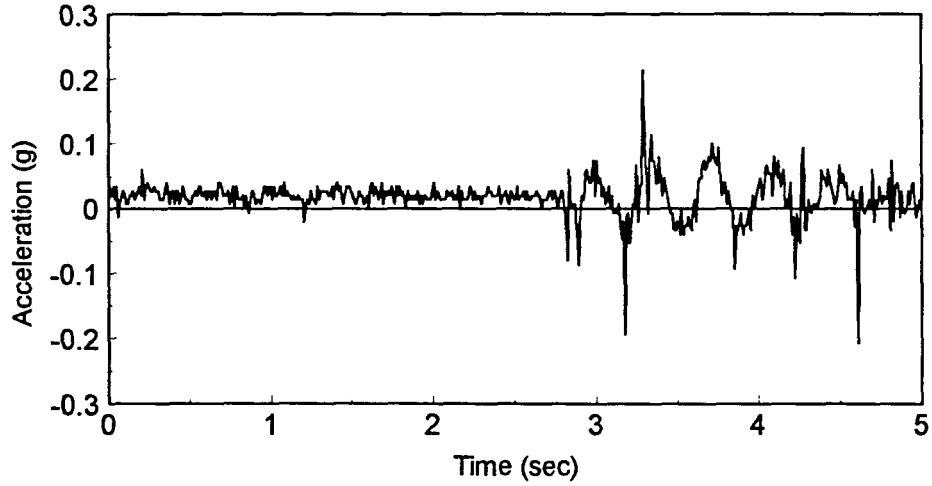

a) vehicle acceleration record, 8.0B mph

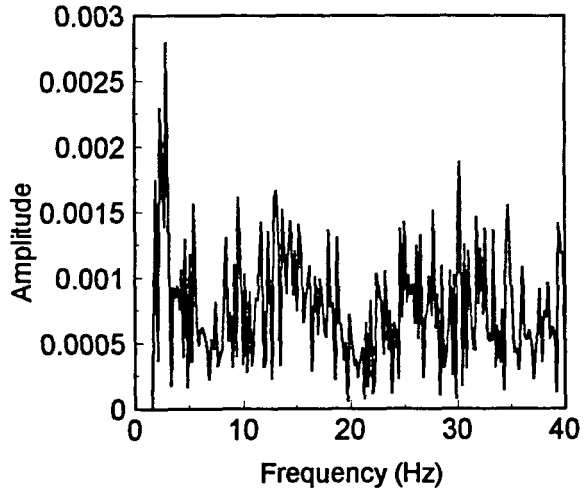

b) frequency content, t = 0 - 2.9 sec

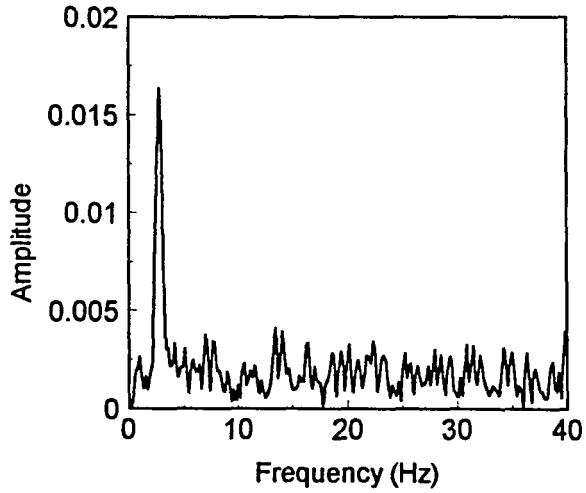

c) frequency content, t = 2.9 - 5 sec

Fig. 4.40 Acceleration (A2) and frequency content plots for vehicle on Chambers Co. Bridge

nanaraa.co

frequency is prominent after the rear axles passed the bump at the time of 2.9 sec (Fig. 4.40c) - i.e. the bump excites the body bounce mode of the vehicle at low speeds. Figure 4.40b shows the frequency content plot of the acceleration signal between 0 sec and 2.9 sec. It is clear that the low frequency was present in the truck vibration before it entered the bridge. This frequency was further amplified by the bump.

4.6.2 Summary of other observations

- Frequencies inherent to the trucks were observed in the tests on the approach roadway. The frequency of the body bounce was found to be 2.5 to 3.1 Hz and the frequency of axle hop was found to be 10.2 Hz to 10.7 Hz. These observations agree with observations of other researchers [5].

- The analysis of the experimental data investigated the effect of pseudo-resonance between a bridge's natural period and passage of consecutive axles of a vehicle. It was found that the pseudo-resonance amplified the response for the bump approach condition of the vehicle. This fact is logical, since the bump excited the axle hop vibration mode. This led to high axle forces, and made the effect of the axles more prominent.

- Dynamic amplification was analyzed and discussed for each bridge. A summary was presented in section 4.6.1. The largest observed dynamic amplification was 1.38 for

nanaraa.co

the Mud Creek Bridge. This bridge had the highest natural frequency (8.9 Hz) of all of the bridges tested. The largest DAF observed for the other bridges was 1.15. This observation suggests that dynamic amplification can be high for short span bridges.

- Low dynamic amplification was observed for the Span 3 of Wittson Bridge, despite the potential for dynamic coupling of the bridge's natural frequency and the truck's body bounce frequency (2.8 Hz and 3.1 Hz). It is possible, however, that in the limited number of tests performed, the initial conditions of the vehicle were insufficient to cause high amplification.

- The artificial bumps placed at the entrance to the bridges did not result in higher amplifications when compared to the in situ tests. The short bump only excited the axle hop frequency at high speeds. The high amplifications, however, occurred when the bridge response was dominated by the low body bounce frequency of the vehicle. Therefore, the bump did not cause large amplification of the bridge.

- A lower tire stiffness was simulated by decreasing the tire pressure by 20% on the test vehicle for the Chambers Co. Bridge test. The bridge behavior and response amplification were the same as for the original tire pressure, except for the lowest speed of 7.6L mph. At this speed, lower amplification occurred (1.02 compared to

nanaraa.co

1.06 for the original pressure). The frequency of the response remained the same when compared to the test with the original tire pressure.

nanaraa.co

5. SUMMARY AND CONCLUSIONS

5.1 Summary

The study was divided into two parts. In the first part (Chapters 2 and 3), analytical models of the bridge and vehicle, and the interaction were developed and discussed. The second part (Chapter 4) presented an analysis of behavior of four field bridges based on experimentally acquired data.

5.1.1 Bridge model

The timber stringer bridge was modeled using the finite element general purpose ANSYS program. Four basic components were idealized by different types of finite elements. The stringers and deck panels were modeled using shell element SHELL 63. The connectors between the deck and the stringers were modeled using flexible beam element BEAM 4. The transverse stiffeners between adjacent stringers were modeled using tension-only element LINK 8. Particular attention was paid to the degree of composite action exhibited by the cross section of the bridge. The validity of this aspect of the model was based upon data from a reduced scale experiment performed by another researchers.

nanaraa.co

5.1.2 Vehicle model

The vehicle considered in the analytical investigation was a three axle dump truck. The ANSYS program was used to develop the model. The vehicle was idealized as a system of masses (MASS 21), representing the vehicle body (chassis) and axles, and spring-damper-elements (COMBIN 14), representing the suspensions and tires. A significant effort was devoted to a literature study of different types of suspensions, their models, and their effect on the bridge-vehicle interaction. It was found that a majority of commercial vehicles exhibited two vibration modes associated with the vehicle's body and axles. Mechanical properties pertinent to the vehicle were used so that the vibration modes of the model matched the literature findings. The numerical algorithm of the vehicle-bridge interaction was adopted from previous studies done at ISU.

5.1.3 Sensitivity study

A set of parameters to influence the behavior of a bridge under a passing vehicle was identified from a literature study. A sensitivity of the bridge response to some of these parameters was analytically investigated in Chapter 3. A critical speed at which the bridge dynamic response is maximum was found to exist for each bride-vehicle system. The critical speed occurred when the time for the two rear axles to pass a common point was equal to the natural period of the bridge and is referred to as pseudo-resonance. The maximum dynamic deflection always occurred at this speed. The effect of the pseudo-resonance was particularly prominent when the vehicle passed a bump placed on the

nanaraa.co

entrance of a bridge. The variation of DAF with speed was found to be affected by different axle spacing of the vehicle. Participation of bridge normal modes in the frequency response was found to change with speed. Generally, higher bridge modes were excited at higher vehicle speeds. The bridge response was dominated by one mode for the speed, when the pseudo resonance occurred.

5.1.4 Experimental findings

The behavior of three field bridges (a total of four different spans) and three vehicles was investigated experimentally. Different vehicles were used at each of the three bridges. Several types of tests were performed at each bridge depending on approach conditions (in situ and artificial bump) and/or transverse position of the vehicle on the bridge. Bridge deflection and acceleration data and vehicle acceleration data was acquired. The acquired data was analyzed in time and frequency domain. Three different patterns of the bridge response were observed at low, medium and high vehicle speeds. The maximum deflection always occurred at the high speed interval. The conclusions addressed the influence of the artificial bump placed at entrance of the bridge, pseudo-resonance between the bridge natural period and passage of vehicle's consecutive axles, and the influence of a vehicle with a lower tire pressure. Results of the vehicle analysis were also discussed and compared to observations of other researchers.

nanaraa.co

5.1.5 Comparison of analytical and experimental results

Two of the three bridges investigated experimentally were modeled analytically to validate the concept of the analytical bridge model (Span 3 of Wittson Bridge and Chambers Co. Bridge). These bridges were selected for the purpose of validation, because several normal modes observed experimentally were available for the comparison. The concept of the validation was to compare crawl deflections (experimental) to static deflections (analytical), and observed normal mode frequencies (experimental) to results of mode analysis (analytical). The agreement was found to be good. The analytical model of the vehicle was validated by comparing the observed frequencies inherent to the truck (experimental) to the results of mode analysis (analytical). Again, the agreement was good.

Results of the time domain analysis (analytical) were compared to the experimental observations to validate the vehicle-bridge interaction part of the model. The effect of the pseudo-resonance was observed both analytically and experimentally. Also, both analytical and experimental results show that this effect is more prominent when high axle forces are excited by passage of the vehicle over a bump.

The three patterns of the bridge behavior observed experimentally were not observed analytically. Regardless of the vehicle speed, the bridge response was always dominated by some of the bridge normal modes. This discrepancy should be explained by initial conditions of the vehicle. Experimentally it was observed that the vehicle was vibrating even before it entered the bridge. Zero initial conditions, however, were assumed in the analytical investigation. It is possible that since the vehicle stays on the bridge only

nanaraa.co

for a short time (about 1 sec) at the high speeds, the initial conditions necessary to cause the low frequency vibration cannot be developed.

5.2 Conclusions and Recommendations

The following conclusions and recommendations for additional studies are:

- Initial conditions of the vehicle can play an important role in the bridge's response. The vehicle initial conditions in terms of frequency and level of acceleration should be determined from the experimental data. Complimentary analytical investigation should focus on clarification of their effect.
- The analytical model of the vehicle-bridge interaction should be validated using the experimental data to account for the initial conditions of the vehicle.
- The occurrence of low frequency bridge vibration at low vehicle speeds should be clarified.
- The potential for dynamic coupling between bridges with low natural frequencies (e.g. Span 3 of Wittson Bridge) and vehicles should be investigated. Although such behavior was not observed experimentally, analytical investigations should concentrate on finding such vehicle initial conditions that would result in high dynamic amplification. This conclusion would be particularly important from the design criteria standpoint.

ınaraa.cor

REFERENCES

1. Hwang, E. S., Nowak, A. S.: Simulation of dynamic load for bridges, *Journal of Structural Engineering,* Vol. 117, No. 5, May, 1991, pp.1413 - 1434.
2. Inbanathan, M. J., Wieland, M.: Bridge Vibrations due to vehicle moving over rough surface, *Journal of Structural Engineering,* Vol. 113, No. 9, September, 1987, pp.1994 - 2008.
3. Casas, J. R.: Dynamic modeling of bridges: some thoughts derived from field testing., *Transportation research board,* 74th Annual Meeting, January 22 - 28, 1995, Washington, D.C.
4. Wang, T. L., Huang, D., Shahawy, M.: Dynamic response of multigirder bridges, *Journal of Structural Engineering,* Vol. 118, No. 8, August, 1992, pp.2222 - 2238.
5. Heywood, R.: Are 'road-friendly' suspensions 'bridge friendly'?, Paper submitted to the TRB Fourth International Bridge Engineering Conference, San Francisco, August 1995.
6. Chang, D., Heehyun, L.: Impact factors for simple span highway bridges, *Journal of Structural Engineering,* Vol. 120, No. 3, March, 1994, pp.704 - 715.
7. Green, M. F., Cebon, D., Cole, D. J.: Effect of vehicle suspension design on dynamic of highway bridges., *Journal of Structural Engineering,* Vol. 121, No. 2, February, 1995, pp.227 - 282.

ınaraa.cor

8. Paultre, P., Chaallal, O., Proulx, J.: Bridge dynamic and dynamic amplification factors - a review of analytical and experimantal findings., *Canadian Journal of Civil Engineering,* Vol. 19, 1992, pp.260 - 278. 9.

9. Winkler, B. C., Hagan, M.: A test facility for the measurement of heavy vehicle suspension parameters, *Technical Papers Series 800906,* Society of Automotive Enginers, Warendale, Pa.

10. Drosner, S., Sedlacek. G.: Numerical calculation of traffic induced vibrations in roadway bridges., Structural Dynamic, 1990, pp. 977 - 984.

11. Hardy, M. S. A., Cebon, D,: Importance of speed and frequency in plexible pavament response., *Journal of Engineering Mechanics,* Vol. 120, No. 3, March, 1994, pp.463 - 482.

12. Winkler, B. C.: Measurement of inertial properties and suspension parameters of heavy highway vehicles., *Technical Papers Series 730182,* Society of Automotive Enginers, Warendale, Pa.

13. Francher, P. S., Ervin, R. D., MacAdam, C. C., Winkler B. C.: Measurement and representation of the mechanical properties of truck leaf springs., *Technical Papers Series 800905,* Society of Automotive Enginers, Warendale, Pa.

14. Barton, F. W., Baber, T. T., Yen, W. H., McKeel, W. T.: Dynamic field test of a flexible simple span bridge., Development in Short and Medium Span Bridges Engineering '90, Third Conference on Short and Medium Span Bridges, Vol. 1, August 7 - 10.

15. AASHTO. Standard Specifications for Highway Bridges, Washington, DC, American Association of State Highway and Transportation Officials, 1992.

ınaraa.cor

16. Ritter, M. A.: Timber Bridges - Design, Construction, Inspection and Maintenance, EM 7700-8. Washington, D.C.: USDA Forest Service, 1990.

17. ANSYS User's Manual for Revision 5.0, Swanson Analysis Systems, Inc., Houston, Pa, 1992.

18. Gutkowski, R. M., Goodman J. R., Pault, J. D.: Test and analysis for composite action in Glulam Bridges., *Trasportation Research Record 676,* National Academy of Sciences, Washington, D.C., 1978.

19. Wijesooryia Chintaka: Behavior of stress laminated timber bridges., M.S. Thesis, Iowa State University, Ames, Iowa, unpublished.

20. Bakht, B., Pinjarkar, S. G.: Review of dynamic testing of highway bridges, Structural Research Report SRR-89-01, Ministry of Transportation of Ontario, Diwnsview, Ontario, 1989.

21. Ritter, M. A., Wood, D. L., Wipf, T. J., Wijesooriya, C., Duwadi, S. R.: Dynamic Response of Stress Laminated Deck Bridges, Paper submitted to the TRB Fourth International Bridge Engineering Conference, San Francisco, August 1995.

22. Barton, F. W., Baber, T. T., Yen, W. H., McKeel, W. T.: Dynamic field test of a flexible simple span bridge., Development in Short and Medium Span Bridges Engineering '90, Third Conference on Short and Medium Span Bridges, Vol. 1, August 7 - 10.

23. Dodds, C. J., Robson, J. D.: The Description of Road Surface Roughness, *Journal of Sound and Vibration,* Vol. 31, No.2, November, 1973, pp. 175-183.

ınaraa.cor

ACKNOWLEDGEMENTS

The work described in this thesis has been done as a part of the analytical and experimental bridge testing program conducted cooperatively between ISU and Forest Product Laboratory.

I would like to express my thanks to sponsors of this project, the United States Department of Agriculture Forest Service/Forest Product Laboratory for funding the project and Dr. Terry J. Wipf for his guidance and help throughout the project. I would also like to thank to Dr. Hisham El-Arabaty, research associate, and Jason D. Carpenter, graduate student, for their help with evaluation of the experimental data. I also thank Dr. F.W. Klaiber and J.E. Bernard for serving on my committee.

ınaraa.cor

APPENDIX 1

RESULTS OF THE ANALYSIS IN FREQUENCY DOMAIN

ınaraa.cor

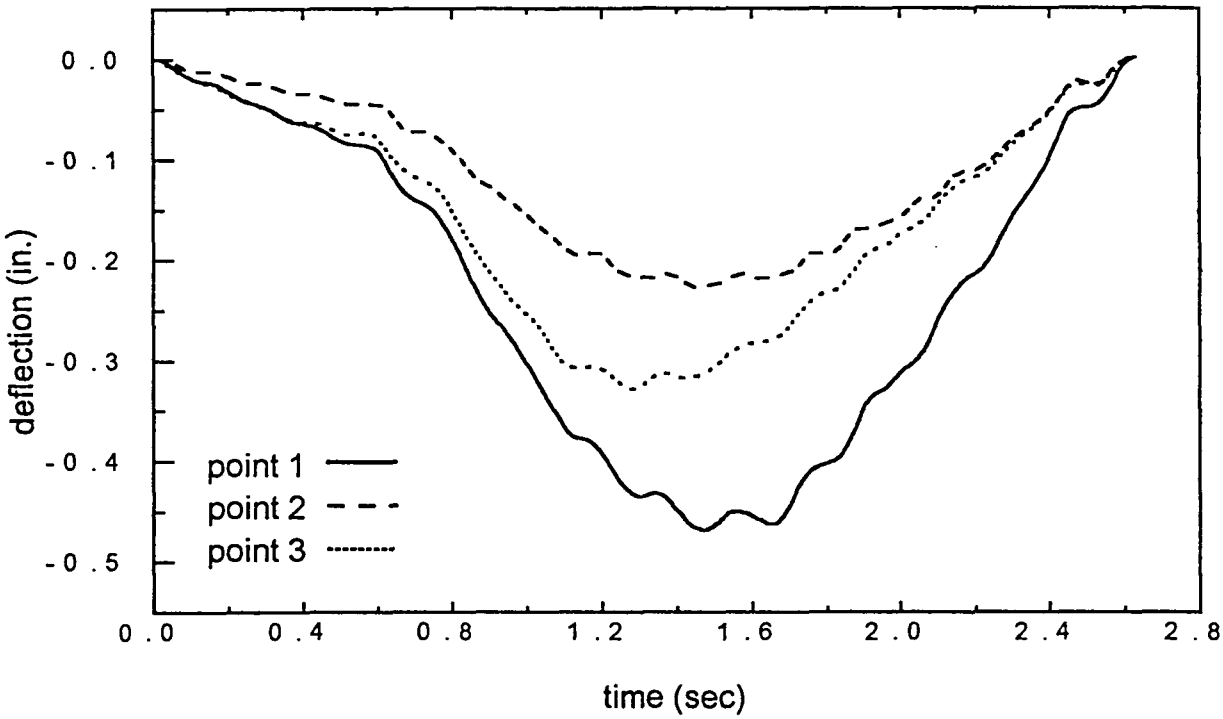

Fig. A 1.1 Bridge 1 response for 15 mph and smooth entry

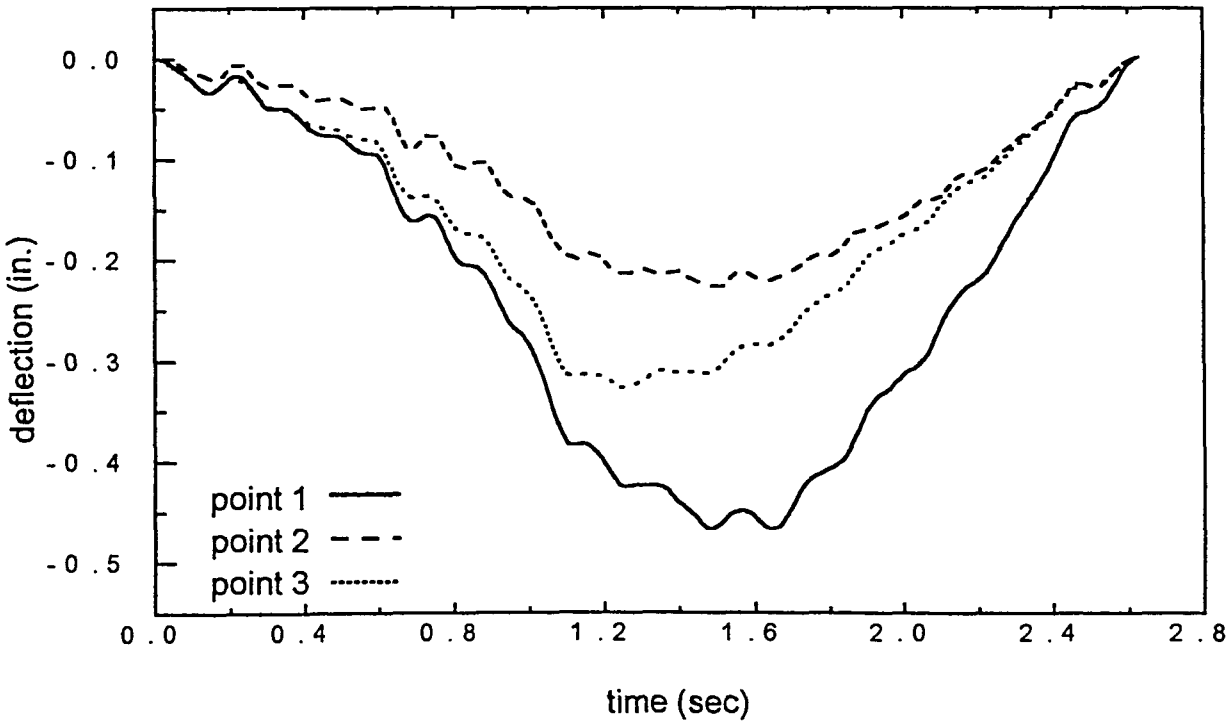

Fig. A 1.2 Bridge 1 response for 15 mph and bump entry

ınaraa.cor

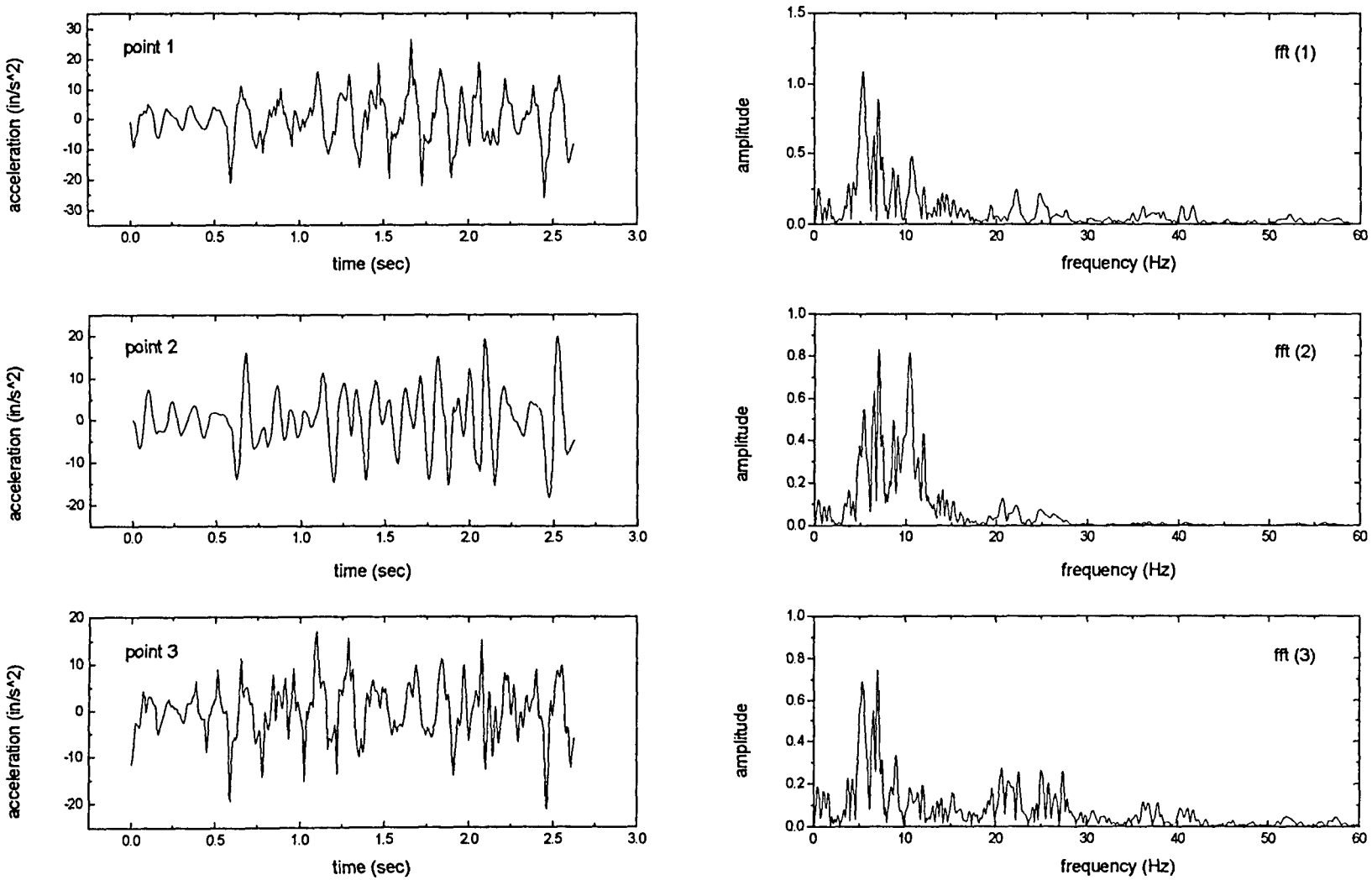

Fig. A 1.3 Frequency domain analysis - bridge response for smooth vehicle entry and speed 15 mph

unaraa.com

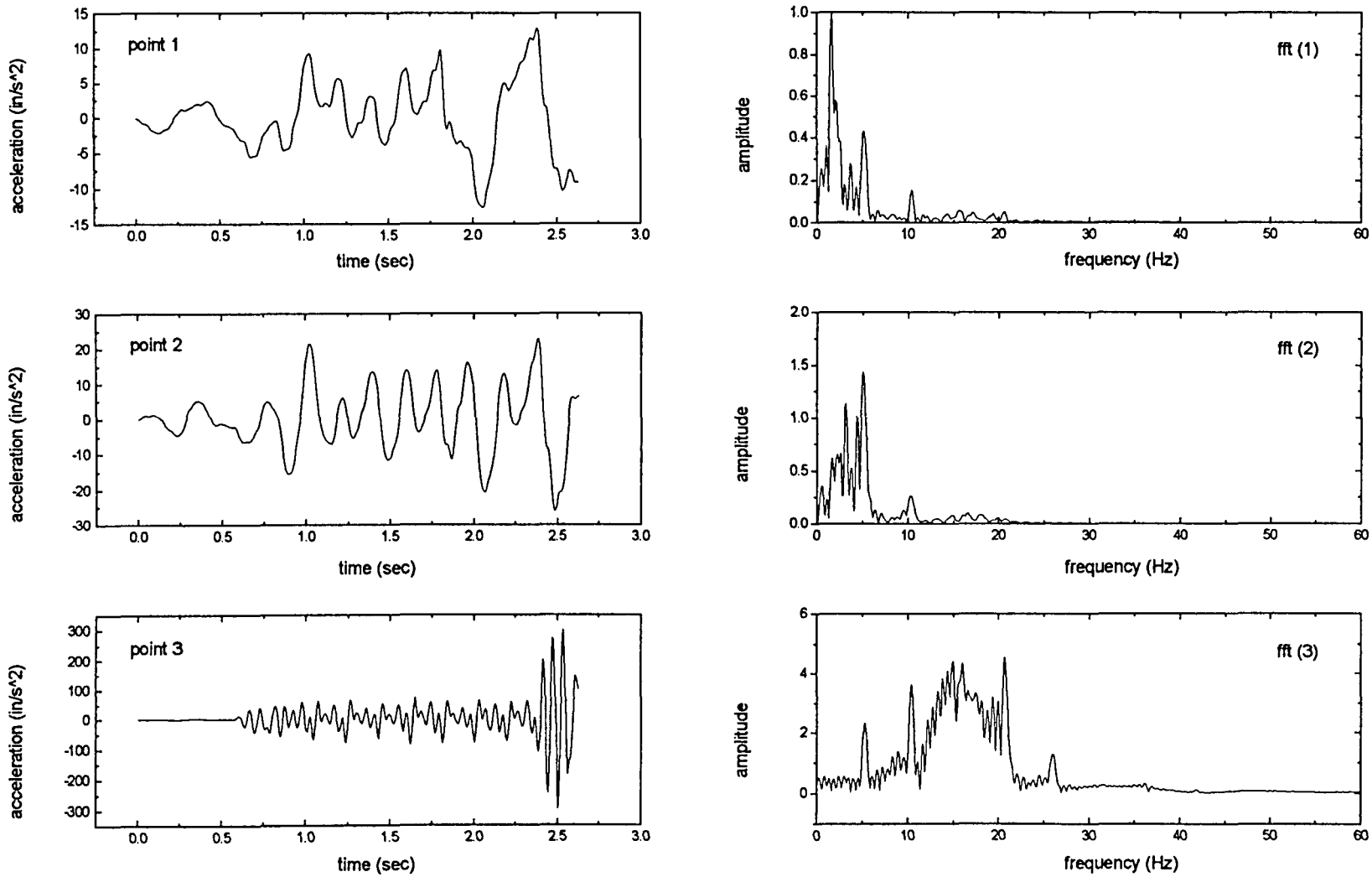

Fig. A 1.4 Frequency domain analysis - vehicle response for smooth entry and speed 15 mph

unaraa.com

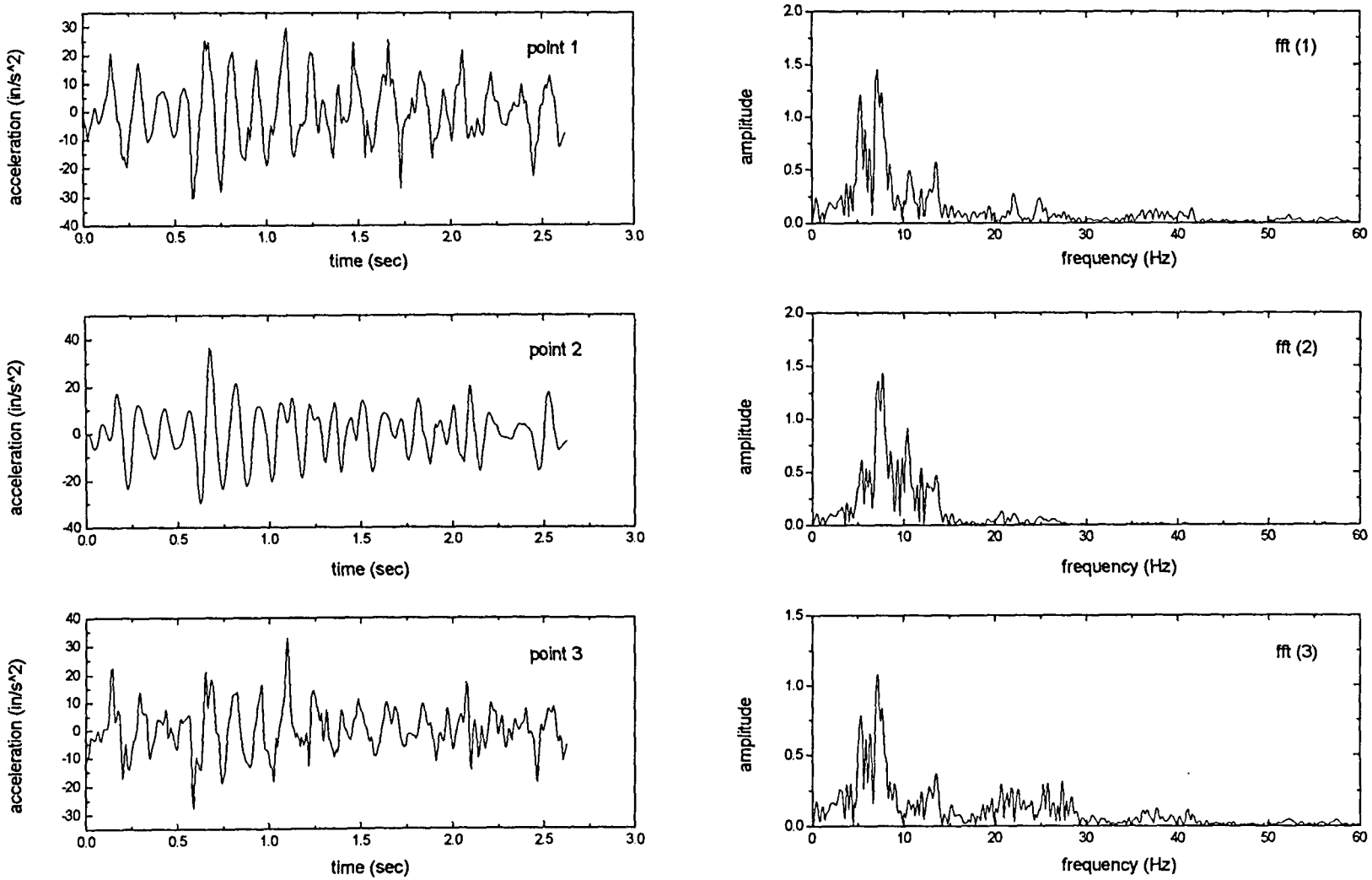

Fig. A 1.5 Frequency domain analysis - bridge response for bump vehicle entry and speed 15 mph

unaraa.com

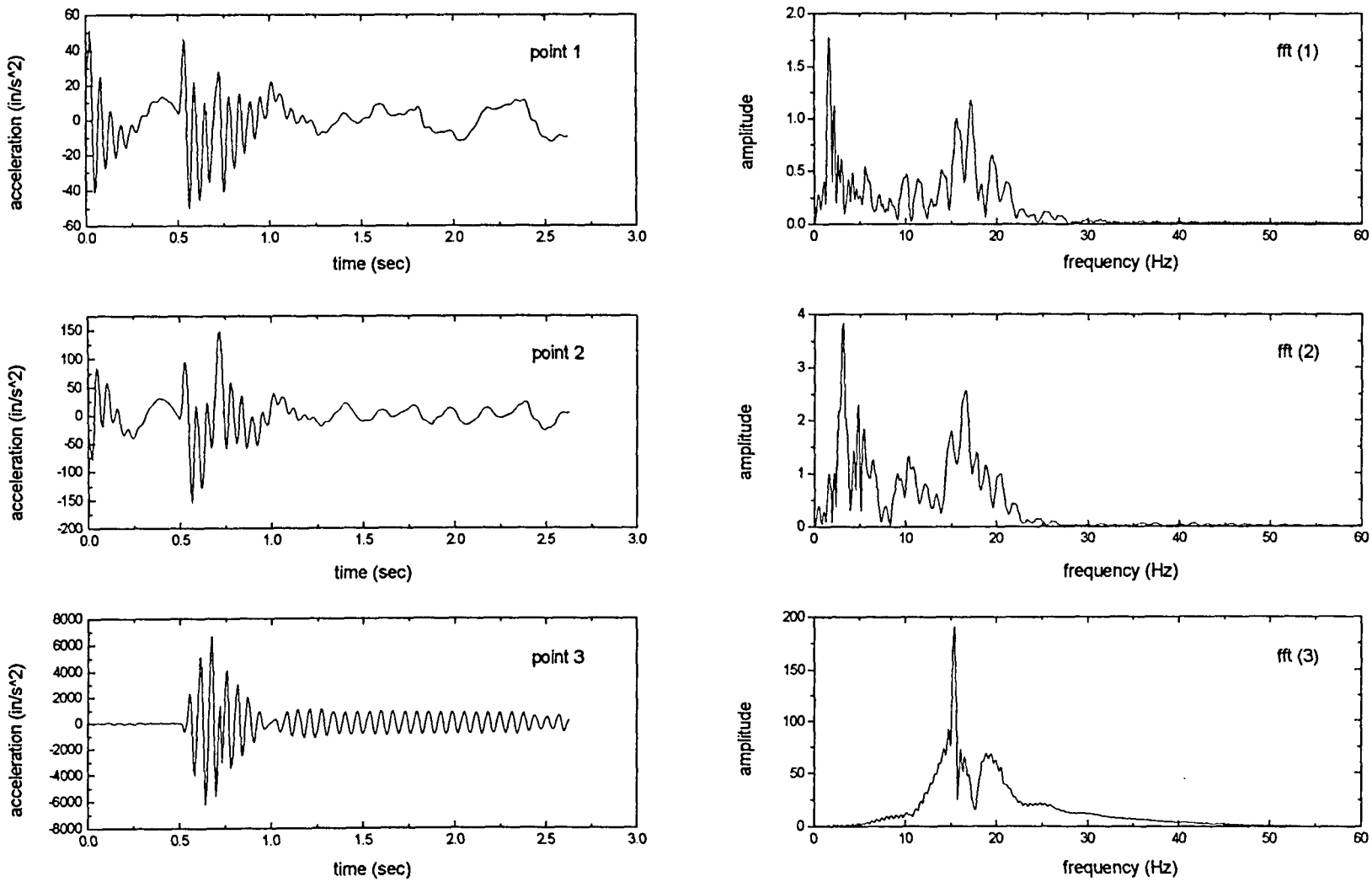

Fig. A 1.6 Frequency domain analysis - vehicle response for bump entry and speed 15 mph

ınaraa.cor

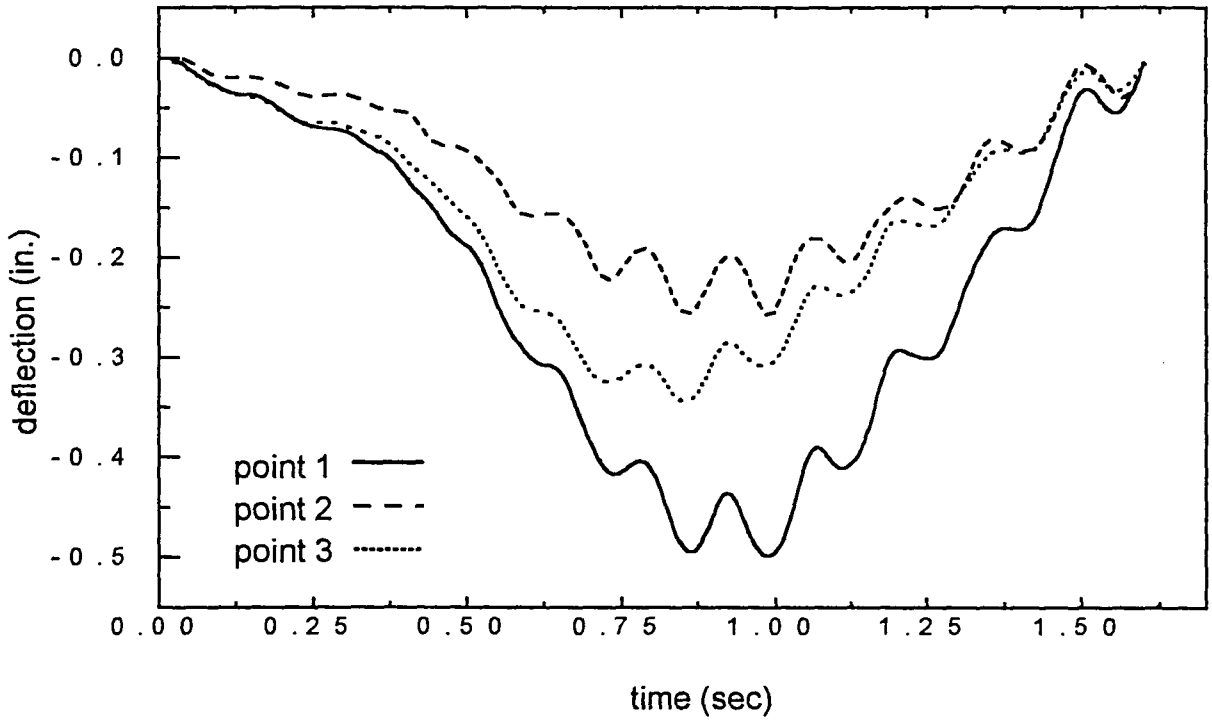

Fig. A 1.7 Bridge 1 response for 25 mph and smooth entry

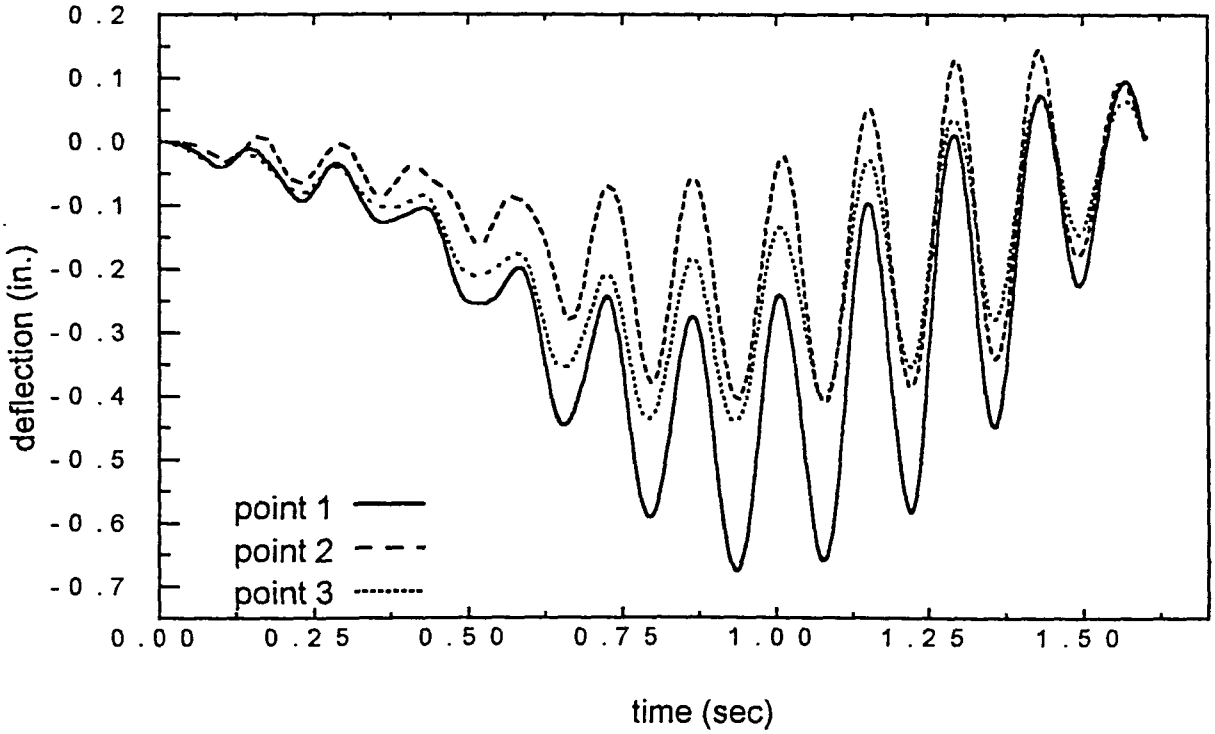

Fig. A 1.8 Bridge 1 response for 25 mph and bump entry

ınaraa.cor

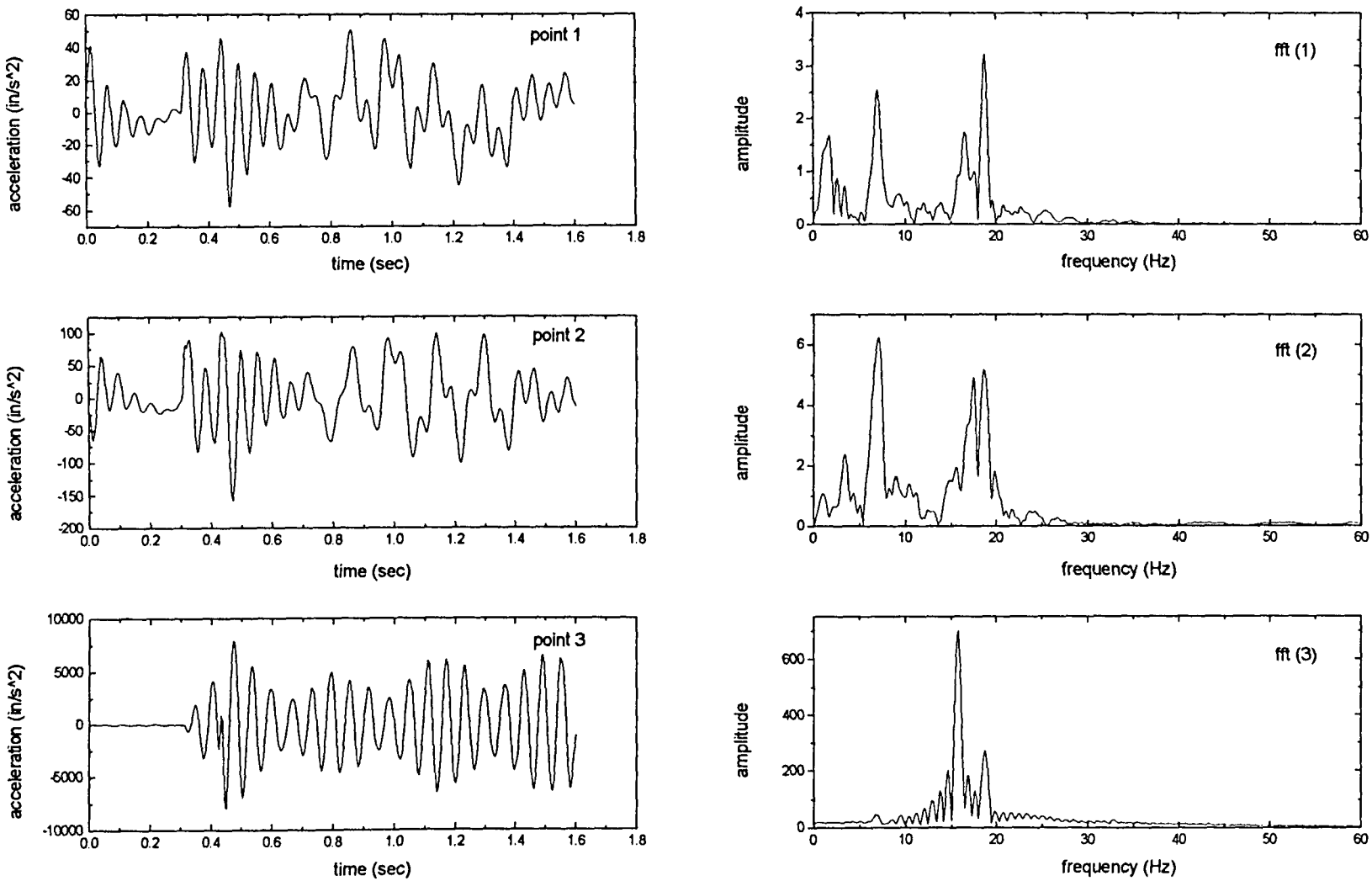

Fig.A 1.9 Frequency domain analysis - vehicle response for bump entry and speed 25 mph

unaraa.com

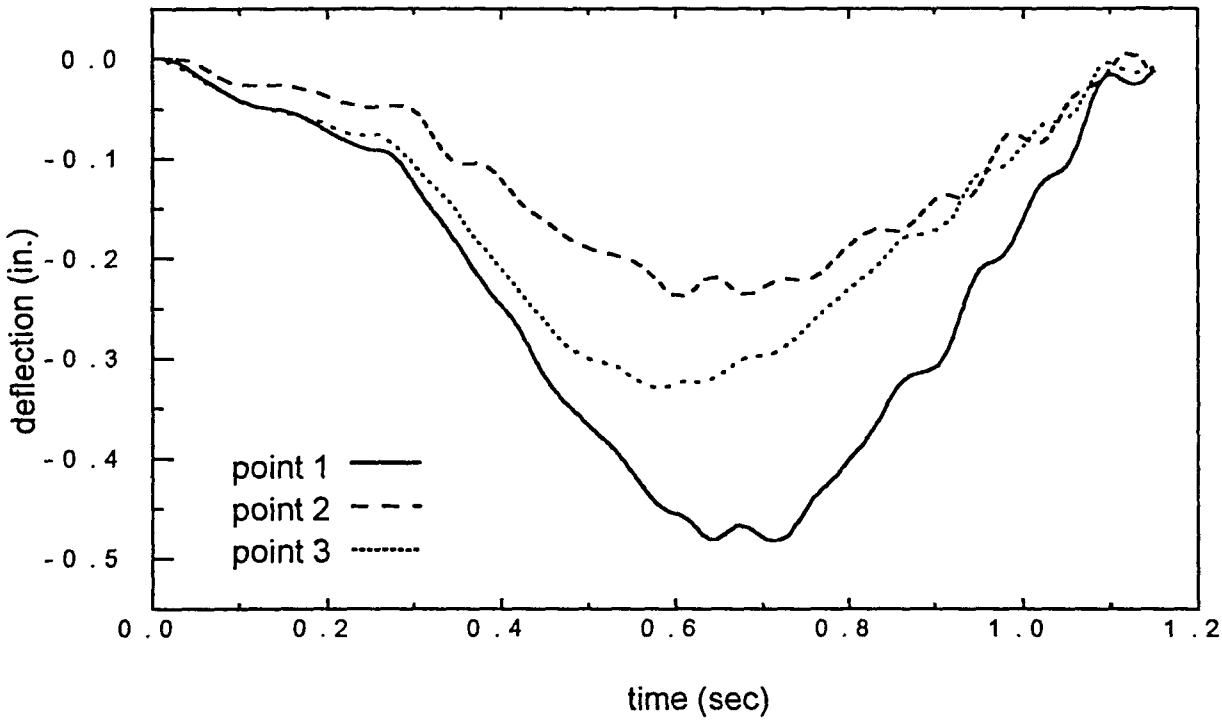

Fig. A 1.10 Bridge 1 response for 35 mph and smooth entry

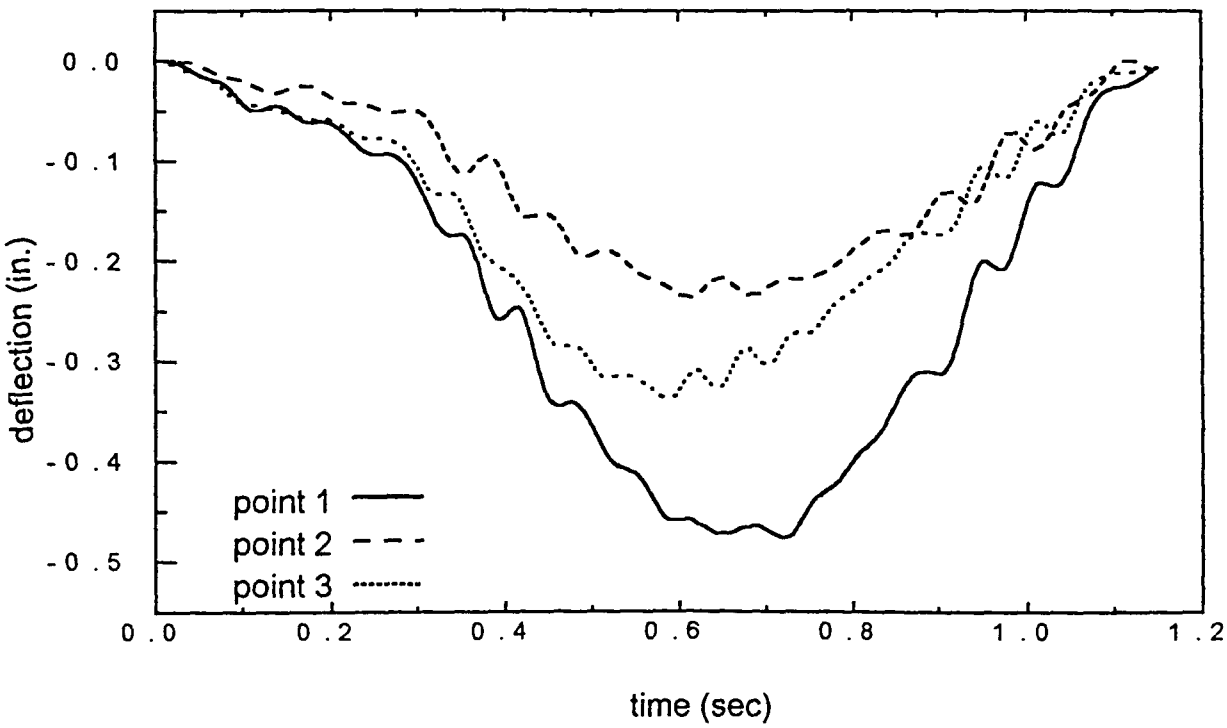

Fig. A 1.11 Bridge 1 response for 35 mph and bump entry

ınaraa.cor

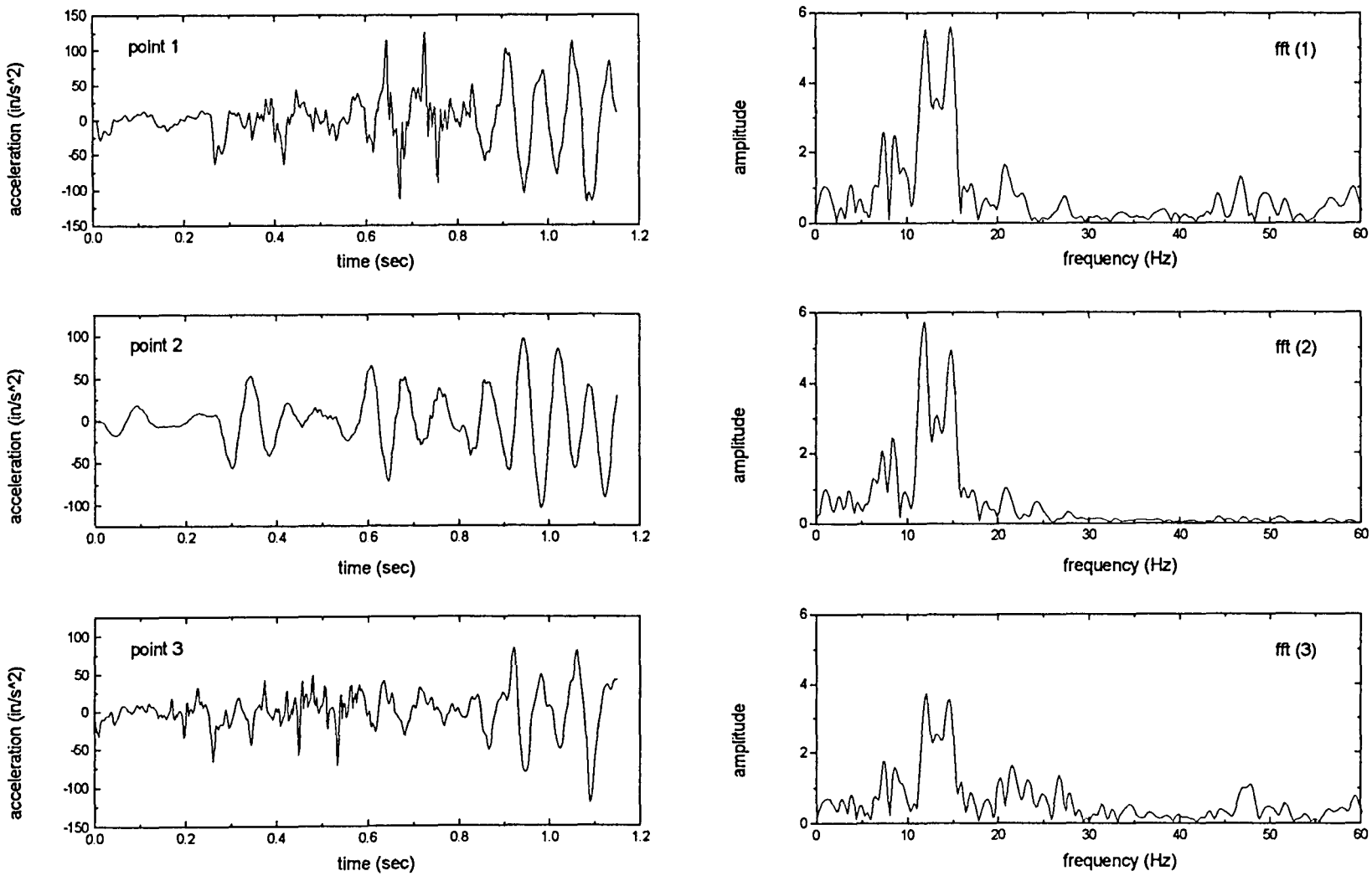

Fig. A 1.12 Frequency domain analysis - bridge response for smooth vehicle entry and speed 35 mph

unaraa.com

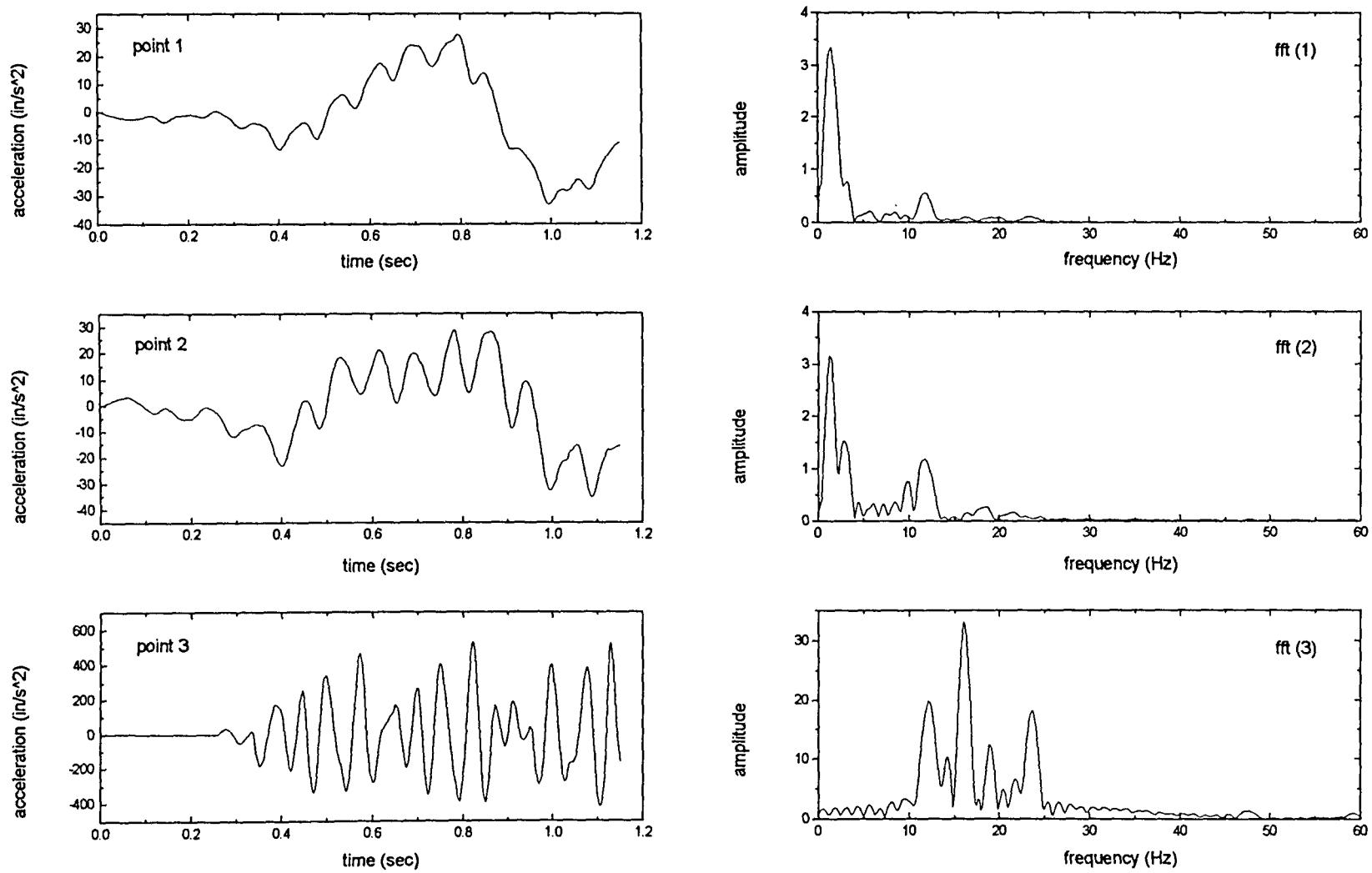

Fig. A 1.13 Frequency domain analysis - vehicle response for smooth entry and speed 35 mph

unaraa.com

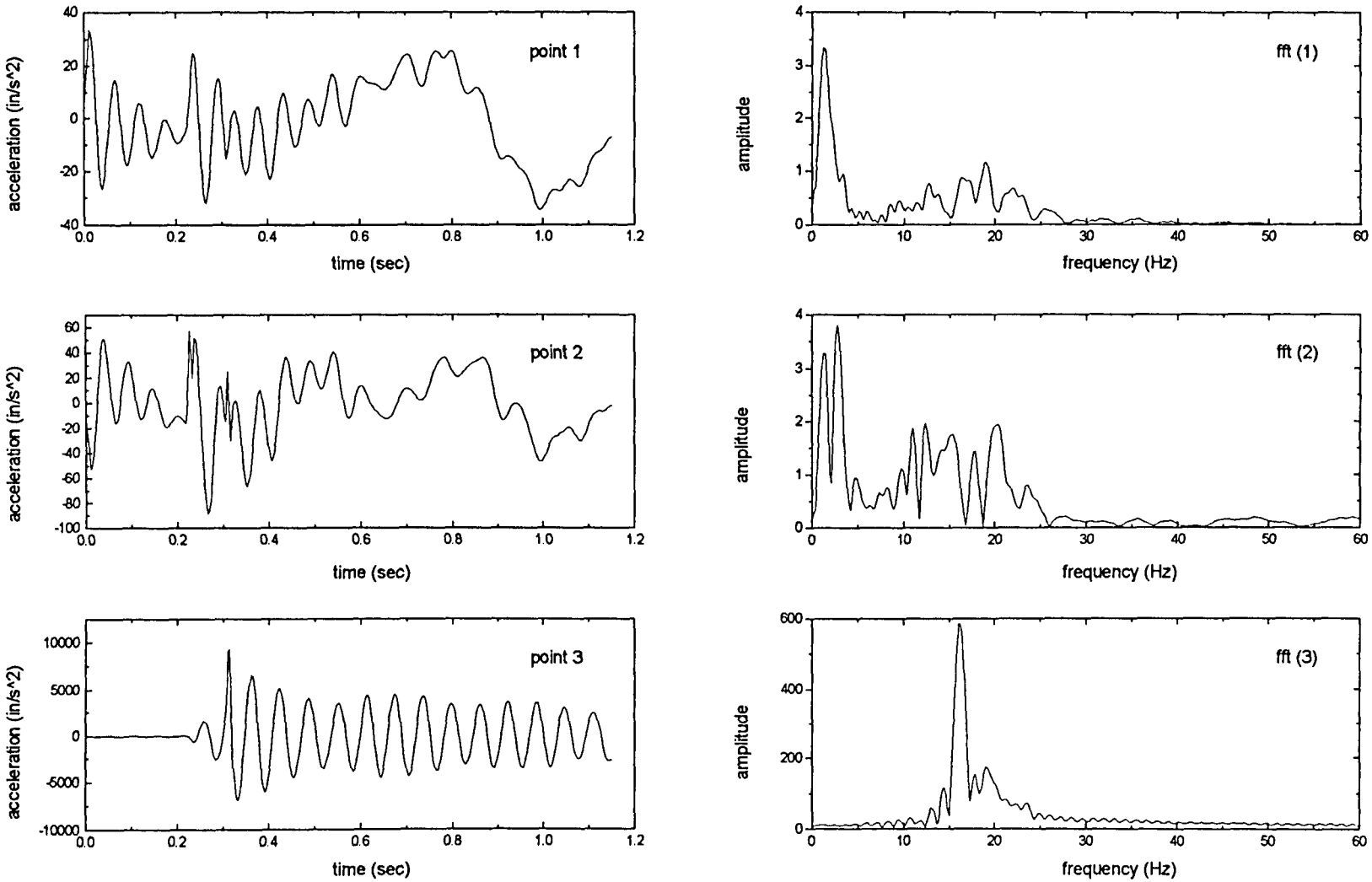

Fig. A 1.14 Frequency domain analysis - vehicle response for bump entry and speed 35 mph

unaraa.com

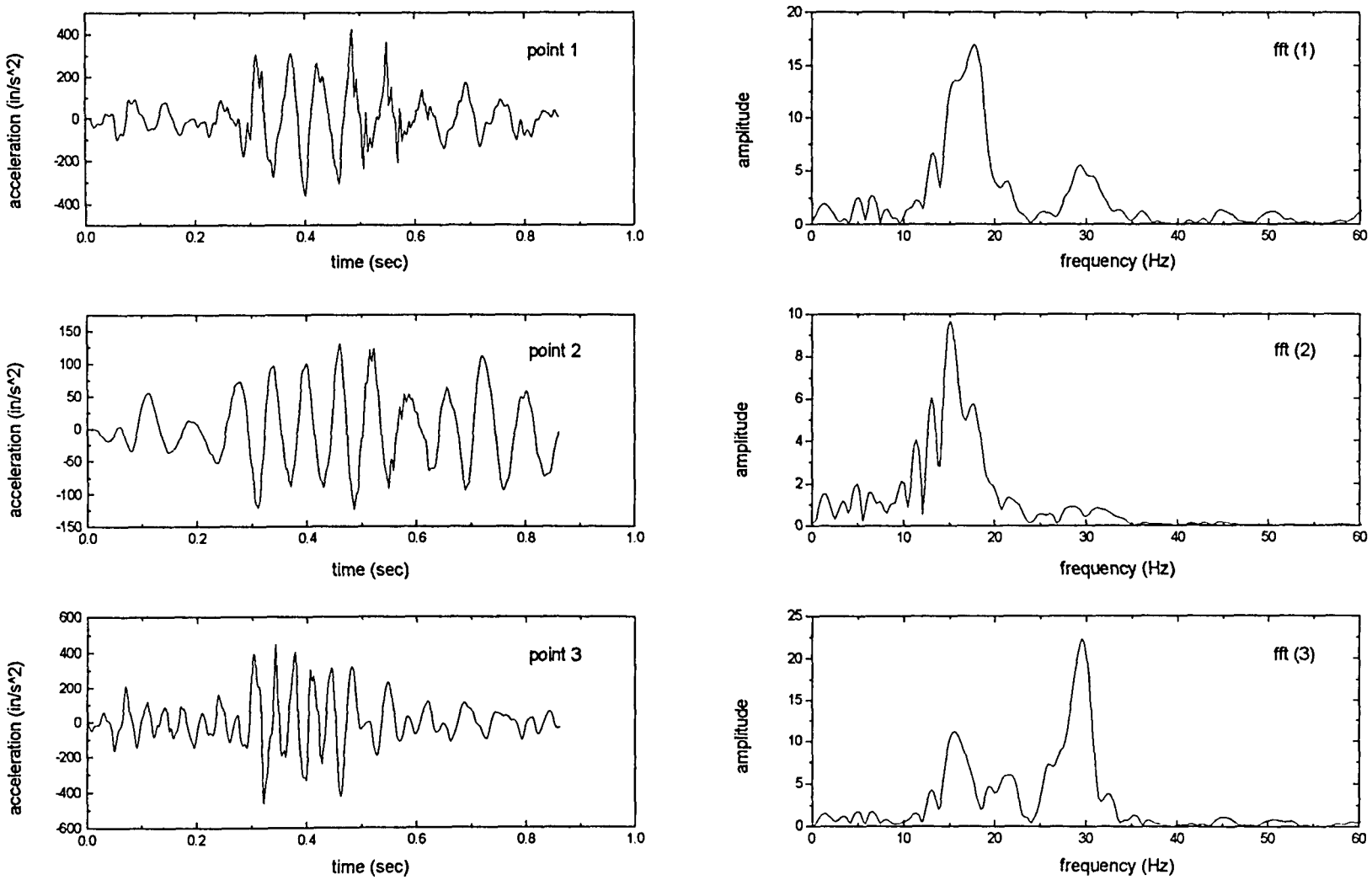

Fig. A 1.15 Frequency domain analysis - bridge response for bump vehicle entry and speed 45 mph

unaraa.com

APPENDIX 2

ADJUSTMENTS FOR DAF CALCULATIONS

In Chapter 4 it was mentioned that calculation of DAF adjustments were made to account for tracking differences of the vehicle for different tests. During the testing, visual records were obtained on each test indicating the vehicle deviation from the projected path. Maximum deflections of all the stringers were observed for the test or tests, where the vehicle visual record indicated that the vehicle perfectly followed the projected path. A distribution of deflection in the cross section was established. For the cases, when the vehicle was off this path, maximum deflections of all the stringers were observed again and compared to the established deflection distribution. The deflections were subsequently modified to match transverse deflections of the test with good tracking. That way the difference due to the tracking problem was offset. The modified deflections were used for calculation of DAF for the particular test. Note, however, that the plots of bridge deflection versus position of the vehicle on the bridge show the observed (unmodified) data.

The following tables A1 through A4 present the maximum observed (unmodified) deflections. Also, the calculated DAFs shown in these tables are based on the unmodified maximum deflections.

ınaraa.cor

Table A 2.1 Summary table for Wittson Bridge - Span 1

OBSERVED DEFLECTIONS - IN SITU CONDITION				
speed (mph)	G1	G2	G3	G4
crawl	-0.328	-0.411	-0.4302	-0.3931
15.0	-0.422	-0.468	-0.447	-0.367
19.5	-0.398	-0.445	-0.431	-0.359
26.3	-0.403	-0.445	-0.419	-0.341
31.4	-0.401	-0.438	-0.399	-0.315
38.2	-0.464	-0.499	-0.471	-0.363
OBSERVED DEFLECTIONS - BUMP CONDITION				
12.7	-0.405	-0.464	-0.445	-0.371
16.2	-0.379	-0.460	-0.468	-0.424
20.9	-0.413	-0.462	-0.444	-0.376
27.0	-0.399	-0.436	-0.392	-0.308
30.8	-0.390	-0.443	-0.423	-0.351
36.4	-0.413	-0.472	-0.455	-0.374
42.3	-0.376	-0.429	-0.401	-0.325
DAF - IN SITU CONDITIONS				
speed (mph)	G1	G2	G3	G4
15.0	1.29	1.14	1.04	0.93
19.5	1.21	1.08	1.00	0.91
26.3	1.23	1.08	0.97	0.87
31.4	1.22	1.07	0.93	0.80
38.2	1.42	1.21	1.10	0.92
DAF - BUMP CONDITIONS				
12.7	1.23	1.13	1.03	0.94
16.2	1.16	1.12	1.09	1.08
20.9	1.26	1.12	1.03	0.96
27.0	1.22	1.06	0.91	0.78
30.8	1.19	1.08	0.98	0.89
36.4	1.26	1.15	1.06	0.95
42.3	1.15	1.04	0.93	0.83

Stringers G1 to G4 are shown in Fig. 4.14

ınaraa.cor

Table A 2.2 Summary table for Wittson Bridge - Span 3

OBSERVED DEFLECTIONS - IN SITU CONDITION				
speed (mph)	G1	G2	G3	G4
crawl	-0.91545	-0.918471	-0.979758	-0.952791
8.9	-1.017	-1.020	-1.047	-1.034
15.2	-0.947	-0.950	-0.975	-0.964
24.6	-0.993	-0.996	-1.013	-0.984
29.3	-0.995	-0.998	-1.021	-0.988
36.3	-0.946	-0.949	-1.003	-1.022
39.4	-0.956	-0.959	-0.991	-0.970
OBSERVED DEFLECTIONS - BUMP CONDITION				
9.7	-1.026	-1.029	-1.049	-0.988
15.6	-0.985	-0.989	-0.970	-0.914
19.4	-0.979	-0.982	-1.013	-0.986
24.6	-0.987	-0.991	-0.990	-0.940
27.9	-0.999	-1.003	-1.018	-0.947
34.1	-0.948	-0.952	-0.992	-0.966
38.0	-0.944	-0.947	-1.012	-0.992
DAF - IN SITU CONDITIONS				
speed (mph)	G1	G2	G3	G4
8.9	1.08	1.11	1.07	1.09
15.2	1.02	1.04	1.00	1.01
24.6	1.05	1.08	1.03	1.03
29.3	1.07	1.09	1.04	1.04
36.3	0.98	1.03	1.02	1.07
39.4	1.04	1.04	1.01	1.02
DAF - BUMP CONDITIONS				
9.7	1.10	1.12	1.07	1.04
15.6	1.07	1.08	0.99	0.96
19.4	1.05	1.07	1.03	1.04
24.6	1.04	1.08	1.01	0.99
27.9	1.09	1.09	1.04	0.99
34.1	0.96	1.04	1.01	1.01
38.0	1.00	1.03	1.03	1.04

Stringers G1 to G4 are shown in Fig. 4.22

ınaraa.cor

Table A 2.3 Summary table for Mud Creek Bridge

OBSERVED DEFLECTIONS - CENTRIC RUN					
speed (mph)	G1	G2	G3	G4	G5
crawl	-0.136	-0.261	-0.318	-0.244	-0.142
7.5	-0.152	-0.314	-0.398	-0.314	-0.178
10.4	-0.156	-0.312	-0.388	-0.300	-0.167
14.1	-0.144	-0.268	-0.334	-0.268	-0.153
19.0	-0.145	-0.267	-0.344	-0.277	-0.169
25.4	-0.158	-0.310	-0.398	-0.333	-0.202
28.7	-0.180	-0.345	-0.423	-0.327	-0.183
33.3	-0.187	-0.360	-0.440	-0.348	-0.192
OBSERVED DEFLECTIONS - ECCENTRIC RUN					
crawl	-0.383	-0.362	-0.268	-0.110	-0.009
10.4	-0.380	-0.373	-0.284	-0.116	-0.004
14.2	-0.347	-0.367	-0.292	-0.125	-0.013
18.7	-0.399	-0.389	-0.309	-0.146	-0.037
24.1	-0.464	-0.423	-0.310	-0.134	-0.024
24.8	-0.440	-0.428	-0.323	-0.146	-0.020
26.4	-0.467	-0.450	-0.342	-0.146	-0.005
28.7	-0.520	-0.488	-0.355	-0.149	-0.012
30.6	-0.512	-0.480	-0.355	-0.145	-0.005
DAF - CENTRIC RUNS					
7.5	1.112	1.205	1.251	1.288	1.251
10.4	1.146	1.197	1.220	1.231	1.177
14.2	1.058	1.028	1.050	1.101	1.079
19.0	1.063	1.026	1.079	1.136	1.191
25.4	1.160	1.189	1.249	1.367	1.423
28.7	1.320	1.325	1.328	1.342	1.288
33.3	1.374	1.381	1.382	1.427	1.353
DAF - ECCENTRIC RUNS					
10.4	0.991	1.031	1.062	1.054	0.462
14.2	0.905	1.015	1.091	1.133	1.462
18.7	1.041	1.076	1.153	1.325	4.308
24.1	1.209	1.169	1.160	1.217	2.846
24.8	1.149	1.182	1.207	1.331	2.308
26.4	1.218	1.245	1.277	1.325	0.615
28.7	1.358	1.350	1.328	1.355	1.385
30.6	1.335	1.328	1.328	1.319	0.538

Stringers G1 to G5 are shown in Fig. 4.7

ınaraa.cor

Table A 2.4 Summary table for Chambers Co. Bridge

OBSERVED DEFLECTIONS - ECCENTRIC RUN, INSITU CONDITION						
speed (mph)	G1	G2	G3	G4	G5	G6
crawl	-0.043	-0.218	-0.415	-0.524	-0.457	-0.300
7.8	-0.048	-0.225	-0.421	-0.536	-0.475	-0.319
8.8	-0.047	-0.229	-0.419	-0.541	-0.473	-0.318
15	-0.051	-0.215	-0.408	-0.518	-0.462	-0.321
18.8	-0.068	-0.244	-0.441	-0.538	-0.462	-0.330
22	-0.066	-0.235	-0.423	-0.551	-0.493	-0.349
29.7	-0.048	-0.219	-0.417	-0.550	-0.502	-0.373
34.8	-0.075	-0.259	-0.484	-0.593	-0.502	-0.346
OBSERVED DEFLECTIONS - ECCENTRIC RUN, BUMP CONDITION						
9.9	-0.062	-0.239	-0.430	-0.547	-0.510	-0.334
11.2	-0.057	-0.231	-0.418	-0.530	-0.450	-0.310
14.8	-0.060	-0.225	-0.412	-0.520	-0.469	-0.326
16.8	-0.099	-0.241	-0.435	-0.547	-0.484	-0.378
20	-0.081	-0.233	-0.441	-0.553	-0.539	-0.334
27.5	-0.058	-0.229	-0.419	-0.537	-0.478	-0.334
30.6	-0.077	-0.252	-0.447	-0.542	-0.466	-0.319
DAF - ECCENTRIC RUN, INSITU CONDITION						
7.8	1.104	1.032	1.015	1.023	1.038	1.065
8.8	1.089	1.051	1.011	1.033	1.034	1.061
15	1.181	0.989	0.984	0.988	1.011	1.072
18.8	1.565	1.121	1.062	1.028	1.011	1.101
22	1.519	1.078	1.021	1.052	1.079	1.165
29.7	1.120	1.008	1.005	1.050	1.097	1.245
34.8	1.749	1.189	1.168	1.133	1.099	1.154
DAF - ECCENTRIC RUN, BUMP CONDITION						
9.9	1.442	1.100	1.037	1.044	1.115	1.116
11.2	1.319	1.063	1.007	1.011	0.985	1.034
14.8	1.381	1.035	0.994	0.993	1.025	1.087
16.8	2.301	1.109	1.050	1.044	1.060	1.263
20	1.871	1.072	1.064	1.055	1.180	1.114
27.5	1.350	1.051	1.011	1.025	1.045	1.114
30.6	1.779	1.158	1.078	1.035	1.019	1.065

Stringers G1 to G6 are shown in Fig. 4.30

ınaraa.cor

Table A 2.4 continued

OBSERVED DEFLECTIONS - CONCENTRIC RUN, INSITU CONDITION						
speed (mph)	G1	G2	G3	G4	G5	G6
crawl	-0.194	-0.364	-0.515	-0.487	-0.307	-0.134
7.6	-0.202	-0.391	-0.560	-0.526	-0.332	-0.154
13.7	-0.156	-0.343	-0.517	-0.519	-0.345	-0.170
15	-0.168	-0.344	-0.501	-0.505	-0.335	-0.176
15.7	-0.180	-0.344	-0.501	-0.514	-0.352	-0.178
19	-0.226	-0.378	-0.515	-0.498	-0.314	-0.170
23	-0.208	-0.368	-0.506	-0.469	-0.289	-0.134
31.3	-0.203	-0.203	-0.203	-0.203	-0.203	-0.203
33	-0.211	-0.395	-0.559	-0.527	-0.341	-0.168
OBSERVED DEFLECTIONS - CONCENTRIC RUN, BUMP CONDITION						
8	-0.163	-0.356	-0.527	-0.526	-0.350	-0.245
12.6	-0.163	-0.352	-0.529	-0.525	-0.344	-0.182
17.7	-0.198	-0.350	-0.532	-0.545	-0.370	-0.229
19	-0.219	-0.370	-0.549	-0.543	-0.359	-0.217
24.2	-0.175	-0.344	-0.517	-0.513	-0.324	-0.178
29.7	-0.122	-0.314	-0.485	-0.503	-0.336	-0.224
34.5	-0.190	-0.367	-0.536	-0.512	-0.332	-0.171
DAF - CONCENTRIC RUN, INSITU CONDITION						
7.6	1.044	1.076	1.087	1.081	1.081	1.151
13.7	0.808	0.944	1.003	1.066	1.122	1.265
15	0.866	0.948	0.973	1.037	1.092	1.310
15.7	0.931	0.946	0.973	1.055	1.148	1.330
19	1.170	1.041	0.999	1.022	1.023	1.265
23	1.075	1.014	0.982	0.962	0.942	0.998
31.3	1.051	0.559	0.395	0.417	0.662	1.517
33	1.088	1.087	1.085	1.082	1.109	1.256
DAF - CONCENTRIC RUN, BUMP CONDITION						
8	0.842	0.979	1.023	1.081	1.142	1.826
12.6	0.842	0.968	1.027	1.078	1.120	1.355
17.7	1.023	0.962	1.032	1.120	1.206	1.712
19	1.133	1.017	1.066	1.115	1.170	1.618
24.2	0.903	0.946	1.004	1.053	1.056	1.330
29.7	0.630	0.865	0.941	1.033	1.094	1.672
34.5	0.982	1.010	1.040	1.051	1.081	1.275

ınaraa.cor

Table A 2.4 continued

OBSERVED DEFLECTIONS - CONCENTRIC RUN, LOW TIRE PRESSURE						
speed (mph)	G1	G2	G3	G4	G5	G6
7.8	-0.153	-0.338	-0.509	-0.507	-0.335	-0.166
11.36	-0.168	-0.358	-0.534	-0.523	-0.344	-0.177
15	-0.156	-0.324	-0.493	-0.514	-0.362	-0.194
19.5	-0.195	-0.343	-0.492	-0.508	-0.350	-0.207
21	-0.172	-0.323	-0.488	-0.514	-0.354	-0.211
28.2	-0.144	-0.381	-0.562	-0.542	-0.364	-0.194
27.1	-0.194	-0.360	-0.537	-0.528	-0.351	-0.187
DAF - CONCENTRIC RUN, LOW TIRE PRESSURE						
7.8	0.791	0.931	0.987	1.041	1.092	1.236
11.36	0.869	0.986	1.037	1.074	1.120	1.320
15	0.804	0.891	0.957	1.056	1.178	1.449
19.5	1.006	0.944	0.954	1.044	1.139	1.548
21	0.890	0.889	0.946	1.056	1.154	1.578
28.2	0.746	1.048	1.091	1.113	1.187	1.449
27.1	1.003	0.990	1.042	1.085	1.144	1.395

ınaraa.cor

APPENDIX 3

MODE SHAPES

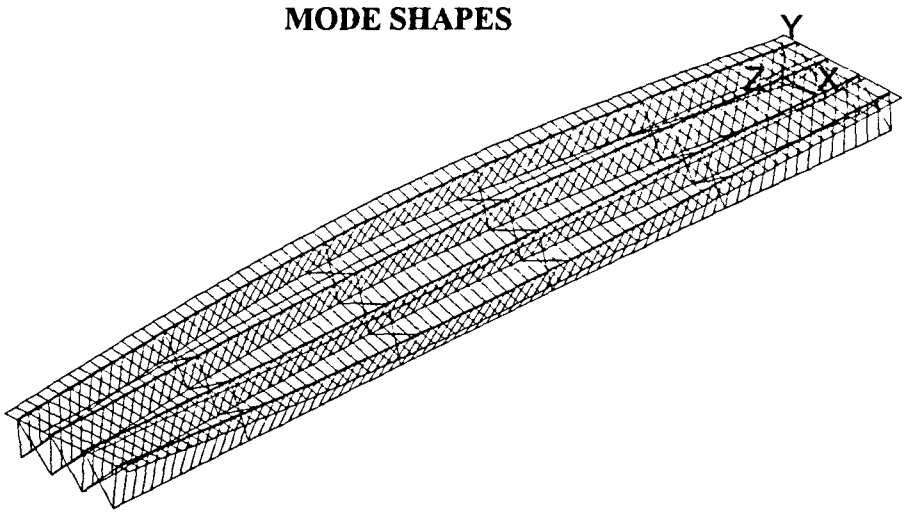

a) first mode shape, f = 2.5 Hz

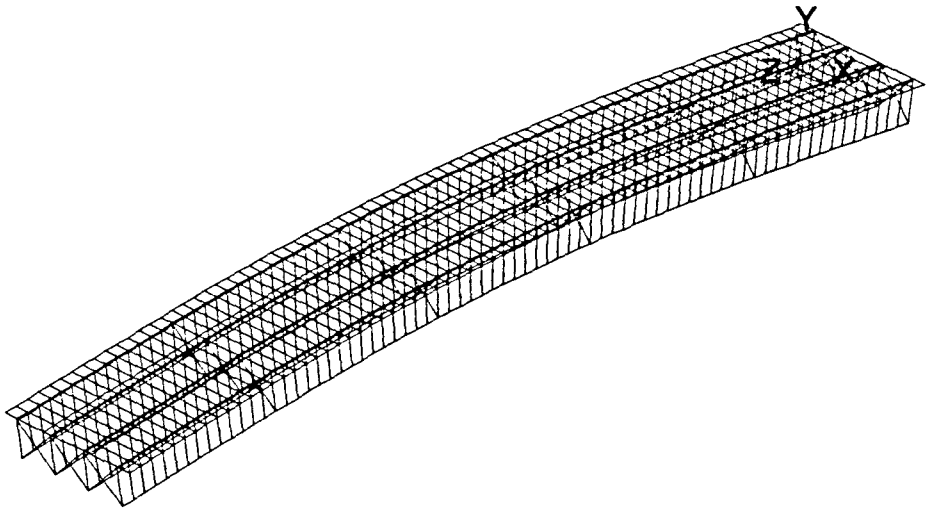

b) second mode shape, f = 2.7 Hz

Fig. A 3.1 Mode shapes of Wittson Bridge - Span 3

naraa.com

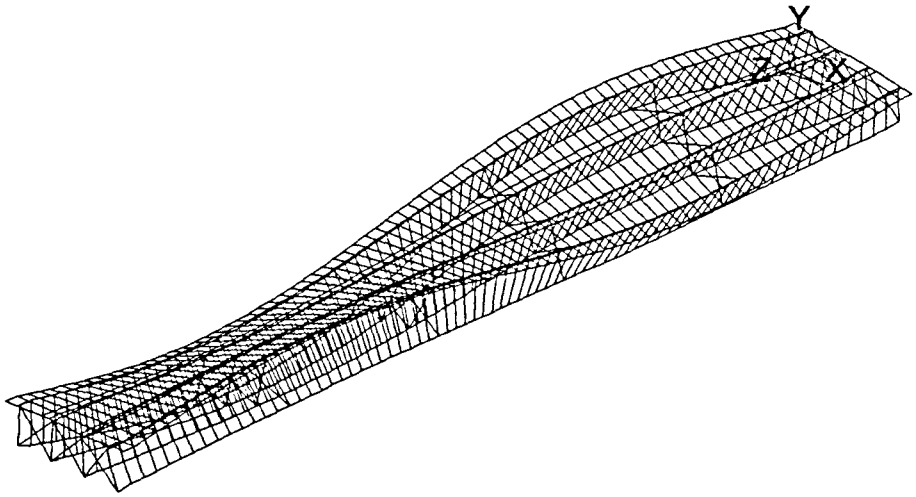

c) third mode shape, f = 9.4 Hz

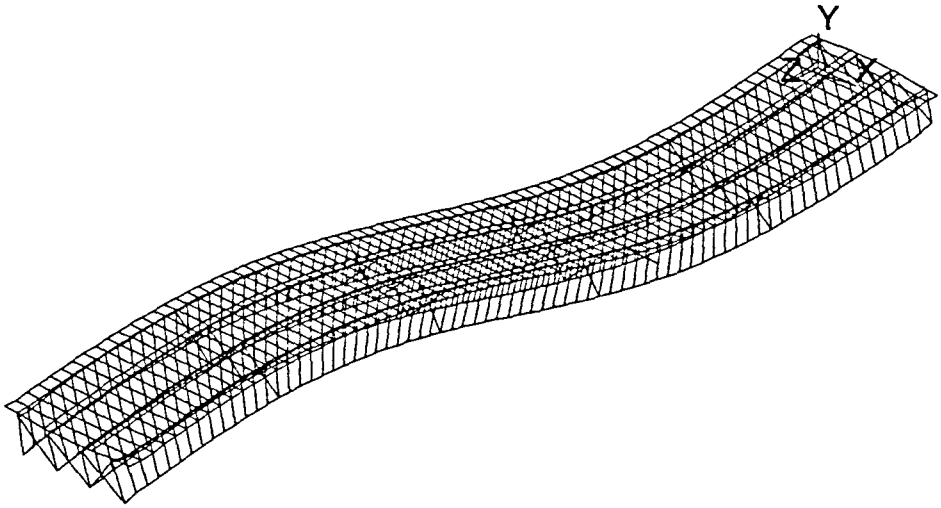

d) fourth mode shape, f = 9.5 Hz

Fig. A 3.1 (continued)

ınaraa.cor

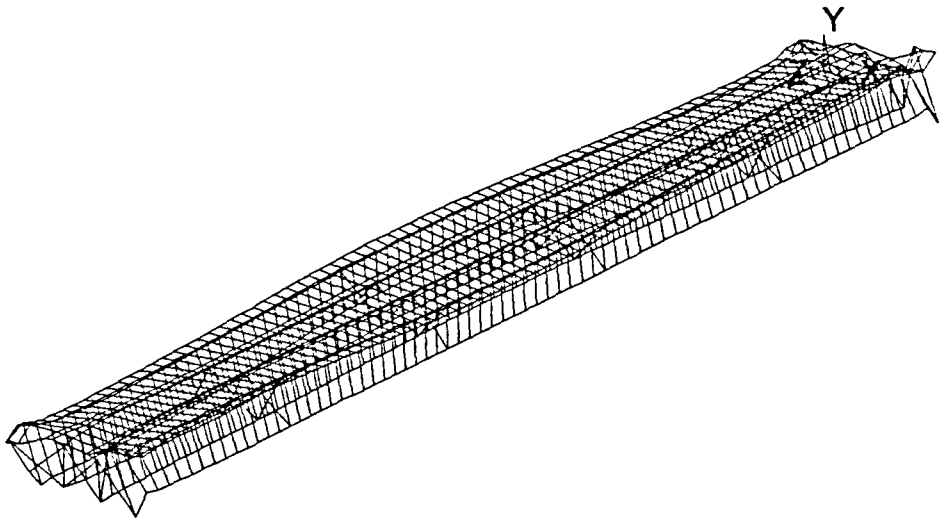

e) fifth mode shape, f = 11.7 Hz

Fig. A 3.1 (continued)

ınaraa.cor

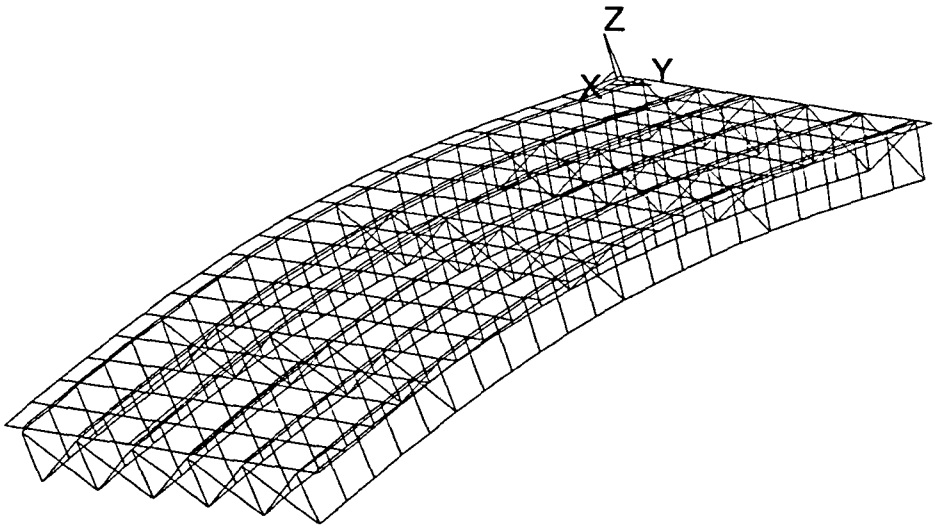

a) first mode shape, f = 6.6 Hz

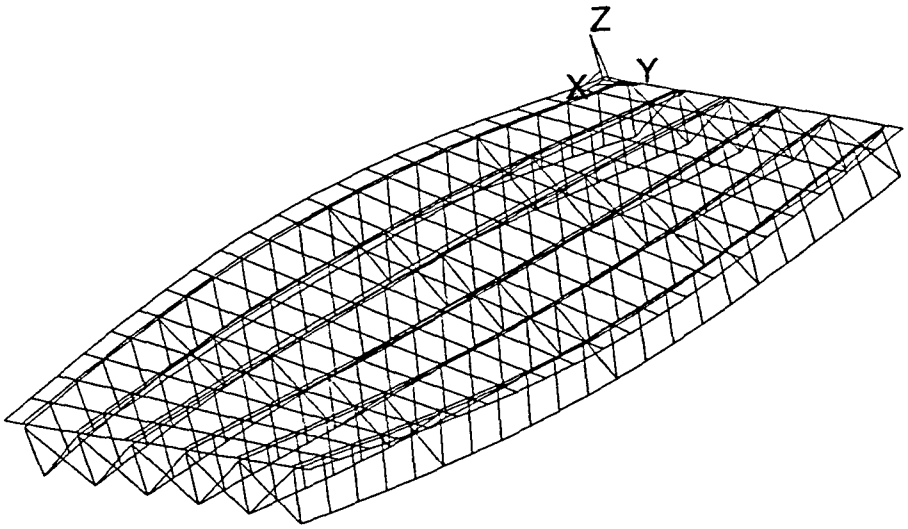

b) second mode shape, f = 6.9 Hz

Fig. A 3.2 Mode shapes of Chambers Co. Bridge

ınaraa.cor

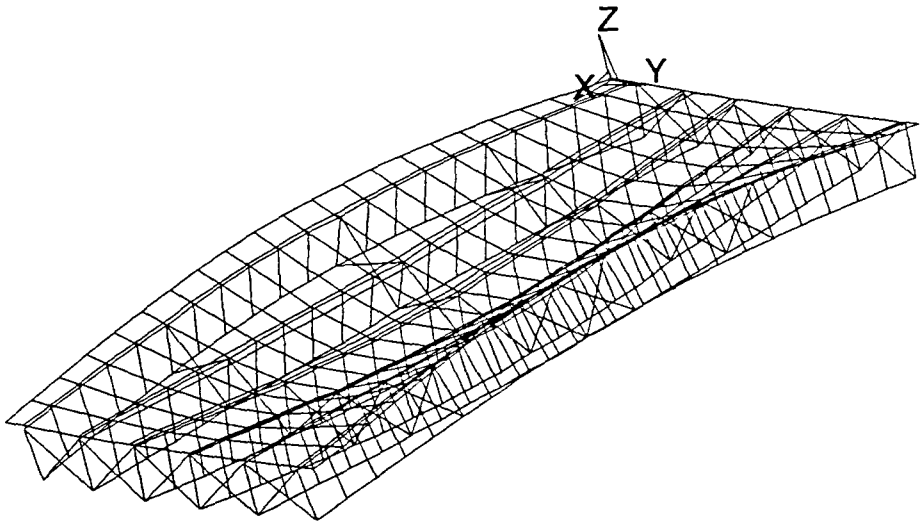

c) third mode shape, f = 10.7 Hz

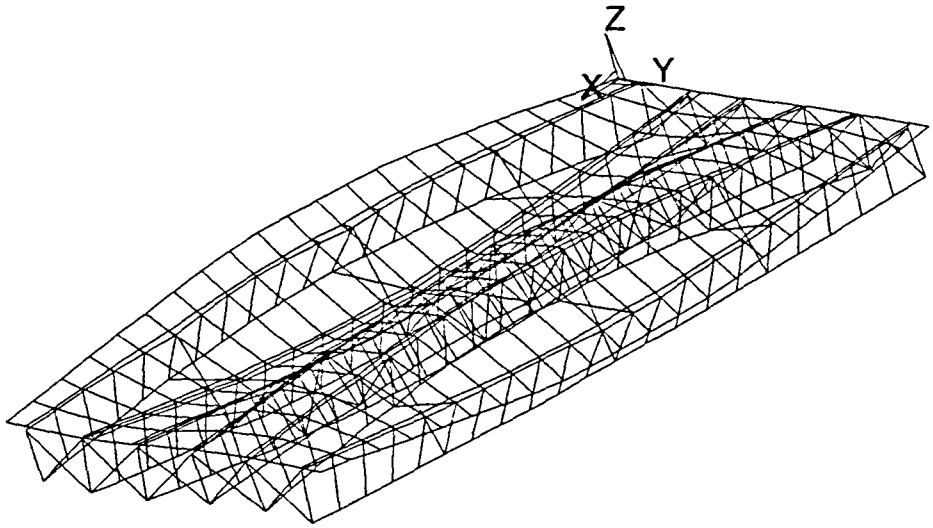

d) fourth mode shape, f = 20.8 Hz

Fig. A 3.2 (continued)

ınaraa.cor

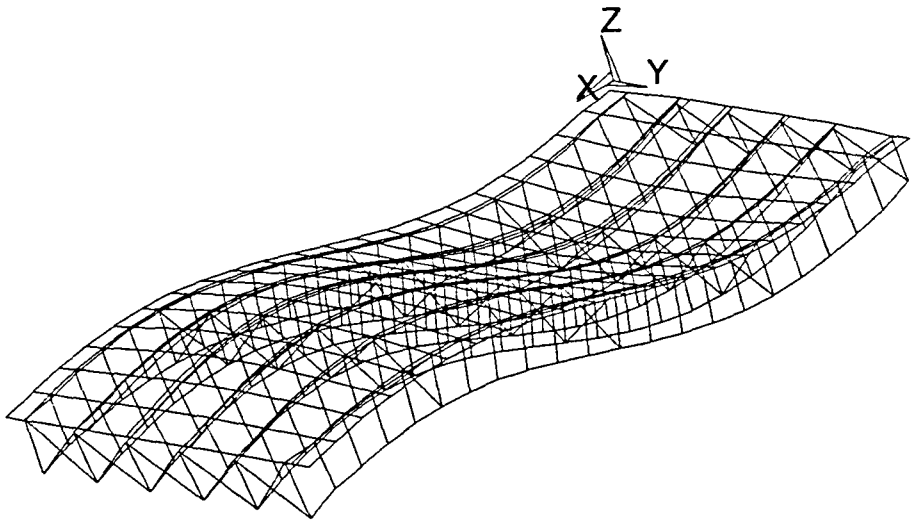

e) fifth mode shape, f = 22.3 Hz

Fig. A 3.2 (continued)

ınaraa.cor